The Thesis Committee for Pedro Rogelio Escamilla
Certifies that this is the approved version of the following Thesis:

Proving 2-Aminobiphenyl Nitric Oxide Probes in Cells
and
Designing Sequence-Defined Oligomers for Sequencing

APPROVED BY
SUPERVISING COMMITTEE:

Eric Anslyn, Supervisor

Jason Shear

Hung-wen Liu

Simon Humphrey

Jonathan Sessler

Proving 2-Aminobiphenyl Nitric Oxide Probes in Cells
and
Designing Sequence-Defined Oligomers for Sequencing

by

Pedro Rogelio Escamila

Thesis

Presented to the Faculty of the Graduate School of

The University of Texas at Austin

in Partial Fulfillment

of the Requirements

for the Degree of

Doctor of Philosophy

The University of Texas at Austin

May 2021

Dedication

To God

Acknowledgements

Foremost and above all, I thank God.

Next, I thank my wife and sons for their encouragement and patience when I could not be the husband or father that I wanted to be. My parents, brother, and sisters, too. It is finally over.

Dr. Anslyn has supported me throughout, and I thank him for his patience and understanding. One of the reasons I chose him for my PI was his consideration for an atypical graduate student – married and with two children. Of course, this is the *only* way I was an atypical graduate student.

UT Austin and its Chemistry Department for providing me with my undergraduate and graduate education and for equipping researchers with the tools to succeed. My favorite instruments were the LCMS and the cryoprobe NMR. Ian Riddington and Steve Sorey were always helpful. Betsy Hamblen for not growing impatient but always helping me with registration/graduation deadlines.

The Anslyn group cultivated so many friendships that I remember warmly. I would call my first few years the winter to spring season. Pedro Metola, who adopted me and Boris my first year, guiding us to good eating with quirky humor. John Lin, curt and impatient, but also kind, helpful, and ready to bounce off ideas. Maggie Meadows and Brette Chapin, encouraging, caring, and somewhat preoccupied with me. Since they celebrated me as "old man" (with the corresponding birthday paraphanelia), they were probably much more patient with me than with others. Alex Gade and Diana Zamora-Olivares, my PhysOrg TAs; Alex is unique, and she livened up the East office with her higher-than-average volume output and Norweigan exclamations, provoking Katherine Diehl to stressfully rub her legs. Helen Seifert, reserved but friendly, slow to melt.

Hannah Jo, quiet and peculiarly easily startled. Ram Edupuganti, always friendly and offering experienced counsel, which I should have adopted more often. Amber Johnson, who discussed her thiourea oligomer research with me, without any visual aids, and thus without my understanding the majority but sapiently nodding.

With time, summer came, and there was a transition to a more vivacious bunch. Jimmy I'd rather Reuther, Xiaolong Sun (eccentric and generous family friend), Lugan technicolor Bachman, Chris Wight (who will clearly and effectively teach you the steps to breathing), Sam House of Dahl – never, ever a second-rate cholesterol drug. Many antics, all under Brenden Herrera's eye of paternal concern, whom I believe I plunked twice, an innocent bystander, and who did share with me many an interesting article, seminar, and audited class out of a curiosity to learn, and seemed to delight in my morning conversations with Sam, freshly arrived to work.

And fall arrived, as the friends graduated before me, it became my turn to graduate. The shades of autumn, Sweet Caroline, BuLi, Kari McDuffee, Jaime Coronado – so reserved at first, Stephanie Valenzuela – hood appropriator and hoarder, Doo-Hee Lee, Liz Gratton (sigh), Sarah Moor – who along with Brenden tried so hard to recover my corrupted hard drive, Ling Yu – a foil to Xiaolong, postdocs CJ, Jongdoo, Josef, and Matt Minus (with some of the strangest disciplined approaches to life).

Gusts that blew in and then left: Xing Li, my WAH! collaborator during my first year, serious Xuanxuan Chen, engaging Linda Lijuan Xie, and bemused Maosen Yuan. Ngong Kodiah Beyeh

Two I have reserved. Crazy Man Erik Hernandez, catalyst to so many stories, a vibrant source of energy, and a very sweet person if given a chance. And my enantiomer (Anslyn group terminology) – Tweedledee, aka Igor Koleschevenko. These two could have a thesis chapter to themselves, and in the battle of greats, E2 blinked and Boris won.

And my undergrads, Kenny Mao, Sam Glass, Jasper Shei, and Doug Saunders. Thank you for your commitment and your company in the lab and for tolerating Igor and his music.

Also Dr. Shear for making his lab and fluorescence microscope available. Derek Hernandez for teaching me how to culture and image cells. Mindy Fitzpatrick and Allison Myers for accommodating my use of the microscope and the cell hood (i.e., being in the way). Janine Elliot and Olja Simoska for collaborating on simultaneous NO probe imaging and electrode measurements.

Abstract

Proving 2-Aminobiphenyl Nitric Oxide Probes in Cells
and
Designing Sequence-Defined Oligomers for Sequencing

Pedro Rogelio Escamilla, PhD

The University of Texas at Austin, 2021

Supervisor: Eric Anslyn

The simple diatom radical nitric oxide (NO) has numerous roles in biology. In organisms, healthy nanomolar NO levels are highly regulated. Deficiencies in NO can lead to atherosclerosis, diabetes, glaucoma, and many other conditions. Yet organisms also purposefully increase NO concentrations to micromolar levels in combatting pathogens. However, these high levels can backfire and damage cells and tissues, as found for Parkinson's disease and ischemia, among others.

Fluorescent NO probes enable live cell, tissue, and sometimes whole-animal imaging with minimal perturbation of their biological environment. 2-aminobiphenyl-based probe NO_{550} brought about a novel mechanism of detection in which NO-surrogate nitrosonium cation is assimilated into the nascent cinnoline fluorophore, resulting in low background and increased sensitivity. A family of second-generation 2-aminobiphenyl based probes were designed, producing four top performers in abiotic conditions.

Chapter 1 describes the synthesis of these top candidates and their evaluation in cells. Two emerged as promising options for NO researchers.

Chapter 2 describes the design and synthesis of sequence-defined non-natural oligomers that are sequenceable. Biological polymers peptides and DNA/RNA's exquisitely complex properties are dictated by their sequence; changing the sequence sufficiently may have detrimental effects on their performance. Both their synthesis and sequencing continue being optimized; a human genome that once required thirteen years to sequence now takes one day.

Not as developed but growing rapidly is the field of non-natural sequence-defined polymers. Without the constraints of biology, limitless options exist for backbone structures and sidechains. Such diversity discourages the focused development of sequencing technologies on par with those for biological polymers. Consequently, tandem MS is the favored form of analysis.

We sought to change the approach to polymer design by factoring in the sequencing of the polymer in addition to its synthesis. Oligourethanes based on β-aminoalcohols were designed so that the terminal unit could be derivatized to sequence by cyclizing upon itself and thereby releasing the remainder of the oligomer. Several derivatizations were investigated, to find that the oligomer sequenced itself without any terminal unit transformation, rather by self-immolation under conditions that slowed the "unzipping" of the polymer sufficiently to be able to detect the intermediate sequences.

Table of Contents

List of Tables

List of Figures

List of Schemes

Chapter 1: Synthesis and Cell Studies on 3'-(N,N-dialkylamino)-2-aminobiphenyl Fluorescent Dosimeter for Nitric Oxide Surrogate N_2O_3[1]

1.1 INTRODUCTION

The uncharged diatomic radical gasotransmitter nitric oxide (NO) participates in a variety of biological processes, an effector molecule for the cardiovascular, immune, and nervous systems. Research from 1972 to 1989 determined this hydrophobic gas, commonly known as a noxious pollutant in vehicle and factory emissions, to be the Endothelium-Derived Relaxing Factor (EDRF) – the chemical that initiates the process of dilation of blood vessels. That such an inconspicuous molecule could play a prominent role in signaling in the cardiovascular system resulted in its being named Molecule of the Year in 1992, and then the Nobel Prize was awarded in 1998 to Furchghott, Ingarro, and Murad for their research establishing NO as the EDRF. Over time, scientists have revealed the pleiotropic roles of NO in physiology and pathology, either through indirect methods, such as quantification of NO-producing enzymes, or through direct detection of NO or its reaction by-products. Electro-paramagnetic resonance (EPR), electrochemistry, chemiluminescence, and fluorescence comprise most of the direct measurement methods. The multitude of fluorescent probes fall into five main approaches to detection. Among these are the probes based on the 2-amino-4´-dialkylamino-biphenyl core, with NO_{550} as the progenitor. Seeking to improve upon NO_{550}'s poor hydrophilicity and reactivity, a second generation of probes was developed and compared to NO_{550} abiotically. We

[1] Most of the content from pages 58 to 84 was published in Escamilla, P. R.; Shen, Y.; Zhang, Q.; Hernandez, D. S.; Howard, C. J.; Qian, X.; Filonov, D. Y.; Kinev, A. V.; Shear, J. B.; Anslyn, E. V.; Yang, Y., 2-Amino-3′-dialkylaminobiphenyl-based fluorescent intracellular probes for nitric oxide surrogate N_2O_3. Chemical Science 2020, 11 (5), 1394-1403. Shen, Zhang, Qian, and Yang synthesized probes **1** to **15** and determined their fluorescence properties in the absence and presence of NO in abiotic media. I wrote the article and performed the cell studies to produce cell images and quantification of cellular fluorescence intensity.

evaluated the top two performers in cells versus NO_{550} and versus DAF-FM, the most published, "gold standard" fluorescence NO probe.

1.1.1 Chemical Properties and Reactivity of Nitric Oxide

Nitric oxide is a neutral radical that exists as a gas at biologically relevant temperatures. The molecule has a bond order of 2.5, with a 115 pm bond length. Its lack of charge and low polarity (0.159 D dipole moment, ten times less than water)[1] results in greater solubility in hydrophobic than hydrophilic environments. In fact, a solution in water saturates at 1.9 mM,[2] whereas organic solvents retain five to ten times the concentration.[3] With a diffusion rate of 3300 μm^2/sec in water at 37 °C (1.4 times that of O_2[4] - corresponding to approximately one length of a cell per 25 milliseconds),[5] NO diffuses across cells readily, and its lipophilicity obviates the need for membrane receptors. Due to the larger electronegativity of oxygen over nitrogen, the radical, located in an anti-bonding pi orbital, has a greater orbital contribution at the nitrogen atom, and molecular orbital theory correctly predicts that most reactions with NO form bonds at the nitrogen. The reduction and oxidation potentials of NO, calculated at -0.76 V[6-7] and -1.2 V[8-9] (1M in H_2O vs. NHE), respectively, testify to NO's weakness as an oxidizing or reducing agent and consequently to its inertness towards diamagnetic species. As such, nitric oxide predominantly reacts with paramagnetic species.

$^{\bullet}NO + 1\ e^- \rightarrow {}^3NO^-$ (-0.76 V/-0.56 V pH 7) $\qquad$ $^{\bullet}NO \rightarrow NO^+ + 1\ e^-$ (-1.2 V)

1.1.2 Sources of NO

1.1.2.1 Nitric Oxide Synthases

The oxidation of L-arginine to L-citrulline by nitric oxide synthases (NOSs) is the main source of nitric oxide in organisms. In mammals, the two constitutively-expressed

synthases, endothelial (eNOS, or NOS 3)[10] and neuronal (nNOS, or NOS 1),[11] produce nanomolar levels of NO of seconds to minutes in duration.[12] In contrast, the inducible synthases (iNOSs, or NOS 2),[13-14] whose increased expression is activated in immune response, for example by cytokines or by lipophilic polysaccharides (LPS) in bacterial cell walls, output micromolar levels of NO over hours – until the synthases are degraded.[15-17] Endothelial, epithelial, cardiac myocyte, platelets, erythrocyte,[18-19] fibroblasts, skeletal muscle, bone, motor neuron, and astroglia[20] cells are known to contain eNOS, and the Ca^{2+}/calmodulin-dependent NO they produce promotes vasodilation to regulate blood pressure. NO from nNOSs, localized in neurons, astrocytes, and neuronal stem cells, reinforces glutamatergic synapses for learning and memory and for synaptic plasticity. The higher levels of NO from iNOS in macrophages, hepatocytes, smooth muscle cells, chondrocytes, glial cells, astrocytes, neurons, and myocytes channel into pathogenic functions necessary for immune response.[21]

The enzymatic conversion of L-arginine to nitric oxide proceeds through reduction of molecular oxygen to first produce ω-N-hydroxy arginine (NOHA) and, in a second cycle, NO and L-citrulline (Scheme 1.01).

Scheme 1.01: Enzymatic conversion of L-arginine to L-citrulline and NO

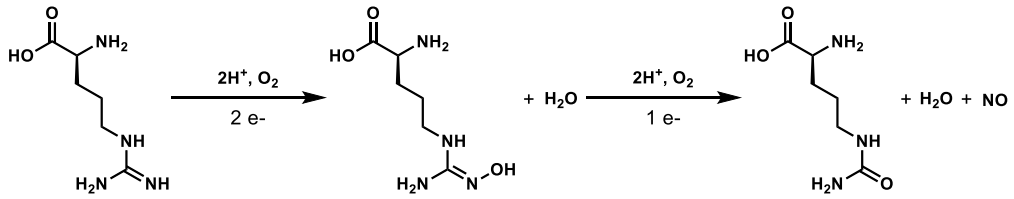

This intricate process requires substrate nicotine adenine dinucleotide phosphate hydride (NADPH) and cofactors flavin adenine dinucleotide (FAD), flavin mononucleotide (FMN), heme B, and (*6R*)-5,6,7,8-tetrahydro-L-biopterin (H_4B). Cytochrome P450,

which also reduces oxygen to then oxidize a wide variety of compounds, has most of these cofactors and substrates in common.

1.1.2.1.1 NOS Structure

The three isoforms of NOS, though encoded by different genes,[22-23] share many similarities in structure, with iNOS the most divergent. All three have a reductase domain at the C-terminus and an oxidase domain at the N-terminus, separated by an alpha-helix region in which the small Ca^{2+}-binding protein calmodulin (CaM) docks.[24-25] NADPH, FAD, and FMN bind in the reductase domain, where the electron transport to the oxidase domain originates. In the oxidase domain, cysteine-thiol-ligated heme B accepts these electrons and exchanges electrons with the neighboring H_4B. Both nNOS and eNOS have an autoinhibitory loop[26-28] in the FMN subdomain of the reductase region as well as an electron-transfer-repressing C-terminal extension,[29-31] necessary to regulate their nanomolar output of NO as constitutive enzymes. The autoinhibitory loop is absent in iNOS, whose greater output depends upon the extent of induction to express a large population of the enzyme. Unique to nNOS is an N-terminal extension known as the PDZ domain, which localizes the enzyme near the cell membrane, at the cytoskeleton, and at post-synaptic receptor locations.[32-33]

Although NOSs may exist as monomers or heterodimers with regulating proteins, only the homodimers bind L-arginine and H_4B and catalyze NO synthesis (Figure 1.01).[34] Within the same monomer subunit of the homodimer, NADPH substrate transfers a hydride to FAD, which reduces FMN, located a mere 5 Å away in nNOS, one electron at a time, first to the semiquinone and then to the hydroquinone.[35-36] This FMN hydroquinone, sufficiently activated for a one-electron reduction of ferric heme,[37] can do so efficiently only to the more proximal ferric heme residing in the oxidase domain of the partner subunit of the homodimer.[38-40] Neither the monomer alone nor any heterodimers

efficiently transfer electrons to heme, as the greater degree of conformational change in the protein required for FMN hydroquinone to reach the ferric heme on the same monomer proves insurmountable. Furthermore, the two H_4B cofactors in the enzyme, which hydrogen bond to the proprionate arms of the heme, also reside in proximity (13 Å) to each other, with a tryptophan aromatic residue in between. This proximity enables electron exchange, possibly also channeled through the tryptophan residue, to an H_4B radical in one monomer from H_4B in the other monomer.[41] Essential to homodimer formation and cooperative in H_4B binding is a tetrahedral zinc-ion bridge with four cysteine residues, two from each monomer, as ligands.[42-43]

Figure 1.01: NOS homodimerization is necessary for the production of NO

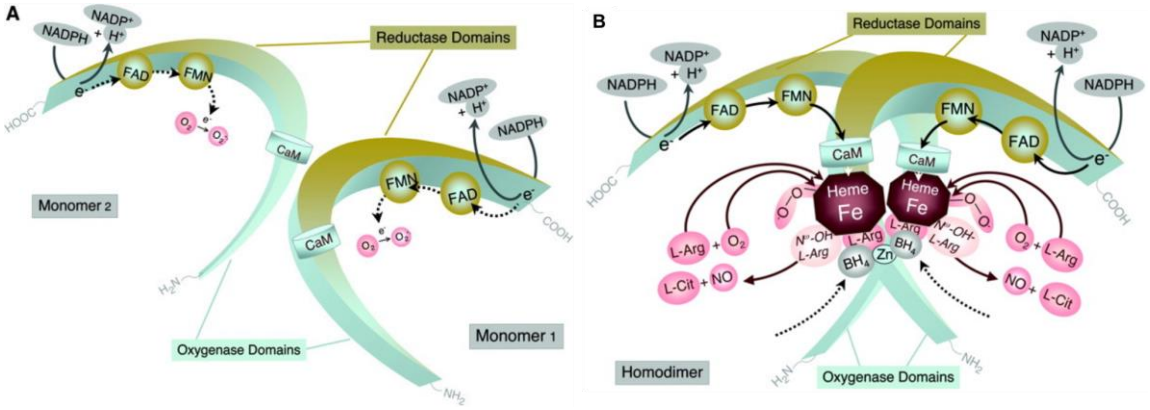

A) Depiction of eNOS non-associated monomers. Without heme present, reductase domain activity is limited to the low-capacity reduction of oxygen to superoxide. B) Heme binding promotes the formation of NOS homodimers, stabilized by Zn^{2+} binding by thiol fingers, which also stabilizes BH_4 cofactor binding. Calmodulin protein binding promotes NADPH/FAD/FMN electron transport chain. FMN on one monomer transfers electrons not to the heme bound to it but rather to the heme bound to its dimer pair, firing up the catalytic production of NO. Figure used with permission from[44]

Equally vital to NO synthesis is calmodulin (CAM), a small protein which binds to a thirty-amino-acid residue between the FMN subdomain and the oxidase domain.[25] For the constitutive NOSs, raised intracellular Ca^{2+} levels activate eNOS and nNOS (200 to 400 nM for half-maximum activation).[45] CAM binds four calcium ions in a penta-

coordinate manner in each of four EF loops (the EF name derives from the last two of six helix regions A-F in the first crystal structure describing this substructure),[46] provoking a change of conformation that increases exposure of hydrophobic side chains. This greater hydrophobic surface enhances quaternary interactions with eNOS and nNOS, although it is not necessary for iNOS, whose more complementary sequence binds CAM regardless of resting Ca^{2+} levels (40 nM half-maximum activation).[45, 47] The C-terminal domain and the autoinhibitory loop in the reductase region of eNOS and nNOS interfere with CAM binding, proven by selective mutation of residues in these constructs.[33] They therefore require the more optimal, Ca^{2+}-induced, hydrophobic CAM conformation.

Although CAM binding affects several processes in NOS homodimers, such as enhancing reduction rates of the reductase flavins, it crucially increases the rate of one-electron reduction of heme by FMN hydroquinone, the overall rate-limiting step for NO synthesis.[48-49] FMN gets reduced by FAD in the reductase domain, distant from the heme in the oxidase domain. A flexible hinge region enables a change in conformation through which FMN swings closer to heme, away from FAD. The hinging occurs more readily in the open, rather than closed, conformation induced by CAM binding.[50]

1.1.2.1.2 NOS NO Production Mechanism

The mechanism for NO production from L-arginine has not been fully elucidated, although there is agreement on parts of the synthesis. A large consensus describes the first cycle oxidation of arginine to NOHA as analogous to the Cytochrome P450 radical-rebound mechanism (Scheme 1.02).[51] Arginine and molecular oxygen substrates localize in the binding pocket above the ferric heme. The NADPH to FAD to FMN electron transport chain reduces the ferric heme to ferrous, thus enabling complexation of oxygen. The incipient peroxo anion in this complex,[52] due to π-back-bonding from the electron rich iron to the anti-bonding orbitals of oxygen, is stabilized by electrostatic interactions

with arginine and by hydrogen bonding to both a guanidinium proton of the arginine substrate and an active-site water molecule.[53] Another electron, this time from H_4B,[54-55] the pterin cofactor hydrogen-bound to the proprionate arms of the heme, reduces the complex to the ferric-peroxy intermediate that then dehydrates to Compound I, the oxo-Fe (IV) heme cationic radical.[51] The ferryl oxygen abstracts a hydrogen radical from arginine substrate, forming the guanidinyl radical which in turn abstracts the Fe(IV)-bound OH radical to produce NOHA and ferric heme.

Scheme 1.02: Possible mechanism for the first cycle in NO production – NOS conversion of L-arginine to NOHA

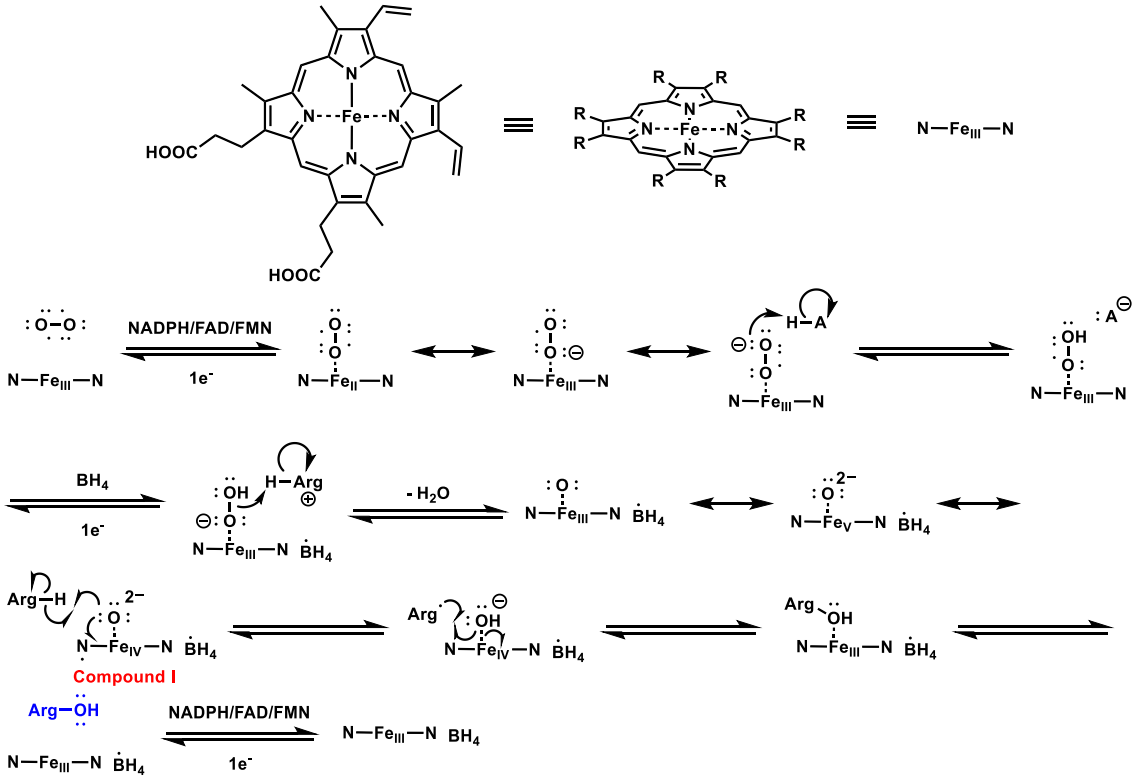

The second cycle (Scheme 1.03) requires only one electron from NADH, signaling a different mechanism from the first. The one agreement for the second cycle is the necessary NADPH/FAD/FMN reduction of ferric heme to ferrous with binding of

oxygen. Most suggested mechanisms also incorporate further reduction with H_4B to the peroxy anion, subsequently protonated to the hydroperoxy complex. The proton source in this case is purported to be the more acidic hydroxyguanidinium proton,[56] rather than the water/arginine hydrogen-bonded network for the first cycle.[57] Partly due to this difference in proton sources is attributed the change in heme catalysis from the first to second cycles. A concerted, six-membered transition state could be envisioned, in which a pi bond forms between the NOHA ω-nitrogen and its hydroxyl oxygen, a sigma bond forms between the guanidinyl carbon and the distal hydroperoxyferryl oxygen as the peroxo bond breaks, and the proximal hydroperoxyferryl anionic oxygen deprotonates the hydroxyl. The resulting ferric hydroxide would then deprotonate the resulting tetrahedral intermediate, expelling nitroxyl anion to form L-citrulline. Nitroxyl anion could then replace water in the experimentally-observed ferric aqua complex.[57] This ligand exchange enables reduction of the H_4B radical and results in dissociation of NO radical from ferric heme.[53]

Scheme 1.03: Possible mechanism for the second cycle in NO production – NOS conversion of NOHA to L-citrulline and NO

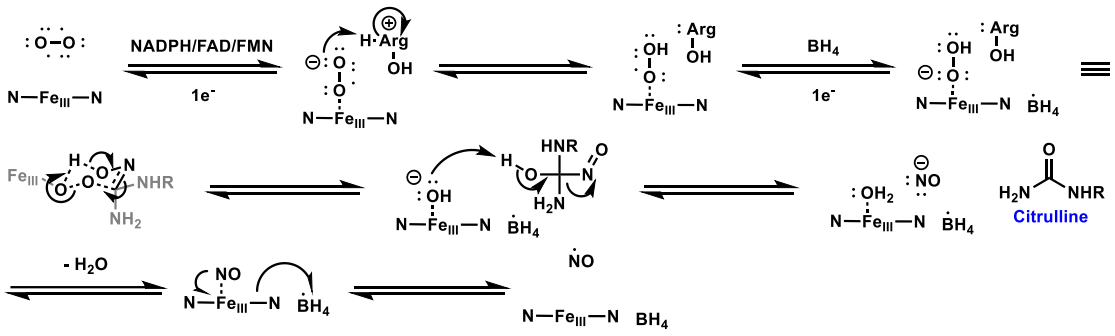

1.1.2.2 Nitrate / Nitrite / NO Pathway

Endogenous NO also derives from the nitrate-nitrite-NO pathway, in which nitrate and nitrite are reduced to NO. The most abundant of these three nitrogen oxides in plasma (roughly 100:1:0.1 nitrate/nitrite/NO)[58], nitrate was at first considered the physiologically inert end-product of NO chemistry, but it actually functions as a stable storage of the more reactive NO. Molybdenum-based oral-commensal-bacteria nitrate reductases[59] efficiently reduce nitrate to nitrite,[60] and salivary glands extract approximately 25% of circulating plasma nitrate, which derives from diet and from the oxidation of endogenously produced NO.[61] For mammals, xanthine oxidoreductase seems to also perform as a nitrate reductase, especially in hypoxic and low pH conditions.[62-63]

Reduction of nitrite to NO does not depend on prokaryotic enzymes. Nitrite derives from nitrate reduction or from reactions with downstream products of NO, such as N_2O_3 and peroxynitrite. Gastric acidity does non-enzymatically reduce some of the nitrite to NO,[64] but most nitrite is absorbed into circulation with a half-life of ten minutes.[65] Multiple mammalian nitrite reductases convert nitrite to NO, particularly in hypoxic or even apoxic and/or lower than physiological pH conditions. Among these are the molybdenum-based xanthine oxido reductase, sulfite oxidase, and aldehyde oxidase; the mitochondrial amidoxime reducing components III and IV; the hemo, myo, neuro, and cytoglobin family, eNOS, and possibly carbonic anhydrase.[66] The nitrate-nitrite-NO production pathway, optimal under hypo-aerobic conditions, performs complementarily to the NOS pathway, optimal under aerobic conditions. In fact, the output of NO from nitrite in ischemic conditions rivals that of constitutive NOSs.[67]

1.1.3 Sinks for NO

The diatom nitric oxide, with an average half-life varying from 0.1s to 6 seconds[68] (more recently estimated at 0.002 to 2 seconds),[68] depending upon its environment, readily permeates membranes, diffusing according to its concentration gradient away from its point of production. A stable radical resistant to oxidation or reduction, it reacts with paramagnetic partners. Its primary partner in the bloodstream is the metalloprotein ferrous oxyhemoglobin in red blood cells (erythrocytes), with reaction rates on the order of $10^5\ M^{-1}s^{-1}$. Their interaction results in heme oxidation to ferric and in oxidation of NO to nitrate, an apparently insignificant end to the signaling radical, except for its ability to be stored as NO_3^- as discussed above.[69] Interestingly, studies have revealed that hemoglobin in erythrocytes frequently carries NO in its S-nitroso form. When hemoglobin adopts its oxygen-binding relaxed state, the Cysβ93 thiol tends to be nitrosylated,[70] as shown by mass spectroscopy[71] and by x-ray crystallography,[72] without much consequence to its bioactivity. Similar to hemoglobin's ability to carry nitrosonium, the major component (> 5 μM) of S-nitrosoproteins in human plasma is serum albumin, with an S-nitroso Cys-34, indicating the S-nitrosation of plasma proteins as a significant NO sink.[73]

For the constitutive NOSs, NO's intended reaction partner is the soluble Guanylate Cyclase (sGC), a ferrous heme protein that binds O_2 very poorly[74] but NO strongly. This binding catalyzes the conversion of guanosine triphosphate to the secondary messenger cyclic guanosine monophosphate (cGMP).[75] NO binding to histidine-coordinated ferrous hemes displaces, due to strong π-backbonding between the metal and NO, the trans histidine, thereby activating the sGC.[76-77] Other signal transduction targets for NO include mitochondrial cytochrome oxidase,[78] cytochromes P450,[79] vitamin B2 Cobalamin,[80] nuclear factor kappa B (NF-κB),[81] Ca^{2+}-related G-

proteins,[82] apoptosis caspases and poly (ADP-ribose polymerase),[83-85] partially oxygenated hemoglobin,[86] the chelated iron pool,[87] the cardiac calcium-release channel,[88] NMDA channels,[89] and (at high concentrations) calcium-dependent potassium channels in vascular smooth muscle.[90] When nitrosylating higher oxidation state metalloproteins [M(X)], the complex has greater M(X-1)-NO^+ character, and the complex can stoichiometrically (not catalytically) nitrosate diamagnetic nucleophiles, such as water, amines, and thiols. The reduced metal may bind NO, but with prohibitively less NO^+ character and unable to reductively nitrosylate another nucleophile. Nitrosothiols can transnitrosate other thiols, thereby acting as a storage of this nitrosonium chemistry of NO.

Apart from interactions with metalloproteins, NO reacts with other radicals. Nitrosylation of thyil radicals provides another route to nitrosothiols and their nitrosonium storage capabilities. In tissue, the main consumption is by hydroxyl and superoxide radicals. HO radicals neutralize NO to nitrite. Superoxide ($O_2^{\bullet-}$) reacts with NO at near diffusion-limited rates to form peroxynitrite (Scheme 1.04A). Protonation of peroxynitrite (pK_a ~6.6) weakens the peroxide bond and leads to disproportionation to the radicals nitrogen dioxide ($^{\bullet}NO_2$) and hydroxyl ($^{\bullet}OH$) in their solvent cage that recombine to yield nitrate or further react with NO to give nitrite and dinitrogen trioxide (N_2O_3, Scheme 1.04C). Peroxynitrite may also react with carbon dioxide to form the nitrosoperoxycarbonate anion (Scheme 1.04B);[91] homolytic cleavage gives NO_2 and carbonate radicals that can rearrange in the solvent cage to nitrate and carbon dioxide. If they escape the solvent cage, the two radicals can further react with NO to give N_2O_3 and nitrite and carbon dioxide, respectively. Carbon radicals react to form organic nitroso compounds that tautomerize to oximes in the case of primary or secondary radicals.

Scheme 1.04: Physiologically relevant reactions of NO with radicals

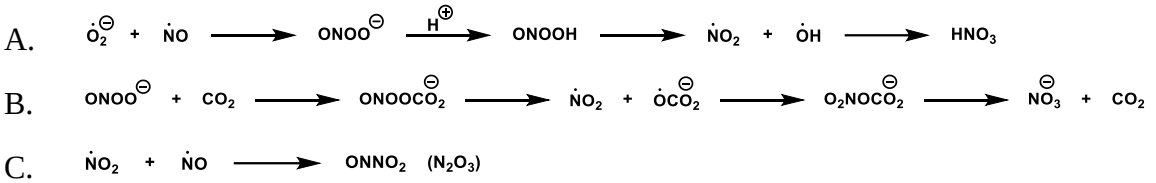

A) NO and superoxide combine under near-diffusion-limited rates to form peroxynitrite, which decomposes after protonation (pKa ~ 6.6) to NO_2 and OH radicals that can reassociate to form nitric acid. B) Peroxynitrite reacts readily with carbon dioxide to the nitrosoperoxycarbonate, which disproportionates to NO2 and carbonate radicals. These can recombine and heterolyze to nitrate and carbon dioxide. C) If NO2 radical escapes the solvent cage from homolysis in (A) or (B), it can react with NO to form asymmetric N2O3, a nitrosating agent.

The two unpaired electrons in oxygen entail a third-order reaction with two NO molecules (Scheme 1.05). The resulting product disproportionates to two molecules of NO_2, again with the unpaired electron primarily on the nitrogen but also more oxidizing than NO. NO combines with NO_2 to form N_2O_3 (Scheme 1.04C), and the greater oxidation potential of NO_2 means that N_2O_3 has some nitrosonium character, making it a nitrosating agent. Typical biological NO levels range from 10 nM to 1 µM, and at this dilution, for reaction with physiological levels of oxygen, NO has a half-life of nine to 900 minutes.[92] However, both NO and O_2 are more soluble in hydrophobic environments, and so higher local concentrations in membranes and hydrophobic pockets enhance reaction rates about 300-fold.[93]

Scheme 1.05: Reaction of NO with oxygen to form nitrogen dioxide

Another circumstance increases local concentrations of NO and O_2. As stated before, eNOS, which are mostly expressed in endothelial cells, produce approximately 70% of circulating nitrite from oxidation of NO. Diffusion of NO away from its point of synthesis takes it towards the proximal blood stream to be converted into nitrite by oxyhemoglobin in erythrocytes – or in the opposite direction, penetrating into tissues.

Released O_2 from oxyhemoglobin similarly diffuses away from the blood stream and into tissues, and so the concentration gradient for NO and O_2 is higher close to the bloodstream than average NO and O_2 values, especially in hydrophobic environments, enabling N_2O_3 nitrosative chemistry.

1.1.4 Physiology of NO

Nearly thirty years after its discovery as the EDRF, a myriad of physiological roles for NO has been elucidated. Nitric oxide influences vasodilation;[94] glaucoma;[95] proliferation and migration of vascular smooth muscle cells,[96] platelet adhesion and aggregation;[97] cell inflammation and leukocyte adhesion that can lead to thrombosis;[98] vascular permeability;[99-100] angiogenesis;[101-102] fibrinolysis;[103] bronchodilation;[104] β-adrenergic stimulus;[105] cytokine production and mast cell inhibition;[106] wound and muscle repair;[107-108] penile erection;[109] spermato/oogenesis and fertilization;[110] colon, rectum, and sphincter relaxation;[111] glomerular filtration and renin secretion;[112-113] brain vascular tone regulation;[114] thermoregulation;[115] neurotransmission;[116-117] regulation of neurotransmitter uptake and reward learning;[118] sleep regulation;[119] pain sensitization;[120-121] hormone secretion;[122-123] long-term potentiation and depression in synaptic plasticity;[124-127] neurogenesis;[128] stem cell differentiation;[129] immune response to bacteria, parasites, and viruses;[130] and tumor suppression.[131] It is the relaxation factor produced by eNOS in endothelial cells that binds to sGC to activate the synthesis of cGMP, which in turn acts on protein kinases, gates cation channels, and regulates phosphodiesterase to cause relaxation of smooth muscle cells in veins and arteries.[132-133] This vasorelaxation increases blood flow, lowers blood pressure, and decreases platelet adhesion. cGMP also triggers mitochondrial biogenesis[134]

An equally major target for NO is nitrosylation (via transition metal intermediates) or nitrosation (via nitrosonium chemistry) of cysteine thiols in proteins.[135] This type of post-translational modification is regulated and site-directed and applies to nearly all protein categories, with effects such as directing proteins to subcellular locations; preparing proteins for degradation; and regulating interactions between proteins, ion-channel activity, membrane trafficking, phosphorylation, cellular redox stress, enzyme activities, cellular metabolism, transcription-factor activity, and apoptosis.[136] For example, cancer cell death derives from s-nitrosylation of matrix metalloproteinase 9 (MMP-9) and NF-κB.[137]

S-nitrosothiols, whether in proteins or deriving from low-molecular weight thiols such as cysteine and glutathione readily transnitrosate other thiols, performing as NO carriers. In the circulatory system, when hemoglobin is in its oxygen-binding relaxed state, S-nitroso Cys93β resides in a hydrophobic cavity. Hemoglobin's tense conformation that releases oxygen also exposes the S-nitrosothiol to the cytoplasm.[138] Trans-nitrosation, particularly to membrane-associated proteins or to low-molecular-weight thiols, results in the extracellular delivery of nitrosonium, according to a decreasing arteriovenous oxygen gradient, with subsequent vasodilation. The mechanism of this vasodilation has not been established and may not proceed through the NO/sGC activation mechanism.[139] Hydrogen sulfide may denitrosylate S-nitrosothiols via its disulfide, forming perthionitrite. Homolysis releases NO and persulfide radical, initiating sulfide polymerization.[140] Whether this sequence of reactions occurs at biological levels has not been determined.

In addition, NO competes with oxygen for binding to Cytochrome C oxidase in mitochondria, inhibiting respiration and prolonging O_2 diffusion into tissues.[141] Also, due to its resistance to oxidation or reduction, NO acts as a radical quencher. It

transforms highly oxidative hydroxyl radicals to the much more benign nitrite anion. The oxidative NO_2 radical reacts with NO to form N_2O_3, a milder nitrosating species. NO can also quench allylic and peroxy radicals in lipids to stop the propagation of lipid peroxidation that can disrupt cell membranes.[142]

NO levels range from constitutive NOS picomolar/nanomolar resting levels to inducible NOS micromolar full output concentrations. At the lower end, 500 pM to 5 nM steady-state NO concentrations activate sGC to augment cell proliferation and protection, but 100 nM concentrations are needed to activate extracellular signal-regulated kinase (ERK). Increasing up to 150 nM, Akt get phosphorylated, triggering the phosphorylation of caspase-6 and Bad, which disrupts apoptosis.[143] NO inhibits non-heme iron oxygenases at 100 to 400 nM levels, and levels above 1 μM promote nitrosation of proteins, thiols, zinc fingers, and DNA.[144] In general terms, at lower concentrations, NO influences cell survival and proliferation. Mid-level NO modulates metastasis, the vascular endothelial growth factor, and angiogenesis. High NO concentrations tend to induce apoptosis and enact DNA nitration (nitrosative stress).[145]

1.1.5 Pathology of NO

The two extremes of NO concentration typically produce pathological results. A deficiency of NO negates NO benefits and leads to hypertension; thrombosis; atherosclerosis; hypercholesterolemia; infarction; diabetes;[146] chronic and acute inflammation disorders, including arthritis; stroke; hyperlipidemia; digestive tract issues, such as irritable bowel syndrome; chronic kidney disease;[147] erectile disfunction; asthma; cystic fibrosis; loss of memory and learning;[148] dementia;[149] β-amyloid deposition in Alzheimer's disease;[150] Many of these hypo-nitric oxide symptoms were isolated by

infusing or injecting NOS inhibitors based on L-arginine derivatives, such as L-N-monomethyl arginine (L-NMMA) or by knocking-out NOS expressing genes.

Low NO levels can result from the uncoupling of NO synthesis in NOS, for instance from lack of L-arginine substrate or H_4B cofactor. This uncoupling reduces oxygen to superoxide through the oxy-ferrous heme complex or by flavins FAD or FMN.[151] Various other enzymes also leak electrons to reduce oxygen when the catalytic system is not fully aligned, especially in the mitochondrial electron transport chain, whereas other enzymes such as NADPH oxidase and xanthine oxidase primarily produce superoxide for immune response. NO and superoxide combine to form peroxynitrite that, when protonated (pK_a 6.8) can disproportionate into the much stronger oxidants $^{\bullet}OH$ and $^{\bullet}NO_2$, and the 30% that escape the solvent cage[152] either nitrate or oxidize unsaturated lipids and nitrate tyrosine, tryptophan, guanosine, and DNA. Similarly, the peroxynitrite / CO_2 adduct disproportionates to $^{\bullet}OCO_2$ and $^{\bullet}NO_2$, and the 35% that escape the solvent cage[153] similarly corrupt the lipid bilayer, proteins, and DNA.

Whereas a deficiency of NO subtracts its beneficial modulatory properties, when concentrations reach maximum micromolar levels, NO and its metabolites themselves wreak pathological havoc. At these concentrations under normoxic conditions, both NO oxidation to NO_2 and N_2O_3 and NO's reaction with superoxide anion to form peroxynitrite become more relevant, leading to nitrosative stress. The most common indicator of nitrosative stress is the conversion of tyrosine residues to 3-NO_2 tyrosine, stemming from radical (e.g., NO_2 and OH - from disproportionation of peroxynitrous acid - or NO_2 and CO_3^- - from the nitrosoperoxycarbonate adduct of peroxynitrite and CO_2) abstraction of a hydrogen *ortho* to the phenol followed by combination of the aryl radical with NO_2. Subjects with rheumatoid arthritis;[154] renal septic shock;[155] celiac disease;[156] cerebral ischemia;[157] Alzheimer's, Parkinson's, Huntington's, Lou Gehrig's,

and Prion diseases[158] exhibited increased levels of nitrotyrosine versus healthy ones, mainly due to conformational changes to the nitrotyrosine-containing protein. The three radicals also abstract allylic protons from unsaturated lipids, and the lipid allylic radicals then form other radical adducts or initiate lipid peroxidation.[159] The potent HO radical reacts with sugars in polysaccharides and in DNA strands, breaking the polymers.[160] Furthermore, peroxynitrite, its acid form, and nitrogen dioxide react with guanine in DNA to cause single strand breakage.

Insomuch as the diffusion-limited reaction between NO and peroxynitrite, sometimes with the involvement of CO_2, delivers NO_2, CO_3^-, and OH radicals, the diffusion limited reaction between NO and NO_2 generates the nitrosonium equivalent N_2O_3 to react with diamagnetic nucleophiles, such as water, amines, and thiols. The prohibitively slow (unless at high NO concentrations and in hydrophobic environments with oxygen) autoxidation of NO, homolysis of peroxynitrous acid, disproportionation of peroxynitrosocarbonate, and oxidation of nitrite all contribute to NO_2 availability, and this neutral radical also diffuses through membranes, imparting relevance to the N_2O_3 chemistry of NO. Most damaging of this chemistry is the eventual deamination of primary amines through N-nitroso adducts, to the extent that the public was admonished to avoid nitrite-preserved meats, despite vegetables being a better source of nitrite. Cytosine, adenosine, and guanine DNA bases de-aminate to uracil, hypoxanthine, and xanthine, respectively, upon reacting with N_2O_3, and these point mutations (G to A translation and G to T transversions)[161] may cause cancer.[162] Enzymatic hydroxylation, e.g., cytochrome P450, oxidizes secondary nitrosamines to the geminal N-nitrosamine alcohol that heterolyzes to the carbonyl and N-hydroxy-N'-alkyldiazene fragments. Dehydration produces the alkyldiazonium salt, a powerful alkylating agent that has been observed to react indiscriminately with the gamut of available nucleophilic sites on DNA,

even phosphates.[163] Alkylation interferes with base pairing, DNA repair, and other normal enzymatic processes upon DNA, also leading to mutations and eventually cancer.[164]

Through reactive nitrogen species (RNS), excess of NO (beyond the regulatory mechanisms of the cell) can result in necrosis or apoptosis. Necrosis from ATP depletion, which blocks apoptosis, results from pathological levels of NO that eventually irreversibly repress mitochondrial respiration, induce mitochondrial permeability transition, inhibit glycolysis, and poly-ADP ribose polymerase (PARP) activation.[165] The impeded respiration provokes glutamate release; in glia neighboring neurons, the released excitatory transmitter glutamate overwhelms the sensitive neurons, resulting in their excitotoxicity.[166] Peroxynitrite was directly implicated in multiple sclerosis in provoking demyelination and damage to axons,[167] except when uric acid, an $ONOO^-$ scavenger, was administered.[168] Excessive nitrotyrosination of proteins leads to Alzheiemer's disease, provoking aggregation (by favoring β-sheet secondary structure) of fibrillar amyloid beta and paired helical filaments of tau and triosephosphate isomerase proteins, compromised glucose consumption and thus cholinergic deficiency, and tubulin-network damage.[20] Similarly, Lewy-bodies α-synuclein protein aggregates in Parkinson's disease, responsible for the death of 70% of Substantia Nigra dopaminergic neurons, contain nitrotyrosinated α-synuclein, and this nitration has been shown to induce aggregation.[169]

1.1.6 NO Detection and Measurement

Understanding the varied roles that nitric oxide plays in the plentitude of biological processes highlights the need for proper methods of detection and quantification. Ideally, these methods would measure and discriminate the subnanomolar to nanomolar concentrations of resting NO levels, up to the micromolar levels produced

by iNOS, with the measurement not altering or consuming the analyte. A sensor should also produce a signal within the lifetime of NO, or at least within the duration of the change in NO concentrations brought about by an interrogation to the system. Furthermore, a sensor with subcellular resolution would inform on NO kinetics, from its origin to its diffusion and consumption. Finally, sensors for NO's metabolites would provide a full picture of the biology of NO. To date, although many sensors and methods exist – a tribute to the importance of studying NO – none exhibit all the desired characteristics.

One way to categorize the sensor population is according to their ability to detect with subcellular resolution. Among those lacking this ability are chemiluminescent detection, NO electrodes, electroparamagnetic resonance (EPR) probes, and the Griess assay.

1.1.6.1 Griess Assay

Perhaps the most global and indirect measurement of NO is the Griess assay, which colorimetrically measures NO oxidation termini nitrite and nitrate. Oxidation of NO is one of the main sinks in NO metabolism, and the sum of nitrate and nitrite concentrations has been considered proportional to NO production, although systems that incorporate ingested nitrate and nitrite cannot claim a direct proportion. For NO-related hypoxia studies (e.g., ischemia-reperfusion and its treatment), however, nitrite quantification is highly relevant as a prominent source of NO. The Griess diazotization assay comprises reacting nitrite in acid to dehydrate nitrous acid and form nitrosonium equivalent N_2O_3 in the presence of a primary amine nucleophile, such as sulfanilimide (Scheme 1.06). The resulting primary nitrosamine tautomerizes and dehydrates to the diazonium salt, and then addition of second amine nucleophile, such as N-

naphthylethylenediamine, makes the colored diazo compound whose absorbance (with these reagents – 540 nm) linearly reflects nitrite concentration at the correct dilutions.

Scheme 1.06: Detection of NO oxidation-sink nitrite via typical Griess-assay reagents

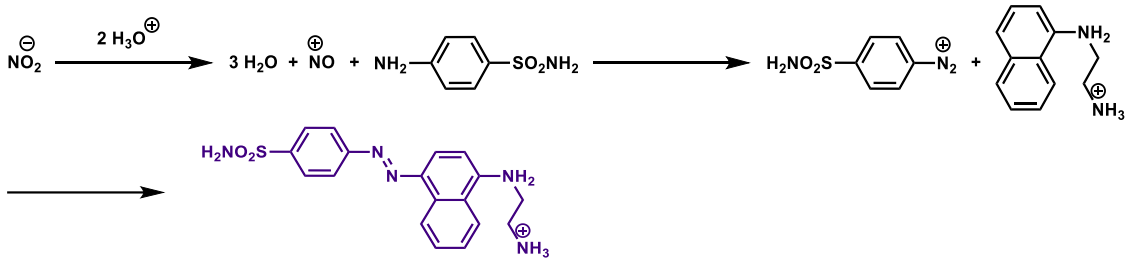

The Griess assay is normally applied to cell culture supernatants, serum, plasma, or urine. Proteins, with nucleophilic side chains, interfere with the assay and are typically filtered off. Other interferants include NADH and NADPH, anticoagulants, azide, ascorbic acid, and small molecular-weight thiols. Only nitrite, not nitrate, reacts to form the diazonium products, but application of nitrate reductase to samples efficiently reduces nitrate to nitrite, enabling independent quantification of total NO oxidation products. Typical limits of detection are 2.5 μM, unless the sample is first purified by HPLC, which resolves most interferants and concentrates the NO_x analytes to their peak elution volume, resulting in 1 nM detection limits.

1.1.6.2 Chemiluminescence

For the highly sensitive (~ 10 pM)[170] chemiluminescence technique, emitted NO gas, for example that escapes or is sparged out of a tissue sample or a cell culture, is directed by a stream of inert gas (or even air at low NO concentrations) to a vessel containing ozone. The exothermic reaction of NO with ozone produces oxygen and nitrogen dioxide (Scheme 1.07), with a portion of the population of nitrogen dioxide in an excited state. Relaxation to the ground state emits a broad spectrum of photons centered

around 1200 nm[170] with a quantum yield of 0.12 to 0.18.[171-172] The rate for this reaction is 10^7 $M^{-1}sec^{-1}$.[173] Selectivity for NO derives from its fairly unique nIR chemiluminescence. However, most commercially-available photomultiplier tubes (PMTs) that convert emitted photons to electrical signal do so poorly at wavelengths greater than 875 nm. This limitation results in loss of most of the NO signal, so the 600 – 875 nm signal is optimized by placing long-pass filters with a 600 nm cutoff to eliminate most interferences from other chemiluminescent impurities. This assay has been expanded to include detection of NO released from as low as 10 nM S-nitrosothiols by reaction with Cu (I) and cysteine, 10:1 hydroquinone/quinone in alkaline conditions (to form the semiquinone radical), or vanadium (III). Triiodide (which also displaces the more weakly-bound heme-NO) measures not only NO released from S-nitrosothiols but also from reduction of nitrite, again at 10 nM lower limit of detection (LOD).[174]

Scheme 1.07: Chemiluminescence from the reaction of nitric oxide and ozone

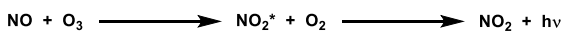

1.1.6.3 NO-selective Electrodes

NO electrodes, particularly microelectrodes, provide more localized measurements than chemiluminescence. Some microelectrodes have been constructed at 7 μm in diameter,[175] well below the average cell diameter of 20 μm, permitting single-cell measurements. Depending on the electrode material, a potential of 0.6 to 1.0 V (Ag/AgCl)[176] oxidizes NO to NO^+. Electrodes have been fabricated from platinum, carbon fiber, graphene, graphite, gold, and glassy carbon, the latter exhibiting high inertness, good conductivity, and ease of modification. The high potential required to oxidize NO also oxidizes common interferants, such as carbon dioxide, ascorbic acid, peroxynitrite, nitrite, hydrogen peroxide, hydrosulfide, dopamine, and acetaminophen.[177]

Coating the transducer surface with hydrophobic (often perfluorinated) polymer membranes; such as Nafion (also sulfonated), polystyrene, Teflon AF, chitosan or cellulose acetate; filters out charged or larger molecules. Conversely, the small, uncharged, and lipophilic NO is able to approach the junction, along with other small gases, including O_2, CO_2, and H_2S.[178] In addition to functioning as NO sieves, membranes also serve to protect the electrode from contamination by the biological medium, although proteins tend to foul hydrophobic membranes more than hydrophilic ones due to the hydrophobic effect.[179] Nafion membranes provide a compromise between NO-favored lipophilicity and water-ordering non-polar groups. Membrane thickness also enters the equation, since the longer NO takes to diffuse to the electrode, the longer the response times and lower sensitivity.[180] Further manipulations to improve selectivity and sensitivity have involved incorporating metalloporphyrins and metallophthalocyanines; gold, ferric oxide, or alumina nanoparticles; and single or multi-walled carbon nanotubes. Optimized electrodes have reached an LOD of 55 pM[181] and can linearly detect NO from 200 pM to 4 μM.[182] Typically the electrode is placed at a small distance above the cell or tissue, and carefully reproducing this distance enables comparisons between experiments.[183] Incorporating the electrodes onto the surface to which the cells adhere eliminates distance variability from improper positioning of the electrode above the cell.[184-185] Some complications derive from the high electrode potentials destabilizing the polarization of cell membranes,[186-187] from causing injury to cells or tissue and inducing NO response (the measurement itself increasing analyte levels), and from hampered function and limited reusability of electrodes after exposure to the complex biological matrix. More worrisome is the variability (up to six orders of magnitude) among electrode-based measurements in similar experiments.[188-189] One issue was determined to be the size of the electrode; those with diameters greater than 30

μm consumed the local NO in the unstirred media, thus reporting that only 50 nM NO affected vascular smooth muscle in arterioles, whereas electrodes with diameters less than 15 μm reported hundreds of nanomolar NO for the same process.[190] The authors concluded that resting NO concentrations lie in the mid 300 nM on the outer walls of arterioles.

1.1.6.4 EPR

Electron paramagnetic resonance (EPR) spectroscopy rounds out the common nitric oxide analysis techniques that cannot distinguish subcellular entities. Due to typical spatial resolution on the order of millimeters (although micron and sub-micron resolution with EPR have been reported) most imaging applies to tissues, organs, limbs, and whole animals. One of the main advantages of EPR is that it detects only paramagnetic signals, greatly simplifying complex matrices like those found in biology, due to the normally short lifetimes of radical species. Like magnetic resonance imaging (MRI) (and often overlayed with MRI spectra), the lower energy microwaves employed by EPR penetrate tissue and enable *in vivo* imaging. Analogous to nuclear magnetic resonance (NMR), the quantized electromagnetic-energy photons needed to promote an electron whose spin is aligned with an external magnetic field to a higher energy level in which the spin is aligned against the field have wavelengths in the order of millimeters, depending on the field strength. Furthermore, nuclei that also align with and against the magnetic field affect the electron's local magnetic field, leading to hyperfine splitting (e.g., doublets, triplets, multiplets). The equivalent of chemical shift in NMR, g values are dimensionless (proportionality constants relating the strength of the field to the frequency of excitation) and describe the magnetic local environment of the electron relative to a free electron, with a g value of 2.0023.[191]

The EPR spectrum for short-lived and dilute NO in biological specimens is broad and indistinct from various endogenous signals, so paramagnetic metal-NO complexes or NO-adducts that produce more defined spectra and stabilize the paramagnetic species are preferred. The less reactive and more selective NO radical does not form adducts with nitrone spin-traps, requiring the more reactive nitronyl nitroxides, such as PTIO. These and their iminonitroxide product from oxidizing NO to NO_2 both exhibit well-defined and distinct spectra. NO_2 can react with another molecule of NO to form N_2O_3, changing the stoichiometry from 1:1 PTIO to NO to 1:2 PTIO(NO_2) to NO (Scheme 1.08).[192] Superoxide,[193] ascorbate, thiols, and other reducing agents shorten the lifetime of both species by reducing them to EPR-silent diamagnetic species. Consequently, although nitronyl nitroxides have been used in imaging, they have fallen out of favor.

Scheme 1.08: Additional reactivity of ntironyl nitroxide spin trap for NO

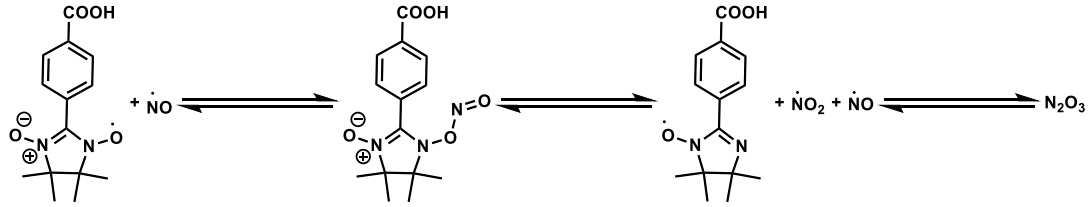

Further reaction of nitronyl nitroxide spin trap for NO to produce NO_2, whose reaction with another molecule of NO can distort probe to NO stoichiometry

Ferrous dithiocarbamates (DTCs, Scheme 1.09A) are more robust traps for NO. Their lifetime in air is on the order of a day, versus the minute lifetimes of organic spin traps.[194] The simple reaction of amine with carbon disulfide yields dithiocarbamate, accessing a wide variety of these ligands; such as N,N-diethyl-dithiocarbamate (DETC), N-methyl D-glucamine dithiocarbamate (MGD), and N(dithiocarboxyl)sarcosine (DTCS); from their respective amines (Scheme 1.09B). These dithiocarbamate traps detected NO in living mice that were exposed to LPS[195] and in mice that had experienced

septic shock,[196] as well in many other experiments.[194, 197] In rat aortas exposed to LPS, an EPR system achieved an LOD of 6 pmol for NO-Fe(DETC)$_2$, albeit at 77 Kelvin.[198]

Though widely used, Fe(DTC)$_2$ traps interfere with the production and consumption of the analyte they measure. Their dithiocarbamates' capacity as ligands has been demonstrated in DETC's reported ability to strip Cu^{2+} form superoxide dismutase (SOD), disabling the superoxide scavenger.[199] DETC and other variants inhibit NF-κB transcription factor, thereby decreasing iNOS induction and immune system NO response.[200] When added to a solution of isolated and purified nNOS, Fe(DTCS)$_2$ and Fe(MGD)$_2$ inhibited NO production with IC_{50}'s of 10 and 25 μM, respectively.[201]

Scheme 1.09: EPR imaging of NO with dithiocarbamate spin traps

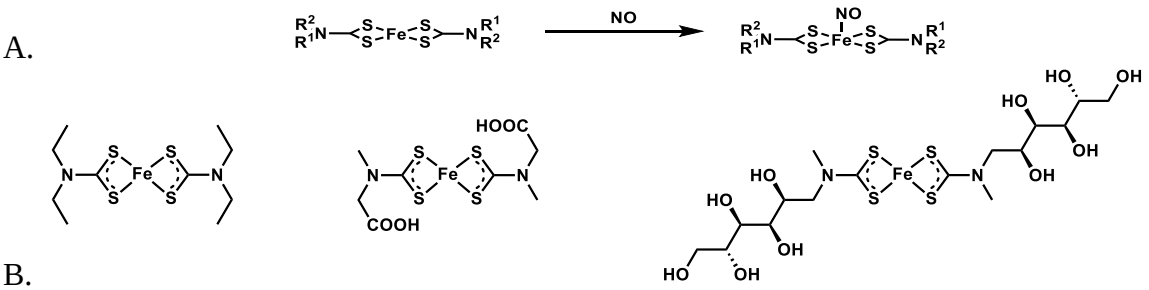

A) Complex formed between spin trap and NO B) From left to right: DETC, MGD, and DTCS spin traps.

Iron hemes also provide an EPR-visible detection of NO. Ferric oxyhemoglobin oxidizes NO to nitrate with concomitant reduction to ferrous heme, and the aquo-methemoglobin complex produces a g signal in the 6, not the more common 2, region. This complex is not stable at room temperature, so temperatures of 77 K or less are needed. Not useful therefore for live imaging, aquo-methemoglobin EPR imaging can provide NO levels in the otherwise complicated blood or plasma matrices.[202] Oxygen-free hemoglobin binds NO with high affinity, but the four hemes, two α and two β, that

comprise hemoglobin complicate the spectrum. Furthermore, the relaxed and tense states result in two different signals, deriving from the extent of interaction between the trans histidine and Fe in the nitrosyl α-hemes. Using other techniques, basal levels of heme-NO have been estimated at 20 nM,[203] well below the ~ 200 nM LOD in EPR.[192]

1.1.6.5 Fluorescence

Fluorescence, renowned for its subnanometer spatial and submillisecond temporal resolution,[204] enables subcellular imaging of NO activity over time. The process of fluorescence starts with the absorbance of a photon of light by a molecule (fluorophore), which excites an electron from its ground-state orbital residency to its corresponding excited-state orbital (for longer-wavelength fluorophores, these are π to π* and n to π* transitions) of the same spin state (e.g., singlet or triplet), on a time scale of 10^{-15} s. The quantized energy difference between these orbitals corresponds to the product of Planck's constant and the frequency of the absorbed photon; often, the photon energy is specified by the wavelength of light ($\lambda = c / \nu$). As stated in the Frank-Condon principle, significant nuclear motion is not possible within ~10^{-15} s, and so the efficiency of absorbance of a photon of certain energy depends directly upon the extent of population density overlap (similar molecular geometries) between the ground state and the excited state that corresponds to that wavelength of excitation. Quantum mechanical interpretation of the Franck-Condon principle states that the probability of absorbing a photon depends on the square of the integral overlap for the vibrational-level wavefunctions populated by the electron transitioning from the ground to the excited electronic state. For fluorophores with distinctively different geometries in the excited state versus the ground state, photon absorbance is limited to the high vibrational energy levels in the excited state that overlap in geometry with the ground state, whereas for

fluorophores with highly similar ground/excited state geometries, photon absorbance may occur from any of the vibrational energy levels in the ground state to all the vibrational energy levels in the excited state. The molar absorptivity coefficient (ε), a wavelength and solvent-dependent constant, empirically relates the amount (or efficiency) of photons absorbed to the concentration of the chromophore, according to Beer's law.

A molecule contains a myriad of vibrational levels, according to the number of bonds and to the degrees of vibrational freedom in its bonds. These vibrational levels multiply when the molecule is dissolved, due to stabilizing interactions with the solvent. Although quantized, these numerous levels may overlap in energy, and non-radiative relaxation occurs if overlap exists. There is usually sufficient overlap in vibrational levels among excited states, and Kasha's rule describes the propensity for molecules to first relax vibrationally (due to the relative speed of relaxation: 10^{-14} to 10^{-11} s) from higher-energy excited states to the lowest-energy excited state of conserved spin before another relaxation process can become a factor. Flexible molecules (acyclic alkanes) contain a continuum of vibrational levels, to the extent that complete relaxation after excitation may occur via vibrational relaxation. Rigid and constrained molecules lack this continuum, and so vibrational relaxation is limited to the lowest-energy excited state.

At this time, the excited electron may emit (fluoresce, 10^{-9} to 10^{-7} s) a photon of light of frequency corresponding to the energy gap as it relaxes back to an accessible vibrational level in the ground state. Particularly in solution, a plethora of these levels exist due to vibrational interactions with the solvent, and the population of emission energies therefore resemble a Gaussian peak. Due to vibrational relaxation of the excited electron to the vibrational ground state of the excited electronic state (Kasha's rule), the distribution of photons emitted are of equal or lower energy than those absorbed at temperatures when the Boltzmann distribution of electrons occupy the lower levels of the

ground electronic state. This lower energy results in a Stokes shift – the difference between the excitation and emission peak maxima – that imparts notable sensitivity to fluorescence, as the shorter-wavelength excitation light can be filtered out from the longer-wavelength signal, thereby eliminating most background signal.

If other relaxation pathways (vibrational, rotational, collisional, energy transfer) compete with fluorescence relaxation, the quantum yield of fluorescence – in a population of molecules, the ratio of photons emitted due to fluorescence versus total photons absorbed – decreases from 1. The brightness of a fluorophore is typically defined as the product of the extinction coefficient (how much light a molecule absorbs) and the quantum yield (how much of that light is emitted). Both variables are temperature and solvent, even microenvironment (i.e., cytosol, cell membrane, protein), dependent.

Both fluorescent proteins (FPs)[205-209] and organic fluorescent probes[210-214] have provided valuable information to the field of NO detection. While the fluorophore itself can be the binding or reacting moiety, typically a chelating or reactive moiety is connected to perturb the fluorophore's fluorescence. Photoinduced electron transfer (PET),[215-218] internal charge transfer (ICT),[204, 212, 219] heavy-atom quenching, and FRET[219-221] are among favored means of modulating fluorescence.

PET quenching of fluorescence occurs under two scenarios. In one scenario, an occupied ground-state orbital exists at higher energy than the fluorophore's ground-state orbital (HOMO, or S_0) from which an electron is excited. Non-bonding lone-pairs typically reside in these higher-energy orbitals. Excitation of an electron from S_0 leaves a vacancy in that orbital, and an electron of like spin from the higher-energy ground-state orbital occupies that vacancy. Consequently, the excited electron can no longer radiatively relax to its now fully occupied S_0, and fluorescence is quenched (Figure

1.02A). If the quenching ground-state orbital's energy is lowered below the fluorophore's S_0 by partaking in a covalent, coordinative, or ionic bond (protonation or chelation), its electrons cannot transfer to a higher-energy S_0, eliminating PET-quenching, and the excited electron can radiatively relax to its partially filled ground state orbital (Figure 1.02 B).

Figure 1.02: Donor PET-quenching of fluorescence

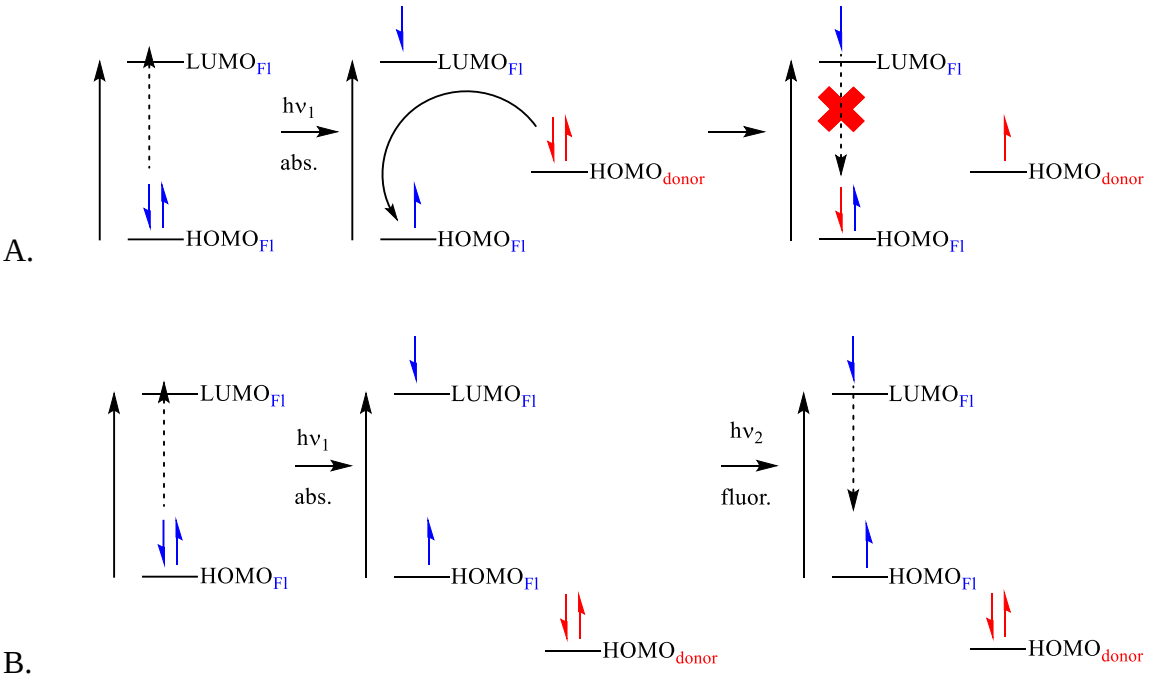

HOMO/LUMO$_{Fl}$ are the fluorophore's molecular orbitals.

In the second scenario, an orbital not involved in fluorescence has an accessible lower-energy lowest unoccupied molecular orbital (LUMO, or S_1) than the fluorophore's LUMO. After the fluorophore's electron is excited, it can relax to occupy the lower-energy LUMO whose S_0 is fully filled, once again impeding radiative relaxation (Figure 1.03A). If the accessible LUMO orbital is higher in energy than the fluorophore's LUMO, no transfer occurs, and fluorescence proceeds accordingly (Figure 1.03B) In

either scenario, electron transfer is believed to occur through hopping, tunneling, or superexchange between the relevant molecular orbitals.[222]

Figure 1.03: Acceptor PET-quenching of fluorescence

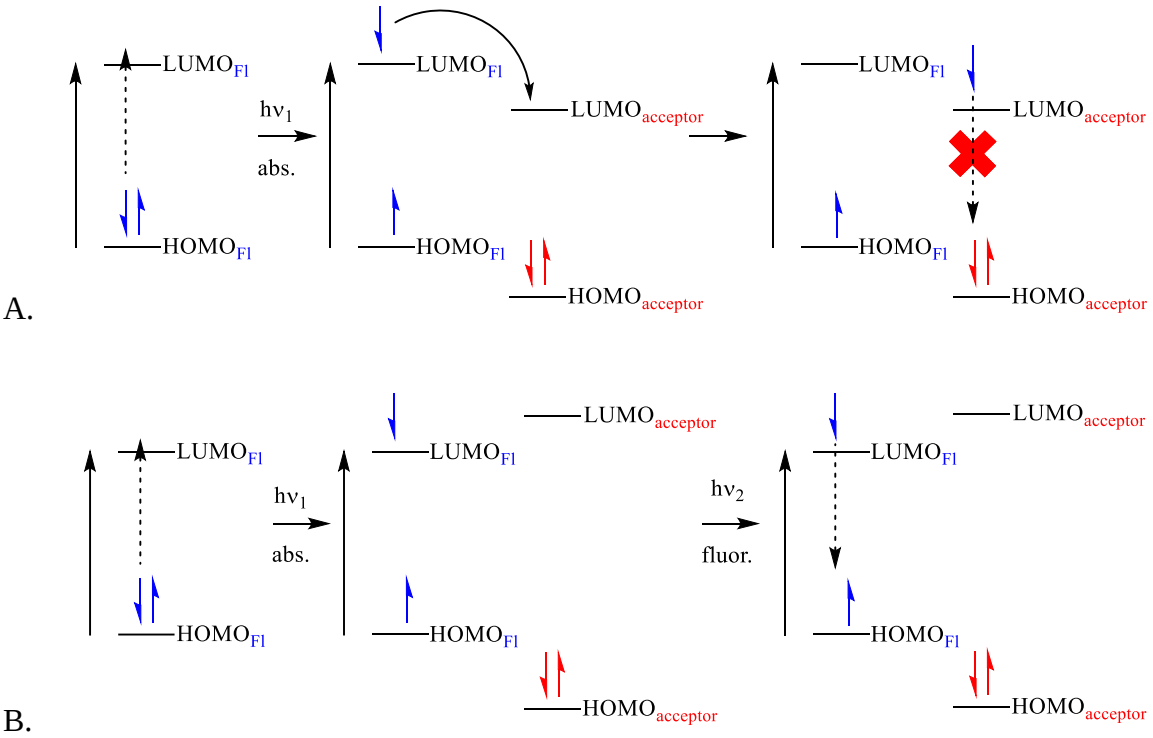

HOMO/LUMO$_{Fl}$ are the fluorophore's molecular orbitals.

1.1.6.5.1 Fluorescent Proteins

The Nobel prize in 2008 to Shinomura, Chalfie, and Tsien recognized the importance of adapting and improving upon proteins that fluoresce in nature to study protein localization, movement, and processes in cells and organisms. Employing this technology, the location of a genetically-expressed eNOS fused to green fluorescent protein (GFP) was monitored in response to various stimuli known to provoke changes in NO levels / NOS activity.[223-224] Moving from NOS localization to NO concentration measurements, the geNOps sensors were assembled by incorporating a bacterial (to avoid participation in eukaryotic signaling processes), non-heme Fe(II) binding domain for NO

that is fused near the fluorescing moiety of a green, cyan, yellow, or orange-fluorescing protein; and NO-binding quenches fluorescence.[225] This binding is reversible, with return of fluorescence upon dissociation of NO. In one study, NO production was correlated to Ca^{2+} levels by co-imaging either green or orange geNOps with Fura-2 calcium ion indicator.[226] The geNOps pKa's range from 4.8 to 6.6; apart from the orange geNOps, their fluorescence intensity changes by at most 3-4% per 0.1 pH unit.[225]

A second approach to direct NO measurement involves metallothioneins (MTs). These proteins abound in cysteines that bind zinc and copper metal ions, and interaction with NO results in release of the metal ions and a change in structure. Often, a significant change in structure points to Förster Resonance Energy Transfer (FRET) based imaging. When two different fluorophores A and B have complete overlap in the emission spectrum of A with the excitation spectrum of B and their dipoles are aligned well within the Förster radius (the distance between dipoles at which FRET efficiency is 50%), the excitation of A solely provokes emission of B. The amount of emission of A versus emission of B therefore measures the extent of spectral overlap, dipole alignment, and Förster proximity. To detect NO binding to MTs, FRET pairs Cyan FP (CFP) and Yellow FP (YFP) were fused to the C and N termini of human type IIa MT. Exposure to NO leads to a decrease in FRET efficiency; the greater the concentration of NO, the higher emission from CFP and lower from YFP, resulting in a ratiometric response to NO.[227] The maximum possible response, deriving from application of 1 mM NO, was ~40% decrease, and application of calcium ionophore 4-Br A23187 caused a ~ 20% decrease. Whether perturbation by NO is reversible is not known,[228] but the sensor did show in sheep pulmonary artery endothelial cells that metallothioneins mediate Zn^{2+} release in response to NO.[229]

A third construct responds to cGMP produced by sGC when the latter is activated by NO. The FRET protein CGY[230] fuses CFP and YFP to opposite termini of a truncated yet still active protein kinase G that has two binding sites for cGMP. This FRET protein is then fused separately to each of the α and heme-containing β monomers of the sGC heterodimer. The CGY fusion does not prevent formation of the α,β heterodimer (the active form of sGC), and the NO-bound, CGY-fused sGC heterodimer maintains its activity of catalyzing cyclization of GTP to cGMP at 3000 - 6000 molecules/minute. This cGMP can bind at the CGY domains flanking the same NO-bound sGC heterodimer; flanking another sGC heterodimer, whether NO-bound or not; or fused to non-associated α or β monomers. No matter the target, this binding triggers an increase in FRET efficiency (increased yellow emission, decreased cyan emission). Since binding of NO induces hefty cGMP output that can increase FRET efficiency in various CGY-containing constructs, this approach amplifies the signal produced by NO-binding, engendering the name NOA (NO Amplified). Such amplification of signal results in a detection limit of 100 pM for NO. This sensor determined the resting levels of NO in endothelial cells in serum-supplemented media to be 1 nM, as opposed to non-detectable levels in eNOS-lacking CHO cells.[231] One drawback to this indirect sensing of NO through cGMP is that mechanisms other than NO binding to sGC exist to modulate cGMP levels, such as cGMP synthesis by natriuretic peptides and cGMP degradation by phosphodiesterases.[232-233]

Similar FRET approaches have produced fluorescent proteins for both nitrate and nitrite. Fusion of bacterial proteins NasT and NasS with CFP and YFP, respectively, led to the FRET pair as the heterodimer sNOOOpy (sensor for NO_3^-/NO_2^- in physiology, yellow fluorescence dominant due to FRET).[234] Only NasS-YFP binds either NO_2^- or NO_3^-, and this binding elicits dimer dissociation, with loss of FRET, and CFP-NasT's

blue fluorescence dominates. The acellular buffer dissociation constants of NasS-YFP for NO_3^- and NO_2^- are 39.5 and 256 μM, respectively, and changes in NO_3^- levels between 1 μM and 1 mM could be detected in seconds. Since tissue, blood, and plasma nitrate levels range from 3 to 50 μM, the sensor properties seemed promising. In HeLa cells, however, sNOOOPy's sensitivity and responsivity were attenuated, even though cells were programmed to synthesize both monomers at equal rates.

In summary, fluorescent proteins provide direct and indirect measurement of NO. With their low LODs, they have helped establish basal levels of NO in various cell types. Most reporting occurs via FRET imaging, giving a conformationally-based ratiometric response to changes in analyte levels. These responses typically increase or decrease by 2 to 3-fold, according to the extent of change in analyte concentration provoked by the applied stimulus. To a certain degree (at most 20% of the signal), some FPs are pH sensitive. For FPs that detect NO indirectly, non-NO-dependent processes that produce, conserve, or consume the analyte factor in the reporting by the sensor. Not membrane permeable, these proteins require transfection or transduction into cells, and the relative rates of production of different monomers that form heterodimers may require programming to have similar output. With the appropriate gene encoding, fluorescent protein synthesis and translocation may be directed to subcellular locations. Along with analyte levels, FPs can report protein movement within the cell in response to stimuli.

1.1.6.5.2 Fluorescent synthetic small molecules

Non-protein, synthetic small-molecule fluorescent probes tend to be brighter and have greater sensitivity and dynamic range than fluorescent proteins, along with greater photostability. Fluorescein, rhodamine, cyanine, bodipy, naphthalimide, and coumarin derivatives are frequently chosen as fluorophores. Unfortunately, no biologically-useful reversible synthetic probes exist; instead, synthetic probes act as dosimeters for NO – the

measurement consumes the NO being measured. Ideally, interaction with NO would be reversible, so that the measurement would minimally interfere with cellular processes. Depending on the brightness of a fluorophore, 0.5 to 50 μM amounts are normally loaded into cells, and intracellular concentrations may reach much higher levels if the probes are sequestered in the cytosol, subcellular compartments, and/or hydrophobic regions. At typical low NO outputs by nNOS and eNOS, sufficiently large concentrations of a dosimeter could scavenge NO and quench the NO-dependent, downstream physiological processes.

Whereas fluorescent proteins require transfection or transduction to appear in cells, synthetic fluorophores or fluorophore precursors cannot be genetically encoded into production by cells. Non-charged fluorophores passively permeate cell membranes to distribute into the more hydrophobic compartments of cells. Ionically charged fluorophores may be masked, commonly by acetates or acetoxymethyl esters (similarly to pro-drugs), so that they too passively permeate membranes, and intracellular non-specific esterases then hydrolyze the masking groups (with acetate or acetate / formaldehyde by-products) to reproduce the charged fluorophores that tend to locate in the cytosol. For non-masked loading of charged fluorophores, techniques include electroporation, ATP-induced permeabilization, cell-penetrating peptides, liposomes, hypoosmotic shock, and single-cell microinjection or patch-clamping.[235]

Synthetic fluorescent probes can also be directed to subcellular compartments.[236] Molecules with an overall delocalized positive charge tend to aggregate in mitochondria, attracted by the negative membrane potential (~ -180 mV)[237]; often triphenylphosphonium, pyridinium, or quinolinium moieties appended to neutral molecules engender mitochondrial sequestration. Lipophilic amine (e.g., morpholine, N,N-dimethylethylenediamine) appendages are protonated (and therefore entrapped) in

lysosomes (~ pH 5). *p*-Toluene sulfonamide moieties direct sensors into the ER, and affixing L-cysteine, linked through the N or C terminus, imparts specificity to the Golgi apparatus. Finally, due to the typically higher brightness of synthetic fluorophores versus fluorescent proteins, SNAP Tag[238] and HALO Tag[239] technologies have been developed. Cells are transduced to synthesize the protein of interest with a fused peptide that recognizes and covalently bonds to a specific tag – O^6-benzylguanine for SNAP and chlorohexyl/aminoethyl glycol ether for HALO – attached to the fluorescent probe. The probe can thus be directed to the subcellular compartment in which that protein resides.

Perhaps the greatest testimonial to the favoring of fluorescent NO-imaging is the gamut of non-protein, synthetic fluorescent probes that have been published over the years. The majority of these probes indirectly measure NO by reaction with nitrosonium equivalent N_2O_3, the product of NO autoxidation via the combination of NO_2 and NO. Those that react directly with NO do so mainly through paramagnetic transition metals, often incorporating the reduction of high-valency metals by NO that also produces a nitrosonium equivalent.

1.1.6.5.2.1 Small-Molecule Synthetic Probes that React Directly with NO

1.1.6.5.2.1.1 Fluorescent Chelotropic Traps

Certainly, to minimize experimental variables, the probe should react directly and selectively with NO. The inertness of NO towards diamagnetic reagents points to paramagnetic probes containing either transition metals or organic spin traps. Most radical spin traps fail the selectivity requirement, as they react readily with OH, NO_2, O_2^-, and other biologically relevant radicals. However, *o*-quinodimethanes do react selectively with NO to form the corresponding nitroxides. Although the nitroxides fail to sufficiently extend the radical lifetime or fluoresce significantly due to paramagnetic quenching, their hydroxylamine reduced product fluoresces well and with a distinct

spectrum from the quinodimethane.[240] Indeed, when the weakly fluorescent N,N-dimethyl-2-aminophenanthrene variant of a fluorescent nitric oxide chelotropic trap (FNOTC) reacts with two equivalents NO in the presence of two equivalents ascorbic acid, the reaction is complete within a few seconds (Scheme 1.10). Cellular concentrations of ascorbic acid and glutathione reducing agents are several orders of magnitude more concentrated than the micromolar concentrations used for fluorescence, so the reduction in cells occurs quickly and without significantly affecting reducing levels.

The probe is inert to superoxide, hydrogen peroxide, and hydroxide radicals. It does react with peroxynitrite, first to a fluorescent product, but further reaction with excess peroxynitrite turns it non-fluorescent. Another shortcoming is its UV excitation of 380 nm that causes significant cellular autofluorescence that can overlap with its emission in the blue (460 - 490 nm). Nonetheless, an AM-loadable version of FNOTC applied to alveolar macrophages produced fluorescence nearly twice as bright in cells stimulated to iNOS high-NO production with LPS versus non-stimulated cells.[241]

Scheme 1.10: FNOCT cheletropic spin trap for NO

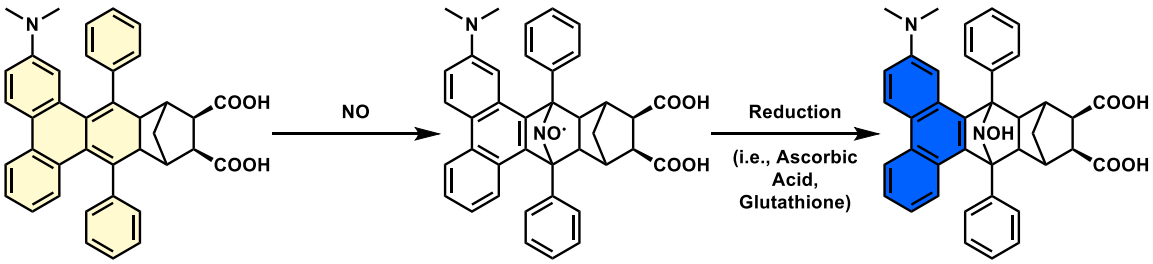

Reaction with NO quenches the initial fluorescence of the extended conjugation system. Conversion to the hydroxylamine by abundant cellular reductants returns fluorescence to a less conjugated system. Note: Fluorophore colors in the structures were assigned according to a website that converts wavelength (in this case, emission wavelength) to RGB values: https://academo.org/demos/wavelength-to-colour-relationship/ For PET-quenched fluorophores, the RGB values were adjusted to lighten the intensity of the color.

1.1.6.5.2.1.2 Transition metal-based probes

Some transition metals afford greater selectivity, mostly due to NO's ability to π backbond with low-valence metals, for example, NO's biological target – the ferrous heme in sGC. In fact, the very displacement of histidine by NO when binding to sGC served as a model for some probes, in which NO displaces an anthracene-TEMPO radical that is fluorescent when bound to a sarcosinedithiocarbamate complex of Fe(II).[242] Increasing levels of NO quench fluorescence, however, a sensing tactic that counteracts the sensitivity of fluorescence stemming from a signal with little background. The same sGC/histidine model was applied to a ferrous cyclam (to loosely mimic heme) with a pendant quinoline as the histidine mimic.[243] The Lewis acid character of Fe(II) greatly enhanced and red-shifted the fluorescence of the quinoline, but binding of NO displaced the quinoline ligand and disrupted the fluorescence enhancement. Although elegant, this probe achieved a LOD of only 1 μM, due in part to the quenching of fluorescence to measure NO.

Some high-valence metals, such as Fe(III), Co(II), and Cu(II), are reduced by the oxidation of NO to nitrosonium, with concomitant nitrosation of a nucleophile, at times, in absence of a better one, the solvent. This process has been adapted to amine-based ligands attached to fluorophores. The paragmagnetic metal quenches the fluorescence of the fluorophore ligand when bound in proximity. NO binding results in the metal oxidizing it to nitrosonium, which nitrosates the ligand amine. Reduction of the metal along with N-nitrosation of the ligand reduces the affinity of the ligand for the metal. Furthermore, in the case of copper, Cu(I) is diamagnetic and non-quenching. Any PET-quenching by the amine on the ligand also terminates with N-nitrosation. With the many quenching pathways eliminated, this type of probe exhibits fluorescence enhancement in an NO-dependent manner. Two CuFL family provides two examples.

CuFL1 (Scheme 1.11A) incorporates an 8-aminomethylquinaldine ligating moiety at the 4´-position of 7´-chlorofluorescein that, together with the 3´-phenolate binds Cu(II) with a dissociation constant (K_d) of 1.5 μM.[244] The aniline alone, without Cu(II) present, PET-quenches fluorescence to a quantum yield of 7.7%. Cu(II) complexation drops the fluorescence by 18%. N-nitrosation of the aniline as NO reduces Cu(II) to Cu(I) brings the quantum yield to 58%, with a ~16-fold increase in fluorescence, establishing an LOD of 5 nM. Of the typical competing analytes in cells (ClO^-, O_2^-, H_2O_2, HNO, NO_2^-, NO_3^-, $ONOO^-$), only ClO^-, O_2^-, and $ONOO^-$ provoked responsed of 3-fold, 2-fold, and 2-fold, respectively.[245] In fact, autoxidation of NO failed to compete with CuFL1's scavenging prowess, as an aerobic titration with NO showed no difference from an anaerobic one. Furthermore, CuFL1 could detect cNOS production of NO in neuroblastoma cells stimulated by Ca^{2+} influx due to estrogen application, lighting up the neuroblastoma with greater contrast over non-stimulated cells than a popular alternative probe (to be discussed below) DAF-2 DA. CuFL1 also detected the higher NO levels brought about by LPS/interferon-γ stimulation of iNOS in RAW 264.7 cells. Moreover, 80% of neuroblasts and 90% of macrophages survived five-day incubation with CuFL1, proving the probe slightly toxic to cells, and not within typical experiment time frames of less than 24 hours. However, a relatively small dianion, the product of CuFL1 reaction with NO, FL-NO is rapidly extruded from cells by organic anion transport enzymes, causing a time-dependent decrease in fluorescence.

In response to this "leakage" issue, Cu_2FL2A (Scheme 1.11B) was developed, with two 8-aminomethyl-6-carboxymethylether-quinaldine ligands at the 4´ and 5´ positions.[246] The tetranion is less susceptible to transport outside the cell. Doubling the PET quenching ligands drops FL2A's quantum yield lower than FL1 to 1.8%. After complexation of two Cu(II) ions and exposure to NO, fluorescence enhances 27-fold.

This larger enhancement compared to CuFL1 does not translate to lower LOD, established as 35 nM for Cu_2FL2A. Cu_2FL2A maintained the selectivity for NO over competing analytes, except that it became a little more sensitive to peroxynitrite and hydrogen peroxide, and it binds NO_2. The carboxylates require masking esters, in Cu_2FL2E's case – ethyl esters, to passively permeate the cell membrane, and this version has enabled various studies monitoring NO in cells. 86% of neuroblasts were viable after three days incubation with 5 μM Cu_2FL2E.[247]

Scheme 1.11: CuFL probes for NO

A.

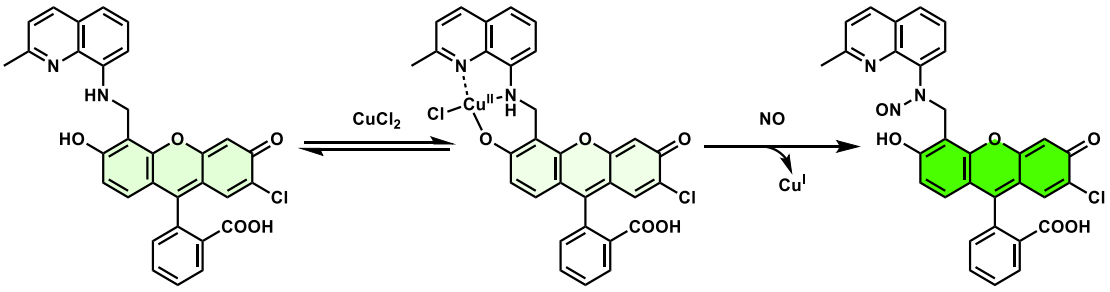

B.

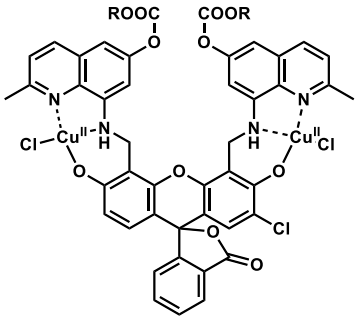

A) Reductive nitrosylation of the copper (II) complex CuFL1 eliminates both paramagnetic metal quenching and aminoquinoline PET quenching of the fluorescein moiety. B) CuFL2A, R = H and CuFL2E, R = Et

An interesting variant of the CuFL approach was designed in CuRBT: Rhodamine B for which the lactonizable *o*-carboxylic acid is amidated with tris(2-aminoethyl)amine.[248] The equilibrium between fluorescent amide and non-fluorescent lactam forms predominantly favors the lactam at pH 7.2. Acidification opens the lactam to the fluorescent rhodamine amide, but so does the incipient nitrosonium when NO binds

to the bis(2-aminoethyl)amine-Cu(II) complex. Opening the lactam to the N-nitroso amide (Scheme 1.12) results in an impressive 700-fold fluorescence increase of fluorescence, although with a quantum yield of only 0.13. The absorptivity coefficient also suffers at 1445 $M^{-1}cm^{-1}$, but the LOD was a respectable 1 nM. CuRBT selects NO over the standard competing analytes, almost to perfection, and fluorescence fluctuated by less than 10% over the pH range 6.5 to 9. Also, its 580 nm emission peak has less cellular autofluorescence as background.

Scheme 1.12: CuRBT lactam opening by NO

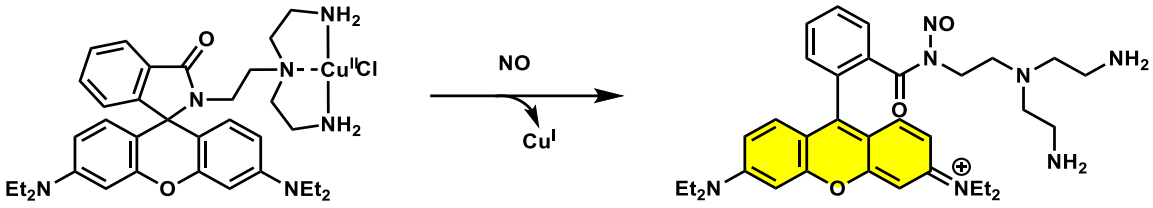

Reductive nitrosylation opens the non-fluorescent lactam form of CuRBT to the fluorescent N-nitroso amide form.

The lactam-opening approach contributed to the design of RPD, a FRET, Cu(II)-based probe.[249] N-(2-aminoethyl)piperazine connects Rhodamine B to Dansyl, with the piperazine connecting to Dansyl and the primary amine terminus to Rhodamine B (Scheme 1.13). The piperazine and sulfonamide groups chelate Cu(II), resulting in a drop of Dansyl fluorescence, with almost no fluorescence from the predominant lactam form of Rhodamine B. Reductive nitrosation with NO opens the lactam to the fluorescent Rhodamine B amide, presumably by nitrosating the amide. Lactam-opening activates FRET from Dansyl to Rhodamine B with 88% efficiency and an absorptivity of 29,000 $M^{-1}cm^{-1}$ and quantum yield of 45%. Competitive binding experiments for Cu(II) versus a series of biologically-relevant metal cations showed explicit preference for Cu(II) over all the metals, and the FRET turn-on mechanism showed similar selectivity to

the CuFL series for NO over other analytes. Cu-RPD loaded into cells and proved more toxic than CuFL, with nearly 80% viability at concentrations of 10 μM. Due to Cu(II)'s quenching Dansyl fluorescence in Cu-RPD, the probe is not ratiometric, as diamagnetic Cu(I) does not quench as effectively or simple leaves the complex. NO therefore produces an emission increase in both yellow and green channels.

Scheme 1.13: Cu-RPD FRET probe for NO

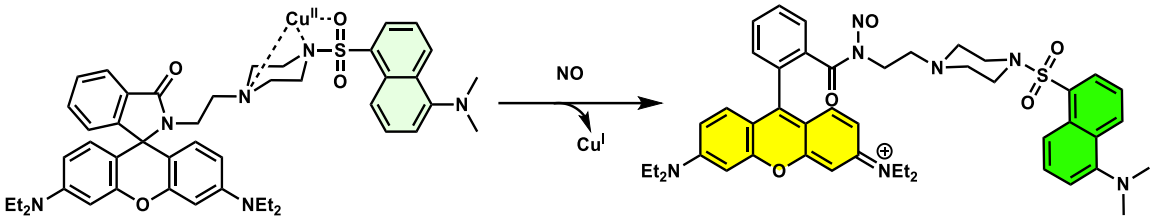

Reductive nitrosation of the lactam of rhodamine 6G and dissociation of diamagnetic Cu(I) enables FRET from Danysl to the open form of Rhodamine 6G

The Cu(II) reductive nitrosation probes react directly with NO and can detect low nanomolar to micromolar NO levels. They show some toxicity to cells over time, probably from the increased levels of Cu(II) imported to the cells and deposited as Cu(I). They also react with NO_2, although authors have not been forthcoming on the effects of such reaction. Cu(II) mediates oxidation of thiols to disulfides; thiol and HNO are competing analytes that reduce Cu(II) that seldom appear in analyte selectivity experiments. However, as nitrosation is necessary to disable PET quenching or to open lactams, Cu(II) reduction by other analytes does not produce fluorescence enhancement. It does incapacitate the sensor, removing its quantification ability, although a ratiometric response would correct for such incapacitation. Despite several attempts, no ratiometric Cu(II) reductive nitrosation probe has been developed that can function in cells and detect low nanomolar to low micromolar NO concentrations.

1.1.6.5.2.1.3 Hantschz ester-based probes

In order to avoid mildly toxic and thiol non-selective copper-based probes but still sense NO directly, probes based on Hantschz ester aromatization by NO were developed (Scheme 1.14). The mechanism has been counterintuitively described as hydrogen abstraction by NO to produce HNO and the aminyl radical, based on the deuterium kinetic isotope effect of 3 for N-H vs N-D when reacted in MeCN and under argon.[250] Another NO radical produces the N-nitrosamine, and disproportionation at the 4-position yields the pyridine. When a radical stabilizing group, such as benzyl, allyl, or isopropyl, occupies the 4-position, it disproportionates rather than the hydrogen. The selectivity of NO and not another radical species to aromatize the dihydropyridines complicates the proposed mechanism, as conceivably peroxy or hydroxy radicals could accomplish the same. To muddy the waters further, in dichloroethane this reaction proceeded at faster rates with oxygen present and even made pyridine in 98% yield with only 0.2 equivalents of NO,[251] while the proposed mechanism requires two equivalents NO and does not incorporate oxygen. As discussed, NO reacts with half-equivalent of oxygen to make NO_2, which has a larger reduction potential than NO.

One sensing approach for Hantschz-derived probes is based on the elimination of PET quenching of a fluorophore upon aromatization with NO. Two coumarin variants, one connected through an ethyl linkage (DHP-1, Scheme 1.14A)[252], and another directly connected (DHP-4, Scheme 1.14B)[252], to the Hantschz ester produced LODs of 17 and 74 nM . Aromatization increased the quantum yield from 1 to 91% for DHP-1 and from 6 to 63% for DHP-4. Both proved selective for NO over competing analytes, even hydrogen peroxide and superoxide. 50 μM solutions of DHP applied to RAW 264.7 cells maintained >80% viability, and both probes responded to LPS stimulation of iNOS in

these cells. Unfortunately, they also required cytotoxic and autofluorescence-enhancing UV excitation, and the better performer DHP-1 even emitted UV light.

The same group therefore looked to the visible-wavelength BODIPY fluorophore, and attached the Hantsczh ester at the 2 position, with a triphenylphosphonium targeting group linked through the 8 position to give MITO-DHP (Scheme 1.14c).[253] The NO-activated pyridine quantum yield of 7.5% came short of the coumarin enhancements, and activation took more than ten minutes.

Scheme 1.14: Hantsczh ester-based NO probes

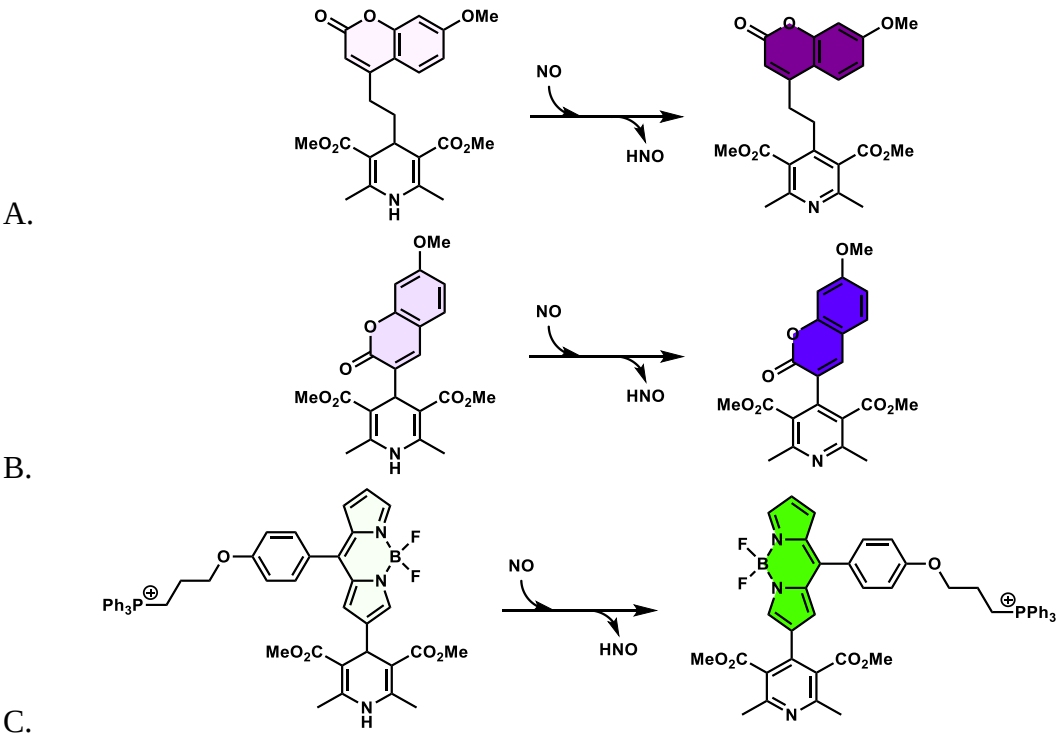

Elimination of PET quenching by dihydropyridine after reaction with NO to form pyridine. A) DHP-1, B) DHP-4, and C) MITO-DHP.

Another sensing approach with Hantzsch esters exploits NO's cleavage of radical-stabilizing moieties at the 4-position in the pyridine-forming disproportionation step. A very intricate design (Scheme 1.15) paired fluorescein with fluorescence-quenching

DABCYL.[254] The pair are sufficiently proximal for FRET to occur, with ~20% of fluorescence quenched. NO oxidation of dihydropyridine proceeds with the cleavage of the benzylic group, rather than the hydrogen, at the 4-position. As the FRET pairs are no longer ligated to each other, DABCYL no longer quenches fluorescein, resulting in strong 525 nm fluorescence when exciting at 490 nm two minutes after NO addition. This probe is selective for NO over the competing analytes tested, including hydrogen peroxide. At 50 μM loading concentrations, it detected 2 mM sodium-nitroprusside exogenously applied NO in HeLa cells and RAW 264.7 cell production of NO with LPS stimulation. Its intracellular fluorescence colocalized with LyTracker Red, suggesting lysosome compartmentalization. When applied *in vivo* to an inflamed mouse paw, the 600 nm fluorescence (470 nm excitation) was eight times higher than that for a normal paw. The authors did not address the possible competing mechanism of hydrolysis of the ester linking DABCYL to the Hantzsch ester, which would also break the linkage between the FRET pair.

Scheme 1.15: Cleavage of FRET pairs from Hantzsch ester reaction with NO

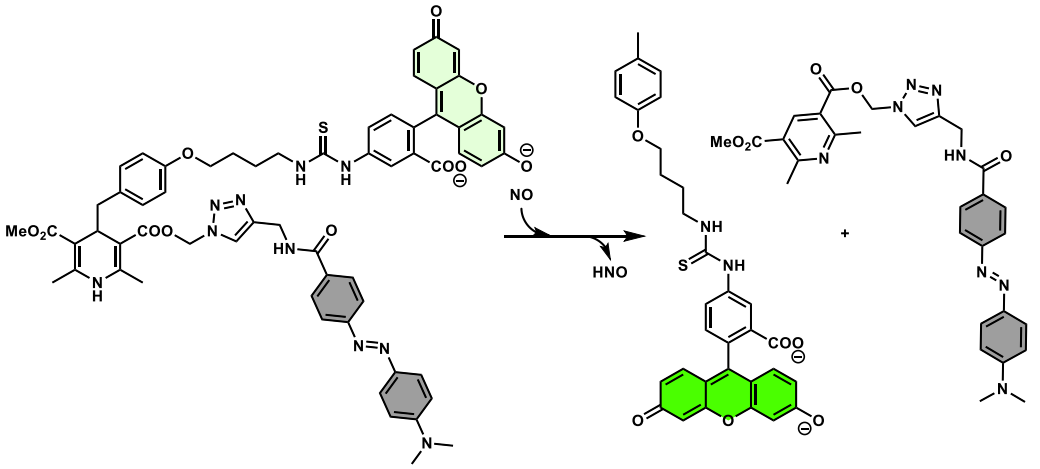

Elimination of FRET quenching between fluorescein (green) and fluorescence quencher DABCYL (gray) after exposure to NO, which promotes cleavage of the benzylic bond, freeing the FTER pairs to separate by diffusion.

1.1.6.5.2.2 Small-Molecule Fluorescent Probes that React with NO/O_2

Three categories of probes respond to the NO metabolite N_2O_3: *o*-diaminophenyl to benzotriazole probes, secondary aniline nitrosation probes, and 2-aminobiphenyl to cinnoline probes. The three categories rely on elimination of PET quenching, and the first has produced the most reported probes for NO. In cells or *in vivo*, other nucleophiles, in particular biological thiols and amines, compete with the probes for N_2O_3, leading to very different results from those in abiotic buffers.

1.1.6.5.2.4 o-*Diaminophenyl-based probes*

N_2O_3 can be considered a nitrosonium (dielectrophile) donor that releases nitrite. *o*-Diaminophenyl (ODP) moieities are electron rich, with high-energy non-bonding lone pair orbitals that can efficiently PET quench fluorescence. They also react readily with N_2O_3 to produce an N-nitroso adduct that is attacked by the remaining vicinal aniline. Elimination of water yields the benzotriazole, whose lower-energy lone-pair orbitals cannot participate in PET quenching. Using anilines, rather than their higher pK_a counterparts aliphatic amines, ensures that PET quenching is not impeded by protonation at physiological pH. The ODP sensing moiety has been applied to naphthalenes (LOD 10-30 nM),[255] coumarins (LOD 24 nM),[256] napthalimides (LOD 5 nM),[257-258] bodipies (LOD 0.83 nM), [259-261] [260-262] [259-261] [260-262] [260-262] [259-261] fluoresceins (LOD 3 nM),[262-263] calceins,[264] rhodamines (LOD 7 nM),[265] cyanines,[266] Nile Red (LOD 9 nM),[267-268] and more, at times with subcellular directing-group appendages.

Probably the most popular of all NO probes is DAF-FM (diaminofluorescein - fluoro, methyl). This ODP's quantum yield of 0.05% increases to 81%, upon forming the benzotriazole (Scheme 1.16), with an LOD of 3 nM. The 2,7-difluoro substitution drops the fluorophore pK_a to 4.38, well below physiological pH. The methyl group on the amine conjugated to the fluorophore replaces a proton that is susceptible to deprotonation

after formation of the triazole at pH higher than 7. This deprotonation in the non-methyl triazole derivative resulted in a high-energy lone-pair orbital that could PET quench, albeit inefficiently, fluorescence and counteract nitrosonium signaling. The authors do not mention the pK_a of the probe itself; protonation of one of the vicinal diamines would decrease the extent of PET quenching. (Fluorescence enhancement occurred for a cyanine congener as pH dropped below 6, reaching triazole intensities at pH ~3.7.)[266]

DAF-FM is passively loaded across cell membranes as the lactone diacetate (DAF-FM DA), whereupon non-specific cellular esterases hydrolyze the acetates to produce the membrane-impermeable dianionic fluorescent sensing form. Intracellular concentrations of DAF-FM loaded this way may approach 750 µM,[269] as influx continues while DAF-FM DA is available, but efflux stops with hydrolysis of acetates (not considering "leakage", discussed below). The slow reactivity of DAF-FM with NO prevents it from wholly buffering NO and its cell-signaling processes that approach diffusion-controlled reaction rates. In cell types with active organic anion transporters (CHO cells), DAF-FM is actively extruded (termed "leakage") from cells. It has detected the range of NO levels from cNOS stimulation by bradykinin on the low end to iNOS stimulation by LPS on the high end.

Scheme 1.16: ODP-type probe DAF-FM

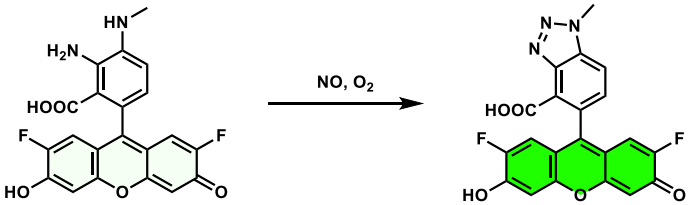

DAF-FM reacts with oxidized NO to form the highly fluorescent benzotriazole product.

Most ODP probes are designed with the vicinal diamine sensing moiety linked by a phenyl group to the fluorophore, but three recent designs incorporate different

connectivity. The first, SIRD (Scheme 1.17A, bypasses the phenyl group in linking one of the amines directly to the silyl rosamine (i.e., rhodamine without the lactonizable carboxylate) fluorophore. This fluorophore emits in the nIR region (λ_{ex}/ λ_{em} 690/710 nm), since the less electronegative dimethylsilyl group increases the HOMO for the fluorophore verses the oxygen equivalent in rhodamine. The directly-linked ODP moiety quenches efficiently to a quantum yield of 0.06%, and aerobic reaction with NO makes the triazole, with a quantum yield increase to 31%.

Rosamines react as conjugate acceptors with thiols; the ODP group is too poor a leaving group for thiol displacement to be relevant, but thiols can readily replace the benzotriazole group. Cysteine displacement of benzotriazole, via conversion of the reversible thiol-adduct kinetic product to the α-amine-adduct thermodynamic product (based on Anslyn group results with EVA conjugate acceptor)[270], shifted the fluorescence wavelengths to λ_{ex}/ λ_{em} 480/620 nm. Glutathione with the more distant N-terminus did not react. In fact, the N-silylrosamine-benzotriazole is quite selective as a fluorescent probe for cysteine versus glutathione in cells. Apart from cysteine, SIRD maintained selectivity over the standard competing analytes, including peroxynitrite. When applied to cells, SIRD's positive charge directed it to mitochondria, and LPS-stimulated RAW 264.7 cells showed both 620 (cysteine adduct) and 710 nm (benzotriazole) emission.

A second design resembles one that we attempted and that will be discussed later. An asymmetric rhodamine ROPD incorporates the ODP at one of the fluorophore nitrogens (Scheme 1.17B). Formation of the benzotriazole shifts the absorbance maximum from 546 nm to 470 nm and eliminates PET quenching, with increasing emission at 581 nm. The LOD of 68 nM derives from a relatively small increase (F/F_o only ~6) in fluorescence upon full reaction with NO oxidation products.[271] Based on our experience with a similar motif, the ethyl ester may serve to prevent its carboxylic acid

precursor from lactonizing, as the equilibrium between the non-fluorescent lactone and the fluorescent open forms probably favors the lactone form.

Scheme 1.17: SIRD and ROPD ODP-based NO probes

A.

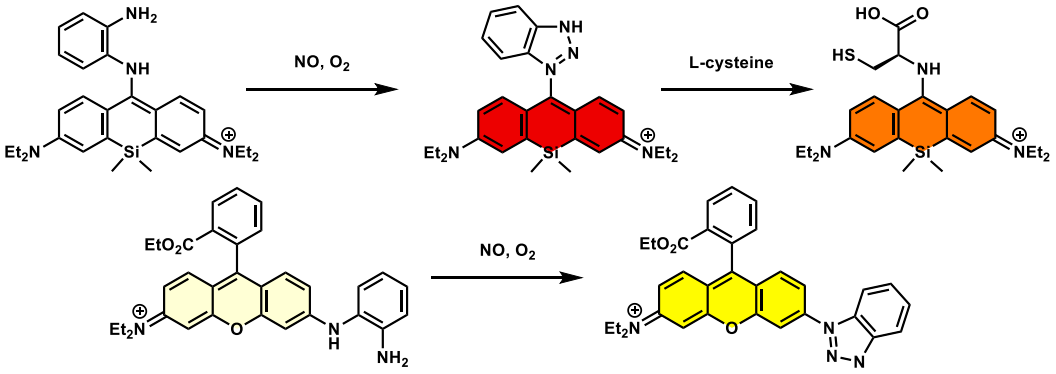

B.

A) SIRD red fluorescence detection of oxidized NO with subsequent substitution by L-cysteine B) ROPD NO detection

DALR, connects the diaminophenyl group through the amine to form a lactam on Rhodamine B (Scheme 1.18A).[272] The equilibrium between the non-fluorescent lactam form and the fluorescent amide form favors the lactam until pH drops below 3, meaning the sensor is dark at physiologic pH. The authors propose that the free amine of the vicinal diamines binds nitrosonium from N_2O_3, tautomerizes, and then loses water to form the diazonium. Then an intramolecular reaction with the lactam nitrogen opens the lactam to form the fluorescent benzotriazole amide. This sensing approach differs from the typical elimination of PET-quenching approach typical to ODP probes, and the 2400-fold increase in fluorescence due to NO saturation produced an LOD of 3 nM.

DALR was selective for NO over the standard competing analytes, except for peroxynitrite, which produced a response very similar to that of aerobic NO. The authors postulated that peroxynitrite reversibly dissociates to NO and superoxide at pH 7; separate applications of peroxynitrite and NO at pH 12, at which $ONOO^-$ is stable, produced a strong response for NO and a much reduced one for $ONOO^-$.

Unfortunately, benzotriazole is a good leaving group, and after 30 minutes in aqueous solution, hydrolysis of the amide (λ_{ex}/ λ_{em} 570/592 nm) to Rhodamine B (λ_{ex}/ λ_{em} 554/574 nm) is complete. L-cysteine displaces benzotriazole to form the cysteine lactam thermodynamic product (Scheme 1.18A). Both reactions produce a change in fluorescence not dependent upon NO concentrations.

To avoid hydrolysis, the amide in DALR was converted to an aminomethyl connection in deOxy DAL-Si-R (Scheme 1.18B).[273] The Rhodamine B fluorophore was also replaced with the nIR silyl rhodamine fluorophore. Unreacted probe was dark from pH 4 to 10, despite the absorbance spectrum showing the spiroclactam opening below pH 7, due to the reinforcing effect of PET quenching by ODP. Reaction with NO under aerobic conditions produced a 6300-fold increase in 680 nm emission within 40 seconds, producing an enviable LOD of 0.12 nM. Fluorescence of the triazole product was stable over the pH range of 5 to 10. A thorough screen versus potentially competing analytes (including thiols) demonstrated great selectivity for NO, even in cells with exogenous application of the analytes. Deoxy DAL-Si-R detects basal levels of NO (and their attenuation with NOS inhibitor aminoguanidine), as well as LPS-stimulated micromolar levels of NO in RAW 264.7 cells. In HeLa cells, it localizes primarily in lysosomes. With its deep red emission, NO in LPS-inflamed live mice could be located by DAL-Si-R.

Scheme 1.18: DALR and DAL-Si-R lactam and deoxylactam ODP probes for NO

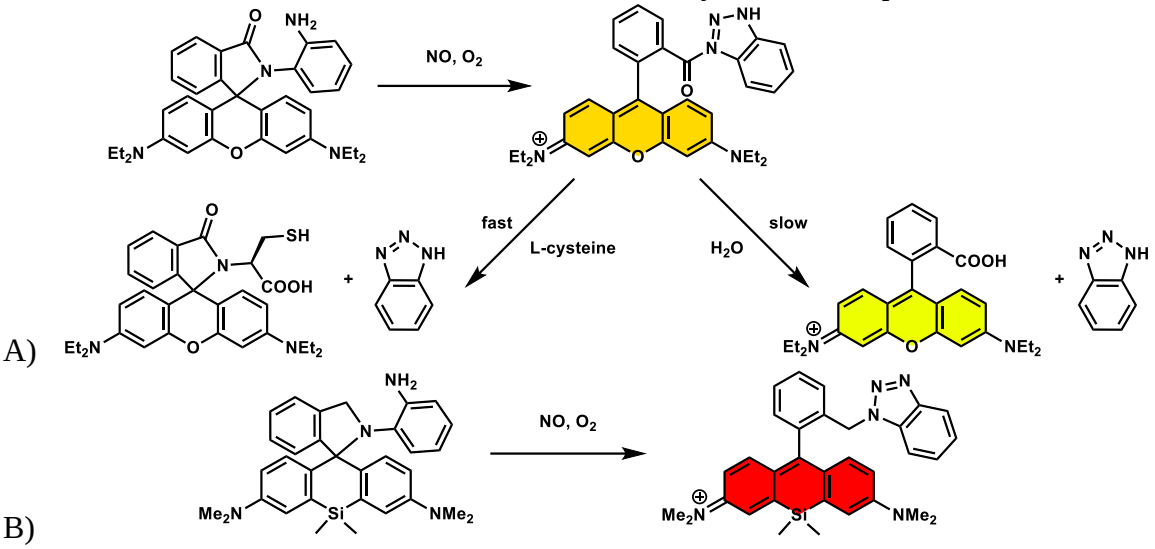

A) DALR non-fluorescent lactam reacts with oxidized NO to the fluorescent benzotriazole amide, an activated amide that reacts further with cysteine or water. B) near-IR DAL-Si-R is not susceptible to hydrolysis or to trans-amidation by L-cysteine

The ODP probes have been found to exhibit some cross-reactivity. As dinucleophiles, they can react well with other dielectrophiles found in cells like methyl glyoxal and ascorbic acid/dehydroascorbic acid (Scheme 1.19A). In fact, a variant of DAMBO, a bodipy ODP published as an NO sensor,[259] has been published as the methyl glyoxal sensor MBo (Scheme 1.19B).[274] The authors for the latter publication postulated that, although MBo does react with N_2O_3, at physiological pH a portion of the non-alkylated benzotriazole is deprotonated, quenching the fluorescence response to the NO metabolite (Scheme 1.19C). The methylquinoxaline formed from reaction with methylglyoxal abolishes the donor PET quencher orbital, and it has no physiologically relevant acidic proton, so emission enhancement would arise mostly from condensation upon methylglyoxal, not N_2O_3. Both DAMBO and MBo publications focus on optimizing the fluorescence reporting for the analyte (N_2O_3 or methylglyoxal) but ignore that binding to competing analytes that does not evoke fluorescence may be irreversible and result in consumption of probe, which would cause saturation (and therefore

underreporting) of probe fluorescence at high-analyte levels. To avoid undesirable immine-forming condensation (such as with glyoxal and dehydroascorbic acid), Nagano methylated one of the vicinal amines in DAF-FM, imparting reversibility to the cross-reactions but not to N_2O_3 condensation. The methyl group also replaces the acidic hydrogen in benzotriazole, denying the potential for PET quenching from the benzotriolate. For probes in which one of the vicinal diamines connects to the fluorophore directly (Scheme 1.17), not through their phenyl ring, steric constraints strongly minimize these methylglyoxal cyclic adducts.

Scheme 1.19: DAMBO and MBo examples of cross-reactivity of ODP-based NO probes

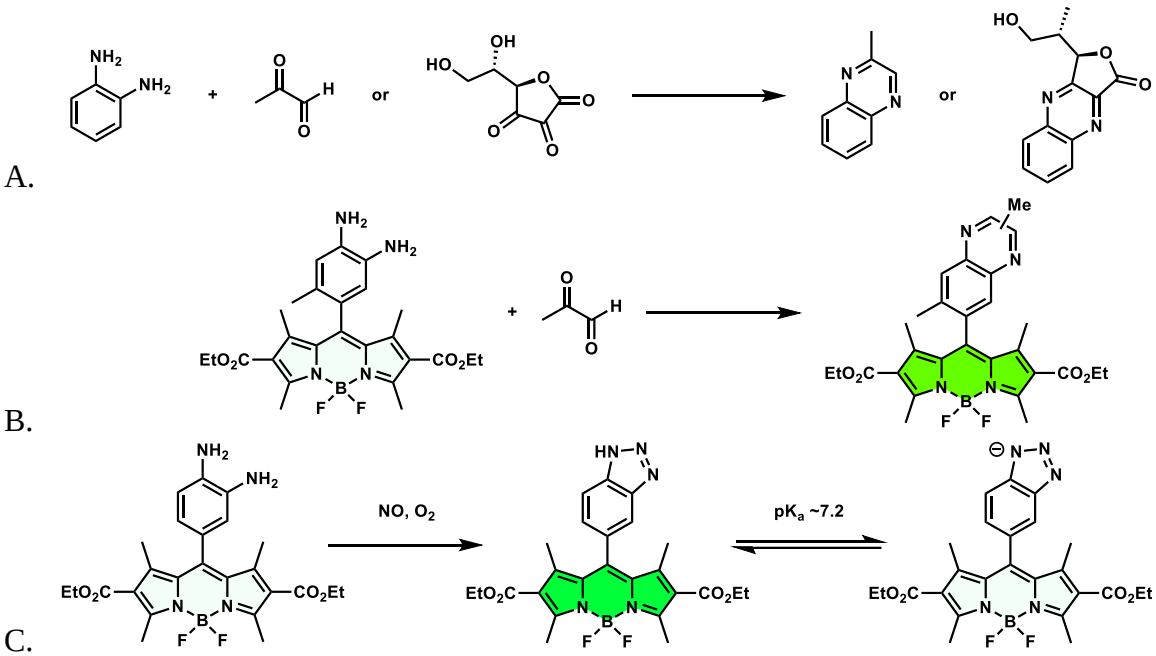

A) Potential cross-reactivity of ODP-based probes with dielectrophiles methyl glyoxal and dehydroascorbic acid. B) MBo reaction with methyl glyoxal results in a strong increase in emission. C) Deprotonation of DAMBO triazole re-instates PET quenching, with 24% of triazole as the anion at pH 7.2.

ODP's also become sensitized to react directly with NO upon abstraction of an anilinic hydrogen by oxidizing radicals such as $^{\bullet}OH$, $^{\bullet}OCO_2^-$, and NO_2.[275] In fact, by mimicking physiological conditions in which superoxide is produced at equal rates to

NO, one study estimated only 20% of DAF (non-fluorinated, non-methylated version of DAF-FM) triazole fluorescence emanated from reaction with N_2O_3, as determined by N_3^- (an N_2O_3 scavenger) competition, and the rest from NO_2.[276] NO_2, an intermediate to N_2O_3, forms from autoxidation of NO, homolysis of peroxynitrous acid (along with $^{\bullet}OH$), and homolysis of nitrosoperoxycarbonate (along with $^{\bullet}OCO_2^-$), all downstream products of NO biology. If these radicals arose exclusively from these sources, then ODP sensitization would merely reflect the biology of NO more globally; unfortunately, other sources of these radicals exist. For example superoxide dismutase makes carbonate radicals from bicarbonate,[277] and ferrous to ferric Fenton chemistry on hydrogen peroxide produces hydroxyl radicals.[278] As another example of cross-talk, DAF was reported to respond to nitroxyl, the reduced form of NO, sourced from Angeli's salt ($Na_2N_2O_3$) in aerobic conditions.[276]

1.1.6.5.2.5 Monoamine-based probes

Monoamine sensors for aerobic NO metabolites minimize the possibility of the NO sensor reacting with other dielectrophiles. They normally have higher reaction rates than ODPs due to the simplicity of N-nitrosation when compared to multiple proton shuttling steps required to form ODP triazole. Primary amines may form diazonium salts when they condense upon nitrosonium, whereas secondary amines cannot due to their degree of substitution. PET-quenching secondary anilines react with N_2O_3 to form N-nitrosamines, with a drop in HOMO energy that disables quenching. In order to compete with vicinal-diamine nucleophilicity, the sensors were designed with an electron-donating group (EDG) *para* or *ortho* to the aniline. These EDGs also help to increase HOMO energy to make PET quenching more effective.

The first generation of these sensors, BNHM, incorporated a phenol as the EDG on a tetramethyl bodipy sensor (Scheme 1.20A).[279] The secondary aniline sensing moiety

further served as a linker to potential cell-directing groups, such as a mitochondrial-directing triphenylphosphonium group in BNHM-MT. Aerobic exposure of the aniline to NO within twenty seconds provoked a 90-fold enhancement in 518 nm emission that resulted in an LOD of 4.8 nM, with the desired selectivity over standard competing analytes, except peroxynitrite. $ONOO^-$ promoted cleavage of the benzyl linker to a non-responsive product (Scheme 1.20B). Substituting the phenol in BNHM with a methoxy group (BNMM) lowered the LOD to 0.4 nM, but BNMM also reacted with peroxynitrite, resulting in an *o*-iminoquinone that disrupts PET quenching, with an LOD of 0.14 nM for peroxynitrite. Both NO and $ONOO^-$ provoked a >800-fold fluorescence enhancement at 518 nm. Strangely, nitroso-BNNM and iminoquinone-BNNM both fluoresce optimally only between pH 7 and 7.5; any larger fluctuations in pH caused a significant drop in emission.[280] This sensing approach has been applied to nIR-emitting silyl rhodamine (LOD 14 nM), benzo[*g*]coumarin (LOD 37 nM), and Cy-7 (LOD 11.3 nM)[281] fluorophores for deep-tissue and live-animal imaging.

Scheme 1.20: Secondary monoamine-based NO probes

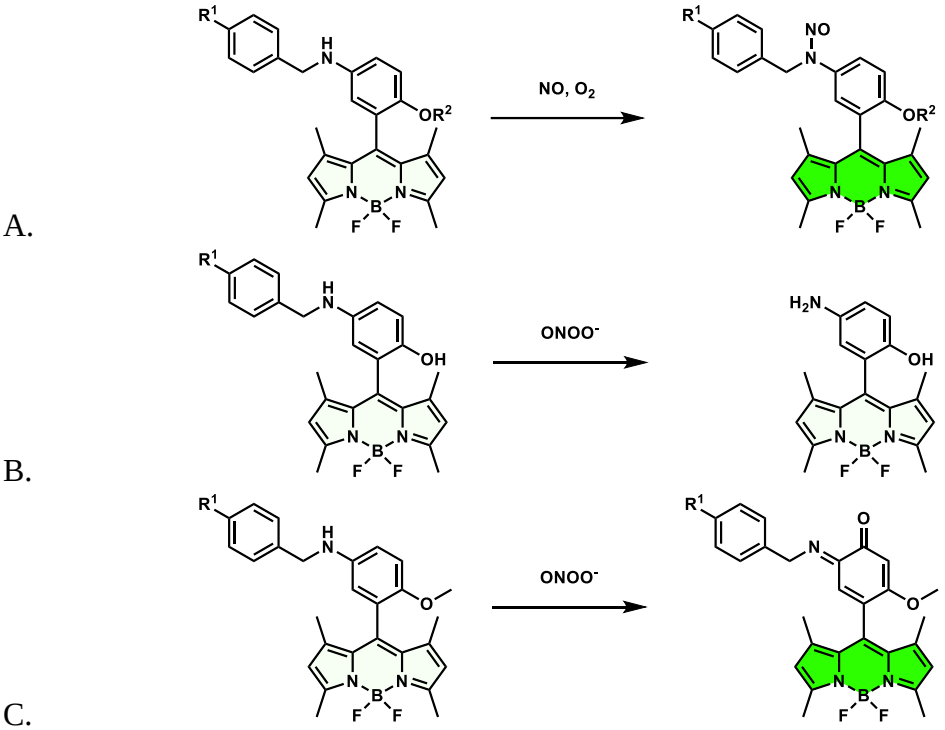

A) Cytosolic (R1 = H) and mitrochondrial (R1 = O(CH2)3PPh3) monoamine BNHM (R2 = H) and BNMM (R2 = Me) probes for oxidized NO. B) Non-fluorescent consumption of BNHM by peroxynitrite. C) Consumption of BNNM by peroxynitrite produces an iminoquinone with similar fluorescent properties to N-Nitroso BNNM.

1.1.6.5.2.6 2-aminobiphenyl-based probes

2-aminobiphenyl (2-ABP) probes combine the selectivity of monoamines with the dinucleophilicity of the ODP's for NO in aerobic conditions. The primary aniline traps nitrosonium, followed by condensation from the connected aryl ring to form fluorescent benzo[*c*]cinnoline. In this manner, NO^+-binding creates the fluorophore, rather than modulating its fluorescence. If the probe is fluorescent and if probe and cinnoline fluorescence wavelengths are well resolved, a ratiometric response to N_2O_3 ensues, with probe emission decreasing as cinnoline emission increases. NO_{550}, the first of these probes (Scheme 1.21), has negligible fluorescence but produces a 1500-fold enhancement of 550 nm emission (quantum yield 11%) upon complete reaction with NO to the

cinnoline product AZO_{550}, with an LOD of 30 nM.[282] Reaction kinetics are comparable to the DAF probes, achieving ~ 80% of saturated signal at 25 seconds, with full saturation after 2 minutes.

In contrast to the pH-susceptible non-N-alkylated benzotriazoles, AZO_{550}'s fluorescence emission is stable from pH 5-9. An array of competing analytes in at least 4-fold excess could produce no signal. A competition assay of NO_{550} in the presence of competing analytes for NO was not performed, however. These assays have become more routine to elucidate side reactions of a probe with competing analytes that may interfere with detection (e.g., other analytes that react with the probe irreversibly to yield a non-fluorescent product that cannot detect NO). When compared to ODP probe DAF-2 DA, NO_{550} fluorescence remained located within PC-12 and astrocyte cells, whereas DAF-2 showed strong extracellular fluorescence from transporter pump extrusion that diminished contrast and clarity. However, to achieve similar brightness to 1 μM DAF-FM loading into cells, NO_{550} required loading concentrations of 50 - 100 μM and 5-25 hours of scavenging N_2O_3.[283] Although at first glance this difference of two orders of magnitude seems to highlight DAF-FM as a brighter, more sensitive probe, one should note that when loaded as the diacetate, DAF-FM accumulates in cells to concentrations of 750 μM.[269] Loading concentrations higher than 100 μM NO_{550} were not attempted because they showed cytotoxicity.[283] NO_{550} localized in cells in a punctate manner that did not overlap with lysosome-staining fluorophores, and the authors speculated the staining pattern might resemble that for caveolae, Golgi bodies, and cytoskeleton, where eNOS activity in endothelial cells has been established.

Scheme 1.21: 2-aminobiphenyl probe NO_{550}

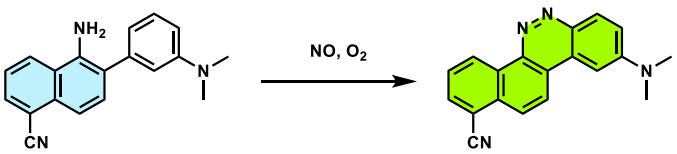

NO_{550} traps oxidized NO and transforms it into the cinnoline fluorophore. In the absence of the N,N-dimethylaniline PET quencher, 5-cyano-1-methylamino naphthalene fluoresces strongly blue in hydrophobic solvents/regions but weakly yellow in aqueous media/cytosol.[284]

The selectivity and high fluorescence enhancement of NO_{550} inspired the development of 2-ABP analogues. The design of one analog (Scheme 1.22) ignores the fluorescence enhancement emanating from nitrosonium constructing the fluorophore, preferring to focus on the PET quenching capability of the 2-ABP moiety. The 2-ABP connects through its aniline phenyl group to the meso position of tetramethyl bodipy, with quenching of fluorescence.[285] Aerobic NO builds the cinnoline, whose HOMO is too low to PET quench effectively, resulting in a 5-fold fluorescence increase at 518 nm and an LOD of 30 nM. Probe and azo product fluorescence are stable between pH 4.5 and 7.5.

Scheme 1.22: 2-ABP probes as PET quenchers

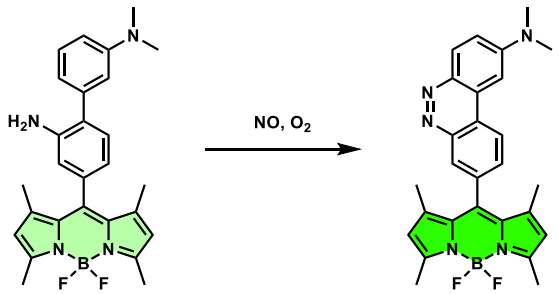

Implementation of the 2-ABP moiety as a PET quencher, with fluorescence turn-on upon condensing with oxidized NO to the cinnoline whose HOMO is lower than 2-ABP.

Another analog, NO-QA5 connects 2-methyl-5-aminoquinoline with N,N-dimethylaniline (Scheme 1.23).[286] Reaction with nitrite in acid yields two isomers of the azo product, a non-fluorescent one deriving from attack at the *ortho* position of the dimethylaniline and the fluorescent, albeit with a low quantum yield of 0.15% in aqueous

PBS buffer, *para*-attack product with well-resolved fluorescence wavelengths (excitation/emission maxima of 430/540 nm) from non-fluorescent NO-QA5. The same reaction on NO_{550} did not produce the *ortho*-attack regioisomer, and it was not determined whether NO-QA5 aerobic reaction with NO yielded isomers. The low background from creating a longer-wavelength fluorophore results in an LOD of 15 nM. Although NO-QA5 is selective for the standard competing analytes, it is sensitive to solvent polarity, revealing emission stemming from ICT. Such solvatochromism means that fluorescence emission changes according to the probes' local environment in the cell. Hydrophobic regions provoke a hypsochromic shift in emission wavelength, along with a strong increase in quantum yield.

Scheme 1.23: NO-QA5 probe and the regional isomers of its cinnoline product

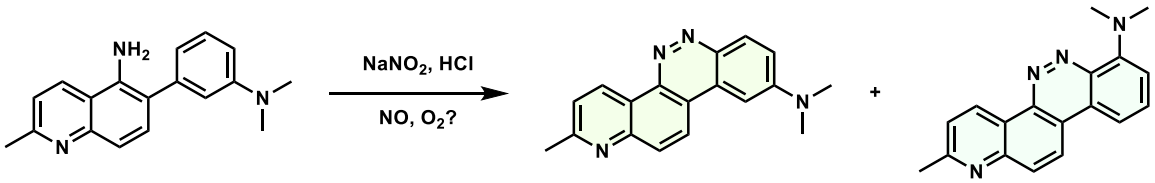

Weakly fluorescent ortho and para products from the reaction of NO-QA5 with nitrosonium derived from acidification of nitrite and possibly from the reaction of aerobic NO.

Mito-N incorporates 6-aminonaphthalimide into the 2-ABP core structure, with the imide connecting a triphenylphosphonium-capped tail for directing into mitochondria (Scheme 1.24).[287] Mito-N emits at 540 nm, but cinnoline formation extends emission to 595 nm. Unfortunately, reaction with N_2O_3 takes twenty minutes to reach 80% completion. The electron-withdrawing nature of the phthalimide renders the 6-amine less nucleophilic, slowing down the reaction pronouncedly relative to NO_{550}. Excitation at 440 nm provokes ratiometric emission at 540 nm and 595 nm, proportional to the amount of Mito-N versus its cinnoline product, respectively, with an LOD of 21 nM. Although

mitochondrial, Mito-N produced weak response, even to exogenous NO, in RAW 264.7 cells, not surprisingly considering its low reactivity.

Scheme 1.24: Mito-N, an emission-ratiometric probe with low nucleophilicity for aerobic NO

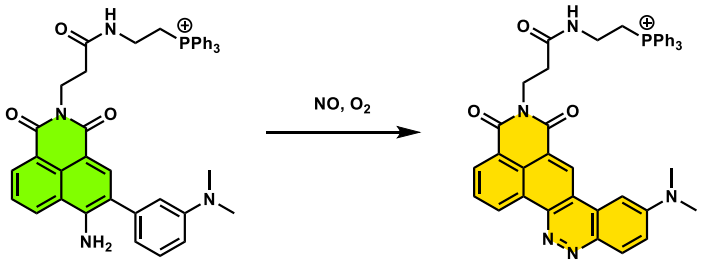

These analogs have informed on the 2-ABP family of NO probes, but the Yang group performed a more systematic study into the optimization of 2-ABP probes. (Portions of this document starting from Table 1 and extending through Figure 1.18 are adapted from [288], published by The Royal Society of Chemistry.) Table 1 shows the permutations synthesized and studied. Positions X and Y on rings A and B were varied due to their pronounced influence on the probes' nucleophilicity, and ring C was appended to induce bathochromic shifts. Substituents at position Z on ring C are not only commercially and synthetically convenient but also distant from (and less inductively and sterically interfering with) the N_2O_3 reaction site. Z was therefore an attractive modification site to introduce hydrophobic, hydrophilic, cell-compartment directing, or tethering functionalities. The Yang group started by evaluating the brightness and fluorescence properties (in 1:4 DMSO / 50 mM PBS at pH 7.4) of the probes and their cinnoline (azo) products accessed from the reaction with nitrite in acid (Table 1).

Table 1: Structures and optical properties of a suite of 2-ABP probes for aerobic NO.

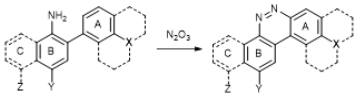

Unreacted Probe						Cinnoline Product				
λ_{abs}[a] (nm)	λ_{em}[b] (nm)	$10^{-3}\cdot\varepsilon$[c] $M^{-1}cm^{-1}$	Φ[d]	Structure	Pr. No.	X or Z	λ_{abs}[a] (nm)	λ_{em}[b] (nm)	$10^{-3}\cdot\varepsilon$[c] $M^{-1}cm^{-1}$	Φ[d]	Relative[e,f] brightness
300	420	10.0	0.54	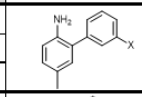	1	OMe	395	488	14.0	0.09	3.0
300	420	11.0	0.47		2	OH	395	490	13.2	0.67	20.0
310	415	9.0	0.27		3	NMe_2	415	510	14.3	0.02	0.7
300	390	14.4	0.003	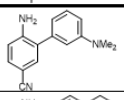	4	-	450	550	16.2	0.003	0.1
310	415	9.9	0.24	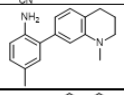	5	-	425	508	20.8	0.62	**29.3**
300	415	9.5	0.1	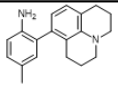	6	-	447	535	11.3	0.36	9.3
350	450	9.9	0.02	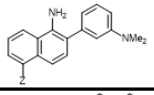	7	NHAc	433	535	13.0	0.08	2.3
330	445	8.0	0.04		8	H	430	530	13.9	0.06	1.9
350	n.d.[g]	3.5	n.d.[g]		9	CN (NO_{550})	450	550	4.0	0.11	**1.0**
370	455	9.4	0.07	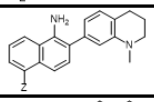	10	NHAc (NO_{530})	445	530	20.1	0.5	**23.0**
355	450	10.3	0.02		11	H	440	525	24.1	0.5	**27.5**
345	510	11.6	0.03		12	CN	450	545	7.3	0.13	2.2
420	465	12.2	0.01	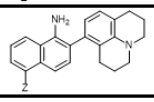	13	NHAc (NO_{562})	470	562	15.5	0.35	**12.3**
350	425	11.3	0.01		14	H	466	555	16.9	0.24	9.3
390	515	12.4	0.02		15	CN	480	580	9.0	0.11	2.3

[a]Wavelength of maximum absorbance for the most bathochromic peak in the UV-vis spectrum [b]Wavelength of maximum emission for the largest peak in the emission spectrum when excited at the most bathochromic absorbance maximum [c]Absorptivity coefficient/1000 [d]Quantum efficiency [e]Brightness relative to the cinnoline product of NO550 (9), previously reported as AZO550. The blue values highlight the best performers in the suite. [f]Cinnoline brightness is defined as the product of its absorptivity and its quantum efficiency. [g]NO550 does not fluoresce in 1:4 DMSO / pH 7.4 phosphate buffer.

The first set of probes studied consisted of simple variants with rings A and B only (no C annulation). The Y substituent was fixed as a methyl group while varying the X substituent on ring A. After nitrosonium is trapped by the primary aniline, ring A attacks the N-nitrosamine, and the *para*-position substituent (X) strongly influences the nucleophilicity of the ring. To X were assigned electron-donating methoxy (OMe, **1**), hydroxy (OH, **2**), and *N*,*N*-dimethylamino (NMe_2, **3**) groups. By far, the hydroxyl variant surpassed the others in brightness due to AZO-**2**'s much higher quantum yield of

67%. Unfortunately, its brightness depends upon the protonation state of the phenol. Fluorescence pH titrations on AZO-**2** and AZO-**3** established their pK_a's as 7.8 and 4.5, respectively (Figure 1.04). These substituent variations indicated that either a methoxy or an amine substituent at Y are required to avoid responding to physiological pH changes.

Figure 1.04: Fluorescence emission pH titration of AZO-2 and AZO-3

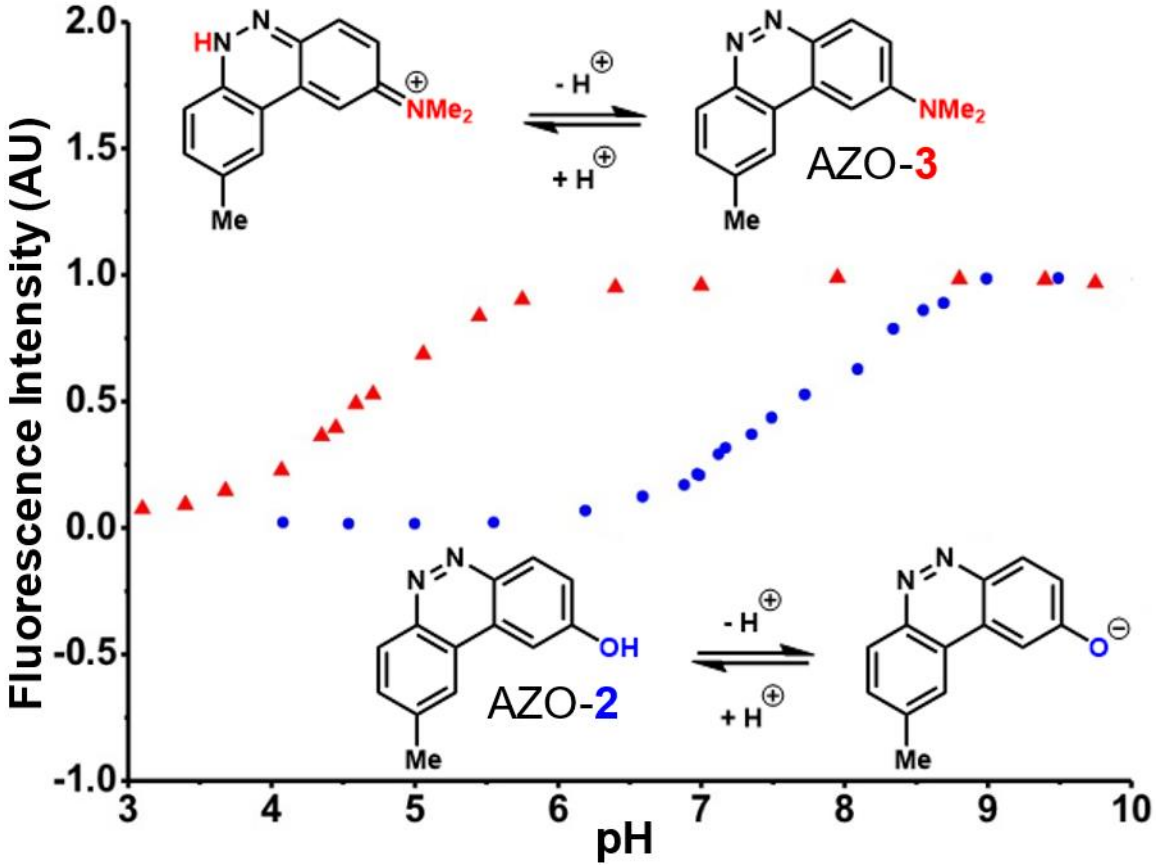

The titrations were conducted with 5 µM AZO-2 (blue) and AZO-3 (red) in 2.5% aqueous DMSO.

The influence of position Y was evaluated by changing it from methyl to cyano, postulating that ICT from NMe_2 to CN would lead to a bathochromic shift of fluorescence wavelengths. The X = NMe_2 and Y = CN cinnoline variant (AZO-**4**) had excitation and emission maxima 35-40 nm longer than AZO-**3**; however, the quantum yield of AZO-**4** was less than 1%, lower than AZO-**3**'s 2%.

When considering AZO-**3** and AZO_{550}'s low quantum yield, the excitation energy is lost to non-radiative relaxation through rotation about the ring-A aryl-NMe_2 bond.[289-290] This bond rotation decreases significantly when the *N*-alkyl groups are fused to the aryl ring, inspiring the *N*-methyl tetrahydroquinoline (**5**) and julolidine (**6**) variants on ring A, with methyl at Y on ring B. The ring fusion in both variants resulted in a remarkable increase in quantum yield, from 2% and 11% for non-fused AZO-**3** and AZO_{550} to 36% for doubly-fused AZO-**6** and 62% for singly-fused AZO-**5**. The molar absorptivity for AZO-**5** also increased, making it the brightest within the biphenyl series - nearly thirty times brighter than AZO_{550}, albeit at shorter wavelengths. The julolidine variant did produce the longest fluorescence wavelengths among **1**-**3** and **5**-**6**, corroborating the greater planarity of the dialkyl-N to aryl bond. However, a steric clash between ring B's aromatic proton and the julolidine benzylic protons (Figure 1.05) disrupts the planarity of the entire fluorophore, possibly explaining AZO-**6**'s lower quantum yield and molar absorptivity when compared to AZO-**5**.

Figure 1.05: Disruption of planarity in AZO-6 due to $A^{1,3}$ strain

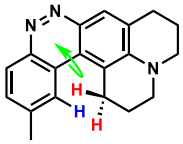

Probe **5** proved to be the brightest candidate, but AZO-**5**'s excitation and emission maxima (425 and 508 nm) fall short of the preferred wavelengths appropriate to the universal FITC filters; benzannulation (ring C) extends fluorescence wavelengths. For these 1-amino-2-phenylnaphthalene-based probes, the *N*,*N*-dimethylamino, *N*-methyltetrahydroquinoline, and julolidine variants at position X on ring A were compared. In each of these X variants, H occupies position Y, and Z on ring C was derivatized with H, *N*-acetamide (NHAc), and CN - a total of nine variants. Focusing on

brightness first, the results listed in Table 1 (probes **7**-**15**) show that both NMe_2 (at X) and CN (at Z) substitutions are detrimental to cinnoline brightness. For the same Z substituent, the NMe_2 series members have lower molar absorptivities and quantum yields than their corresponding N-methyl tetrahydroquinoline or julolidine congeners, i.e., cinnolines **7** versus **10** and **13**, **8** versus **11** and **14**, and **9** versus **12** and **15**. This trend is readily explained by the greater non-radiative relaxation rate caused by rotation about the N-aryl bond for NMe_2 variants versus the singly fused N-methyl tetrahydroquinoline and doubly fused julolidine variants.

Likewise, the Z = CN cinnoline series exhibits lower molar absorptivities than the corresponding Z = NHAc or H series (for the same X substituent). One possible explanation is that the Franck-Condon excited state has significant quinoid character in the Z = CN series (due to internal charge transfer from the dialkylaniline to the nitrile), with less quinoid character in the ground state, such that the poor orbital overlap between the two states results in lower probability of photon absorption. Within the Z = CN series, for the two alicyclic amine variants at X (AZO-**12** and AZO-**15**), the ground state incorporates greater donation of the aligned nitrogen lone pair into the polyaromatic system than from the more freely rotating X = NMe_2 variant (AZO_{550}), leading to better orbital overlap of the ground state with the excited state, as demonstrated by their higher absorptivities. For the Z = H and NHAc variants, both substituents are less electron withdrawing and therefore less accepting of internal charge transfer than CN, meaning that their ground and excited states are more similar and their absorptivities higher.[291-292] The Z = CN series also manifested lower quantum yields. Perhaps the excited state relaxes through internal charge transfer to the nitrile π^* orbital, with subsequent non-radiative relaxation through the increased hydrogen-bonding of this negatively charged complex with buffer. N-methyl tetrahydroquinoline variants proved brighter than their

$A^{1,3}$-strained julolidine counterparts, as discussed for AZO-**6**. Interestingly, for AZO-**13** the greater electron-withdrawing nature of the NHAc Z-substituent (acceptor) acting upon the dialkyl amine (donor) lone pair electrons counters the $A^{1,3}$ strain to promote greater planarity and therefore a higher quantum yield, as compared to Z = H for AZO-**14**.

As anticipated, adding ring C to the biphenyl probes bathochromically shifts fluorescence wavelengths. While benzannulation of fluorones to seminaphthofluorones extends wavelengths by more than 100 nm, only a 15-30 nm shift occurs for the cinnolines.[293-295] For a π to π^* excitation, extending the pi-electron system significantly changes the energy gap, not so much for an n to π^* excitation. Substituting CN at Z (**9**, **12**, **15**) induces the greatest change, but this substitution prohibitively decreases brightness. Variants substituted with NHAc at Z (**7**, **10**, **13**) show only slight shifts (3-7 nm) to longer wavelengths compared to their corresponding H (**8**, **11**, **14**) substituted ones. Varying X in the benzannulated series from NMe_2 (**7**, **8**, **9**) to N-methyltetrahydroquinoline (**10**, **11**, **12**) to julolidine (**13**, **14**, **15**) continues the aforementioned pattern in the biphenyl series of red-shifting fluorescence wavelengths with greater ring fusion. Benzannulated julolidine variants therefore produce the longest-wavelength probes; unfortunately, julolidine substitution also decreases brightness due to $A^{1,3}$ strain, as proposed above.

The spectroscopic data reveal probes **5**, **10**, **11**, and **13** as the brightest in the group. Importantly, as with first generation NO_{550} and AZO_{550}, the absorbance spectra for the probes minimally overlap with the absorbance spectra of their corresponding cinnolines, and probe emission peaks are resolved from AZO emission peaks (Figure 1.06). Consequently, as described below, in cells the probes can be excited independently from their N_2O_3 reaction products to compare intracellular distribution or

compartmentalization of probe and cinnoline product and to maintain a nearly zero background for detecting product (as previously reported for NO_{550}).

Figure 1.06: Absorbance and fluorescence emission traces for **5**, **10**, **11**, and **13**

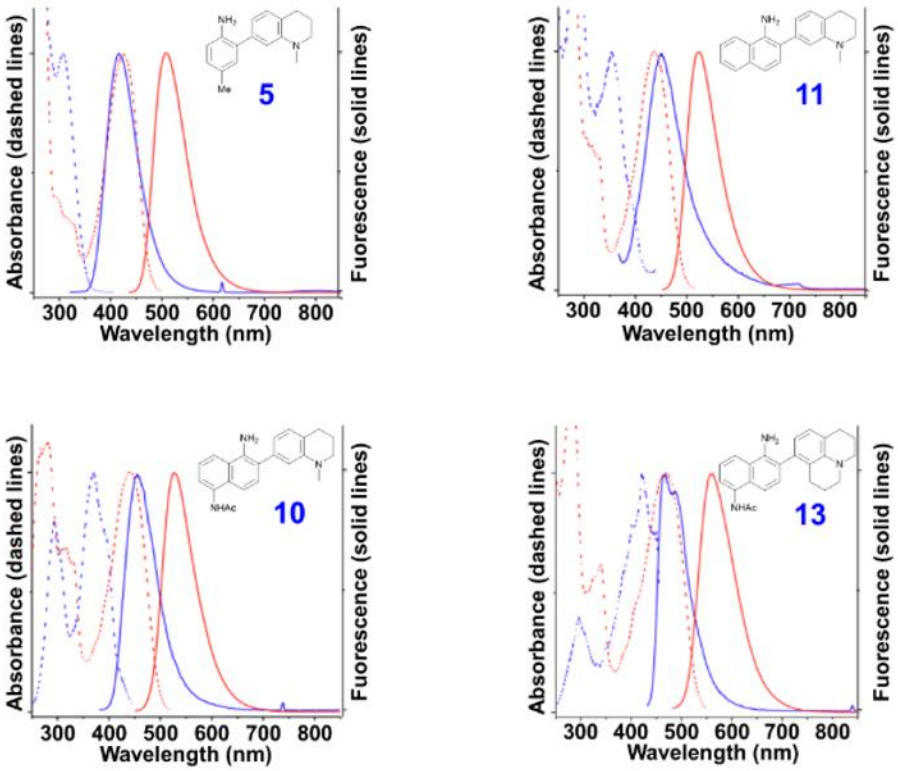

Absorbance (dashed lines) and fluorescence emission (solid lines) traces for probes (blue) and for their azo products (red).

Fluorescence titrations with NO of the probes in acellular, aerobic buffer provide more insight into 2-ABP probes following the same groupings for probes **1**-**16** above. Incremental aliquots of a saturated NO solution (1.9 mM)[15] were added to an air-equilibrated 50 μM solution of each probe variant in 4:1 50 mM PBS / DMSO at pH 7.4 (Figure 1.07).

Figure 1.07: Fluorescence titrations of probes 3, 5-15 with NO under aerobic conditions

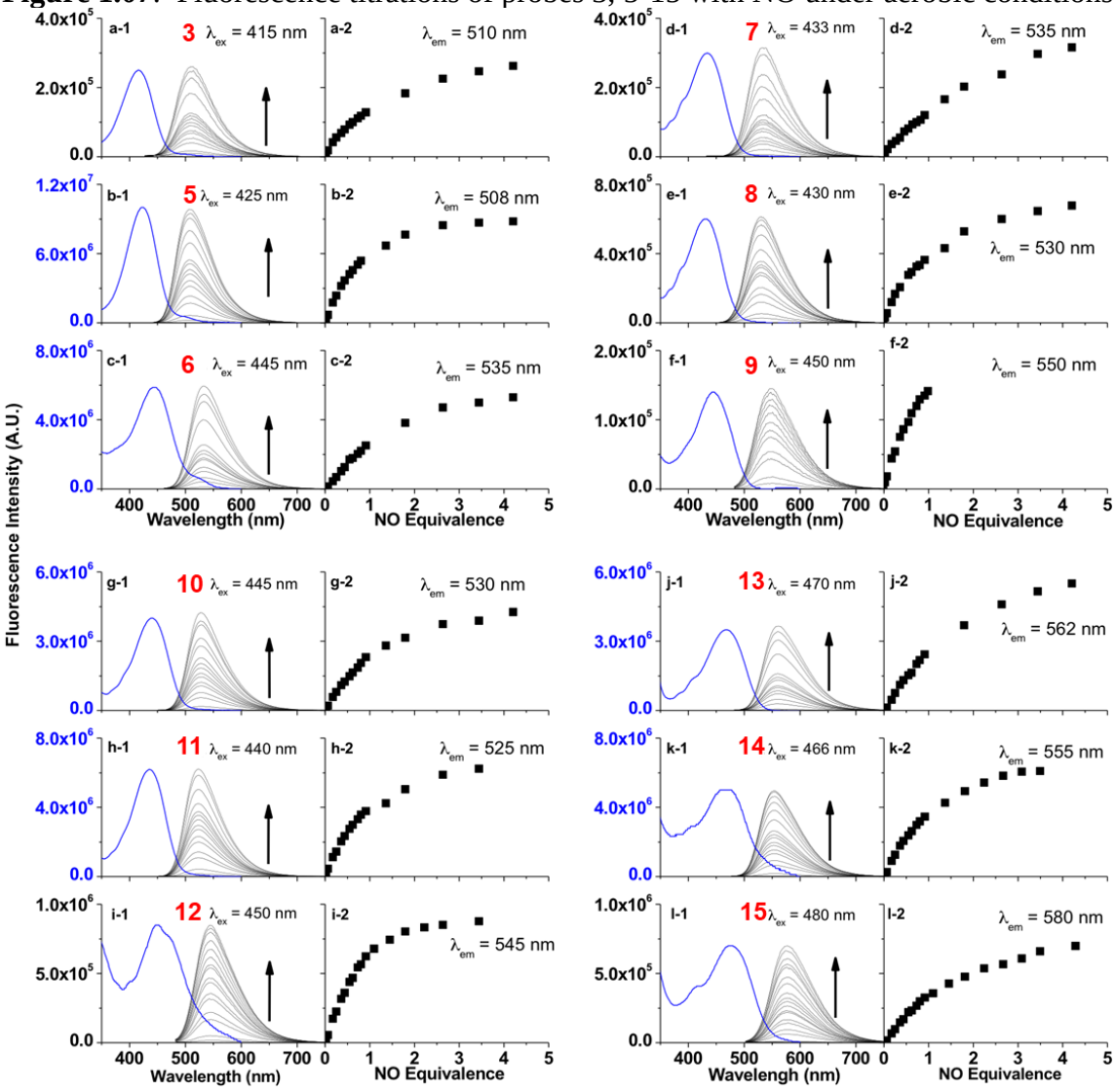

a-1 to l-1) Fluorescence emission spectra (black traces) of titrations with NO of 50 µM probe in 1:4 DMSO / pH 7.4 phosphate buffer at the specified excitation (λ_{ex}). Absorbance spectra (blue traces) of 50 µM solutions of their corresponding cinnoline. a-2 to l-2) Plots of fluorescence intensity of cinnolines at the specified wavelength (λ_{em}) versus added NO equivalents.

Two equivalents of NO react with a half equivalent of oxygen to yield one equivalent of nitrosonium equivalent N_2O_3 (Scheme 1.25), which is susceptible to hydrolysis. To maximize signal, probes should exhibit sufficient nucleophilicity to successfully compete with an excess of water. For the first grouping (the biphenyl system with no ring C and

with Y as Me) the Hammett σ^+ substituent constants for position X on ring A as OMe (**1**), OH (**2**), and NMe_2 (**3**) are -0.78, -0.92, and -1.7, respectively.[296] Variant **1** does not produce sufficient cinnoline product to be detected by fluorescence (Figure 1.08), whereas **2** and **3** provide ample signal, confirming that X must be sufficiently electron-donating ($\sigma^+ < -0.78$) to readily promote nucleophilic attack by ring A. Changing the weakly donating methyl ($\sigma^+ = -0.311$) at Y in **3** to a strongly-withdrawing cyano group, ($\sigma^+ = 0.659$)[297] in **4** (with X set as NMe_2) results in no production of fluorescence; the cyano group decreases the nucleophilicity of the *p*-amine to such an extent that it cannot compete with water for N_2O_3.

Scheme 1.25: Stoichiometry of the oxidation of NO to the nitrosating agent asymmetric N_2O_3

$$2\ NO + O_2 \rightarrow ONOONO$$

$$ONOONO \rightarrow 2\ NO_2$$

$$\underline{2\ NO_2 + 2\ NO \rightarrow 2\ N_2O_3}$$

$$2\ NO + \tfrac{1}{2}\ O_2 \rightarrow 2\ N_2O_3$$

The probes that do form cinnolines from N_2O_3 (**2-3**, **5-15**) for the most part require less than five minutes to almost react fully. The extent of turn-on points to probes **10-11** and **13-14** as the most promising of the longer-wavelength variants (Figures 1.07 and 1.08). More than two equivalents of NO, typically four in most cases, are necessary to reach saturation, however. For low starting concentrations of probe (50 μM, compared to 55.5 M for water), hydrolysis of N_2O_3 competes sufficiently as a side-reaction to warrant the excess NO.[298] Despite requiring at least twice the theoretical amount of NO for full conversion, these probes surpass DAF-2, the predecessor of DAF-FM in reactivity. The fluorescence intensity of a solution of **3** exposed to two equivalents of

NO, when calibrated to varying concentration standards of AZO-**3**, showed 36% cinnoline formation. In comparison, 27% of DAF-2 converted to the triazole when exposed to 2 equivalents of NO under similar conditions.[266]

Figure 1.08: Kinetic traces of the aerobic reaction of the probes with NO

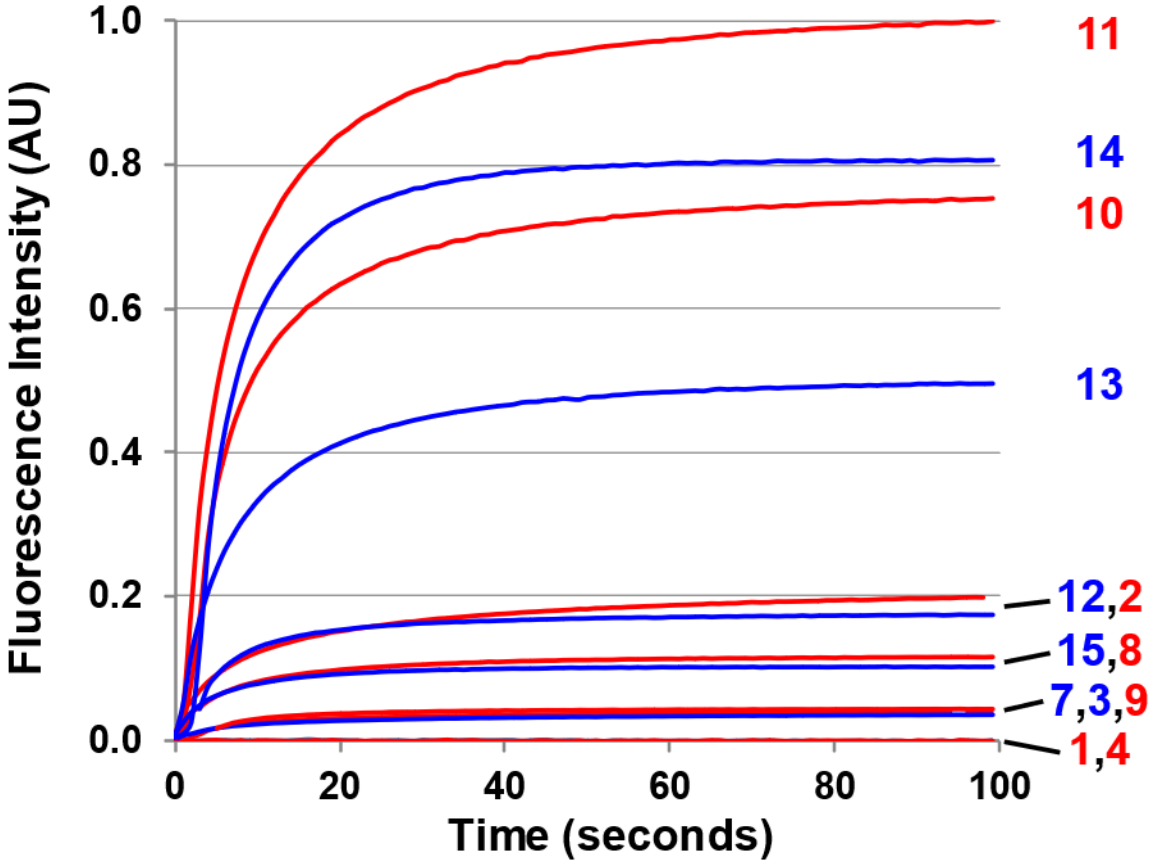

Kinetics of cinnoline emission emanating from exposure to one equivalent of NO of 50 µM solutions of probes 1-4 and 7-15 in 1:4 DMSO / phosphate buffer at pH 7.4 under aerobic conditions. Respective excitation wavelengths were set to the absorbance maximum of each probe's cinnoline product (AZO-1-4 and AZO-7-15).

With the high reactivity of these probes and the creation of signal from virtually no background, excellent detection limits were obtained. The LOD of **9** (NO_{550}) was previously determined to be 30 nM.[282] For the brighter **10**, the detection limit is 2 nM, comparable to DAF-FM's detection limit of 3 nM.[263]

The resolution of the probe and cinnoline emission spectra enables ratiometry when the probes and their cinnoline products share an excitation band (Figure 1.09). Ratiometry corrects for several experimental factors, including variations in intracellular dye concentrations, in optical path due to cell thickness, and in instrumental noise.[299] However, with this set of 2-ABP probes two factors moderate this benefit of ratiometry. First, the shared excitation band is in the cell-damaging near-UV range, shorter than the excitation for the cinnoline alone. Second, the shorter wavelength excites the probe more optimally than its cinnoline product, attenuating the stronger cinnoline emission and increasing unreacted probe background fluorescence, thereby directly counteracting one of the most significant attributes of the 2-ABP system: exciting at the cinnoline absorbance maximum results in virtually no background contribution from the probe.

Figure 1.09: Probe 5 ratiometric response to NO

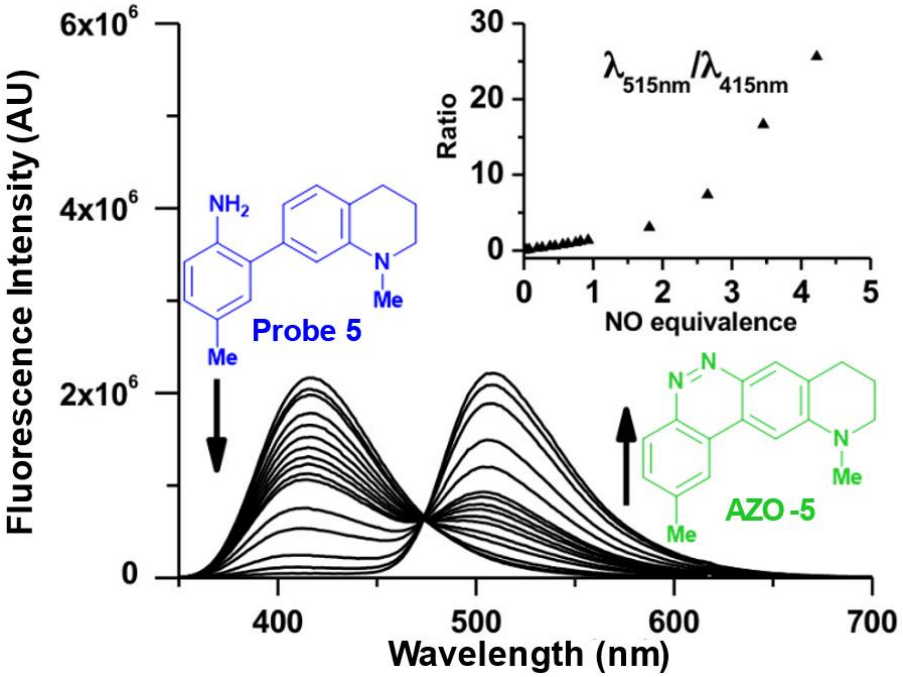

Fluorescence emission spectra depicting the ratiometric response to NO of 5 µM probe 5 solution in 1:4 DMSO / pH 4 phosphate buffer with excitation at 310 nm. The inset plots the ratio of emission intensity of AZO-5 (515 nm) to that of probe 5 (415 nm) versus equivalents of NO.

In conserving the 2-aminobiphenyl core, this set of probes was expected to maintain the selectivity of NO_{550} for NO over other common biological substrates.[282] Indeed this anticipation proved correct; as one example, Figure 1.10 demonstrates fluorescence emission for probe **10** in the presence of NO versus that in the presence of various oxidants. Even at one hundred equivalents of peroxynitrite to probe, at most a five-fold increase of fluorescence was observed, as compared with a greater than 1300-fold increase for merely one equivalent of NO.

Figure 1.10: Probe **10**'s selective response to various physiological analytes

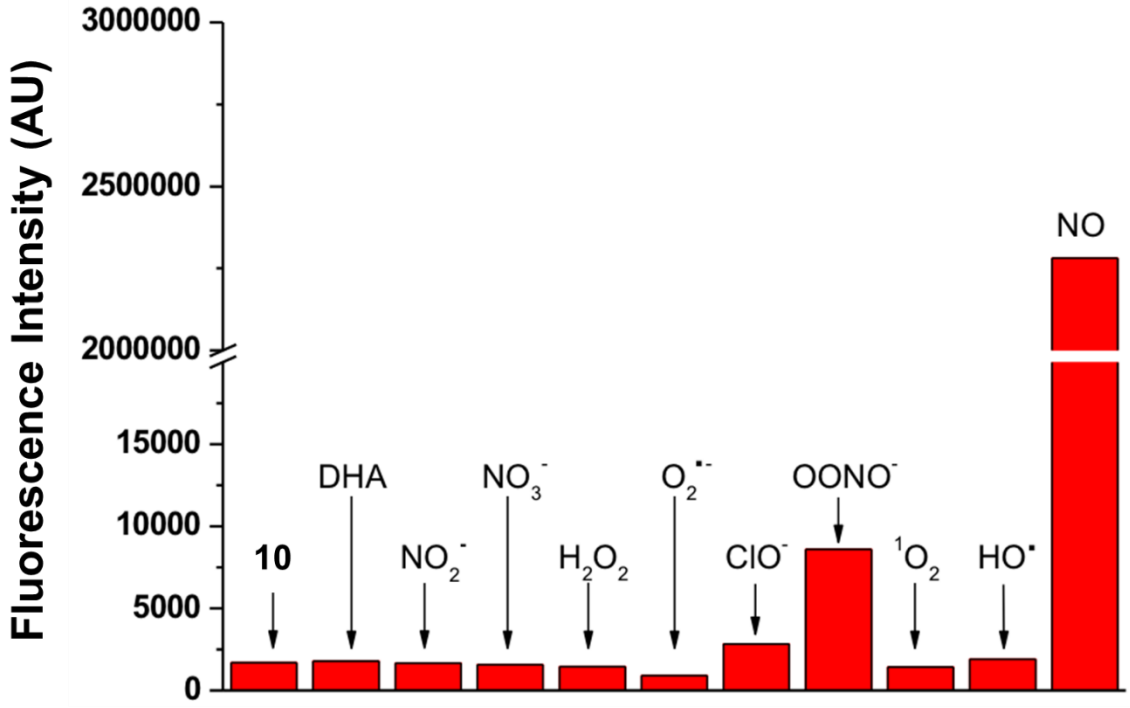

Probe 10 response to competing analytes in 100-fold excess, as compared to its response to one equivalent of NO (last column). The first column quantifies emission from 10 alone. Note the break/change in the vertical axis.

1.2 AIMS

Taking into consideration the probes' spectral properties and response to NO in abiotic aqueous solutions, the top performers consist of probes **5**, **10**, **11**, and **13**. To determine their suitability to the more complex cell environment and to compare their capability with the original 2-ABP probe **9** (NO_{550}) and with the "gold standard" NO probe DAF-FM, we employed fluorescence microscopy. The Anslyn lab was not equipped for cell culturing, nor did it have a fluorescence microscope. Fortunately, the Shear lab shared their cell-culturing equipment and Zeiss Axiovert 135 microscope, as well as their PhD candidate (at the time) Derek Hernandez. In his thesis,[300] Derek reports that, in the loading of probes **5**, **10**, and **13** at concentrations ranging from 10 to 100 μM for 1.5 hours in NIH 3T3 cells, the 50 and 100 μM concentrations produced nuclear fluorescence, pointing to cell damage, mostly absent at lower loading concentrations. In addition, after 24 hours these two highest concentrations provoked cell death in the population that, although not quantified, was easily discernible. In previous experiments, probe **11** within an hour had produced a bright signal comparable to DAF-FM, but this fluorescence faded over 24 hours, indicating some undesired reaction in the cell milieu with AZO-**11**. So concerning was this fading that no further studies were pursued with probe **11**.

Initial studies by Derek on probe **5** proved it similar to probes **10** and **13** in brightness and loading pattern. These studies had to be conducted at the Institute for Cellular and Molecular Biology (ICMB) Microscopy and Imaging Facility because the Shear lab lacked the microscope filter sets required for probe **5**'s shorter fluorescence wavelengths. In transporting the adhered cells from the Shear lab in the Welch building, where they were cultured and loaded, to ICMB for imaging, some would detach and

interfere with the imaging, and their general health seemed to suffer. As a result, we decided to focus on **10** and **13** only.

To verify their response to exogenous NO, we applied separately a saturated aqueous solution of NO and an NO donor, S-nitroso-N-acetylpenicillamine (SNAP). Next, we monitored the effect of dosing cells with NOS substrate L-arginine. Finally, with bacterial lipopolysaccharides (LPS), we provoked high NO production by iNOS enzymes in macrophage-derived RAW 264.7 cells and measured probe response to this endogenous production. For quantification of fluorescence, we developed a method applying available analysis tools in ImageJ software.[301]

The n to π* transition typical to cinnoline probes produces low absorptivity coefficients due to poor Franck-Condon overlap between the ground-state and excited-state orbitals. Even the brightest variant AZO-**5** achieves less than 25% of the brightness (the product of absorptivity coefficient and quantum yield) of DAF-FM triazole (13,000 vs 59,000 respectively). We therefore sought to incorporate the 2-ABP moiety into a rhodamine fluorophore more comparable in brightness to DAF's fluorinated fluorescein to determine if the innate fluorophore brightness would beget a bright AZO product, as detailed in Scheme 1.26. If successful, we anticipated the response to NO would be green-to-red, due to the extended conjugation, emission ratiometric.

Scheme 1.26: Proposed incorporation of 2-ABP into a rhodamine fluorophore

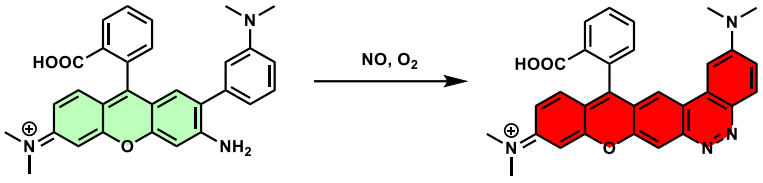

Reaction with aerobic NO should produce a longer-wavelength cinnoline product, perhaps with similar brightness to the starting rhodamine.

Finally, we designed a diphenyl ether probe (Scheme 1.27) that would form a red-fluorescent phenoxazine-based fluorophore if it could trap and condense upon NO under aerobic conditions. Electron-donating dialkyl aniline moieties were placed at the 3, 3´ positions to render the 6, 6´ positions nucleophilic at physiological pH. The alkyl groups terminate in water-solubilizing alcohol or carboxylate groups to prevent quenching from aggregate formation in aqueous media, for which phenoxazinium dyes have a propensity.

Scheme 1.27: Diphenyl ether probe to condense upon aerobic NO to form a phenoxazinium dye.

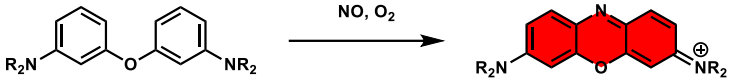

(R = CH_2CH_2OH or CH_2CH_2COOH)

1.3 RESULTS AND DISCUSSION

Since the samples shipped from the Yang group for probes **5**, **10**, **11**, and **13** had degraded, **5** was re-purified and the remaining three re-synthesized according to Schemes 1.28 to 1.31. During the purification of final product, all four probes tended to oxidize (going from clear to yellow-colored), with **5** being the most stable to air and **11** the least, requiring prompt processing to vacuum-dry material and storage at -20 °C.

Scheme 1.28: Preparation of Suzuki-Miyaura coupling partners for probes **10**, **11**, and **13**

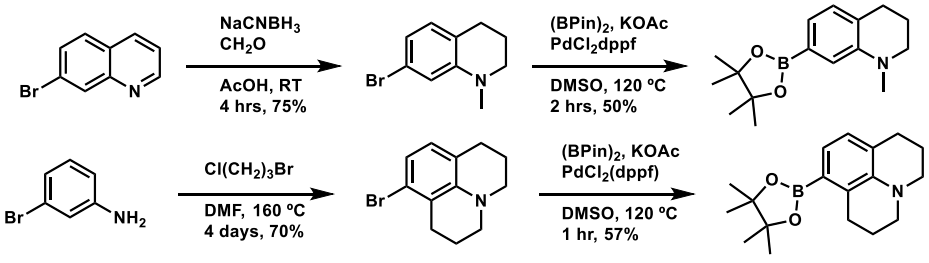

Scheme 1.29: Synthesis of probe **10**

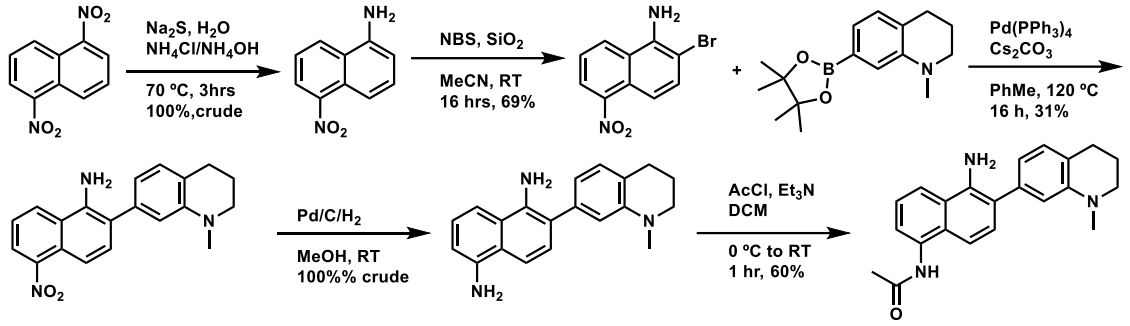

Scheme 1.30: Synthesis of probe **11**

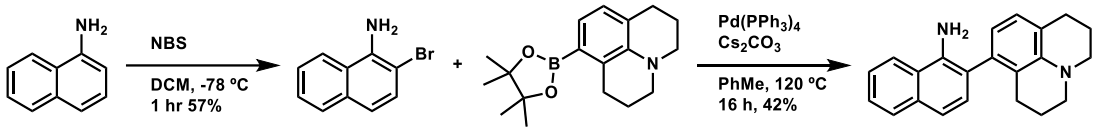

Scheme 1.31: Synthesis of probe **13**

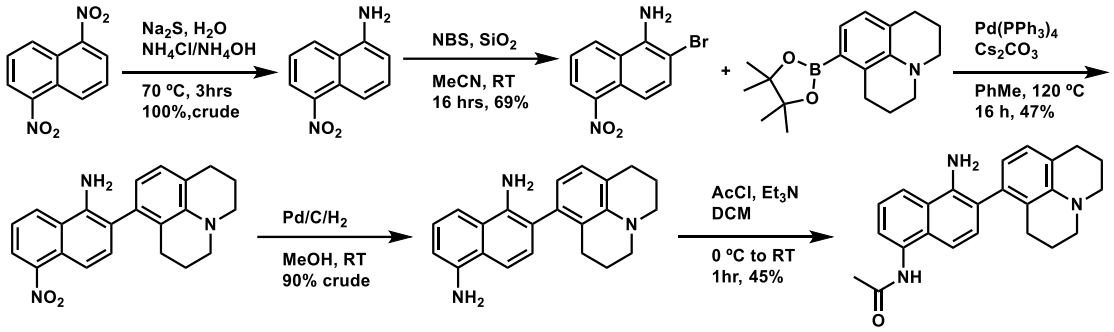

We did not observe toxicity when applying these probes to cells, even after 24 hours of incubation. A representative toxicity assay for probe **10** (Figure 1.11) showed >93% of RAW 264.7 cells remained viable after two hours of exposure to probe concentrations ranging from 1.25 to 40 μM, as compared to >95% in controls where they were either exposed to DMSO only or left untreated. (We did not attempt higher concentrations, since Derek Hernandez had seen cytotoxicity at 50 and 100 μM loading concentrations in NIH 3T3 cells.) In the assay, viable cells have intact membranes that retain highly charged Calcein Blue after non-specific esterases hydrolyze the

acetoxymethyl ester masks that enable passive loading of this polar dye. Propidium iodide cannot passively permeate intact cell membranes in viable cells; but, for dead cells whose membranes are compromised, propidium iodide can diffuse into the nucleus and intercalate into DNA, with a strong enhancement of red fluorescence. Thus, viable cells fluoresce blue and dead cells red.

Figure 1.11: Live / Dead Assay for cells loaded with probe **10**

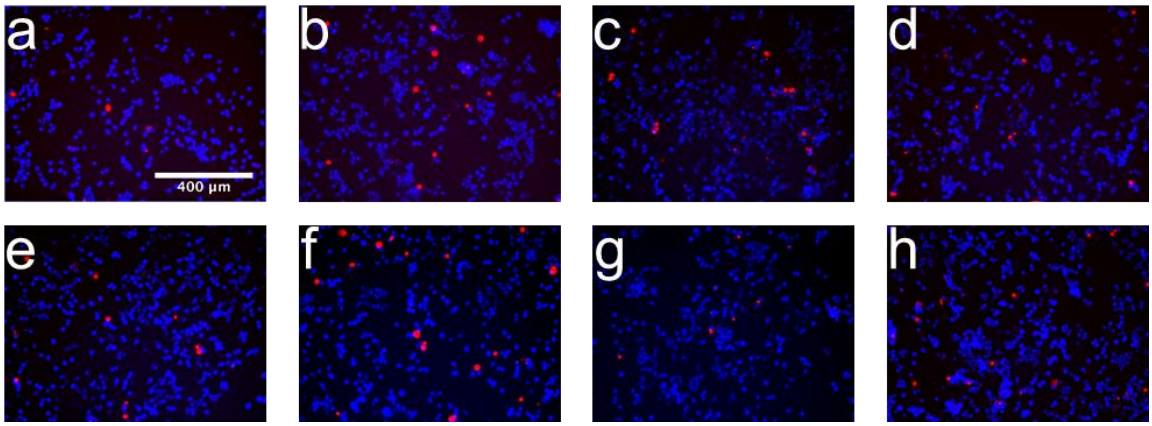

Pseudo-colored, 10X-magnification images of Calcein Blue (live cells) and Propidium Iodide (dead cells) in RAW 264.7 cells incubated for two hours with 1.25 (frame c), 2.5 (d), 5 (e), 10 (f), 20 (g), and 40 µM (h) probe 10, as well as cells left untreated (a) or incubated with 0.25% DMSO only (b).

The popular DAF-FM probe requires strikingly different loading and imaging procedures. The probe itself is negatively-charged and membrane impermeable, but masking it as the lactone/diacetate form DAF-FM DA enables loading. This colorless and non-fluorescent form passively diffuses across cell membranes, and non-specific intracellular esterases hydrolyze the acetate groups, promoting the fluorescent and dianionic non-lactone form that cannot permeat the membrane. However, organic anion transporters (OATs) efficiently pump this NO-responsive form (and its triazole product) out of the cell. Whereas increased loading time would typically yield higher concentrations of intracellular DAF-FM, OATs counteract the trend when the rate of DAF-FM extrusion exceeds that of loading and esterase hydrolysis. Therefore, loading

times and imaging times must be optimized and reproduced, according to cell-type and experiment conditions. This high degree of variability coupled with short experiment times after exposing cells to DAF-FM constrain imaging of NO and limit drawing conclusions of NO dynamics with this probe. In contrast, our 2-ABP probes permeate cell membranes readily and are poor substrates for extrusion by OATs.

The unreacted probes are fluorescent, although not as bright as their cinnoline products, and the excitation/emission profiles (Figure 1.12, excitation: dashed blue lines, emission: solid blue lines) for probes **10** and **13** fit the Zeiss G 365 DAPI filter (Appendix C) fairly well. Consequently, fluorescence imaging with the DAPI filter yields insight on probe loading and distribution. Figure 1.12 shows DAPI-filtered unreacted probe **9** (NO_{550}), **10**, and **13** fluorescence in NIH 3T3 (immortalized mouse embryo fibroblast cell line) and RAW 264.7 (immortalized mouse leukemia-virus transformed tumor macrophage cell line) cells. Fluorescence from probes **10** and **13** is distributed more uniformally throughout the cytosol than from **9**. Table 1 lists the probe form of **9** as non-fluorescent in aqueous solution, so the more punctate fluorescence for **9** probably reflects emission from hydrophobic regions (based on the solvatochromism of 5-cyano-1-methylamino naphthalene).[284] Although nuclear fluorescence is higher than extracellular fluorescence for all probes, the brighter intracellular but extranuclear fluorescence clearly demarcates the nucleus.

Figure 1.12: Probe loading distribution in cells

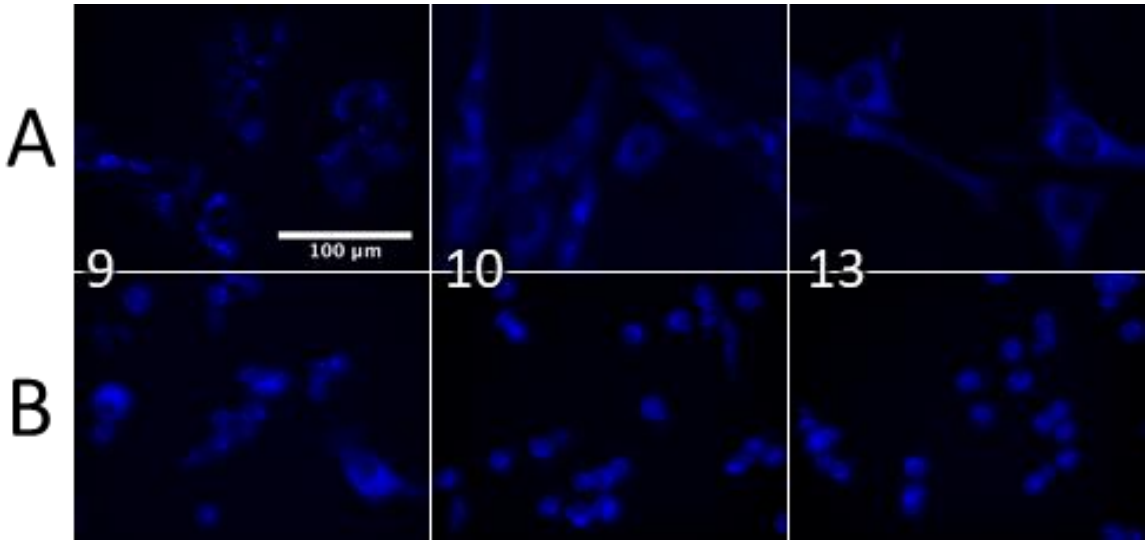

Pseudo-colored DAPI-filtered images (40x magnification) of probes 9, 10, and 13 in A) NIH 3T3 and B) RAW 264.7 cells

We used ImageJ for processing microscopy images, and we developed a protocol to quantify fluorescence intensity, as described in the experimental section of this chapter. Regions of interest (ROI) were defined in the brightfield (not fluorescence) images, since these images capture the full boundaries of the cell, whereas fluorescence images may cut off parts of cells that are not sufficiently bright. Figures 1.13 and 1.14 show the process of defining the ROIs in sample images of NIH 3T3 and RAW 264.7 cells, respectively, and the application of these ROI to the fluorescence image. The morphologically less uniform NIH 3T3 cells required more background and variance adjustments within FIJI sofware than the simpler RAW 264.7 cells. Figure 1.14 also lists sample brightness measurements (defined as area * mean intensity) for all intracellular and extracellular regions with DAPI and FITC filters applied.

Figure 1.13: Sample processing of NIH 3T3 cell images

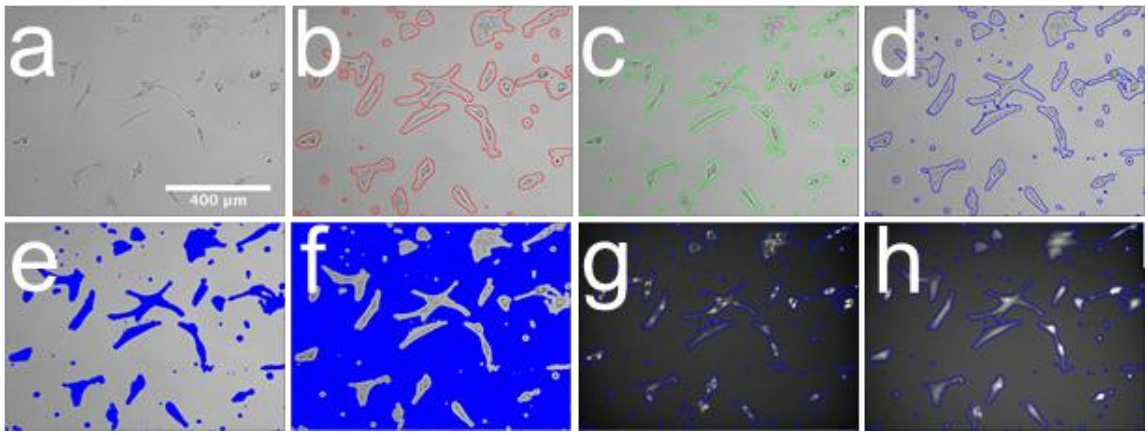

NIH 3T3 celss at 10x magnification. a) brightfield image, b) ROI after background and variance filter processing, c) improved ROI upon adjusting background subtraction and variance filter parameters, d) optimal ROI, e) threshhold mask for cells, f) inverse mask for extracellular region, g) cellular mask applied to DAPI-filtered image, h) cellular mask applied to FITC-filtered image of the same cells

Figure 1.14: Sample processing of RAW 264.7 cell images

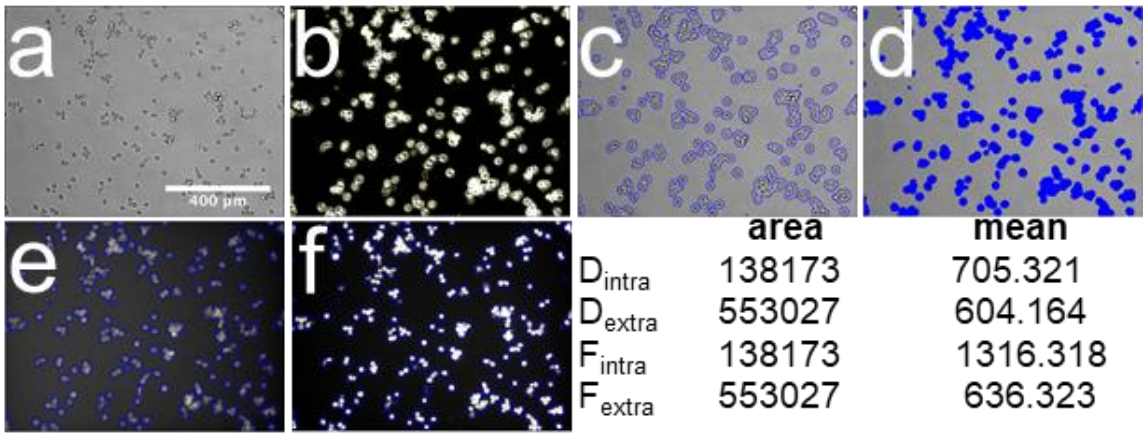

RAW 264.7 cells at 10x magnification. a) brightfield image, b) image after background subtraction and variance filter processing, c) selection of ROI, d) threshhold mask for cells, e) cellular mask applied to DAPI-filtered image, f) cellular mask applied to FITC-filtered image of the same cells, Results: area of cellular ROI is 138,173 pixels and of extracellular ROI 553,027 pixels. D and F are abbreviations for DAPI and FITC channels, respectively. The average intensity per pixel within a region is listed as the mean.

Probes **10** and **13** responded well to exogenous NO in cells. NIH 3T3 and RAW 264.7 cells were pre-loaded with 10 µM solutions of **9**, **10**, and **13** and exposed to 1 mM (releases 300 µM NO) and 200 µM (releases 60 µM NO)[302] SNAP solutions, respectively

(Figure 1.15). The NO released from SNAP (half-life of as much as 37 hours)[303] converted probe to cinnoline under aerobic conditions, as demonstrated by the increase in green FITC-channel intensity, corresponding to cinnoline emission spectra. In SNAP-dosed cells compared to untreated cells, **13** produced the smallest signal increase ($F_{dosed}/F_{un\text{-}dosed}$) among the three probes (Figure 1.15A). This smaller ratio primarily results from a higher resting-level fluorescence ($F_{un\text{-}dosed}$) for AZO-**13** versus AZO-**9**/**10**. The longer-wavelength probe **13**'s excitation and emission overlap slightly with the FITC filter set (Appendix C), such that some unreacted probe fluorescence bleeds into the channel attributed to AZO-**13** cinnoline fluorescence.

Figure 1.15: Probe response to SNAP

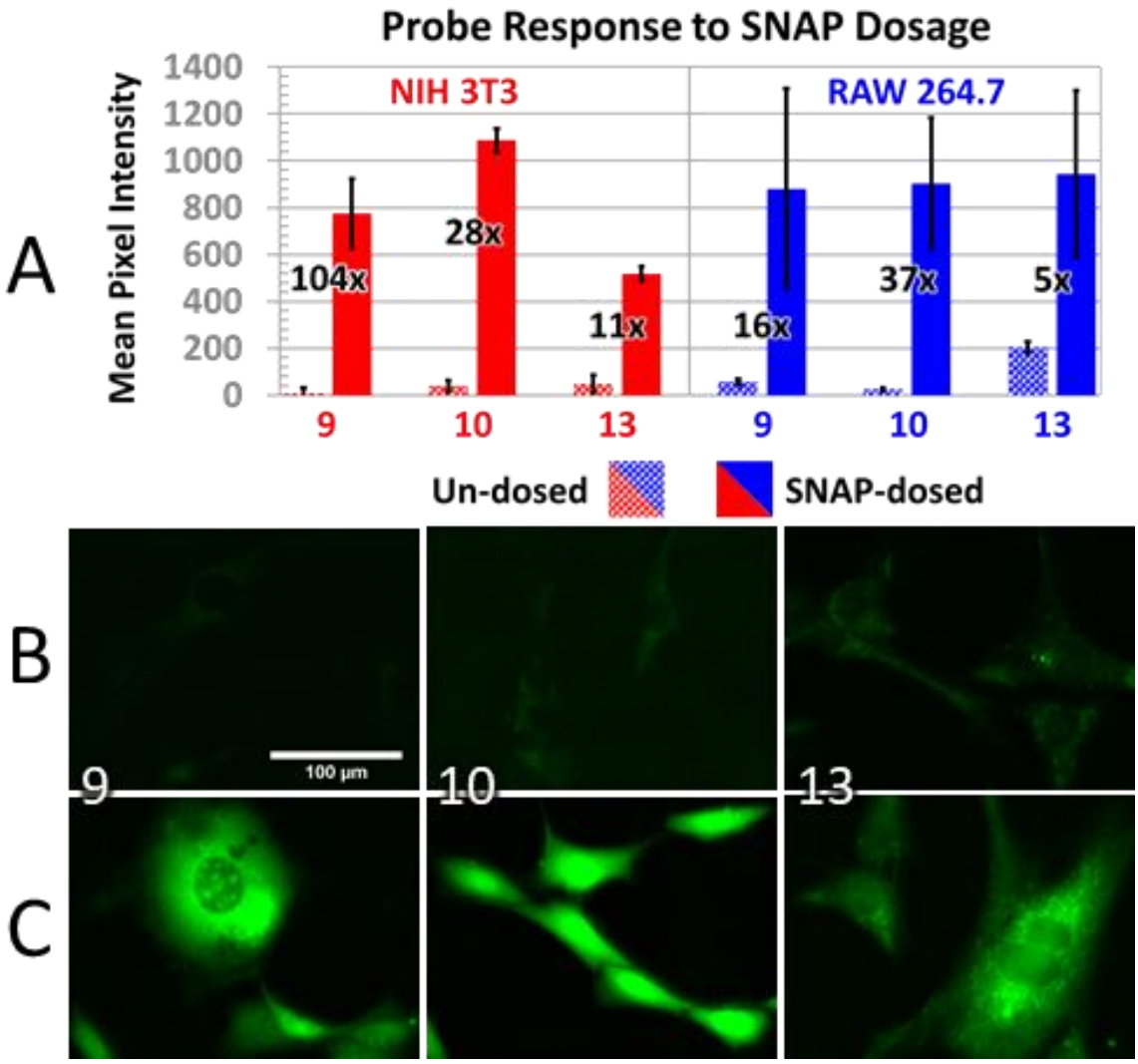

(A) Response of control (dotted bars) versus SNAP-dosed (solid bars) NIH-3T3 (red, dosed with 1 mM SNAP) and RAW 264.7 (blue, dosed with 200 µM SNAP) cells pre-loaded with 10 µM probes 9, 10, or 13. The $F_{dosed}/F_{un\text{-}dosed}$ ratio per probe and cell type is overlaid on the pertinent dotted/solid bar pairs. (B and C) 40x magnification, pseudo-colored, FITC-filtered images of probe 9, 10, and 13-loaded NIH-3T3 cells with no SNAP dosage (B) and with 1 mM SNAP dose (C).

The low AZO emission, slightly above background (defined as emission in cells exposed only to DMSO vehicle but not to any of the three probes), for probes **9** and **10** in un-dosed cells may magnify error or variation in image acquisition. Since the emission intensity is corrected by subtracting the average background from several images, values

for un-dosed cells approached zero. Error in acquiring the images, even if it decreased emission by only 5%, could significantly affect $F_{dosed}/F_{un\text{-}dosed}$. (Case in point, if the background intensity is 90% of the $F_{un\text{-}dosed}$ intensity, 5% error would double the ratio.) With a strong un-dosed signal, 5% error perturbs the ratio minimally. (With a background intensity at 10% of $F_{un\text{-}dosed}$, 5% error increases the ratio by only 1.06.) Therefore, the $F_{dosed}/F_{un\text{-}dosed}$ ratios for probes **9** and **10** may incoporate significant propagation of small error.

A saturated NO solution applied exogenously produced similar fluorescence enhancement to SNAP dosage. Cells loaded with each probe were exposed to 200 μM NO (NIH 3T3 cells) or 320 μM NO (RAW 264.7 cells) by diluting a 1.9 mM saturated NO solution into the cell medium (Figure 1.16). In both cell types, **10** produced the brightest signal and the highest ratio of $F_{dosed}/F_{un\text{-}dosed}$, while **9** was the dimmest and **13** held to its low $F_{dosed}/F_{un\text{-}dosed}$ trend, due to higher $F_{un\text{-}dosed}$.

Figure 1.16: Probe response to NO

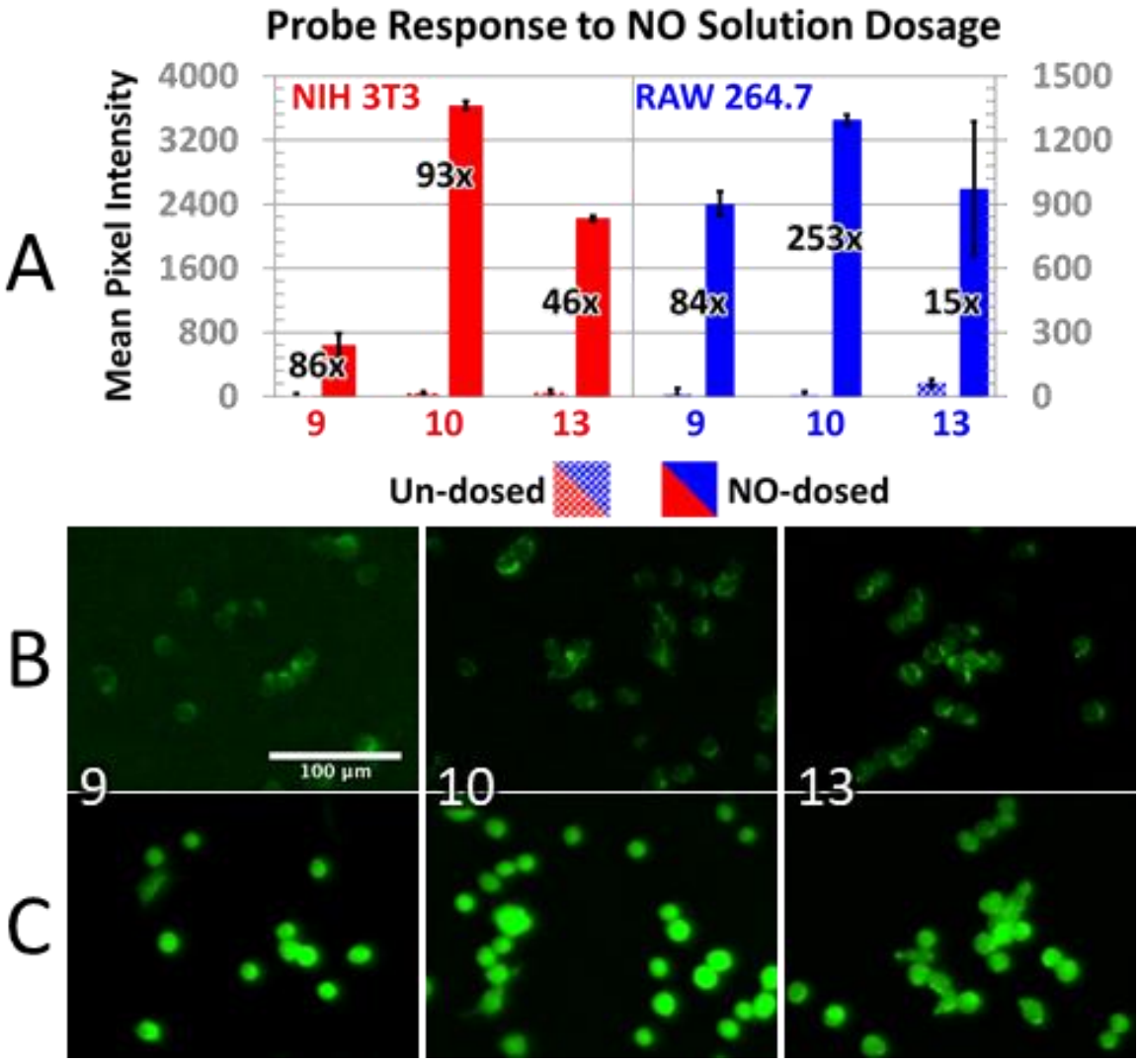

(A) Response of control (dotted bars) versus NO-dosed (solid bars) NIH-3T3 (red, dosed with 200µM NO) and RAW 264.7 (blue, dosed with 320 µM NO) cells pre-loaded with 10 µM probes 9, 10, or 13. The $F_{dosed}/F_{un\text{-}dosed}$ ratio per probe and cell type is overlaid on the pertinent dotted/solid bar pairs. (B and C) 40x magnification, pseudo-colored, FITC-filtered images of probe 9, 10, and 13-loaded RAW 264.7 cells without any NO dosage (B) and with 320 µM NO dose (C).

Having established that the probes could detect applied NO in a cellular environment, we then proceeded to verify if they could detect NO production in cells. Since nitric oxide synthases oxidize L-arginine to L-citrulline and NO, arginine supplementation would at least ensure the synthases would not lack the substrate they

convert to NO. In fact, arginine supplementation was found to significantly enhance fibroblast proliferation in wound healing, purportedly from NO signaling by S-nitrosylation of G-protein $P21^{ras}$ and by known NO activation of the ERK pathway.[304] We found that probe **13**-loaded NIH-3T3 fibroblast-derived cells dosed with 2 mM L-arginine for twenty-four hours produced a 1.7-fold increase in AZO **13** brightness over non-dosed cells (Figure 1.17).

Figure 1.17: Response of probe **13** to L-arginine

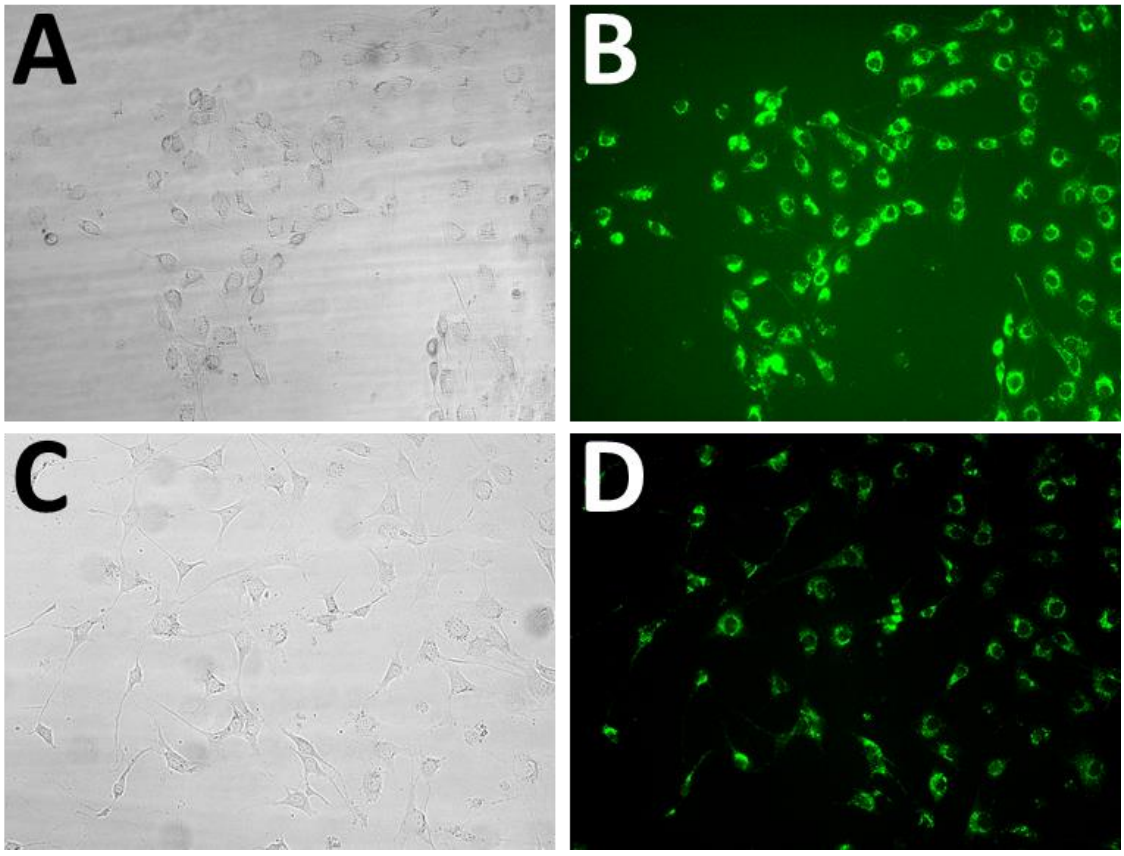

NIH-3T3 cells loaded with 10 µM probe and dosed with 2 mM L-arginine (B) produced a 1.7x increase in brightness versus non-dosed cells (D), after 24 hours. (A) and (C) are brightfield images, whereas (B) and (D) are pseudo-colored FITC-channel images.

To achieve higher NO stimulus, we turned to RAW 264.7 cells. These derive from a macrophage line, which when exposed to LPS, increase expression of inducible

nitric oxide synthase (iNOS), resulting in micromolar level production of NO. We applied 1 μg/mL LPS to the cells overnight, followed by loading with probes **9**, **10**, **13**, and DAF-FM (Figure 1.18). DAF-FM gave the brightest images, whether stimulated or not (Figure 1.18, B and C). The strong DAF-FM fluorescence in non-stimulated cells resulted in only a 1.8-fold increase in brightness from stimulated to non-stimulated cells (Figure 1.18A). DAF-FM also leaked readily from cells, to the extent that imaging was optimal after only 15-20 minutes loading, with strong signal loss after that. At the low extreme of brightness, probe **9** (NO_{550})'s stimulated signal was approximately $1/45^{th}$ that of DAF-FM, with a comparable 1.7-fold response to stimulus. Importantly, probe **10** gave the greatest (4.8-fold) response to stimulus and is brighter than NO_{550}. Due to weak fluorescence in unstimulated cells (Figure 1.18B), the increase of fluorescence ratio (turn on) is larger than DAF-FM. However, stimulated cells achieve less than 20% of DAF-FM brightness. Probe **13** was the brightest performer among the three 2-ABP probes, with a 1.9-fold increase due to LPS. In contrast to the high time-dependence of imaging of DAF-FM, due its extrusion by OATs from the cell, probes **9**, **10**, and **13** and their cinnoline products remain in cells over many hours, with the probes continously available to capture N_2O_3.

Figure 1.18: Response of probes to LPS

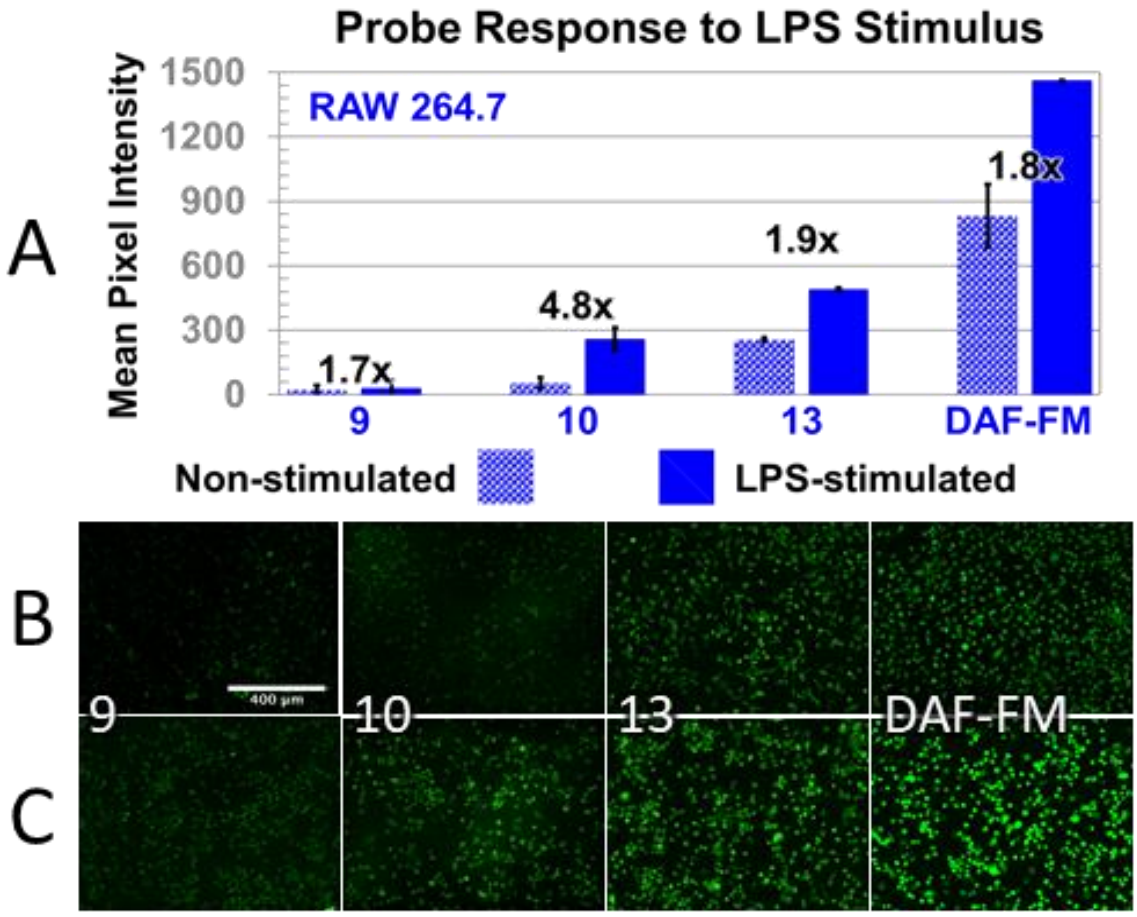

(A) Response of 10 µM 9, 10, and 13 and 2 µM DAF-FM in non-stimulated (dotted bars) versus stimulated (with 1 µg/mL LPS, solid bars) RAW 264.7 cells. The F_{stim}/F_{unstim} ratio per probe and cell type is overlaid on the pertinent dotted/solid bar pairs. (B and C) 10x magnification, pseudo-colored FITC-filtered images of RAW 264.7 cells without any LPS added (B) and with 1 µg/mL LPS added (C).

Despite the strong time-independence of loading and imaging and despite the forementioned cross-reactivity of ODP probes, DAF-FM's brightness (e.g., Figure 1.18B and C) still makes it the most popular probe for studies of NO in aerobic conditions. Rhodamines frequently exhibit similar brightness, with red-shifted fluorescence wavelengths that typically excite less cellular autofluorescence and provoke less cytotoxicity. We sought to apply the 2-ABP selectivity and ability to create a new cinnoline fluorophore from oxidized NO to an intrinsically bright rhodamine derivative,

in hopes of harnessing this inherent brightness to create a bright, long-wavelength, emission ratiometric probe. Scheme 1.32 depicts the synthesis of the asymmetric rhodamine we designed.

Scheme 1.32: Synthesis of asymmetric rhodamine 2-ABP probe.

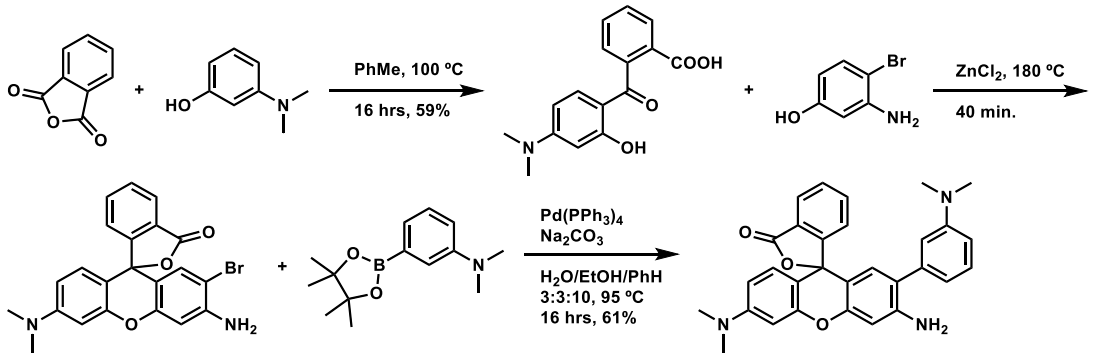

Unfortunately, we saw no fluorescence in the cinnoline product from reacting the probe with sodium nitrite in aqueous HCl. The LCMS chromatogram showed a prominent product peak with visible-wavelength absorbance maxima of 486 and 634 nm and whose peak of 489.2 m/z in the corresponding ESI-positive ion chromatogram agrees with the protonated cinnoline's exact mass of 489.19. In polar (aqueous) environments at neutral pH, the equilibrium between the fluorescent non-lactone form and the non-fluorescent lactone form in simple rhodamine derivatives trends towards the fluorescent form (Figure 1.19). Such is the case with the unreacted asymmetric rhodamine probe. Perhaps the extensively conjugated cinnoline product strongly favors the lactone form, even in an aqueous environment. If not, an efficient PET quenching mechanism could also explain the lack of fluorescence. If the cinnoline product has a higher LUMO than the orthogonally attached benzoic acid, the excited electron could transfer to the benzoic acid's LUMO, followed by non-radiative relaxation (the benzoic acid's HOMO is fully occupied) to the ground state.

Figure 1.19: Equilibrium between non-fluorescent lactone and fluorescent zwitterion forms.

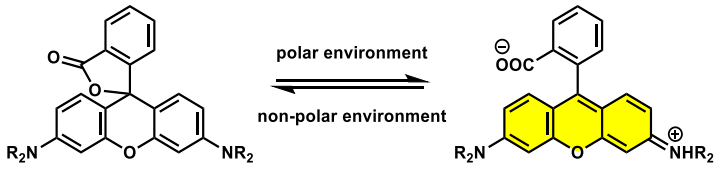

Even worse, no cinnoline product was formed after aerobic exposure of the asymmetric rhodamine to an aliquot of saturated NO aqueous solution. Neither was the N-nitroso intermediate detected by LCMS, only the asymmetric rhodamine probe. Incorporating the primary amine in the rhodamine fluorophore apparently decreases the nucleophilicity of the amine to the extent that it does not readily react with N_2O_3. Given these results, this design was no longer attractive, and no further work was pursued.

In another design, we tested the necessity of an amine to trap NO under aerobic conditions. Scheme 1.33 denotes the synthesis of a 3,3´-diaminophenyl ether probe that we hoped would condense upon NO in aerobic conditions to form phenoxazine fluorescent products. The 3-aminophenyl ether aryl ring has a strong electron-donating substituent in the dialkyl amine (σ^+_p of -1.7 for -NMe_2),[305] along with a mid-level donating substituent in the phenyl ether (σ^+_p of -0.5 for -OPh).[305] Enhanced reactivity notwithstanding, an aqueous solution of the tetra alcohol variant exposed to an aliquot of saturated aqueous NO produced no reaction, and this project was terminated.

Scheme 1.33: Synthesis of N,N,N´,N´-tetraalkyl -3,3´-diaminophenyl ether probes

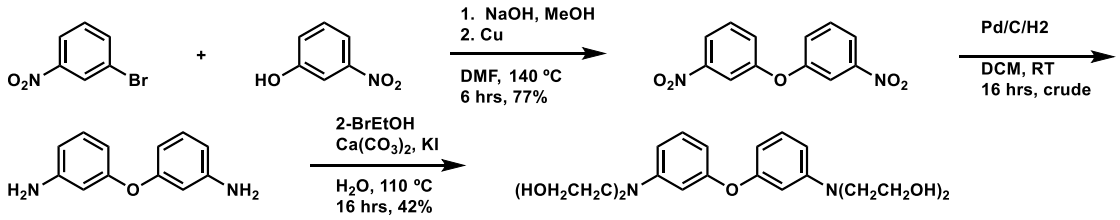

1.4 CONCLUSIONS

Probes based on the 2-aminobiphenyl core structure have proven selectivity for NO over numerous competing analytes that are common to bioimaging in that the other analytes fail to produce the same fluorescent response. The design also ingeniously incorporates nitrosonium to extend conjugation in the newly created cinnoline. The n to π* absorption transition occurs at longer wavelengths well resolved from the 2-ABP's most bathochromic absorbance peak, and cinnoline emission follows suit relative to probe emission. This characteristic leads to a ratiometric response, with probe emission decreasing as cinnoline emission increases upon reaction with NO under aerobic conditions. Alternatively, in non-ratiometric sensing, this same resolution of fluorescence minimizes background emission at the cinnoline wavelength, such that cinnoline fluorescence emanates from "darkness", with remarkable fluorescent enhancement due to NO. Unfortunately, poor orbital overlap between n and π* orbitals results in small absorptivity coefficients when compared to brighter probes, such as those based on bodipy, fluorescein, or rhodamine.

The main brunt of this research sought to ascertain how NO_{550}'s progeny, the second generation of 2-ABP probes designed by Anslyn and Yang (Table 1), would perform in cellular environments. The Yang group thoroughly investigated their performance in abiotic conditions, elucidating reaction kinetics, fluorescence wavelengths and response to NO, and brightness of probe and azo products. They also verified the retention of NO_{550}'s selectivity despite the variations upon the core structure. Perhaps here, the selectivity could have been tested not only as it was - in non-competitive experiments, where the probe is exposed to a potential analyte and the fluorescent response compared to that for NO/O_2 – but also in competitive experiments,

where fluorescent response to NO/O_2 in the presence of a potentially competing analyte is compared to that for NO/O_2 alone.

Preliminary studies by Derek Hernandez showed that probes **5**, **10**, **11**, and **13** all loaded into cells and produced a fluorescent response. Loading concentrations of 50 µM or higher proved toxic, with noticeable cell death at 100 µM. FITC-channel fluorescence from probe **11** faded over time. Since the extracellular fluorescence remained negligible, this fading pointed to further reaction to a non-fluorescent product. The shorter fluorescence wavelengths for probe **5** and its azo product were not compatible with available filter sets in the Shear lab, provoke greater cellular auto-fluorescence, and are more damaging to cells. Thus, we focused on probes **10** and **13**.

The two probes successfully responded to both exogenous and endogenous NO in NIH-3T3 and RAW 264.7 cells. For reasons not yet determined, probe **13** generated more FITC-channel fluorescence than either NO_{550} (**9**) or probe **10** under resting, non-dosed/non-stimulated conditions. Fluorescent enhancement upon dosing/stimulating therefore suffered in comparison to the other two probes. Probe **13** was the most similar to DAF-FM in brightness in resting cells; DAF-FM also produced attenuated enhancement in our hands. Although this attenuation reduces sensitivity to varying levels of NO, the stronger signal in resting cells establishes a value for non-dosed/non-stimulated fluorescence easily discriminated from cellular autofluorescence, reducing error in calculations of fluorescence enhancement from dosing/stimulating. In contrast, NO_{550} and probe **10** in resting cells often fluoresce barely above cellular autofluorescence and experimental noise – unsurprisingly as such is the design of the probes at low NO levels. Higher resting brightness notwithstanding, probe **13** produced a 1.7-fold response to twenty-four hours of exposure to L-arginine.

Probe **10** provides the best compromise between sensitivity/response and brightness. When high levels of NO were applied, whether from the NO donor SNAP or through an aqueous NO solution, true to abiotic results, it was usually the brightest among probes **9** and **13** in both cell types. However, **10** was not the brightest among the two other probes, and certainly not brighter than DAF-FM, in response to LPS stimulation of iNOS production of NO in RAW 264.7 cells. In almost every scenario tested, **10** yielded the greatest enhancement after stimulus. It also proved non-toxic to RAW 264.7 cells in concentrations up to 40 μM, with >93% viability rate after four hours exposure, comparable to >95% for untreated cells.

Both probes **10** and **13** are an improvement over first-generation NO_{550} in brightness, and probe **10** in response. A direct comparison to DAF-FM is difficult due to cellular organic anion transporter pumps' removing loaded probe and triazole product from cells, causing a troublesome and problematic time-dependence of imaging. If imaged within an hour of loading (preferably 20-30 minutes), DAF-FM produces the brightest results, although with small stimulus-provoked signal enhancements. In our hands, even ten minutes between images resulted in discernable DAF-FM triazole signal loss in cells. In contrast, our probes were imaged twenty-four hours after loading, with no noticeable signal loss. The attenuated fluorescence enhancement after stimulus derives primarily from the high non-stimulated fluorescence. Potentially, this high resting fluorescence reflects DAF-FM cross-reactivity, as it is not present in NO_{550} and probe **13**. In abiotic conditions, stoichiometric reaction of **13** with NO showed greater conversion to cinnoline than that reported for DAF-FM to its triazole product. Unless the cellular environment changes this dynamic, the stronger DAF-FM resting fluorescence cannot be attributed to higher reactivity with lower concentrations of NO.

We also attempted a design that incorporates the 2-ABP core into a rhodamine fluorophore in hopes of producing a long-wavelength, emission-ratiometric set of probes with strong, inherent rhodamine brightness. In aqueous solution at neutral pH, the cinnoline product of this asymmetric rhodamine proved non-fluorescent, however, probably due to favoring of the dark spirolactone form. Worse yet, due to conjugation within the rhodamine fluorophore, the primary aniline was insufficiently nucleophilic to trap the nitrosonium moiety when exposed to an aqueous solution of NO in aerobic conditions.

Similarly disappointing was the second design N,N-dialkyl-3-aminophenylether. Rather than condensing upon nitrosonium to form a phenoxazine fluorophore, this probe attempt also failed to react with an aqueous solution of NO. The aryl rings lack the nucleophilicity of an aniline, specifically an aniline with no electron withdrawing groups to lower its nucleophilicity.

1.5 FUTURE WORK

Both probes **10** and **13** are attractive options for bioimaging of NO in cells. SciFinder currently lists twenty-four vendors for NO_{550}, and Sigma-Aldrich also sold it for a time. Named NO_{530} (**10**) and NO_{562} (**13**), both probes should supplant NO_{550} in the market, due to both/either their greater response and and/or brightness and to their more homogeneous distribution in the cell. Certainly, these 2-ABP probes enable more consistent experimentation, as they do not share the DAF series' high time-variability of signal.

At 10 μM loading concentrations, probe **13** somewhat compares to DAF-FM's brightness. Higher loading concentrations, with cytotoxicity established per cell type and length of experiment, could close the gap. The stronger basal fluorescence of DAF-FM

and **13** versus **9** and **10** should be investigated, starting with competing L-arginine substrates and iNOS inhibitors, such as L-N^{ω}-monomethyl arginine acetate (L-NMMA) or L-N^{ω}-nitroarginine methyl ester (L-NAME), to determine if probe **13** fluorescence decreases below that for basal levels of NO production. If the decrease reached basal fluorescence for probes **9** or **10** (slightly higher than cellular autofluorescence and instrument noise), then **13**'s brightness would be attributed to higher reactivity with the resting NO concentrations – the most sensitive of the three. More appropriate excitation/emission filters would eliminate probe bleed-through into the FITC channel that also increases **13**'s resting brightness.

The N-acetamide moiety in probes **10** and **13** provides an elegant synthetic handle to append functionalities, such as cell-compartment directing groups. For example, replacing acetyl chloride with chloroacetyl chloride enables ligation of a nucleophile by S_N2 substitution. We performed such a synthesis on the NO_{562} trisaniline precursor and attached aminodiglycol to enhance water solubility, with qualitatively positive results by eye and by ^{1}H NMR. With the adoption of the parent probes by scientists, the mitochondrial triphenylphosphonium group should probably be the first group appended.

Probe **5** should be evaluated with appropriate filters, as it is easily the brightest of all candidates.

Finally, employing the 2-ABP system as a PET quencher, not as the fluorophore, by the Guo group is an intriguing approach that should be investigated further. One could envision incorporating 2-ABP into the bright and biologically established fluorescein or rhodamine fluorophores (Figure 1.19), with the library of variants available to dial in the desired fluorescence wavelengths. Computational studies would establish which variants provide better matches between the HOMO of the 2-ABP moiety and the HOMO of the xanthene (or other, i.e.; N_R, CR_2, SiR_2, or PO_2; derivatives), with the

HOMO of the former of higher energy than the latter, as well as the LUMO of the resulting cinnoline and the LUMO of the xanthene, with the LUMO of the former of higher energy than the latter.

Figure 1.20: Possible designs for 2-ABP probes as PET quenchers of xanthene dyes

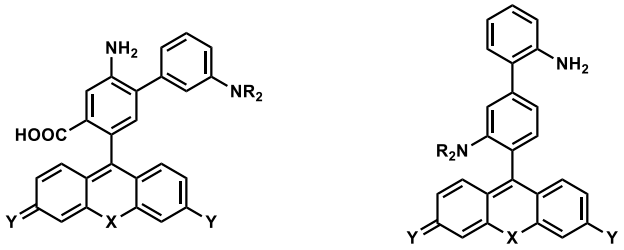

Y = O or NR´$_2$; X = O, NR´, S, CMe$_2$, SiMe$_2$, PO$_2$, etc.; R and R´ = Me, fused alicyclic, etc.

Chapter 2: Sequenceable Carbamate Oligomers

2.1 INTRODUCTION

The tertiary and quaternary structures of biological polymers DNA/RNA and proteins are crucial to their performance in the organisms they inhabit. The sequencing of protein and DNA biological polymers has shown how determining to these higher-order structures are both the order and the identity of their individual components. Substitution and deletion studies reveal that small changes can significantly perturb the efficient performance of these polymers in their environments. Such a dependence on constitution and order should translate to non-biological or non-natural polymers. Potentially, synthetic polymers could achieve the heralded selectivity and efficiency of biological polymers. The allure of this possibility has birthed the field of sequence-controlled and sequence-defined polymers. The synthesis of these types of polymers has been well-established and continues to be developed. Determining the sequence of these polymers, not as much.

2.1.1 Sequence-Defined Polymers (SDPs)

Polymers whose repeating units, or mers, are connected in identical order and number are considered sequence defined polymers. This type of polymer, with a polydispersity index (PDI) of one, stands in contrast to most mass-produced synthetic polymers of higher PDIs found in plastics, synthetic textiles, vulcanized rubber, and the like. The control of sequence and length of SDPs demands a more cumbersome iterative synthesis than the customary one-pot synthesis for most traditional polymers. Historically, SDPs were limited to those produced under biological controls, such as DNA and proteins. With the advent of solid phase synthesis (SPS), iterative syntheses

have been simplified and eventually automated, conquering the fabrication of milligram amounts of a 167-amino-acid protein in less than seven hours, not including time for purification and folding.[306]

2.1.1.1 Biological SDPs

The tight control of sequence ensures reproducibility of biological polymer performance. Among the most famous SDPs, the polynucleotide DNA encodes the genetic blueprint of its organism. For protein synthesis, three sequential base pairs denote a specific amino acid (codons), and the order of the codons specifies the order of connection of their respective amino acids. The DNA sequence must persist throughout all replications to preserve the structure of the proteins, as substituting or deleting a crucial amino acid or several amino acids may provoke deleterious effects. DNA therefore serves as an example of SDPs functioning as data storage devices and has been estimated to be 10^4 times more space-efficient than advanced hard drives (2019).[307]

Enzymes perform as enviably efficient and selective catalysts for their specific functions; few synthetic catalysts can compete with enzymes in reaction rates and/or substrate selectivity. Their sequence, the primary structure of the protein, determines its secondary structure (e.g., α-helices, β-sheets, hairpins) that affect the folding and topology of the protein (tertiary structure). This in turn influences protein affinity for its binding partners; i.e., other proteins, lipids, or ions; and thus its quaternary structure. Selective substrate binding sites, proton or electron transfer shuttles involved in catalysis, and co-factor binding all depend on the amino acid sequence. From an inverse perspective, point-mutation experiments exploit this sequence-dependency to elucidate the amino acids most crucial to protein performance.

2.1.1.2 Non-natural SDPs

The four nucleotides available to DNA or RNA and the twenty amino acids that form proteins capacitate the great diversity found across the organisms of this planet. This diversity has been harnessed for purposes outside biology, for instance to design sensors and as catalysts.[308-317] The successful implementation of these SDPs outside their biological applications inspired a quest to markedly expand the toolkit from the standard nucleotides and amino acids to non-natural ones and then to other molecules, quite different from nucleotides and amino acids, that can perform similar roles in iterative connectivity, structure determination, and catalysis.

2.1.1.2.1 Peptidomimetics

Expanding beyond the limited subset of biological monomers to non-natural repeat units with varying connectivity has resulted in a remarkable variety of SDPs. The closest mimics of peptides consist of alpha-peptides with non-natural side chains, as well as peptoids; aza,[318] aminoxy,[319] and hydrazinyl[320] peptides; and beta,[321-323] delta, and gamma[324] peptides (Figure 2.01).[325-326] The longer beta, delta, and gamma amino acids avail multiple substitutions, if sterically accessible, and ring structures on the backbone of the same monomer, with the potential for greater complexity of the polymer versus natural peptides. A myriad of examples exists for peptoids, and their secondary and tertiary structures have been extensively studied.[327-329] One step further removed from peptides are carbamates (urethanes)[330] and ureas.[331] Ureas are typically more inert than amides and carbamates to hydrolysis, and their disubstituted (N,N´) variants offer two hydrogen-bond donors that tend to enhance secondary structure formation and stability[332] and that can act as a recognition units for anions when not participating in structure-stabilizing hydrogen bonds.[333] Carbamates offer similar stability to ureas, with two hydrogen-bond acceptors per occurrence.

Figure 2.01: Common peptomimetic moieties in non-natural SDPs

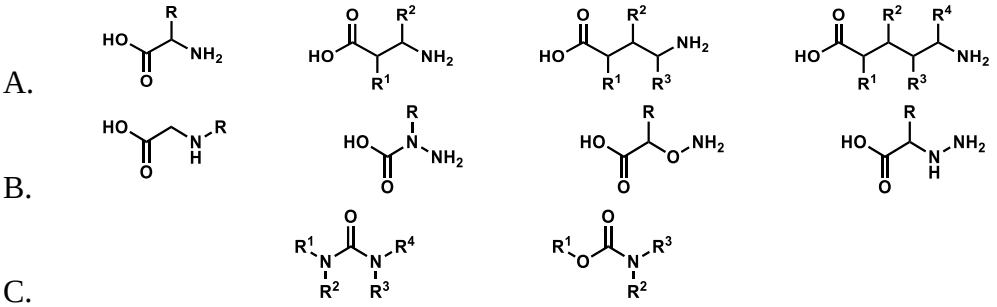

From left to right, A) natural α peptide backbone with non-natural sidechains R, then β, γ, and δ peptides; B) peptoid, aza, aminoxy, and hydrazinyl peptides; and C) ureas and carbamates. Except for peptoids, R substitutions may be occupied by hydrogen.

2.1.1.2.2 Nucleotidomimetics

Non-natural nucleotides exemplify another preliminary step away from the certainty of biological SDPs. As secondary structures for peptides motivated peptidomimetic studies, so did the base-pairing order and the typical resulting single (intra strand) or double (inter strand) helix structures for oligonucleotide mimicry. Whereas most fabrication of peptidomimetics is entirely synthetic, some non-natural nucleotides are amenable to polymerase transcription and replication.[334] To maintain base complementarity, hydrogen bonding interactions between corresponding base pairs are conserved, but some non-interfering variability in structure is introduced. These adaptations resulted in non-natural DNA and RNA synthesized by biological machinery.[335-336] Interestingly, hydrogen-bonding interactions are not essential to base pairing by polymerases. Mimicking the size, shape, and polarity of a natural base pair (such as difluorotoluene for thymine) results in modified polymerases incorporating a non-natural nucleotide according to a natural template. These optimized polymerases tolerated one of these non-natural variants that incorporates varied side chains connected through a rigid alkyne, distant from the enzyme and base pair recognition site (Figure 2.02).[337] Similarly, DNA ligases can function with modified monomers and are also able

to ligate templated non-natural 3-mers and 5-mers, facilitating the incorporation of basic, acidic, aromatic, aliphatic, and hydrophobic/philic side chains into the SDP.[338] Employing RNA or single-strand DNA as a template and incorporating reactive termini into non-natural nucleic acid variants enables templated synthesis, discarding the limitations imposed by enzyme compatibility. Commonly, reductive amination or click chemistry produces the ligation of complementary-sequence monomers paired to their template.[339] Loosening the restraints even further, phosphoramidite-chemistry-enabled non-natural nucleotides are compatible with solid phase synthesis. This approach requires no template or enzyme, but the greater flexibility in monomer design is counteracted by the limitations of the time-consuming process that produces 150-mer oligonucleotides on the average, with a maximum of ~1000,[340] whereas polymerases have achieved 1500 monomer lengths.[341]

Figure 2.02: Non-natural base pairs Ds and Px

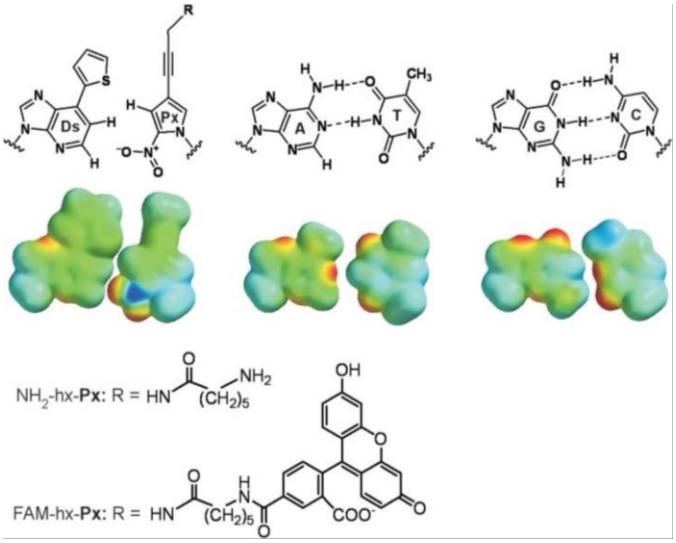

Ds and Px structures compared to natural pairs A to T and G to C, above their space-filling models (deoxyribose not shown, R = Me). The R group in Px is tolerated by a modified polymerase. The aminohexanamide attachment did not interfere with replication, even when amide-coupled to 5-carboxyfluorescein. Thirty cycles of PCR amplification (10^7-fold) of DNA fragments incorporating

the Ds/Px base pair maintained >99.9% fidelity per cycle. Figure reproduced with permission from[337].

2.1.1.2.3 Less Mimicry

Moving further from the imitation of natural SDPs escapes their limitations but also produces a nearly limitless expanse of non-natural SDPs. The manifold synthetic approaches fulfill the goal of synthesizing a wide variety of SDPs; however, doing so to create secondary, tertiary, and even quaternary structures that promote substrate selectivity and catalysis requires significantly more design, often by searching databases and employing artificial intelligence. Aromatic oligoamides retain the amide hydrogen-bonding stabilization of peptides and nucleic acids and tend to adopt similar structures, influenced also by aromatic stacking interactions (Figure 2.03A).[342-344] Some designs have produced trihelices (parallel and antiparallel, depending on solvent polarity),[345] tetrahelices,[346] and even tubular stacks.[347] Bis-aminotriazine polymers contain another backbone rich in hydrogen-bond donors and acceptors and prone to pi-pi interactions (Figure 2.03B). The decreasing reactivity of cyanuric chloride with each substitution imparts stepwise control of substitution, with side-chain attachment at -20 to 5 °C to the unsubstituted trichlorotriazine, polymer chain elongation on the monosubstituted dichlorotriazine at room temperature or with mild heating, and priming of the disubstituted monochlorotriazine for the next monomer addition with heating above 80 °C (Scheme 2.01). According to simulations, this polymer structure has the propensity to self-assemble into helices, sheets, and ribbons.[347-348] A bis-aminotriazine was also incorporated into the backbone of a gamma-peptide with the sidechain emanating from the remaining position on the triazine.[349] Fmoc solid-phase synthesis of triazinyl amino acids with hydrophilic cationic or hydrophobic aromatic residues attached as sidechains provided several oligomers with tunable amphipathicity.

Figure 2.03: Examples of non-natural SDPs based on oligoamide and triazine backbones

A)

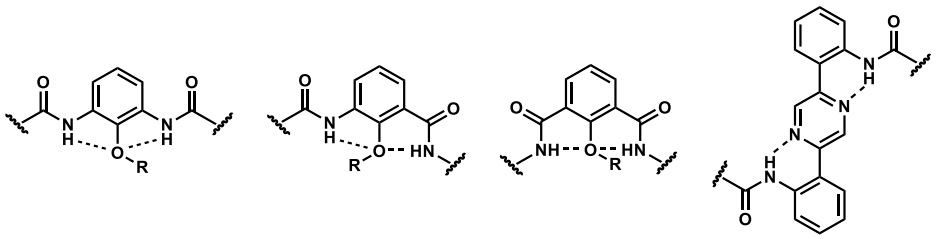

B)

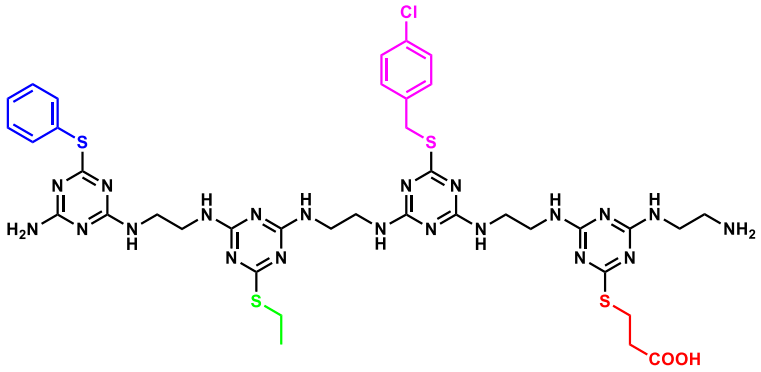

Scheme 2.01: Temperature-controlled stepwise trisubstitution of cyanuric chloride

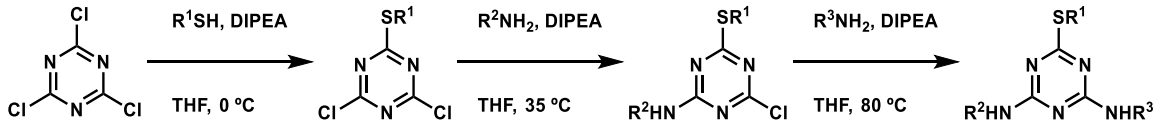

2.1.1.3 Applications of SDPs

2.1.1.3.1 Data Storage

SDPs may function as data encoders; binders, encapsulators, and transporters; catalysts; and therapeutic drugs.[350-353] For data storage, the number of independent monomers establishes the n-ary code, with reports of binary, ternary, and quaternary systems.[354] In one example, collision-induced dissociation (CID), negative-mode MS/MS analysis interpreted a binary code of hydrogen vs methyl-substituted oligocarbamates, with an octamer serving as a byte (Figure 2.04).[355] With CID,

fragmentation occurs only at the backbone O-alkyl carbonyl carbon bond, and the ready ionization of the α-terminus (carboxylic acid) provides facile negative-mode detection. Somewhat akin to random termination in Sanger sequencing (described later in this document), the ionization spectrum provides m/z ratios for fragments starting at the α-terminus up to the point of cleavage, with similar probability of fragmentation at any of the linkages. Subtraction of the largest (unfragmented) mass from the next largest therefore yields the molecular mass of the ω-terminal mer (terminus opposite to the carboxylic acid), and so on moving from the largest ω-terminal mass towards the smallest α-terminal fragment. For longer oligomers, the ionizing yield decreased, but inclusion of a second carboxylic acid, at the ω-terminus, restored the clear detection of each fragment, although it added the signal set of the previously neutral but now negatively charged complementary fragments.[356] Although the simultaneous α-to-ω fragmentation pattern and ω-to-α complementary fragmentation pattern provide a robust doubly confirmed molecular mass for each mer, the ionization spectrum doubles in number of peaks. For longer oligomers, the spectrum could prove prohibitively complicated. Moving to higher number systems (from binary to n-ary) also complicates the spectrum, to the extent that deciphering software was created.[357] Not limited to language code, these SDPs may also function as barcodes; the same binary oligourethanes were embedded in plastic encasing of commercial products for anti-counterfeit measures.[355]

Figure 2.04: Tandem MS sequencing of binary-code oligourethanes

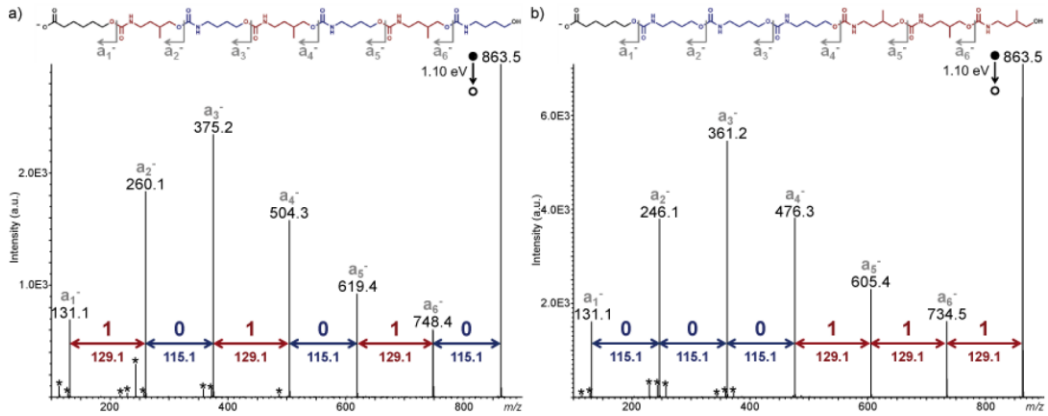

Negative mode ion spectra of two different bytes of non-substituted (0) and methyl-substituted (1) binary-code oligocarbamates. Figure reproduced with permission from reference[356].

2.1.1.3.2 Antimicrobials

With the increasing risk of antibiotic-resistant bacteria, SDPs provide access to intricately designed structures to exploit weaknesses in microbial armor. The enriched anionic phosphate groups, relative to mammalian cells, at the bacterial cell membrane exterior electrostatically attract cationic residues, but the enriched hydrophobic lipid layer repels water-soluble moieties. Fine-tuning of the cationic versus hydrophobic character of an SDP could simultaneously attract membrane disrupting or permeabilizing agents to selectively attack bacterial over mammalian cells.[358-360] A set of triazine-based oligomers incorporated side chains of aliphatic amines or guanidines that are protonated at physiological pH and of hydrophobic phenyl residues. A trimer of two aliphatic amine monomers and one phenyl monomer exhibited significant antimicrobrial activity. The stepwise triazine synthesis obviates the need for protecting groups, so that assembly of the trimer is less expensive and more industrially amenable than that for peptides or peptidomimics.[361] Furthermore, proteases ignore the triazine backbone, overcoming the susceptibility of antibacterial peptides to rapid degradation.

Also resistant to proteases, oligothioetheramides, with aliphatic amine side chains but with varying degrees of hydrophobicity on the backbone – according to chain between the dithiols employed in the synthesis of the oligomer (Figure 2.05)– were toxic to clinically relevant pathogens with minimum inhibitory concentrations of 0.5 to 5 μM. This pathogen toxicity in up to 20% serum-supplemented cell medium did not extend to RBCs or HEK 293 cells.[362] The appropriate combination of hydrophobicity and positive charge, as well as the conformation of the oligomers, factored into the disruption of the cell membrane. The toxicity of a *meta*-substituted phenyl group on the backbone of an oligomer markedly changed versus that of a *para*-substituted, otherwise identical oligomer.

Figure 2.05: Thioetheramide oligomers as antibiotics

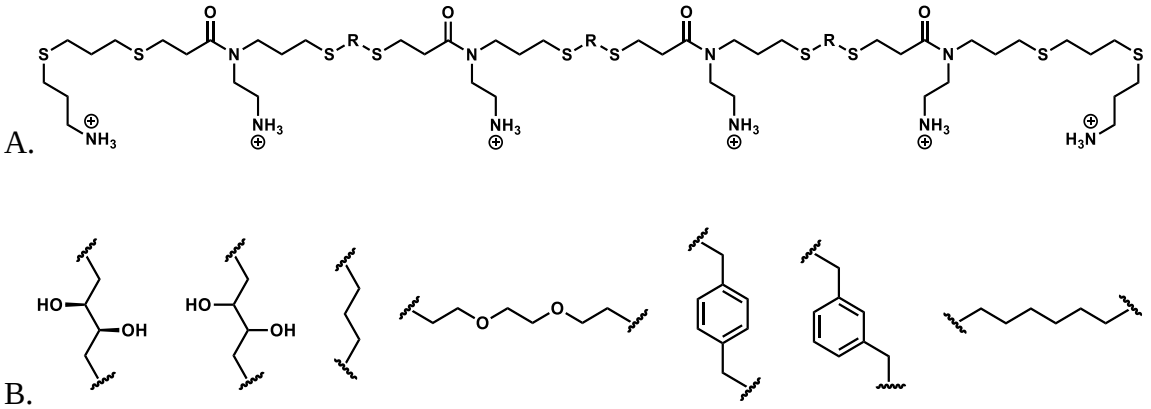

A) Oligothioetheramide core structure with varying hydrophobicity on the backbone to fine tune the antiobiotic balance between positive charge and hydrophobicity. B) The possible R groups incorporated into the oligomer backbone for a combinatorial library of possible antibiotics.

2.1.1.3.3 Catalysts

Higher-order structure imparts the selectivity, enantioselectivity, and catalytic activity to enzymes. Although a helix classifies as only secondary structure, it can certainly affect the approach trajectories between reagents. Its emanating side chains near the binding site may reversibly react with a substrate to lower activation-energy

barriers. In the case of oligoureas, the urea moiety in the backbone may also lower barriers through hydrogen-bonding to a substrate. Enantiomerically pure urea hexamers formed from 1,2-diaminoethane monomers (Figure 2.06) – with a stereogenic methyl, isopropyl, or isobutyl side chain on the ethyl portion – catalyzed the enantioselective conjugate addition of malonates to nitroalkenes (>95% ee, complete conversion with 0.1 mol % catalyst, 10 mol % achiral base). The high enantiocontrol in 2.5-helix-forming pentamers and hexamers was lost with monomers and dimers and diminished in trimers and tetramers.[363]

Figure 2.06: Oligourea catalyst for the addition of malonates to nitroalkenes

A.

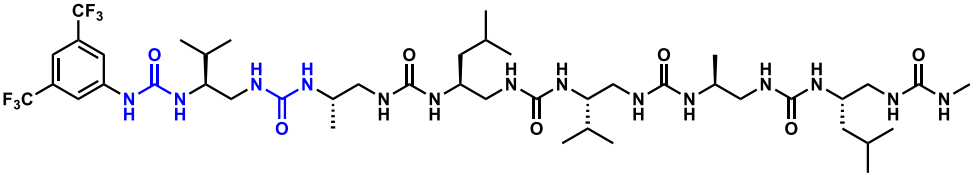

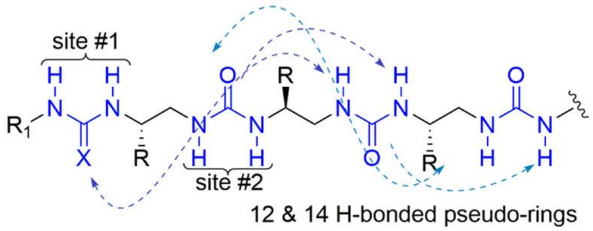

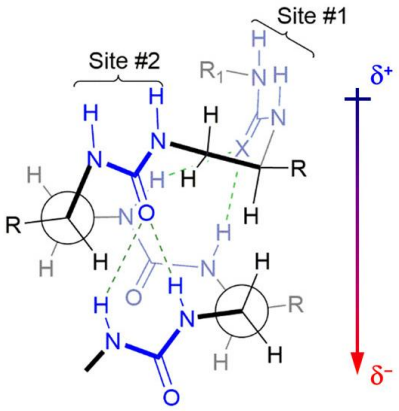

B.

A) Structure of oligourea catalyst. B) top: hydrogen-bonding that foments secondary helical structure, bottom: the helix that begets >95% ee for the reaction, and the molecular dipole of the helix. Figure reproduced with permission from [363], https://pubs.acs.org/doi/10.1021/jacs.7b05802. Further permissions related to the material excerpted should be directed to the ACS.

2.1.1.4 Sequencing SDPs

At times, the sequence of a sequence-defined polymer may not be known. To read SDP memory storage and barcoding, it must be decoded. Promising SDP candidates selected from combinatorial libraries have a particular sequence out of all possible combinations of sequences equal to the number of available monomers to the nth power of an n-mer (for a straight-chain polymer). To gain insight on their structure-activity relationships, their sequence must be elucidated.

Crystal structures are the gold standard for reporting sequence and spatial organization of polymers. The challenge lies in obtaining a crystal that can be analyzed for structure, and high-throughput screening systems have been developed solely for this purpose.[364] Furthermore, the low sensitivity of the analysis requires large amounts of pure sample. Lacking an acceptable crystal, the common approach is to sequence a polymer by clipping it to smaller oligomers or to monomers. Due to the variation in oligomer connectivity, backbone, and side chains, few sequencing approaches exist, mostly directed towards peptides and oligonucleotides.

2.1.1.4.1 Peptides

The amide bond connection in the peptide backbone is resistant to cleavage in physiological conditions without the aid of enzymes. More rigorous conditions can lead to hydrolysis or transamidation, but with little selectivity for one connection over the others. The end result is a mixture that informs on the identity and relative proportion of amino acids that constitute the peptide, without any information on the order in which they were connected.

2.1.1.4.1.1 Edman Sequencing

One method to determines the amino-acid ordering and constitution of peptides was reported by Edman in 1950.[365-366] His iterative approach to peptide degradation

conserves order information. An isothiocyanate, typically phenylisothiocyanate, reacts at the N-terminus to form the corresponding thiourea. Under anhydrous acidic conditions (TFA, to minimize random hydrolysis of the backbone) that activate amide carbonyls to nucleophilic attack, the N-terminal thiourea adds to the most proximal carbonyl, displacing the remainder of the peptide with the formerly penultimate amino acid as the new N-terminus. The resulting unstable thiazolinone cycle, with the sidechain corresponding to the truncated amino acid, has markedly different solubility and volatility from the remaining peptide. Following its separation by extraction, the thiazolinone is converted to the stable cyclic thiohydantoin in aqueous acid for analysis, and then the cycle starts again (Scheme 2.02).

Scheme 2.02: Edman degradation of peptides

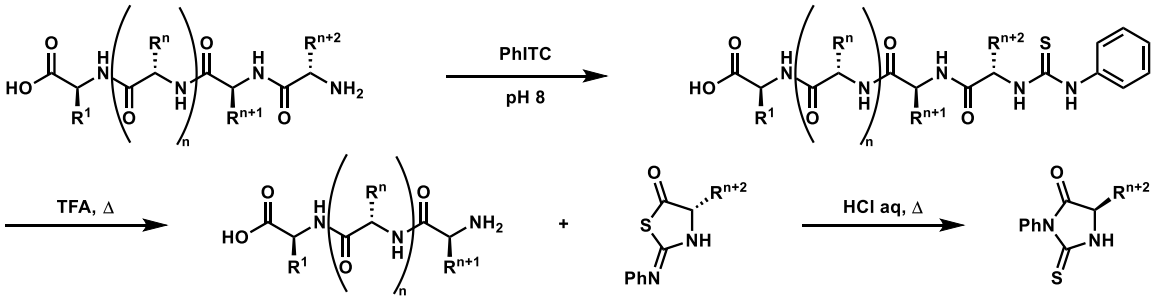

Despite high yields, the iterative nature of the process without stringent purification dictates that n should be less than 50, with higher accuracy for 30 residues.

Despite high yields, this sequencing works well for peptides up to fifty residues in length. To sequence longer ones, including proteins, the peptides are first clipped to smaller pieces with endopeptidases (trypsin, pepsin) or by chemical reaction (cyanogen bromide) that cleave at certain amino acids. The overlap of peptides clipped by one endopeptidase versus another and/or versus chemical cleavage establishes the whole protein sequence.

The Edman degradation has been automated and optimized, given the interest in sequencing not only proteins but also selected peptides from combinatorial libraries. Gas-phase and pulsed-liquid sequencing of a small protein, or of protein digests, individually adsorbed on a membrane have lowered required sample size to picomole levels.[367] Either mass spectroscopy or HPLC, by comparing elution time to thiohydantoin standards of the twenty amino acids and their derivatives that appear in proteins and peptides, reveal the identity of the amino acid. Optimization notwithstanding, one complete cycle takes about an hour.[368] The process times multiply for peptides longer than fifty amino acids that require clipping with at least two endopeptidases and sequence overlap comparisons. Furthermore, proteins with the N-terminus derivatized, from post-translational modifications or from derivatizations in their preparation, purification, and isolation cannot undergo Edman degradation.

2.1.1.4.1.2 Mass Spectroscopy

MS analysis has in general supplanted the more cumbersome Edman sequencing, especially tandem MS sequencing.[369-370] Typically, a single protein or even a mixture of proteins is treated with endopeptidases to obtain several fragments based on the propensity of the enzyme to break the peptide backbone at a certain amino acid recognition unit. These then undergo MS/MS fragmentation (the re-fragmentation – by collision-induced dissociation, photodissociation, or ion-molecule reaction – of selected ions), which breaks both the peptide backbone and sidechains according to the weakness of the bonds. Since the peptide backbone is quite simple, the three fragmentation possibilities are named according to the bond that is cleaved (Figure 2.07). Consequently, the ion spectrum, based solely on backbone fragmentation, for certain sequences can be predicted and assembled into a database of theoretical peptide fragmentation patterns. Screening the results from tandem MS of a protein digest versus

the database, according to the means of digestion, produces hits for the corresponding peptide sequences. If enough of these hits appear in a protein of knowns sequence, then with a certain confidence the digested peptides can be assigned to that protein. Digests from impure mixtures may still reveal peptide sequences, since the resolution of the first ionization (from MS1) purifies the ion that is then subjected to further fragmentation (in MS2).

Figure 2.07: Fragmentation sites on the peptide backbone

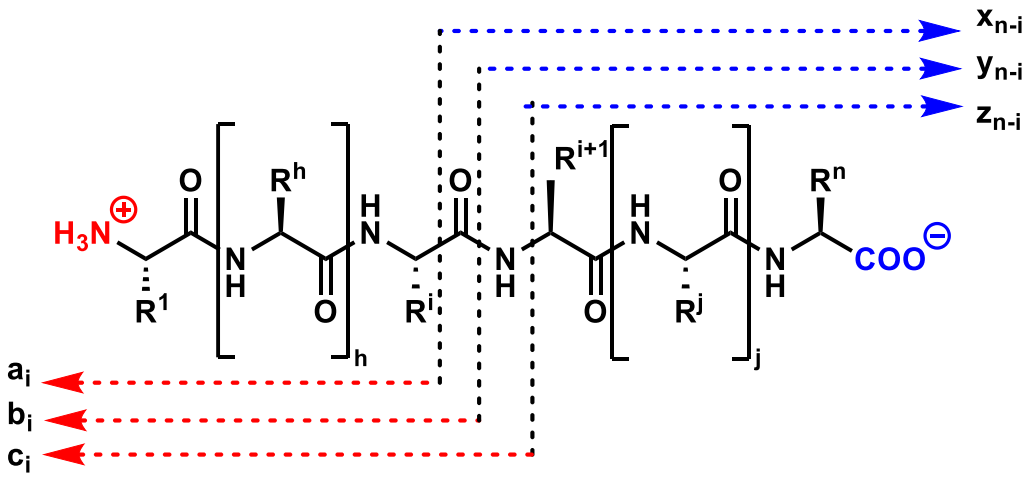

Fragmentation produces a_i, b_i, or c_i masses in positive ionization mode (red) or x_{n-i}, y_{n-i}, or z_{n-i} in negative ionization mode (blue).

Another approach, protein-ladder sequencing, captures peptide sequences, typically by matrix-assisted laser desorption ionization - time of flight detector (MALDI-TOF), after incomplete N-to-C terminus degradation of the protein or its digests.[371] Several Edman cycles of N-termini reacting with phenyl isothiocyanate poisoned with a small proportion of non-cyclizing phenyl isocyanate (Scheme 2.03) produce a population of fragments representing the sequence at each level of truncation. The mild, matrix-assisted ionization tends to yield ion patterns with minimal fragmentation, such that subjecting the Edman-treated sample to MALDI-TOF reveals a ladder pattern pertaining

to each intermediate in the sequencing (capped by a phenyl urea at the N-terminus), from the fully intact peptide to the product of the final Edman cycle. Since each Edman cycle need not fully react, the reaction times for traditional Edman cycles can be shortened or temperatures reduced, leading to fewer side reactions that can complicate the MALDI-TOF readout or remove post-translational modification residues. In fact, a phosphorylated serine survived the multiple Edman cycles and ionization for its mass contribution to appear in the MALDI-TOF spectrum. This ladder approach is also amenable to high-throughput processing, given that ladders for multiple samples may be created in their respective wells, to be then analyzed by MALDI-TOF.

Scheme 2.03: Isocyanate poisoning of Edman degradation

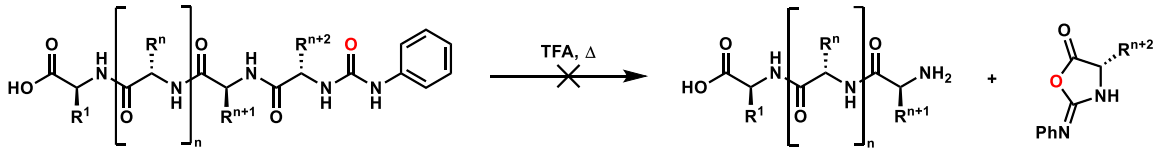

The isocyanate, lacking the sulfur nucleophile, does not cyclize the terminal residue, blocking any further reaction and terminating the sequencing of the peptide.

Figure 2.08: Edman ladder sequencing

HOOC-X_1-X_2-X_3-$(X)_n$-X_{n+1}-PhenylUrea

HOOC-X_1-X_2-X_3-$(X)_n$-PhenylUrea

HOOC-X_1-X_2-X_3-PhenylUrea

HOOC-X_1-X_2-PhenylUrea

HOOC-X_1-PhenylUrea

Illustration of sequencing by Edman ladders created by poisoning the standard Edman degradation reaction mixture with phenyl isocyanide.

2.1.1.4.1.3 Next-generation Sequencing

Single-molecule sequencing enables the high-throughput simultaneous analysis of a matrix of samples. Attaching protein digests by their C-terminus to a surface prepares the peptides for N-to-C sequencing approaches, such as Edman degradation. Certain amino acid sidechains (e.g., lysine, tryptophan, cysteine, and aspartic/glutamic acid) can be color-coded by selectively labeling them with fluorophores.[372] A peptide strand immobilized to a surface would then fluoresce at different wavelengths, according to the labeled amino acids that comprise it, with fluorescence intensity proportional to the number of labeled amino acids in the strand. With each Edman cycle, detecting a loss of intensity of a certain fluorescence would mean that the cycle clipped the corresponding amino acid. No change in intensity means that an amino acid that was not labeled was lost. The strand could then be partially sequenced, with the location of fluorescently labeled amino acids known, but the identity of the non-fluorescent positions ambiguous. Nonetheless, elucidating the number and location even of only two amino acids on a strand of sixteen is sufficient to compare to protein databases and find matches to 75% of uniquely identifiable proteins. Four labels would only increase the match finding.[373]

2.1.1.4.1.4 NMR

Although NMR generates not only sequence but also 3-D structure information for proteins,[374-379] it is a complex process that does not apply to this research and will not be discussed.

2.1.1.4.2 Oligonucleotides

DNA and RNA sequencing take advantage of the highly efficient protease replication of strands. Whereas peptides are degraded when sequencing, oligonucleotide sequencing tracks the order of *building* the complementary strands. Traditional methods require PCR amplification of the oligonucleotides, but next-generation methods multiplex single strands.

2.1.1.4.2.1 Sanger Sequencing

Similar to ladder sequencing (Figure 2.08), this method purposefully randomly disrupts the replication of the full strands being sequenced, such that the various aborted replications comprise every intermediate in the full replication.[380] A portion, typically 1%, of each of four nucleotide triphosphate base types, has the ribose or deoxyribose 3´-OH residue removed. Polymerase catalyzes the phosphoesterification, with loss of pyrophosphate, of this 3´-OH to the 5´-triphosphate of the next nucleotide. Without the 3´-OH, polymerase cannot continue building the strand. Consequently, stochastic incorporation of this "stop" nucleotide results in termination of synthesis at each base-pairing of the replication. Labeling the "stop" nucleotides prior to the replication with fluorescent labels, a different color for each base type, communicates the base identity of the last nucleotide in each fragment. The mixture of full strand and its incomplete fragments is then separated by capillary array electrophoresis, and a well-resolved gel returns a color-coded complementary sequence, with the fastest-eluting band color corresponding to the base at the 3´ terminus and the least-moving one to the base at the 5´ terminus of the complementary sequence (Figure 2.09).

Figure 2.09: Sanger sequencing

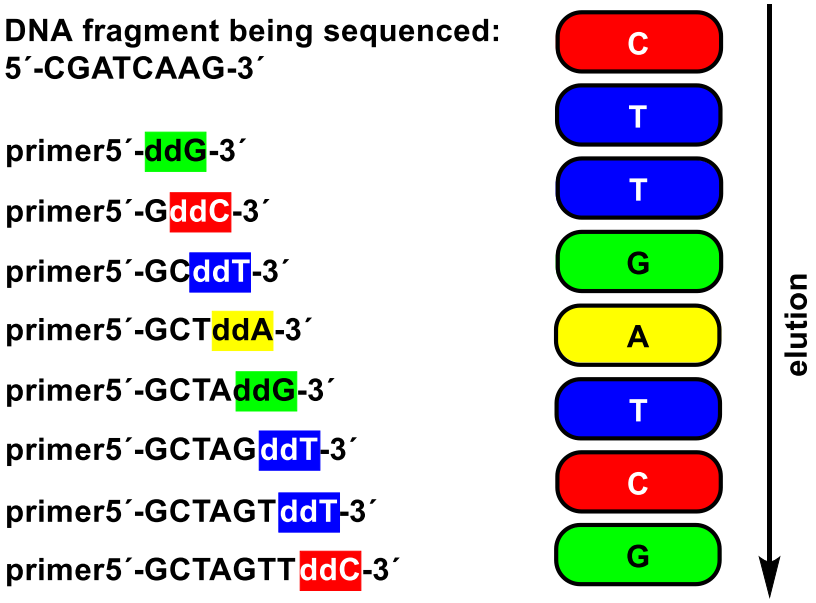

A polymerase builds a DNA strand complementary to the one being sequenced. The cocktail of nucleotides is poisoned with some dideoxyribonucleotides (ddC/A/T/G) that block the next connection and thus terminate the strand. Distinct fluorescent labeling of each ddBase means the fluorescence color of an eluting band (after capillary gel electrophoresis) reports the terminal nucleotide for that length of strand. Smaller strands elute through the gel sieve first. The sequence of elution corresponds to the 5´ to 3´ complementary strand.

Due to the increasing difficulty in resolving an incremented base with oligonucleotide chains of increasing length, the Sanger method is limited to 900 base pairs or less. Like peptides, oligonucleotides can be fragmented by restriction endonucleases to overcome this limit.[381] In 2003, the first human genome in the Human Genome Project was sequenced by the Sanger method over thirteen years and at $2.7 billion cost.[382]

2.1.1.4.2.2 Next-generation Sequencing (NGS)

With NGS, genomes can be sequenced in a day and at much lower cost - $1000 in 2016.[383] Length limits vary from 300 to 20,000 base pairs, depending on the sequencing approach. Most methods simultaneously analyze by CCD camera an array of single oligonucleotide strands, often overlapping fragments produced by different restriction

endonucleases. Various approaches exist; most share in common the detection of a base complementary to the template being added to the strand by polymerase.[380, 382] For example, the pyrophosphate released by polymerase coupling of the 3´ OH to the 5´ triphosphate is converted to ATP by ATP sulfurylase, with luciferase producing a chemiluminescent signal from ATP and luciferin. Addition of the appropriate complementary base makes that location on the array light up. Another approach attaches a polymerase at the bottom of each well, where it engages the template sequence, immersed in a solution of the four distinctly colored fluorescently labeled nucleotide bases. Detection is accomplished through total internal reflection fluorescence (TIRF) of the bottom of the well; only fluorophores within the detection volume at the polymerase are detected. The fluorescence color of base pairs appropriated for ligation to the complementary strand registers until polymerase cleaves the fluorophore label in the process of ligation, and the fluorophore diffuses out of the TIRF detection range. A recording of the signals from the array over time therefore captures the color sequence of each template as the polymerase replicates it. 20,000 base-pair lengths have been sequenced in this manner in less than a day.

2.1.1.4.3 Non-natural Polymers

The broad interest in the narrow fields of peptides and oligonucleotides has produced the increasingly efficient approaches to sequencing. Very few specialized sequencing approaches apply to the wide field of non-natural polymers. Tandem MS is indiscriminate in bond-breaking, so it can be applied to all polymers. In fact, the trends in backbone cleavage of peptoids were compared to those for peptides.[384] Depending on the polymer and the MS/MS settings, the mass spectrum can range from prohibitively complicated to delightfully simple. The oligocarbamates for binary data storage described in the applications section trended towards the latter, as do other storage

oligomers based on alkoxyamine amides.[355, 385] For polymers that provide complicated fragmentation patterns, such as phosphodiesters, a re-design incorporating a much weaker bond, i.e. an aminoxy bond to a tertiary carbon, than those that provoked the complex patterns, with accordingly milder ionization methods, returns a much simpler fragmentation pattern.[386]

Several groups have written software pertinent to their non-natural polymer backbones to quickly interpret tandem MS fragmentation patterns. Oligomer Soup Sequencing (OLIGOSS) software generalizes the software and input requirements to all oligomer types, thus promoted as "a universal sequencing system for unknown oligomers".[387]

Last of all, in 2016 an Edman-like sequencing for peptoids was reported, involving DIC coupling of the N-terminus to bromoacetic acid to form the N-peptoido bromoacetamide (Scheme 2.04).[388] Addition of silver perchlorate traps as insoluble silver salt the bromide expelled by intramolecular cyclization from attack by the proximal amide to form an oxazolinium intermediate. Hydrolysis of this intermediate provides the N-sidechain-substituted morpholine-dione and releases the new N-terminus of the sequenced peptoid. The sequencing occurred at room temperature in much milder conditions than those for Edman sequencing. Although the yields of 70-85% per sequencing step fell short of Edman yields, they are amenable to molecular weight ladders for MS sequencing.

Scheme 2.04: Edman-like sequencing of peptoids with bromoacetic acid and silver perchlorate

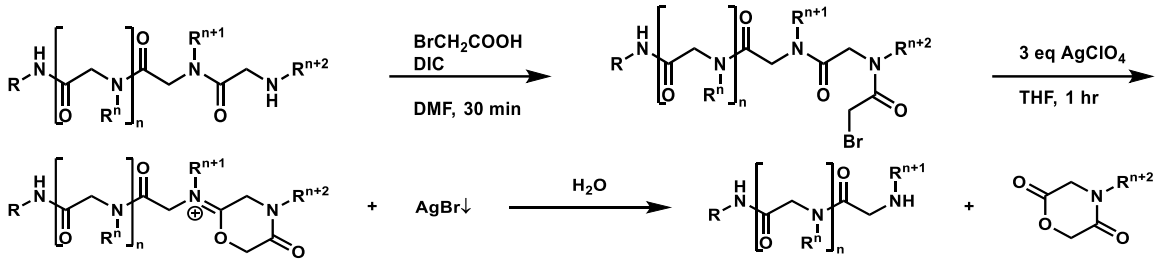

After amidation of the N-terminus with bromoacetic acid, addition of silver ion induces cyclization by removing bromide ion from the reaction. Hydrolysis upon workup produces the sequenced monomer and returns an amine terminus for the next cycle.

2.1.2 Self-immolation of polymers

Polymer self-immolation is the reverse of polymer synthesis. Self-immolative polymers (SIPs) are designed to enable the sequential degradation of the polymer under promoting reaction conditions and, at times, after one reaction event's triggering the response. The triggered release of monomers and the handle starting point from which the polymer was synthesized has found use in drug-delivery, sensing, and photo-resist materials. If each monomer has an output (i.e., fluorescence turn-on or small-molecule drug), the event triggering the self-immolation gets amplified proportional to the monomers present in the polymer.

Carbonate or carbamate junctions employed for facile ligation of monomers in polymer synthesis function optimally for sequential degradation. If the release of the triggering molecule and monomers produces a carbonic or carbamic acid, the acid readily decarboxylates, with the release of CO_2 as a driving force for the degradation. For example, *para* or *ortho*-substituted aminobenzyl alcohol moieties convert to an azaquinone methide intermediate if the alcohol is transformed to a good leaving group, possibly via a carbonic or carbamic ester. The ensuing carbonic or carbamic acid

decarboxylates, yielding another aminobenzyl ester, and the 1,6 elimination-based chain degradation propagates. Disubstitution of an aniline at both *para* and *ortho* positions enables both the continuation of the degradation cascade (1,6 elimination) and the release of a side chain (1,4 elimination) to fulfill its intended application (Scheme 2.05).[389-390] Many variations of the carbonic or carbamic ester eliminations/decarboxylations self-immolation mechanism exist.[391]

Scheme 2.05: Triggered self-immolations by 1,6 and 1,4 eliminations

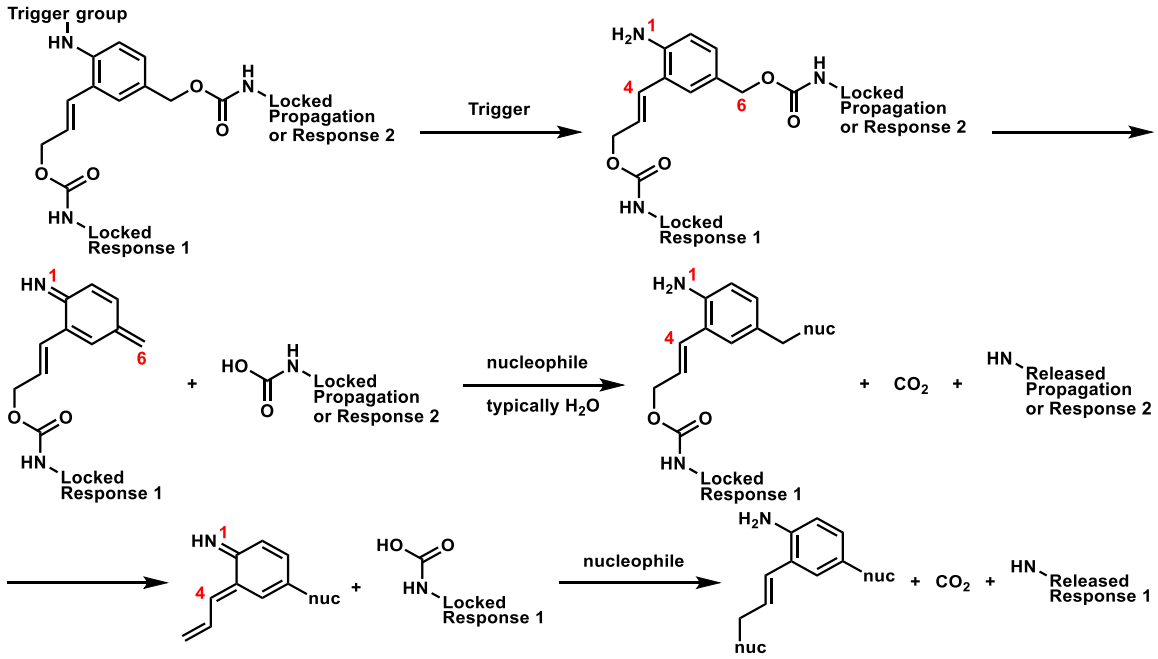

A single trigger provokes a series of 1,6 and 1,4 elimination cascades through which the polymer self-immolates while delivering amplified (proportional to the repeating units of the polymer) Response 1's and a Response 2.

A second approach involves triggering a cyclization degradation cascade. Again, carbamate and carbonate (and their thio derivatives)-linked polymers enable these cyclizations by amines, alcohols, and thiols, released by a trigger. In one case, a released thiol terminus on a dimethylethylene diamine and 2-mercaptoethanol -ligated polymer cyclizes on the proximal carbamate to form the 2-oxathiolone and release the secondary

amine.[392] This amine cyclizes on the proximal thiocarbamate to produce the N,N´-dimethylimidazolidinone and releases the thiol for subsequent cyclization (Scheme 2.06). In this case, the cascade consists of two cyclization events per iteration.

Scheme 2.06: Redox-triggered self-immolation by sequential backbone cyclizations

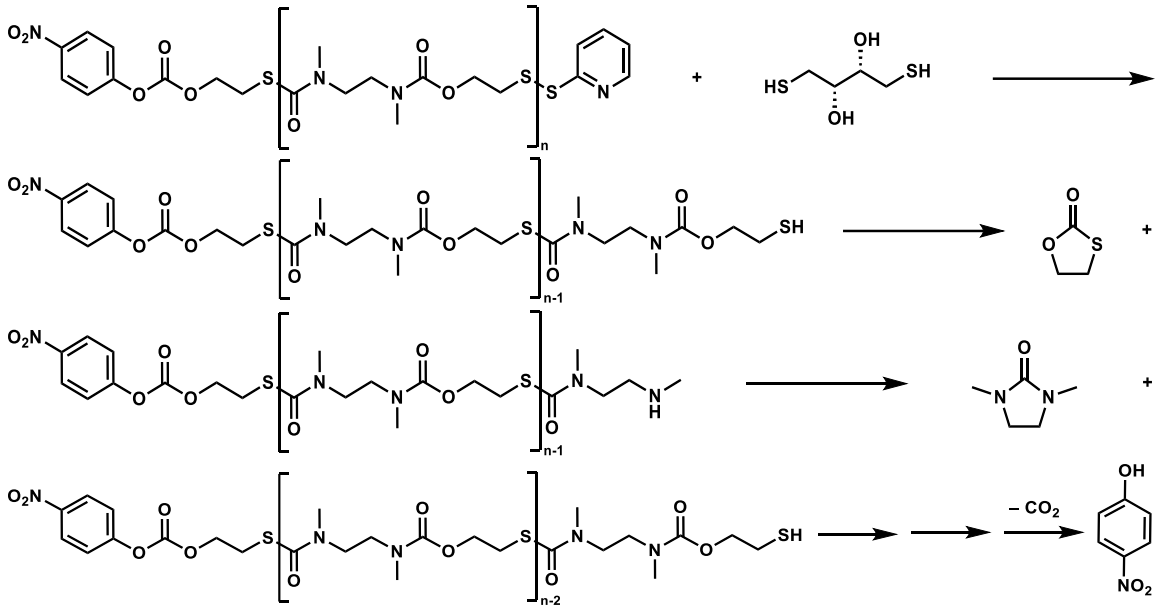

The triggering mechanism is designed according to the application of the SIP. Frequently, a triggering residue at the growth terminus of the polymer incapacitates the degradation cascade initiator (the aniline or the thiol in the examples above). For sensing applications, the analyte provokes a change in the trigger that releases the initiator. For drug-delivery, it can be the redox level of the cell or an over-expressed enzyme; for lithography, a photo-active residue. When deprotonation (pH) is the activating condition, the acidic hydrogen is the trigger.

In iteratively degrading the polymer, self-immolation does sequence it. Like movie film, the sequencing cascade typically proceeds too quickly to capture the

individual frames – the product of each iteration, leaving a soup of truncated monomers with no order information.

2.2 AIMS

Tandem MS is the preferred sequencing method for non-natural SDPs, even more with the availability of universal fragment-predicting / database software. Not all non-natural SDPs produce sufficiently clean spectra to easily interpret sequence, even after adjusting MS ionization parameters. For combinatorial-library applications and structure-activity relationship determination, correct sequences ensure better and faster results. We therefore purposed to find an SDP format amenable to Edman-like sequencing. If successful, it would introduce the idea of designing SDPs with their sequencing in mind for applications such as data storage or combinatorial libraries.

We chose carbamate polymers for their ease of synthesis, peptide-like hydrogen-bonding capabilities conducive to secondary structures, and resistance to degradation by proteases. Our monomers would be 2-aminoethyl alcohols, with sidechain substitution possible at the amine, at either carbon, or any combinations of these options (Figure 2.10), including cyclic sidechains that incorporate the backbone. We would synthesize them in N-to-O fashion by chemoselective reaction with carbonyl diimidazole (CDI), obviating the need for protecting groups, as the amine is more reactive than the alcohol.

Figure 2.10: Possible substitution on proposed oligocarbamate backbone

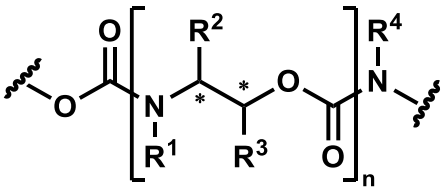

Three possible substitutions per monomer of the polymer. Substitution at the carbons generate stereocenters.

The sequencing approach would involve derivatizing the O-terminus to provoke cyclization on the proximal carbamate junction, clipping the terminal mer and releasing a new O-terminus. Apart from Edman degradation of peptoids, at the time we had no knowledge of other Edman-like sequencing of non-natural SDPs.

2.3 Results and Discussion

As our model for this research was the sequencing of peptides, we envisioned that we would eventually build libraries of our carbamate oligomers once we discovered a cyclization-based sequencing approach. Many peptide libraries have been successfully assembled from solid phase synthesis, and so we anticipated SPS would serve for our libraries. The Rink amide resin appeared to be a logical choice among the resins; the resin linker amine could react with the acylating agent CDI as an anchor point to the start of propagation of the β-amino alcohols, the reaction with 2-aminoethanol derivatives producing a urea less susceptible to degradation than a carbamate. Acid cleavage of the oligomer from the resin would conserve the urea at the N-terminus.

Having an idea of the resin to use prompted us to select a synthetic handle equivalent to the resin-linker for solution-phase chemistry studies of oligomer building and stepwise degradation. In making the functional handle similar to the resin linker, we could screen against any reaction conditions that degrade the handle, making the eventual transition to SPS more robust. Although the similarity score on the first choice of 3,5-dimethoxyaniline certainly would not be very high, we chose it for its chromophoricity at 244 nm and for its simplicity in the ^{1}H NMR spectrum. Due to its unexpected reactivity, we would eventually settle on the more relevant 2,4-dimethoxybenzyl amine.

Our first approach to impart diversity on each monomer consisted of varying the substitution on the amine. Rather than creating chiral centers by derivatizing the alpha or

beta carbons on the beta-amino alcohols, N-substitution would provide the simplest assembly of the oligomers. Secondary β-amino alcohols are also conveniently accessible by ring-opening reaction of a primary amine with epoxide.

With 3,5-dimethoxyaniline as the handle, we first studied the formation of the oligomer. Aniline displacement of one imidazole in CDI occurred smoothly at room temperature in dichloromethane, without need for a base such as triethylamine, as the imidazole mops up the anilinium proton. The resulting mixed urea is stable to LCMS conditions [MeOH (or MeCN) / H_2O + 1% formic acid], as it showed quantitative conversion of the aniline to the urea. LCMS monitoring of the attack on CDI in general revealed complete reaction within two to four hours. Simply adding the β-aminoalcohol, in this case N-benzyl-2-aminoethanol, to the reaction yielded the monomer; again, the displaced imidazole served as a proton sponge (Scheme 2.07A). Upon completion of reaction, the two equivalents of displaced imidazole were washed out with 1M HCl, so as to not interfere with column chromatography of the newly created urea. (The imidazole tended to streak down the column.)

Monomer in hand, we sought to extend it to a dimer, again with N-benzyl-2-aminoethanol. Out of curiosity we tried to purify the mixture after the first displacement of an imidazole from CDI by the monomer alcohol. The reaction was loaded directly onto an SiO_2 column, and the product degraded as it was eluted. The imidazole carbamate is unstable towards the large excess of silanol groups. A repeat of the reaction cleanly produced the mono-displaced carbamate by LCMS, but the second imidazole displacement with N-benzyl-2-aminoethanol proceeded slowly and in poor yield. The LCMS (280 nm chromatogram) showed only 8% conversion by LC after stirring at room temperature overnight. Suspecting that the benzyl group sterically decreases the nucleophilicity of the amine, we reacted the monomer with CDI, then unsubstituted 2-

aminoethanol, with much better yields. Repeating the sequence produced the trimer with the first unit N-benzylated and with the remaining two unsubstituted (Scheme 2.07B).

Scheme 2.07: CDI-mediated synthesis of trimer carbamate from 3,5-dimethoxyaniline handle

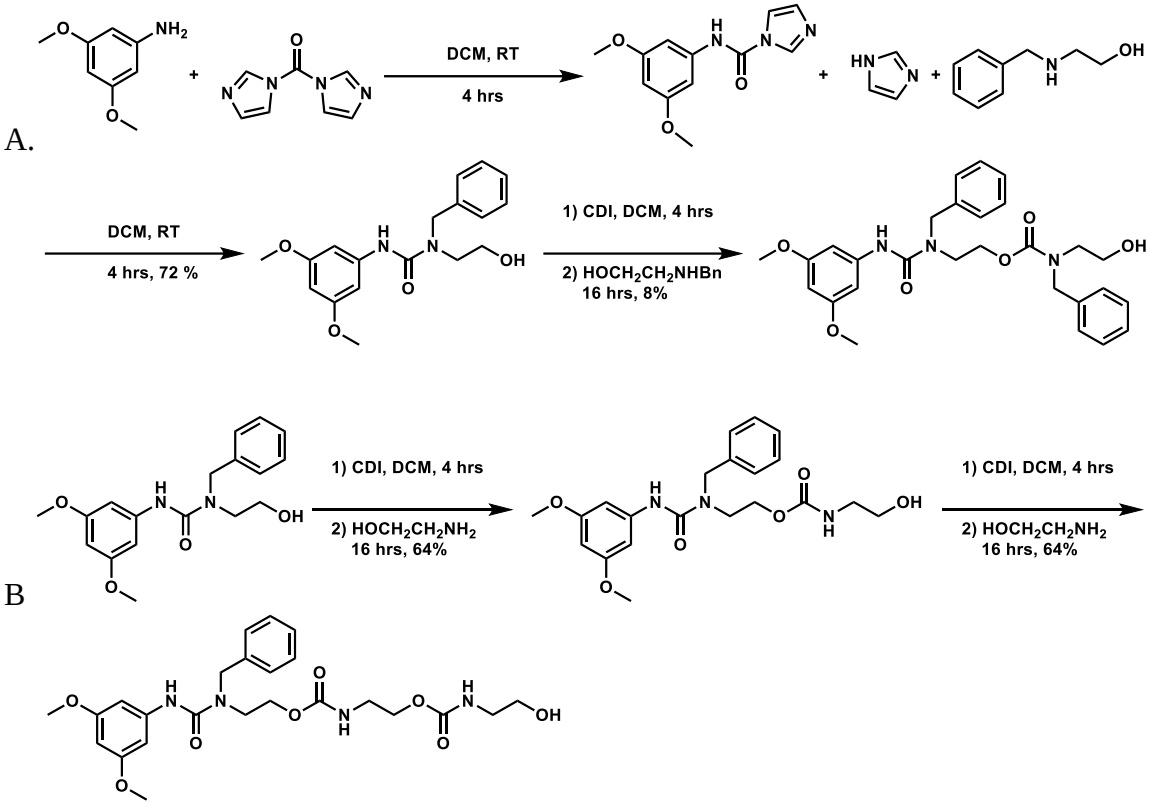

Although not the most ostentatious of oligomers, we desired a speedy synthesis of a trimer to be able to study its stepwise degradation via transformation of the O-terminus into a nucleophilic cyclizing agent. Sequencing of a dimer would produce the urea-based monomer, which we suspected would be resistant to cyclization. With only a dimer, we would not be able to establish whether the sequencing step would clip the terminal monomer only, or if it also would degrade the remaining oligomer.

To convert the alcohol into a better nucleophile, we envisioned esterifying it to an α-cyanoester, which deprotonates readily (pK_a 13.1 in DMSO for ethyl cyanoacetate).

Baldwin's rules favor the 7-exo-trig cyclization from attack of the enolate on the carbonate, which we hoped would form the 7-membered heterocyle product of sequencing. With cyanoacetyl chloride we converted the alcohol into the α-cyanoester. The cyclization was attempted with Hünig's base, DBU, and even NaH at room temperature and with heating to 70 °C, but neither the heterocycle nor the dimer was observed by LCMS, only the oligomer and some hydrolysis of the ester (in the reactions with DBU), most likely due to moisture in the reagent bottle (Scheme 2.08). NaH produced a messy reaction with various products from degradation of the oligomer whose identity were not established. We concluded that cyclization requires a harder nucleophile than the cyanoester enolate.

Scheme 2.08: Failed attempt at cyclization of terminal monomer

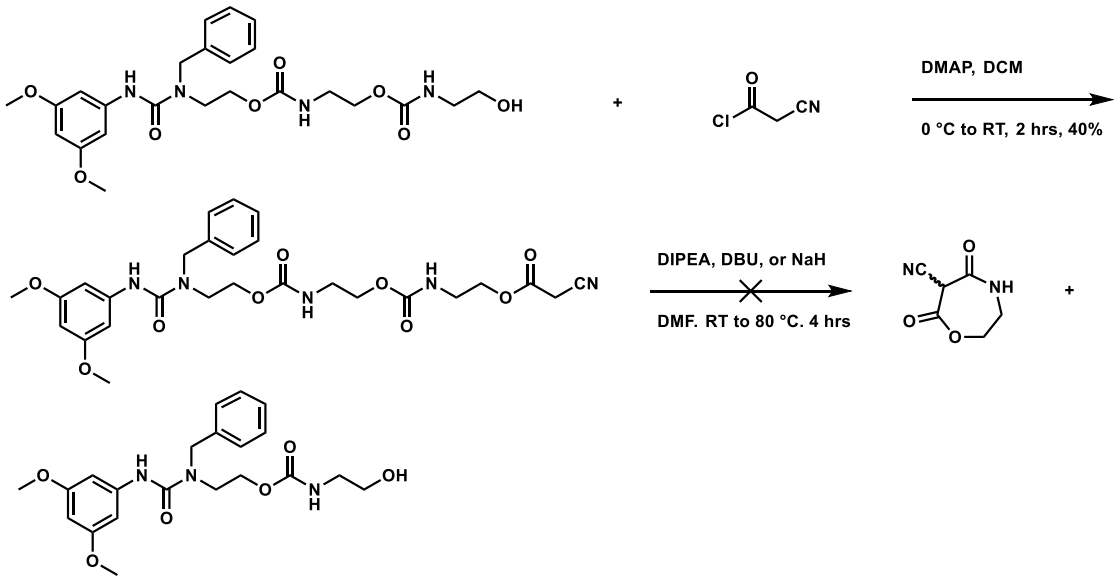

The trimer was esterified with cyanoacetyl chloride, but the enolate could not effect cyclization.

Deprotonation of the O-terminus would produce the hard nucleophile alkoxide. The resulting tetrahedral intermediate from alkoxide attack could expel the remainder of the oligomer, clipping the terminal monomer to a cyclic oxazolidinone – thereby

sequencing the oligomer as we intended. However, the basic conditions necessary for the terminal alkoxide to expel the truncated oligomer alkoxide would enable the latter to attack its proximal carbamate. Given enough time, the oligomer would self-immolate completely to the urea N-terminus, destroying any sequence information.

Converting the O-terminus to a primary amine creates a nucleophile that does not require base. Amine attack on the most proximal carbamate generates a tetrahedral intermediate from which the truncated oligomer O-terminus is the best leaving group. The amine modification should enable sequencing under neutral conditions, avoiding the base-promoted alkoxide self-immolation of the oligomer.

We followed the traditional route of alcohol transformation to an amine (Scheme 2.09A). The trimer was tosylated and displaced by azide; heterogeneous catalytic reduction yielded the amine. The trimer amine was heated at 90 °C in either DMF or water, but LCMS showed no sequencing to the cyclic urea, even after overnight heating. Instead, the primary product was the adduct to a 3,5-dimethoxyaniline acyl species (Scheme 2.09B). This reaction blocks the amine from sequencing.

Out of curiosity, we also investigated the same reaction with potassium carbonate in DMSO. With strong bases, carbamates typically decompose via carbamate N-H deprotonation to the isocyanate, expelling the alkoxide. In the case of β-aminoalcohol-derived carbamates, deprotonation may also occur on the carbon backbone, triggering elimination of the carbamate leaving group, as LCMS of the reaction reported 90% conversion to a peak whose m/z could correspond to the allylic urea (Scheme 2.09C).

Scheme 2.09: Derivatization of the OH terminus to an amine for unsuccessful cyclization

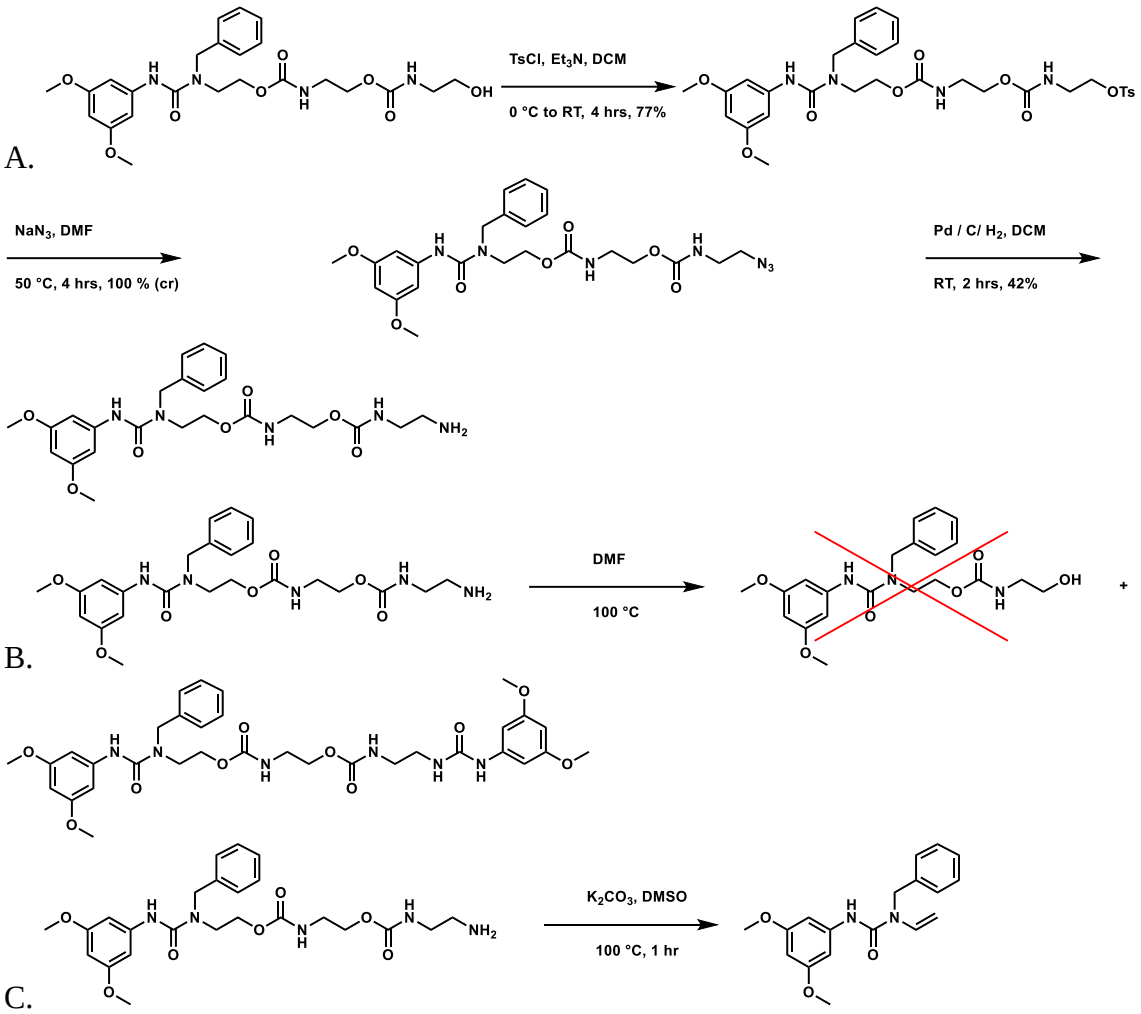

A) Conversion of terminal alcohol to tosyl ester, then azide, and finally amine. B) Cyclization attempts with the amine failed; instead, intermolecular attack on the aryl urea gave the incorrect product. C) Heating the amine with carbonate base degraded the oligomer, possibly by β-elimination at the monomer.

Finally, we followed Edman's example and reacted the trimer amine with phenyl and propyl isothiocyanate, hoping the thiourea would perform the sequencing cyclization in TFA at 50 °C without attacking the dimethoxyaniline mixed urea, as we observed for the trimer amine cyclization. The mixed urea was left intact, but no Edman-like sequencing occurred on the proximal carbamate either (Scheme 2.10). The N-phenyl and

N-propyl thioureas did not react except to oxidize or cyclize in a manner that does not cleave the backbone (-2H peak by LCMS).

Scheme 2.10: Failed Edman degradation of the amino-derivatized trimer

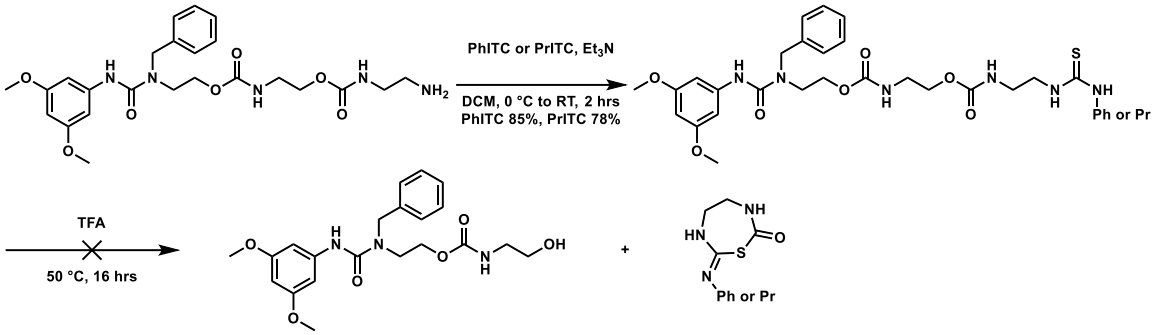

The amine terminus reacted with the isothiocyanate to form the thiourea, which did not cyclize to sequence.

The intermolecular attack by the terminal amine on the mixed urea was troubling. Taking another look at the Rink amide resin showed the linker incorporating a dibenzylic amine, not an aniline. Conceivably the aniline urea is sufficiently acidic that the attempted cyclization conditions deprotonated it, provoking formation of 3,5-dimethoxyphenylisocyanate with expulsion of the remainder of the oligomer. Another trimer-NH2 could then react with the isocyanate to yield the observed product (Scheme 2.11).

Scheme 2.11: Possible pathway to the unexpected bis-urea product of intermolecular reaction

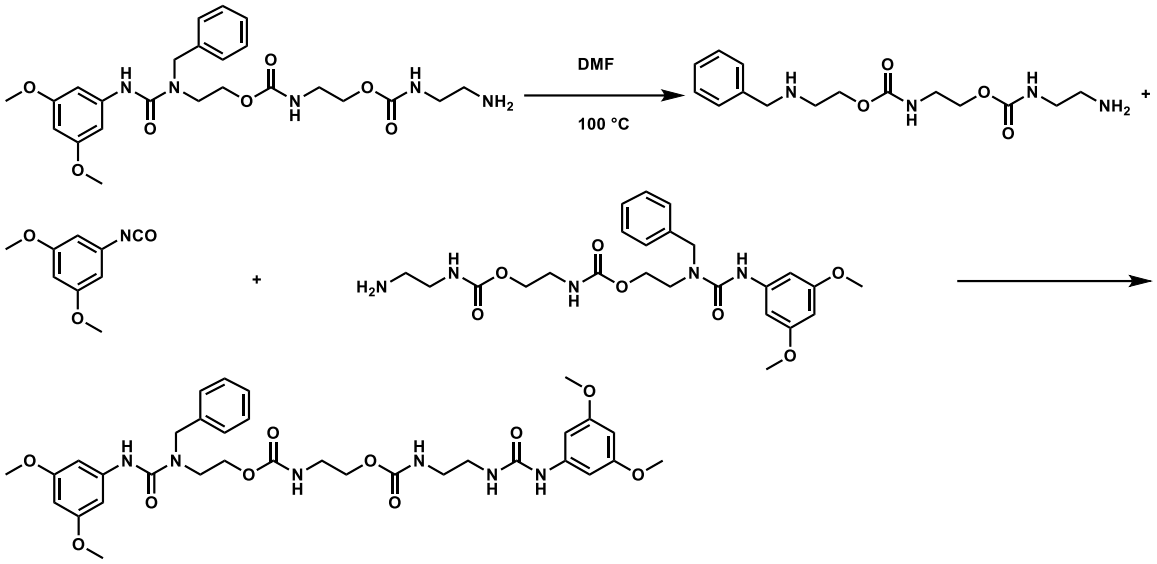

Mixed urea degradation to the aryl isocyanate and the truncated oligomer, followed by isocyanate reaction with another trimer-NH_2 would form the product with a mass equivalent to that observed by LCMS.

2,4-dimethoxybenzylamine was therefore chosen as the more similar handle, and the homodimer of 2-aminoethanol was quickly synthesized (Scheme 2.12) to derivatize at the terminal alcohol and evaluate sequencing strategies, with disregard to the prudence in synthesizing a trimer, not a dimer, discussed above.

Still conjecturing that a terminal amine should cyclize on the nearest carbamate, especially with the competing aryl urea eliminated, we converted the homodimer alcohol to an amine and studied the cyclization reaction (Scheme 2.12). The polarity of the product was not amenable to silica, so we purified it by C_{18} prep LC. Pure fractions containing amine as the as the formate salt (from the 0.1% formic acid additive in the HPLC solvents) were lyophilized. The cyclization was attempted in polar aprotic DMF with aprotic Hünig's base, as well as in a protic 1:1 MeOH/ water solution with phosphate base. Base was added to deprotonate the dimer-ammonium salt. The protic/phosphate base approach cyclized much more effectively than the aprotic/ Hunig's

base. Nonetheless, the reaction required stirring at 80 °C for 40 hours to reach completion. Signals for both the monomer and the cyclic urea products appeared in the LCMS mass chromatogram, well resolved from the homodimer starting material. The reaction was clean, with byproducts amounting to only 2% of the chromatogram at 280 nm. (The absorbance maximum of the peaks was 276 nm.)

To shorten the long reaction times for the sequencing cycle, we turned to microwave heating. Our first trial with MeOH/water/phosphate at 100 °C (250 W) for 15 minutes consumed ~50% of the homodimer to the monomer and cyclic urea. Happily, complete conversion to the two desired products occurred in 45 minutes.

Scheme 2.12: Synthesis of simple dimer from 2,4-dimethoxybenzylamine handle and subsequent cyclization

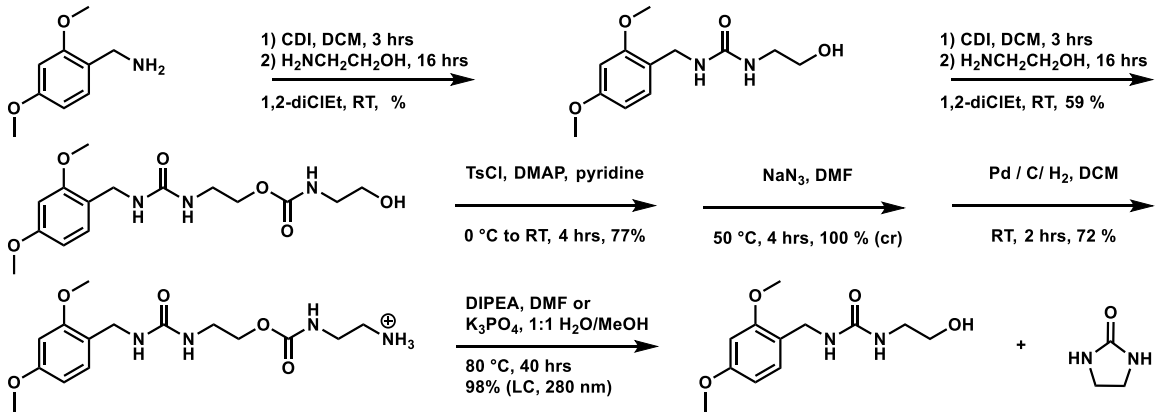

A non-substituted homodimer was synthesized using a 2,4-dimethoxybenzylamine handle to produce an aliphatic mixed urea. The OH terminus was converted to an amine, followed by successful cyclization to the monomer and the imidazolidinone.

Although the transformation of the oligomer alcohol terminus to a primary amine was cumbersome, we were heartened by the cyclization success. The 2-aminoethanol homodimer had served to establish a derivatization of the alcohol and the reaction conditions to promote formation of the heterocycle and monomer. Limited to a dimer, it did not inform us whether the sequencing cyclization would clip only the terminal

monomer, expelling the remaining oligomer with an alcohol terminus as desired. Neither did the homodimer, composed of the simplest β-aminoalcohol, reveal side-chain compatibility with the derivatization and cyclization reactions. At least a trimer, if not longer, comprising more complex and diverse monomers, was necessary to better vet the promising yet nascent design.

With the dimethoxyaniline handle, N-benzyl-2-aminoethanol successfully produced the monomer, but propagation to the homodimer suffered from low yields in a lethargic reaction. Suspecting that steric or electron-withdrawing substituents would adversely lessen the nucleophilicity of the secondary amines, possibly enough to reduce the chemoselectivity of amine over alcohol for the attack on CDI, we abandoned this category of monomers. Monosubstituting sidechains would then be located either alpha to the amine or to the alcohol, their point of connectivity to the backbone a stereocenter. Since steric or elecetron-withdrawing substituents could still influence the nucleophilicity of the adjacent amine or alcohol, it seemed prudent to connect the side chains alpha to the more nucleophilic amine rather than further dampen the alcohol's nucleophilicity. In addition, reduction of stereoisomerically pure amino acids makes this type of monomer readily accessible, with some reduced amino acids commercially available. These include L-phenylalaninol (F), L-alaninol (A), L-leucinol (L), L-methioninol (M), and L-tryptophanol (W).

The reduced amino acids were nicely compatible with CDI-based stepwise oligomer synthesis (Scheme 2.13). With carbon-based side chains, the FAL trimer synthesis was rudimentary. Care was needed to extend the oligomer to FALM; the methioninol sulfide tends to oxidize, but reacting under argon atmosphere and minimizing exposure to air curtailed sulfoxide formation. The pentamer FALMW was readily obtained with these precautions.

Scheme 2.13: Synthesis of FAL-OH trimer and FALMW-OH pentamer

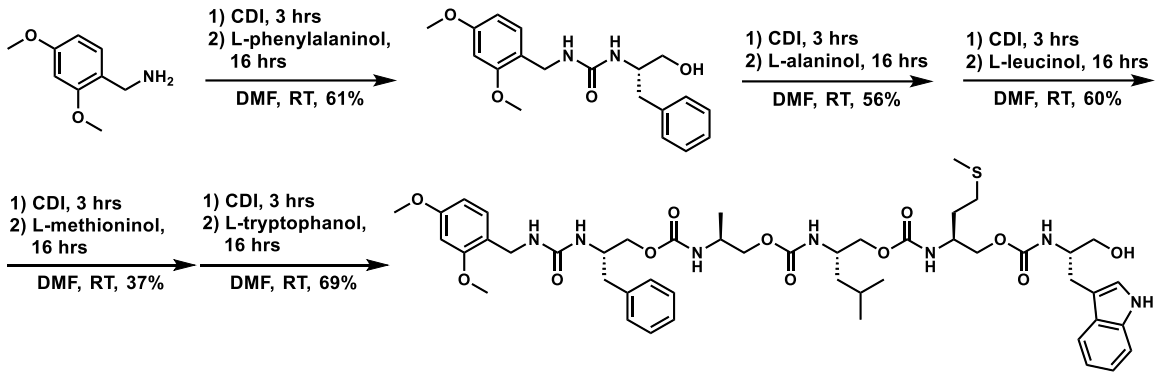

We subjected the FAL trimer to our sequencing procedure. The terminal alcohol was converted to an amine, this time by Mitsunobu reaction with phthalimide, followed by aminolysis with methylamine. FAL-NH_2 was purified by reverse-phase chromatography as the ammonium salt. To our dismay, the 1-hour microwave reaction in MeOH/H_2O/PO_4^{3-}/100 °C conditions degraded the oligomer down to the F-OH monomer, with both leucinol-based imidazolidinone and alaninol-based oxazolidinone present (Scheme 2.14). Subjecting the FAL-NH_3^+ to the same degradation conditions without base resulted in no reaction. Reductive aminations are typically conducted at pH 4, a compromise between activating the carbonyl at low pH and maintaining a neutral amine at higher pH. FAL-NH_3^+ was dissolved in MeOH/ H_2O with NaOAc, and the pH was adjusted to 4 with AcOH. Again, there was no reaction.

Scheme 2.14: Synthesis of FAL-NH_2 and its full self-immolation under sequencing conditions

A.

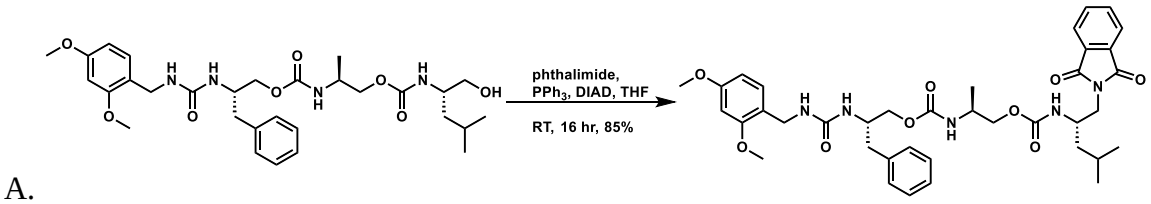

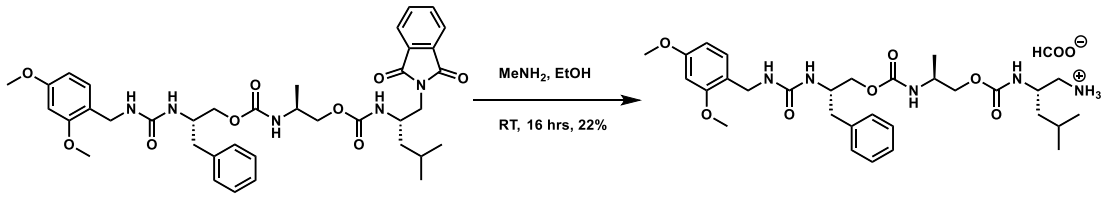

B.

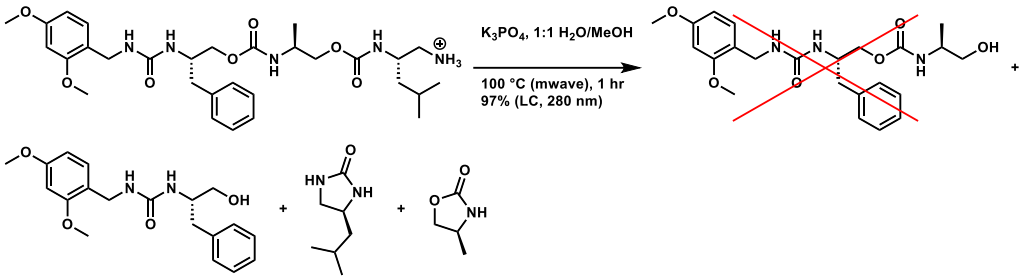

A) Conversion of FAL-OH to FAL-NH_2 B) Unexpected degradation of FAL-NH_3^+ trimer to F-OH monomer and A and L-based oxazolidinones

As a control experiment, we also subjected the FAL-OH trimer directly to the MeOH/water/phosphate microwave cyclization conditions. Surprisingly, even without the amine terminus, this reaction still produced only F-OH monomer and the A and L-based oxazolidinones. We repeated the reaction with FALMW-OH, and even the pentamer degraded completely to the F-OH monomer (Scheme 2.15A). Flabbergasted, we applied the same conditions to FAL-OH, except without base. For the first time, we were able to see the FA-OH dimer expected from a stepwise sequencing, although the F-OH was also present (Scheme 2.15B). After one hour reaction, 88% FAL-OH remained, with 10% dimer and 2% monomer (percentage of chromatogram peak area divided by total peak area at 280 nm, near the absorbance maximum of 276 nm for the oligomers,

presumably due to the 2,4-dimethoxybenzylamine handle). Five hours produced 46% dimer and 21% monomer. We were observing sequencing by sluggish self-immolation!

Scheme 2.15: Self-immolation of FALMW-OH under sequencing conditions

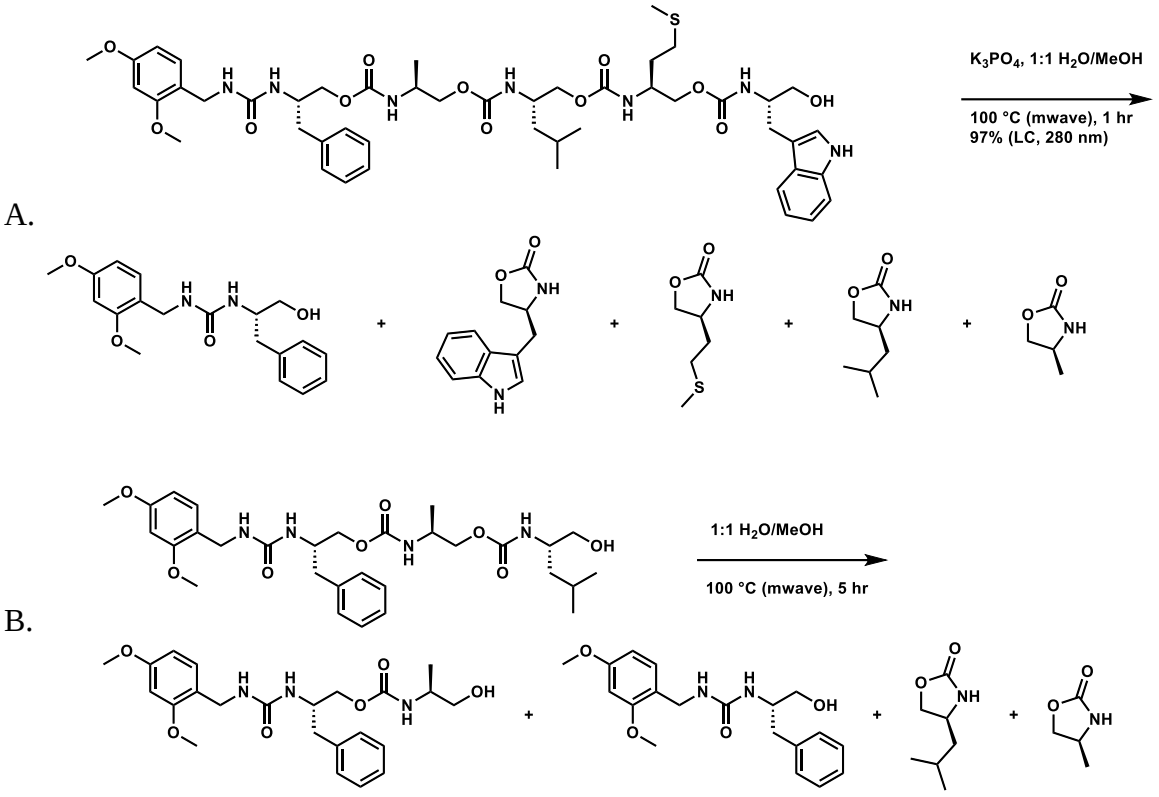

A) FALMW-OH also degrades completely to F-OH and the corresponding oxazolidinones with PO_4^{3-} base at 100 °C. B) Without base, FAL-OH degrades partially, and thereby sequences, to FA-OH and F-OH and the corresponding oxazolidinones.

We had abandoned conventional heating in favor of microwave to shorten reaction times. At 100 °C and without base, the FAL-OH degradation had not completed in five hours. With base at the same temperature, it fully degraded in one hour. We applied a compromise of 50 °C with PO_4^{3-} base for one hour, and it yielded the three species FAL/FA/F in a proportion of 32/47/21 percent. That every species was well represented was promising, and so we applied the same conditions to FALMW-OH. Possibly due to lower solubility, the reaction proceeded more slowly for the pentamer,

reaching only 62/25/8/4/1 percent of FALMW/FALM/FAL/FA/F. Further optimization of temperature and reaction time yielded 90 °C for one hour to nearly degrade the pentamer fully to the monomer. In sampling the reaction at every six minutes, we observed the waxing and then waning of the intermediates as the self-immolization progressed (Figure 2.11).

Figure 2.11: Waterfall plot of the self-immolation of FALMW-OH pentamer.

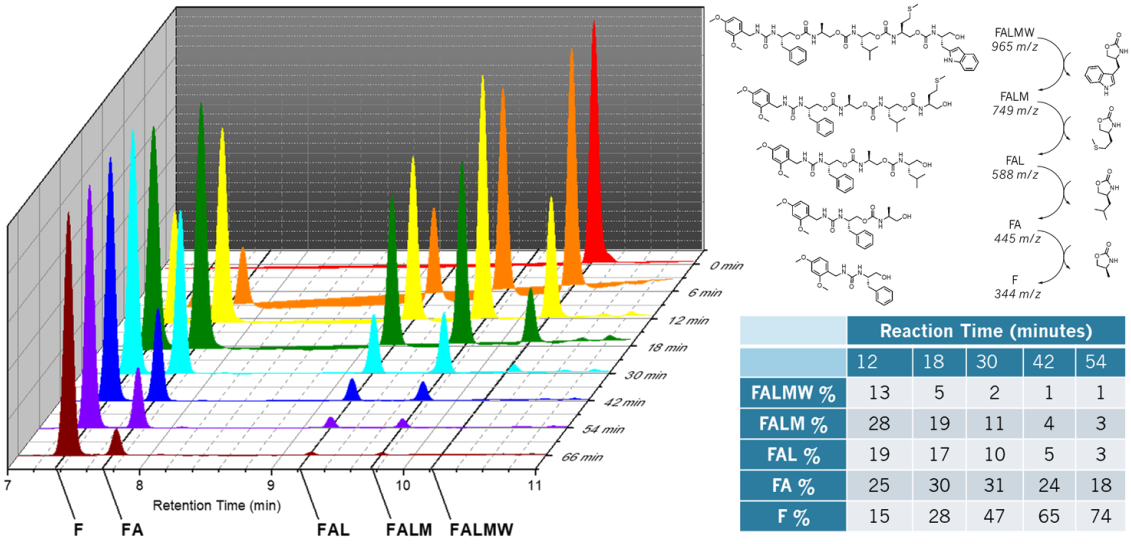

	Reaction Time (minutes)				
	12	18	30	42	54
FALMW %	13	5	2	1	1
FALM %	28	19	11	4	3
FAL %	19	17	10	5	3
FA %	25	30	31	24	18
F %	15	28	47	65	74

LCMS chromatograms (280 nm) showing the time-dependent, stepwise self-immolation of FALMW-OH. The table lists chromatogram peak integrations as percentage of the total area per run. Compounds were assigned to peaks according to their m/z.

Additional experiments revealed more details about the mechanism of the degradation. Polycarbamates tend to degrade via proton transfer from the carbamate amine that produces an isocyanide and expels the alkoxide or by α or β elimination.[393] These pathways would not provide sequence information, so we sought to define their contribution to the degradation. A FAG-OMe trimer was synthesized from FA-OH with CDI and 2-methoxyethylamine. It did not degrade in the sequencing mixture after one hour reaction at 70 °C, but 7% F-OH monomer did appear after one hour at 90 °C

(Scheme 2.16). The low conversion to monomer points to an alternative degradation pathway that proceeds more slowly than the sequencing cyclization pathway.

Scheme 2.16: Degradation conditions applied to control trimer FAG-OMe

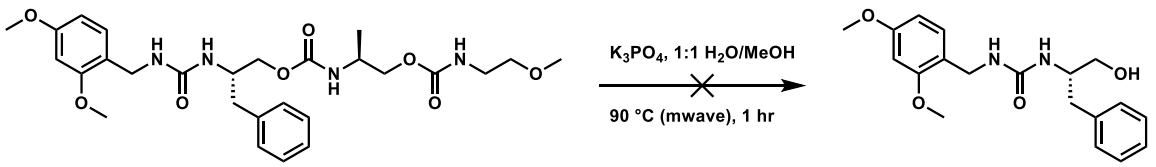

The methoxy-capped trimer degraded minimally to F under conditions that fully converted FAL-OH to F, pointing to the necessity of the OH terminus for self-immolation by cyclization.

Monohydrogen potassium phosphate has a pK_a of 12.3 in water, whereas carbonic acid's is 6.4. Degradation of FAL-OH proceeded much more slowly without base, leading us to suspect that the alcohol must be deprotonated to attack the proximal carbamate efficiently. We again submitted FAL-OH to reaction at 100 °C, but this time with $KHCO_3$ rather than K_3PO_4. Within 15 minutes, the FAL/FA/F percentages were 23/48/28, much faster than without base. FAL-OH degradation at 100 °C with K_3PO_4 yields 97% F-OH in only three minutes. The degradation is a pH-dependent process.

We propose the following mechanism (Scheme 2.17). Base deprotonates the terminal alcohol of an n-mer oligomer to the alkoxide, which is sufficiently reactive to cyclize on the proximal carbamate via a tetrahedral intermediate. Cyclization expels the alkoxide of the remainder of the oligomer (n-1 mer), which deprotonates the conjugate acid of the base, as proton transfers occur at much faster rates than attacks on carbamate carbons. The free base once again deprotonates the n-1 mer terminal alcohol, and cyclization releases the n-2 mer alkoxide that then gets protonated. The cycle continues until the monomer alkoxide, which cannot efficiently cyclize on the urea connection to the 2,4-dimethoxybenzylamine handle.

Scheme 2.17: Proposed specific-base catalysis mechanism of the self-immolation

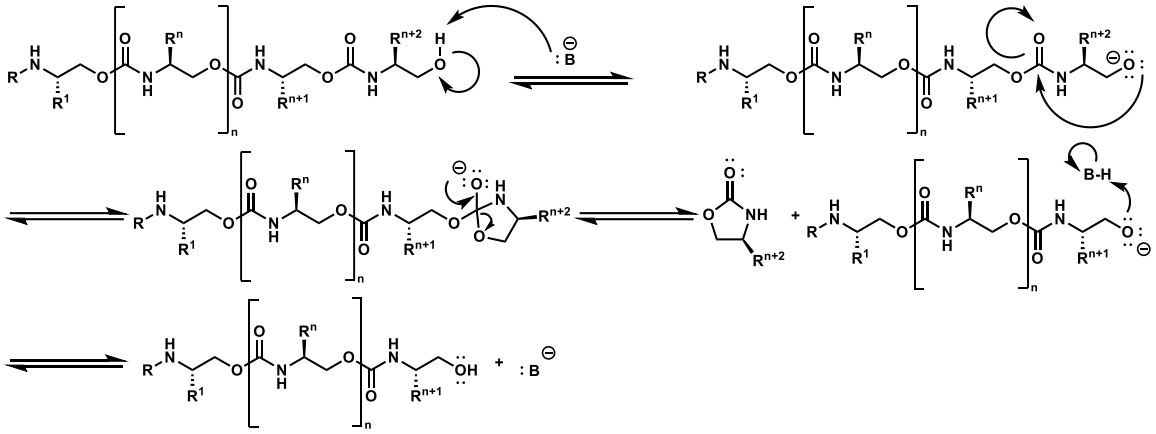

R is a non-reactive handle/linker.

Resolution of intermediates' peaks by HPLC, coupled with low-resolution mass spectroscopy of the peaks, enables determination of the sequence. The peak with the lowest molecular mass corresponds to the handle-derivatized monomer. Subtracting this mass from the second lowest mass reveals the mass of the second monomer, and so on until the parent peak is reached. This ladder sequencing process is quite analogous to sequencing by tandem MS. LC separation resembles mass-ion separation by MS1, and the self-immolation reaction parallels backbone fragmentation by MS2.

2.3 Conclusions and Future Work

We started this research looking for an Edman-type sequencing of N-substituted carbamate oligomers, wherein the terminal alcohol would be transformed into a nucleophilic residue that could cyclize on the proximal carbamate and sequence the terminal mer. In the end we found that self-immolation of carbamates substituted alpha to the carbamate nitrogen could be kinetically slowed enough by controlling temperature

and pH to observe the sequence-dependent waxing and waning of intermediates by LCMS. If the identity of all the monomers that could be incorporated in the oligomer are known (as they would in a combinatorial library or in chemical encoding), then the resolution of intermediates enables facile calculation of sequence by subtracting an intermediate's m/z value from the next largest intermediate's m/z values. If the ionization can be adjusted to ionize only parent peaks, the chromatography would not be necessary, as the self- immolation produces ladder masses.

Further work in our group has synthesized a carbamate heptamer by SPS, labeled the N-terminus with the NBD fluorophore, and sequenced it by slow immolation (Figure 2.12). This study serves as proof-of-concept for building combinatorial libraries and sequencing hits.

Figure 2.12: Ladder MS interpretation of self-immolated heptamer

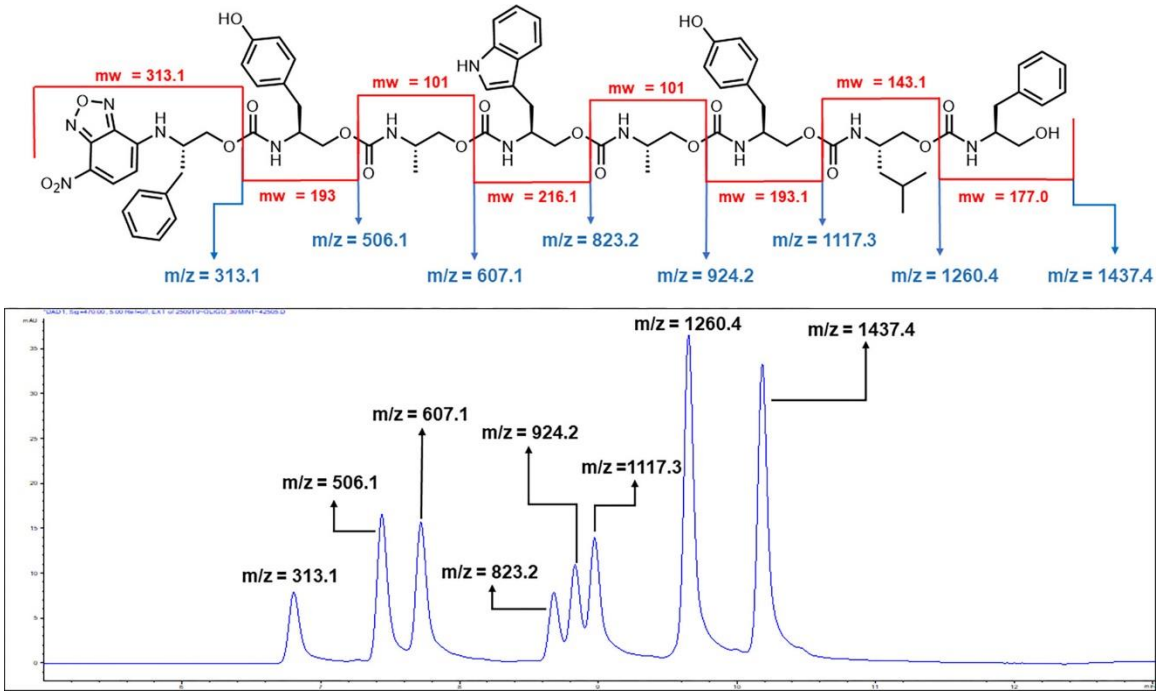

Subtracting the second-highest m/z from the highest gives the m/z of the terminal mer. Subtracting the third-highest from the second-highest gives the m/z of the penultimate mer, and so on. Reprinted with permission from [205]. Copyright 2020 American Chemical Society

The self-immolation has already been optimized with respect to base, solvent, and heat by another research group.[394] They found that sodium hydroxide in ethanol/water mixtures induces slow immolation at room temperature.

If Edman-type sequencing were still desired, the next step would be to look for conditions that would force the terminal amine to cyclize without further base-promoted, uncontrolled cyclizations that degrade the polymer. An oxophilic Lewis acid might catalyze this conversion of a carbamate into an imidazolidinone. In an avenue pursued but then abandoned, the terminal alcohol on the 3,5-dimethoxyaniline handle trimer was oxidized to the aldehyde with DMP. Reaction with hydroxylamine produced the oxime that seemed to cyclize to release dimer, not monomer, by LCMS. Also, Mitsunobu reaction with monoBoc hydrazine or N-Boc hydroxylamine would incorporate supernucleophiles that might cyclize more efficiently than the amine.

The concept of slowing self-immolation to observable intermediates could be applied to other polymers. Under forcing conditions or with the help of a catalyst, transamidation by the N-terminus of a peptide upon the amide residue two mers away would form a six-membered cyclic bisamide with sidechains corresponding to the ultimate and penultimate mers, freeing the N-terminus of the antepenultimate mer to undergo its own cyclization. Under dilute conditions, the high effective molarity of an intramolecular reaction should dominate over intermolecular transamidations. At certain intervals, the reaction would be sampled to determine the dimer rungs of the ladder.

We sought to present to the scientific community the idea of designing a polymer with its sequencing in mind. Instead, our oligomers sequenced themselves by kinetically lethargic self-immolation. In so doing, they may have presented *to us* a sequencing approach with ties to Edman ladders and Sanger sequencing. Future designs may involve

finding how a polymer degrades, if a self-immolative pathway is available, and how to retard the immolation kinetics to observe intermediates.

Appendices

APPENDIX A: GENERAL INFORMATION

Chemicals and reagents were purchased from commercial sources available on UT Market. TLCs, prep TLCs, and SiO_2 were sourced from Sorbtech. NMR spectra were acquired with 400 and 500 MHz instruments in the UT NMR facility. Prep LC purification was performed on Shimadzu binary gradient instrument equipped with a diode array detector with a C18 21.5 mm x 125 mm column. LCMS spectra were acquired by an Agilent 1200 Series HPLC / 6130 single quadrupole mass spectrometer.

APPENDIX B: EXPERIMENTAL DETAILS AND SPECTRA FOR CHAPTER 1 COMPOUNDS

8-bromo-2,3,6,7-tetrahydro-1H,5H-pyrido[3,2,1-ij]quinoline (3-bromojulolidine)

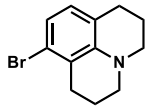

2.18 mL (0.02 mol) 3-bromoaniline, 7.9 mL 1-bromo-3-chloropropane (0.04 mol, 4 eq), and 4 mL DMF were refluxed at 170°C under N_2 for four days, by which point the reaction had solidified. The solid was diluted in DCM and purified by SiO_2 column chromatography, eluting with 2% EtOAc in hexanes to give 3.56 g (70.6% yield) ^{1}H NMR (400 MHz, Chloroform-d) δ 6.93 – 6.82 (d, *J* = 8.1 Hz, 1H), 6.68 (d, *J* = 8.1 Hz, 1H), 3.15 (dq, *J* = 14.4, 8.8, 7.1 Hz, 4H), 2.76 (dt, *J* = 23.2, 6.6 Hz, 4H), 2.13-1.95 (m, 4H). HRMS (ESI+): 300.2137 (M+H, calculated 300.2135).

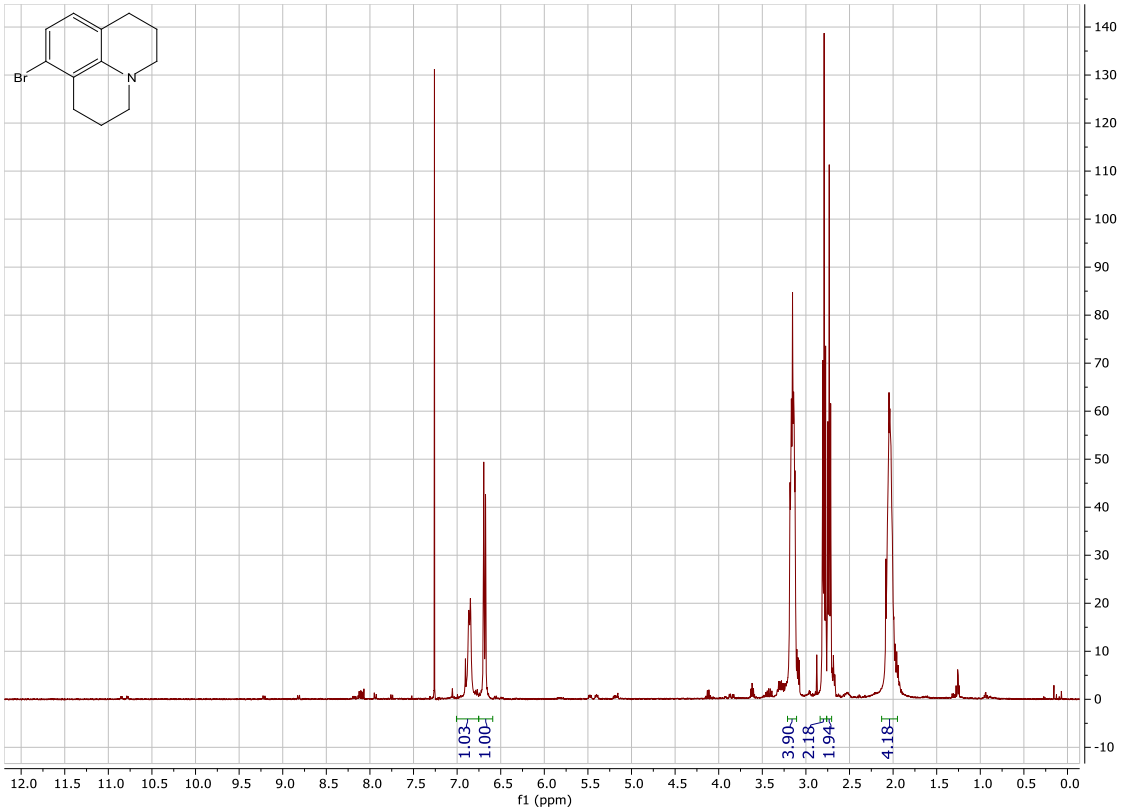

8-(4,4,5,5-tetramethyl-1,3,2-dioxaborolan-2-yl)-2,3,6,7-tetrahydro-1H,5H-pyrido[3,2,1-ij]quinoline

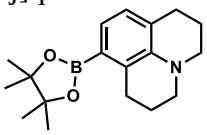

1.008 g (4 mmol) 3-bromojulolidine, 1.22 g (4.8 mmol, 1.2 eq) bis(pinacolato)diboron, and 147 mg (1.5 mmol, 3 eq) KOAc in 3 mL DMSO were sparged for 10 minutes with N_2 to remove O_2 from the system. 30 mg (0.04 mmol, 0.01 eq) $PdCl_2$dppf were quickly added, and the system was sparged with N_2 for another five minutes. The mixture was heated under N_2 balloon at 120 °C for 1 hr. After cooling to RT, the reaction was diluted with EtOAc, and all solids were filtered off. The organics were washed 2x with brine, dried over Na_2SO_4, filtered, and stripped of solvents under reduced pressure. SiO_2

column purification (1% EtOAc in hexanes) provided 681 mg (57% yield). ^{1}H NMR (500 MHz, $CDCl_3$) δ 6.94 (d, *J* = 7.4 Hz, 1H), 6.70 (d, *J* = 7.4 Hz, 1H), 3.03 (t, *J* = 5.7 Hz, 2H), 3.01 (t, *J* = 5.6 Hz, 2 H), 2.96 (t, J = 6.6 Hz, 2H), 2.67 (t, J = 6.6 Hz, 2H), 1.92 – 1.82 (m, 4H), 1.22 (s, 12H). ^{13}C NMR (126 MHz, $CDCl_3$) δ 143.12, 128.56, 126.34, 125.18, 124.02, 83.14, 50.65, 50.17, 28.31, 27.39, 24.94, 22.42, 22.16. HRMS (ESI +): 300.2137 (M+H), Calculated $C_{18}H_{27}BNO_2$ 300.3125

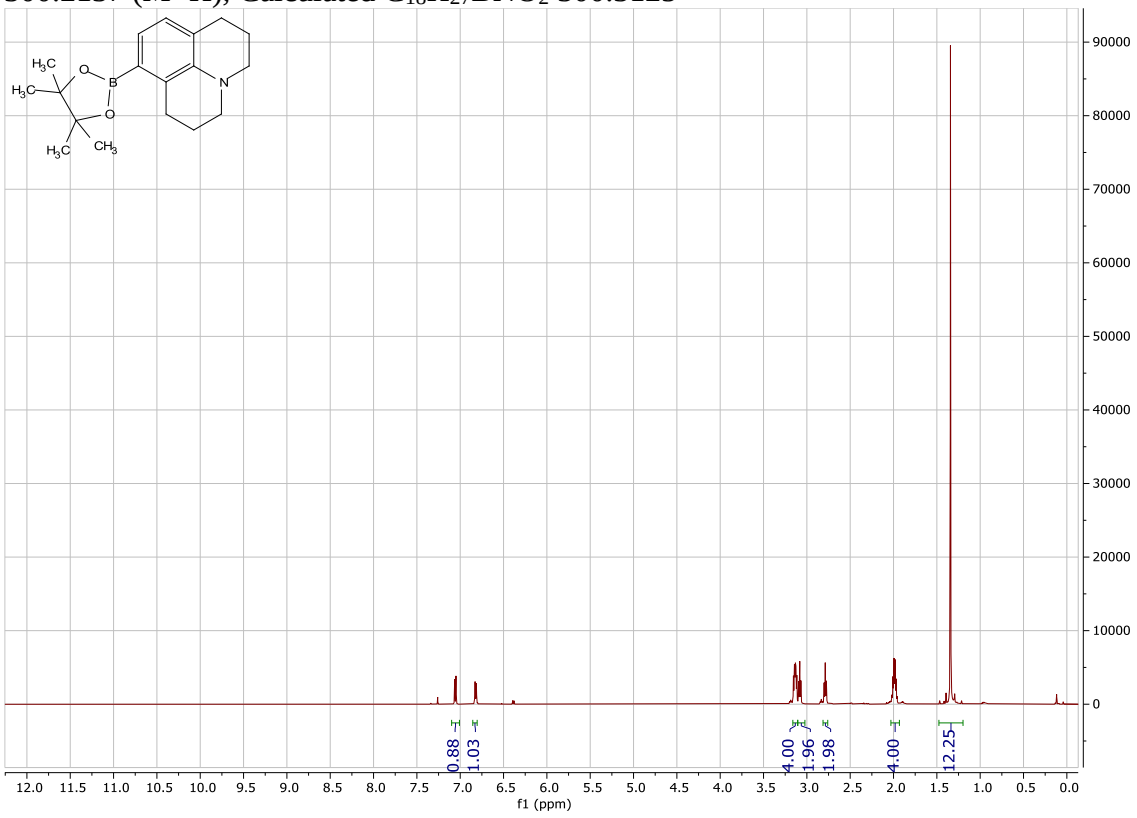

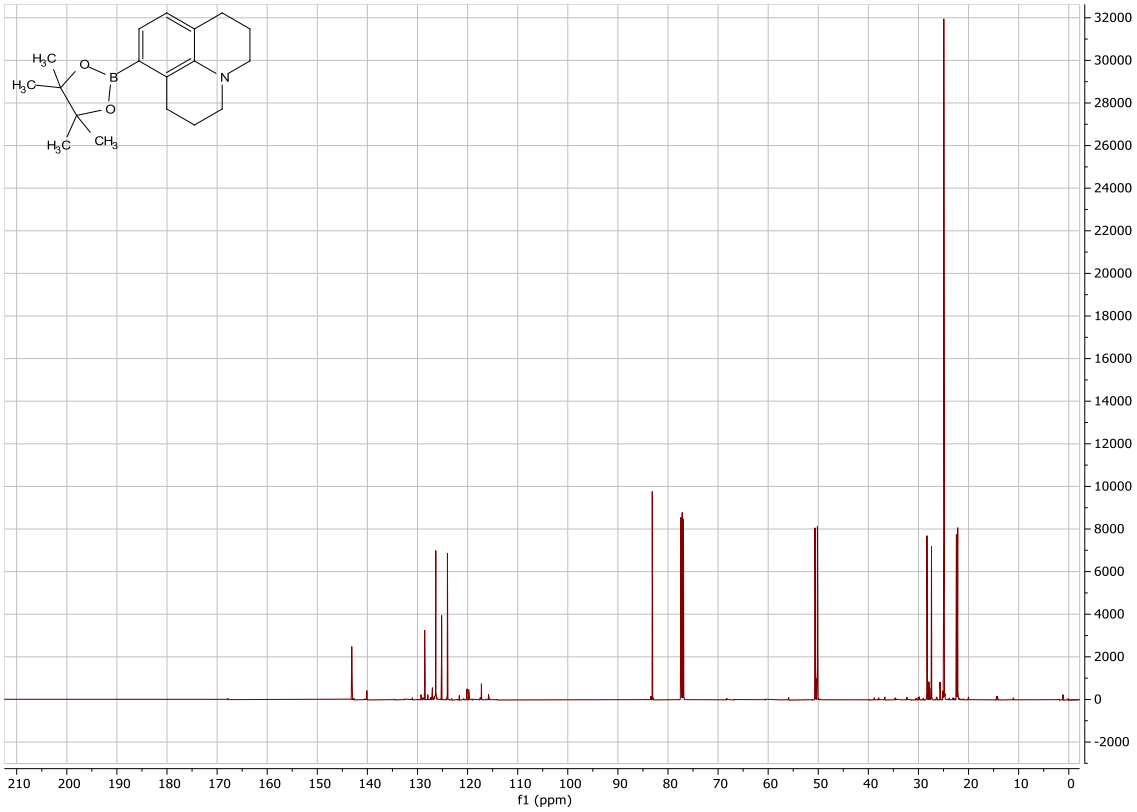

7-bromo-1-methyl-1,2,3,4-tetrahydroquinoline

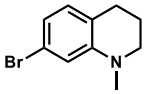

2.1 g (10 mmol) 7-bromoquinoline, 1.26 g (20 mmol, 2 eq) $NaCNBH_3$, and 330 mg (11 mmol, 1.1 eq) paraformaldehyde in 50 mL AcOH were stirred at RT for 4 hrs. The reaction was poured over ice, and the pH was adjusted to neutral with 7 g NaOH. The aqueous mixture was thrice extracted with DCM, and the combined organics were washed with brine, dried over Na_2SO_4, filtered, and stripped of solvents under reduced pressure. SiO2 column chromatography (3% EtOAc in hexanes) provided 1.7 g (75% yield). ^{1}H NMR (500 MHz, $CDCl_3$) δ 6.791 (dt, *J* = 7.8, 1.1 Hz, 1H), 6.700 (dd, *J* = 7.8, 1.9 Hz, 1H), 6.676 (d, *J* = 1.9 Hz, 1H), 3.235 (t, *J* = 5.5 Hz, 2H), 2.876 (s, 3H), 2.698 (t, *J* = 6.8 Hz, 2H), 2.013 – 1.899 (m, 2H). ^{13}C NMR (126 MHz, $CDCl_3$) δ 147.81, 129.92,

121.59, 120.70, 118.55, 113.32, 50.96, 39.00, 27.47, 22.18. HRMS (ESI+): 226.0226 (M+H), Calculated $C_{10}H_{13}BrN$ 226.0231

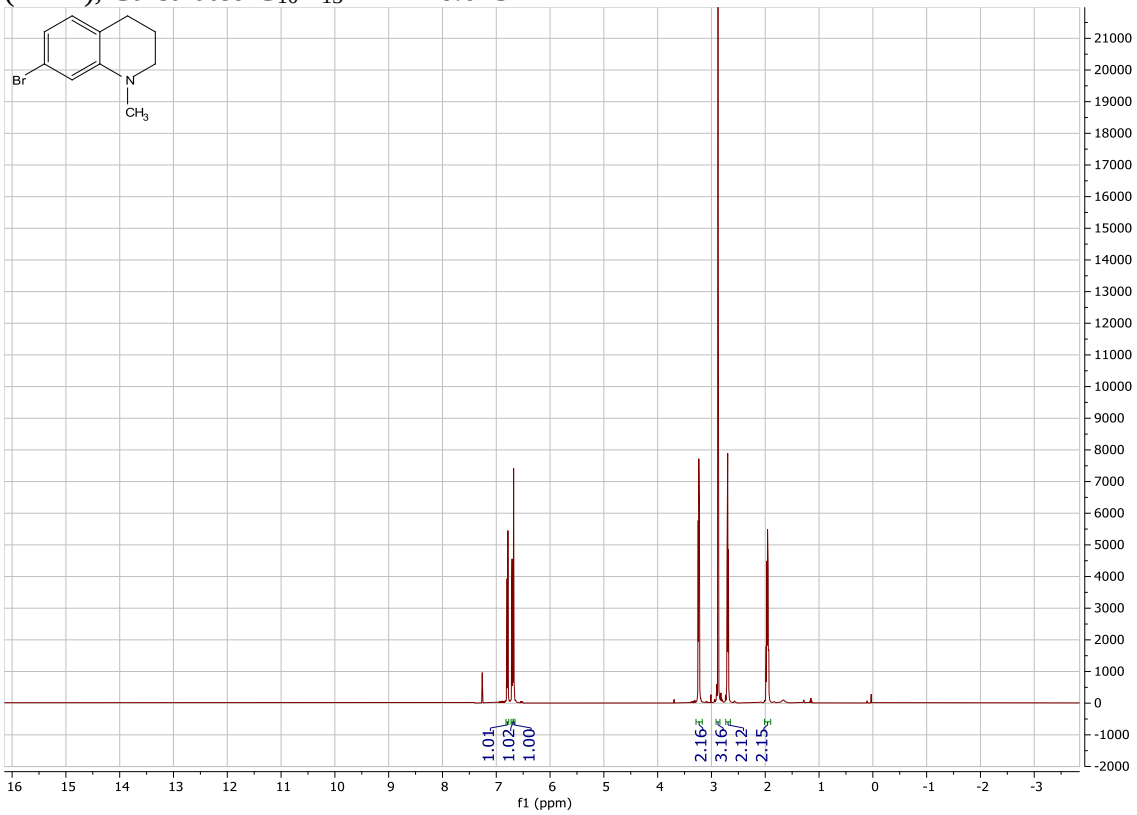

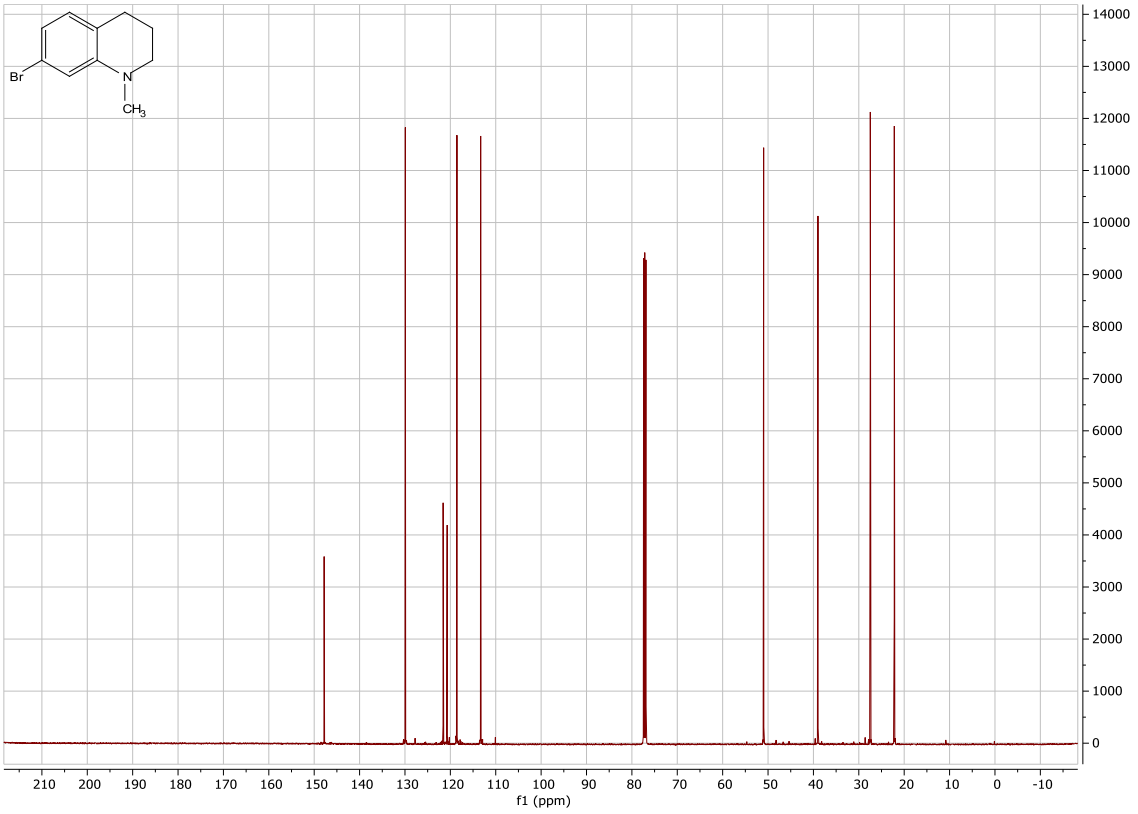

1-methyl-7-(4,4,5,5-tetramethyl-1,3,2-dioxaborolan-2-yl)-1,2,3,4-tetrahydroquinoline

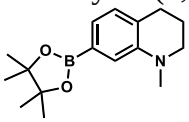

330 mg (1.46 mmol) N-methyl-7-bromo-1,2,3,4-tetrahydroquinoline, 408 mg (1.65 mmol, 1.1 eq) bis(pinacolato)diboron, and 507 mg (5.16 mmol, 3.5 eq) KOAc in 5 mL DMSO were sparged for 15 minutes with N_2 to remove O_2 from the system. 32 mg (0.044 mmol, 0.03 eq) $PdCl_2$dppf were quickly added, and the system was sparged with N_2 for another ten minutes. The mixture was heated under N_2 balloon at 120 °C for 2 hrs. After cooling to RT, the reaction was diluted with EtOAc, and all solids were filtered off. The organics were washed 2x with brine, dried over Na_2SO_4, filtered, and stripped of solvents

under reduced pressure. SiO_2 column purification (1% EtOAc in hexanes) provided 200 mg (50% yield).

^{1}H NMR (500 MHz, Chloroform-*d*) δ 7.07 (dd, *J* = 7.3, 1.1 Hz, 1H), 7.03 (s, 1H), 6.96 (d, *J* = 7.3 Hz, 1H), 3.20 (t, *J* = 5.7 Hz, 2H), 2.93 (s, 3H), 2.77 (t, *J* = 6.5 Hz, 2H), 2.00 – 1.93 (m, 2H), 1.33 (s, 12H), 1.27 (d, *J* = 2.6 Hz, 9H), 1.24 (s, 4H). ^{13}C NMR (126 MHz, $CDCl_3$) δ 146.42, 128.46, 126.66, 123.20, 117.00, 83.57, 51.47, 39.38, 28.20, 24.93, 22.48. HRMS (ESI+): 274.1984 (M+H), Calculated $C_{16}H_{25}BNO_2$ 274.1978

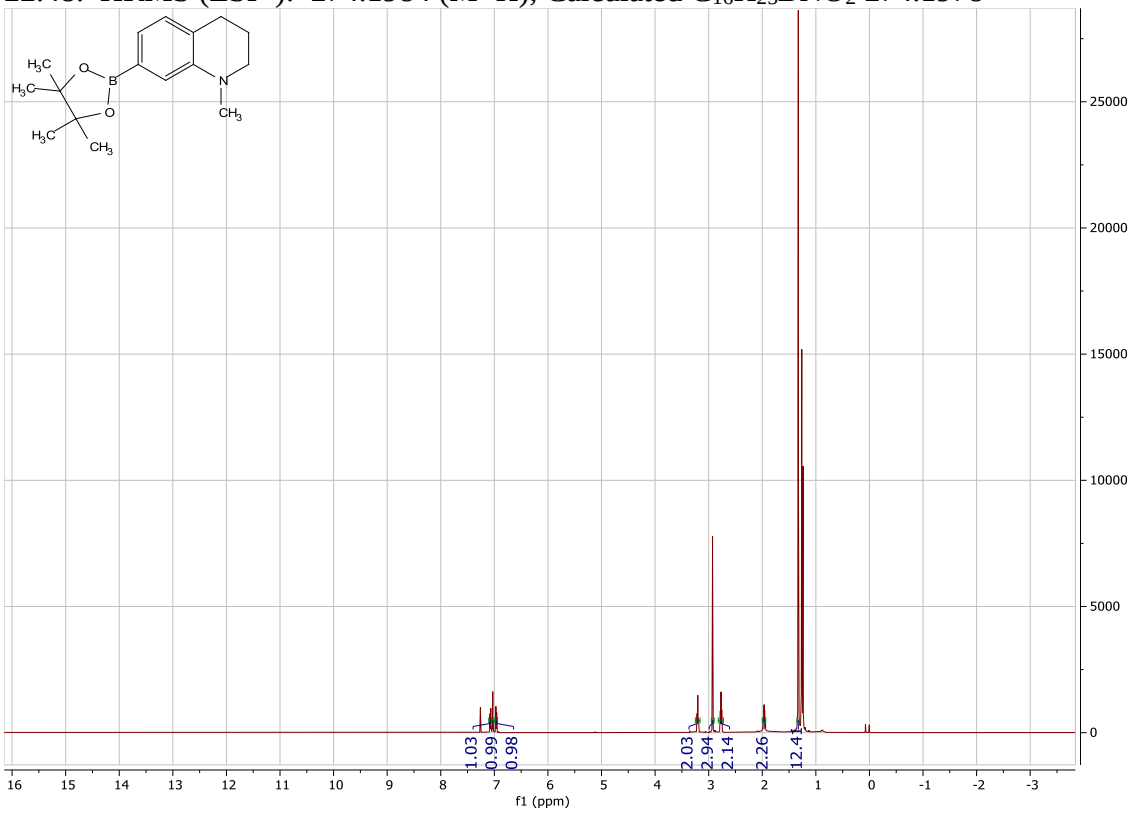

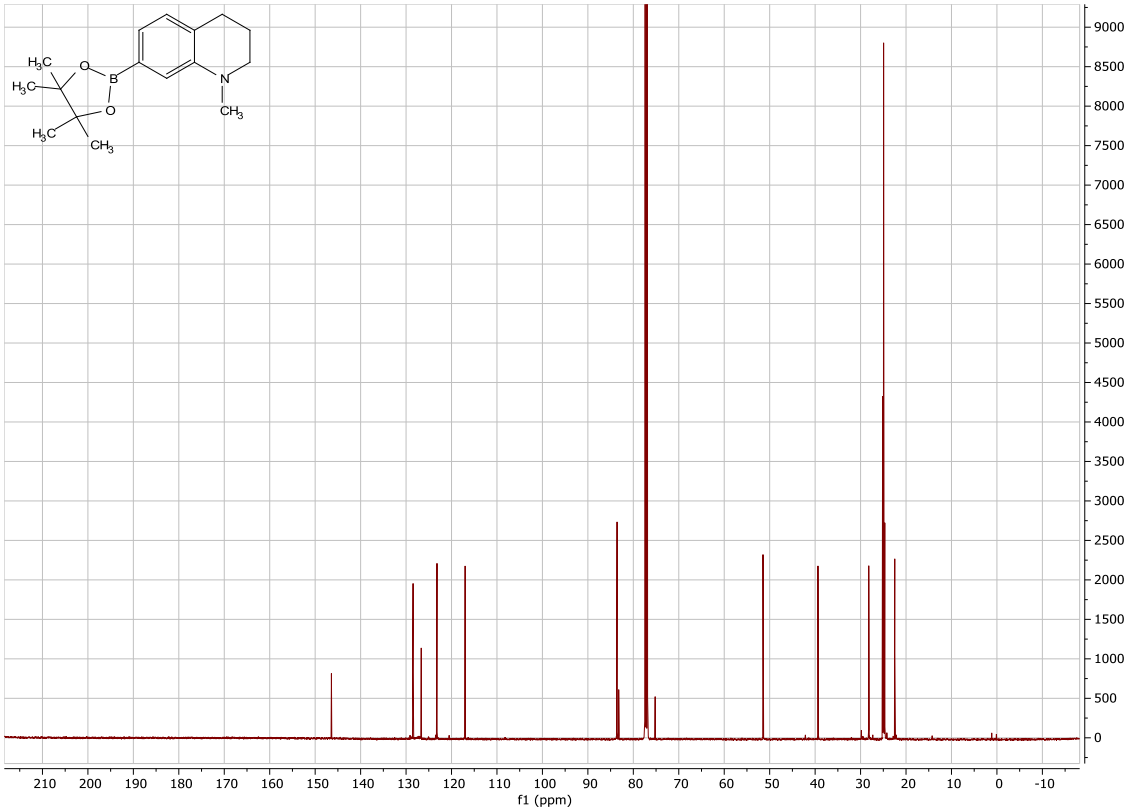

5-nitronaphthalen-1-amine

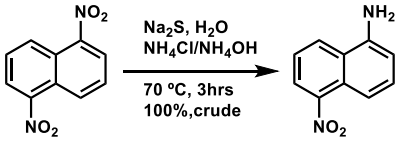

1.1 g (5.0 mmol) 1,5-dinitronaphthalene was dispersed in a solution consisting of 1.86 g (7.11 mmol) ammonium chloride in 10 mL water plus 0.31 mL (4.6 mmol) saturated (28%) aqueous ammonia. The mixture was heated to 70 °C, and 4.0 g (16.7 mmol, 3.3 eq) were added in six portions over 1.5 hrs. to ensure the temperature remained at 70 °C. Red solid forms after addition of the second portion. LCMS shows trace amounts of starting material and of over-reduction to the diamine. The reaction was poured over ice, filtered, and air-dried – 940 mg (100% yield).

2-bromo-5-nitronaphthalen-1-amine

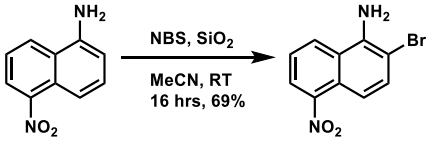

To 1 g 5-nitronaphthalen-1-amine (5.3 mmol) in 50 mL MeCN were added 35 mg SiO_2, followed by 1 g (5.62 mmol, 1.06 eq) N-bromosuccinimide. The reaction was stirred at RT for 7 hrs. Solvents were removed under reduced pressure. SiO_2 column chromatography (2:1 hexanes/ethyl acetate) to remove dibromo and succinimide impurities provided 1.37 g (69% yield). ^{1}H NMR (400 MHz, DMSO-d_6) δ 8.635 (d, J = 8.6 Hz, 1H), 8.212 (dd, J = 7.5, 0.9 Hz, 1H), 7.707 (d, J = 9.2 Hz, 1H), 7.643 – 7.558 (dd, J = 8.6, 7.6 Hz, 1H), 7.374 (d, J = 9.2 Hz, 1H), 6.331 (s, 2H).

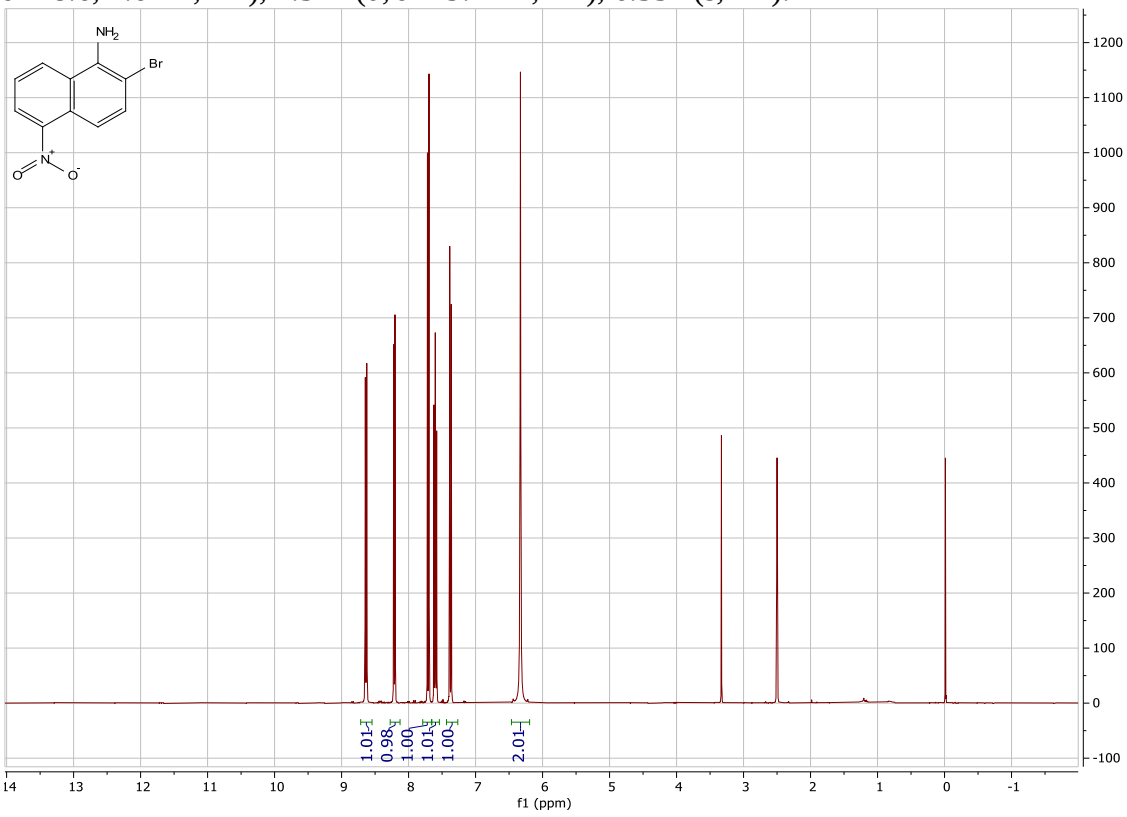

2-(1-methyl-1,2,3,4-tetrahydroquinolin-7-yl)-5-nitronaphthalen-1-amine

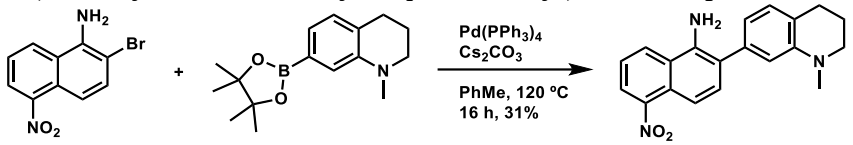

186 mg (0.696 mmol) 2-bromo-5-nitronaphthalen-1-amine, 190 mg (0.696 mmol, 1 eq), and 340 mg cesium carbonate in 3 mL toluene were sparged with N_2 for 10 min. to remove O_2. 80 mg (0.0696 mmol, 0.1 eq) $Pd(PPh_3)_4$ were added quickly and the mixture was sparged with N_2 for another 10 min before refluxing at 120 °C under N_2 for 16 hrs. After cooling to RT, the reaction was diluted in EtOAc and washed with brine. The organics were dried over Na_2SO_4, filtered, and stripped of solvents under reduced pressure. SiO_2 column purification (3:1 hexanes/EtOAc) provided 130 mg (56% yield). ^{1}H NMR (400 MHz, DMSO-d_6) δ 8.598 (dt, J = 8.6 Hz, 1.0 Hz, 1H), 8.175 (dd, J = 7.6, 1.0 Hz, 1H), 7.557 (dd, J = 8.6, 7.6 Hz, 1H), 7.537 (dd, J = 8.6 Hz, 0.9 Hz, 1H), 7.437 (d, J = 8.8 Hz, 1H), 7.022 (d, J = 7.4, 1.0 Hz,1H), 6.626 (dd, J = 7.3, 1.7 Hz, 1H), 6.610 (d, J = 1.7 Hz, 1H), 5.702 (s, 2H), 3.242 (t, J = 5.7 Hz, 2H), 2.856 (s, 3H), 2.752 (t, J = 6.4 Hz, 2H), 1.977 – 1.893 (m, 2H).

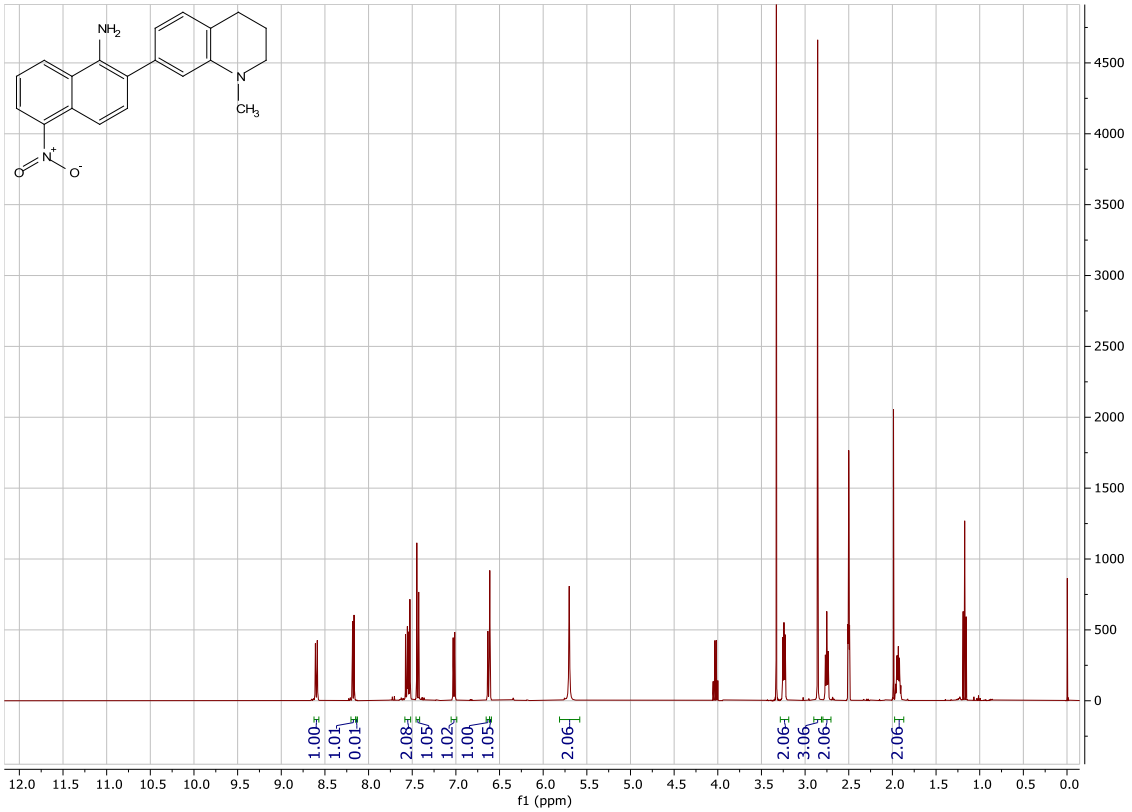

2-(1-methyl-1,2,3,4-tetrahydroquinolin-7-yl)naphthalene-1,5-diamine

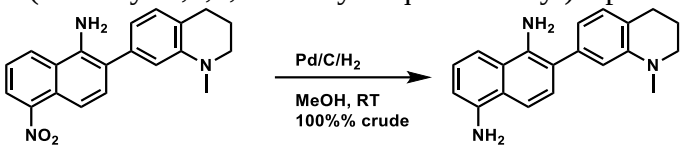

130 mg of the nitro compound were dissolved in 15 mL MeOH (with heating), and 22 mg 10% Pd/C were added after reaching RT. The suspension was sparged with hydrogen for 15 minutes and then stirred at RT overnight under H_2 balloon. Solids were filtered off, and the filtrate was stripped of solvents under reduced pressure to 118 mg (100% yield) crude.

N-(5-amino-6-(1-methyl-1,2,3,4-tetrahydroquinolin-7-yl)naphthalen-1-yl)acetamide

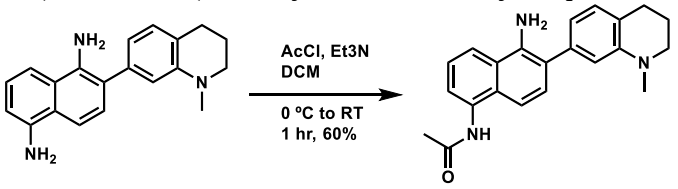

118 mg (0.389 mmol) diamine and 65 µL (0.467 mmol, 1.2 eq) in 5 mL DCM were cooled in an ice bath for 10 min. 28 µL AcCl were added dropwise via syringe over 20 min. The ice bath was removed, and the reaction stirred while warming to RT. Residual diamine and diacetamide impurities in the crude mixture were removed by SiO_2 column chromatography (2:1 hexanes/EtOAc) to give 80 mg (60% yield) mono acetamide product. ^{1}H NMR (500 MHz, Methanol-d_4) δ 7.916 (d, *J* = 8.5 Hz, 1H), 7.549 (d, *J* = 7.3 Hz, 1H), 7.415 (d, J = 8.6 Hz, 1H), 7.413 (dd, J = 8.6, 7.1 Hz, 1H), 7.277 (d, *J* = 8.5 Hz, 1H), 6.998 (d, *J* = 7.5 Hz, 1H), 6.662 (d, *J* = 1.6 Hz, 1H), 6.649 (dd, *J* = 7.5, 1.6 Hz, 1H), 3.220 (t, *J* = 5.6 Hz, 2H), 2.853 (s, 3H), 2.775 (t, *J* = 6.5 Hz, 2H), 2.257 (s, 3H), 1.983 (p, *J* = 6.4 Hz, 2H). ^{1}H NMR (400 MHz, DMSO-d_6) δ 9.796 (s, 1H), 7.994 (d, *J* = 8.4 Hz, 1H), 7.634 (d, *J* = 7.4 Hz, 1H), 7.398 (d, *J* = 8.3 Hz, 1H), 7.388 (t, *J* = 8.2 Hz, 1H), 7.234 (d, *J* = 8.6 Hz, 1H), 7.008 (d, *J* = 7.5 Hz, 1H), 6.634 (dd, *J* = 7.4, 1.5 Hz, 1H), 6.622 (d, 1H), 5.316 (s, 2H), 3.226 (t, *J* = 5.6 Hz, 2H), 2.853 (s, 3H), 2.743 (t, *J* = 6.4 Hz, 2H), 2.183 (s, 3H), 1.927 (p, *J* = 6.1 Hz, 2H). ^{13}C NMR (126 MHz, MeOD) δ 172.76, 148.48, 140.62, 139.90, 134.23, 130.24, 130.12, 129.94, 126.07, 125.25, 124.80, 123.77, 123.36, 121.58, 118.38, 113.11, 113.09, 52.36, 39.48, 28.62, 23.61, 23.25. ^{13}C NMR (101 MHz, dmso) δ 168.83, 146.88, 140.21, 138.55, 133.61, 129.01, 128.36, 127.99, 123.76, 123.68, 121.29, 121.08, 120.95, 119.89, 116.49, 111.43, 110.94, 50.62, 38.75, 27.10, 23.46, 21.97. HRMS (ESI+): 346.1915 (M+H), Calculated $C_{22}H_{24}N_3O$ 346.1919.

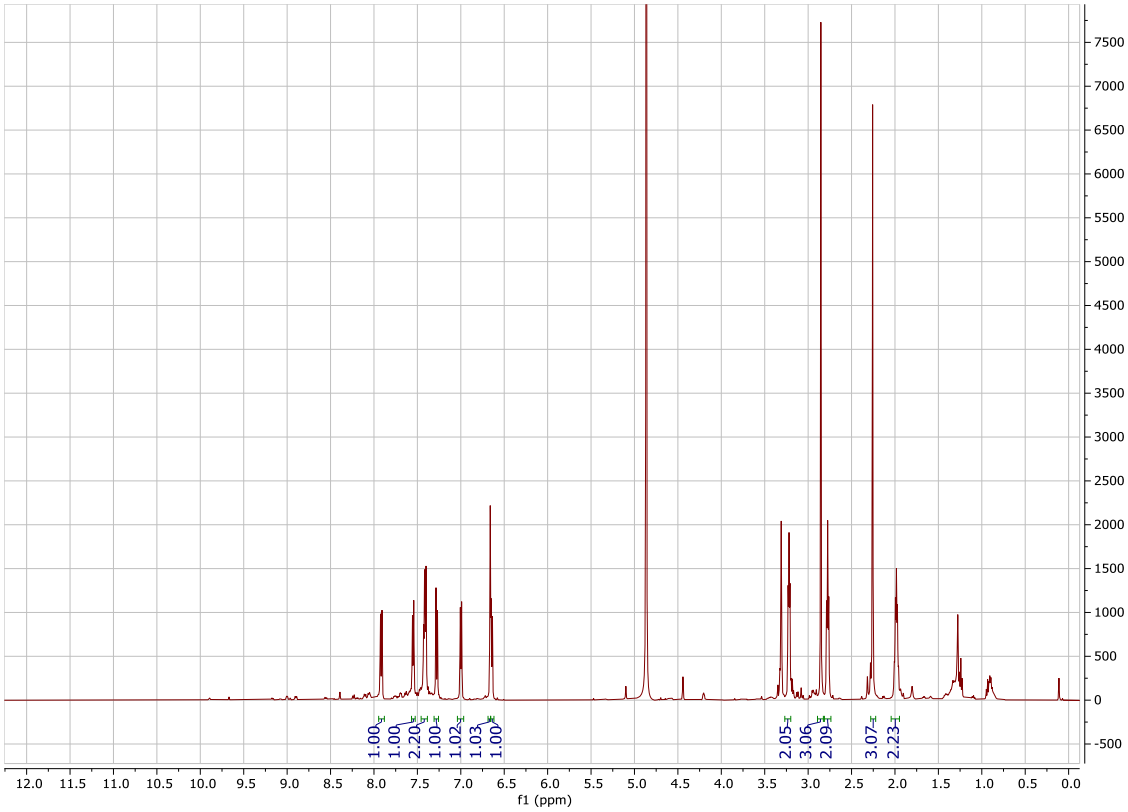
1.00
1.00
2.20
1.00
1.02
1.03
1.00
2.05
3.06
2.09
3.07
2.23
f1 (ppm)

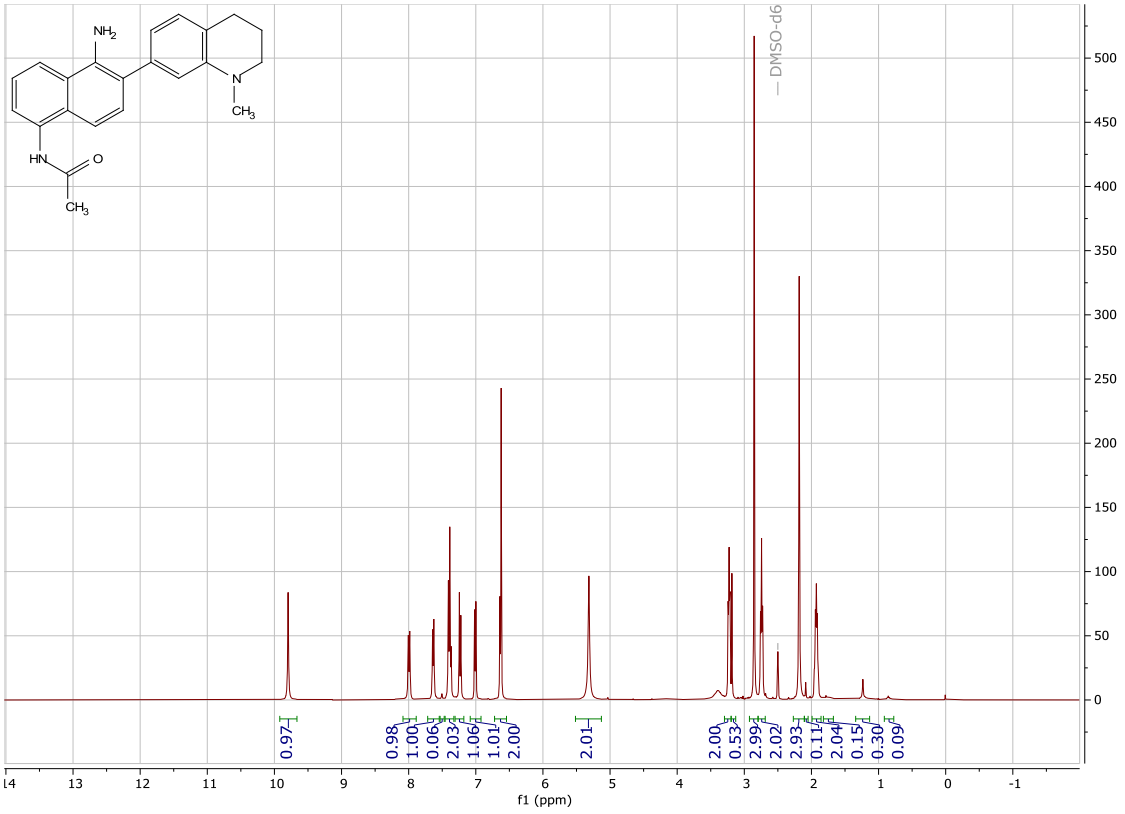
NH2
N
CH3
HN
O
CH3
DMSO-d6
0.97
0.98
1.00
0.06
2.03
1.06
1.01
2.00
2.01
2.00
0.53
2.99
2.02
2.93
0.11
2.04
0.15
0.30
0.09
f1 (ppm)

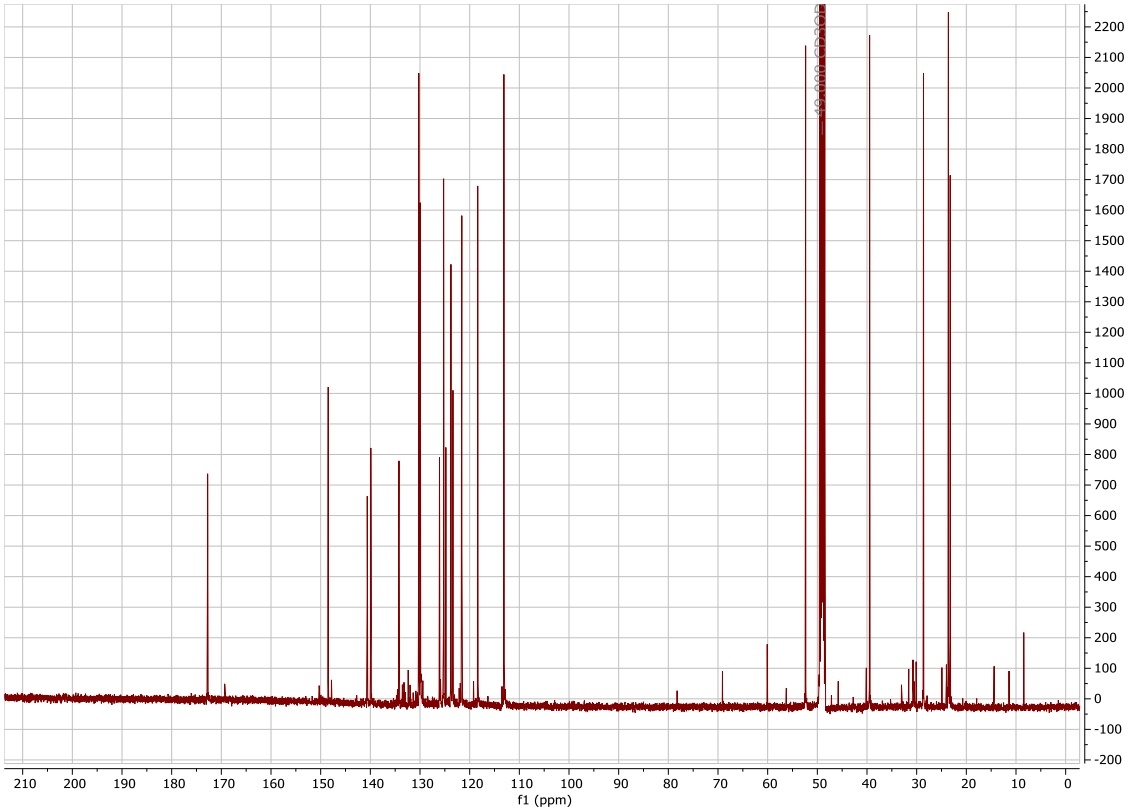
2200
2100
2000
1900
1800
1700
1600
1500
1400
1300
1200
1100
1000
900
800
700
600
500
400
300
200
100
0
-100
-200
210
200
190
180
170
160
150
140
130
120
110
100
90
80
70
60
50
40
30
20
10
0
f1 (ppm)

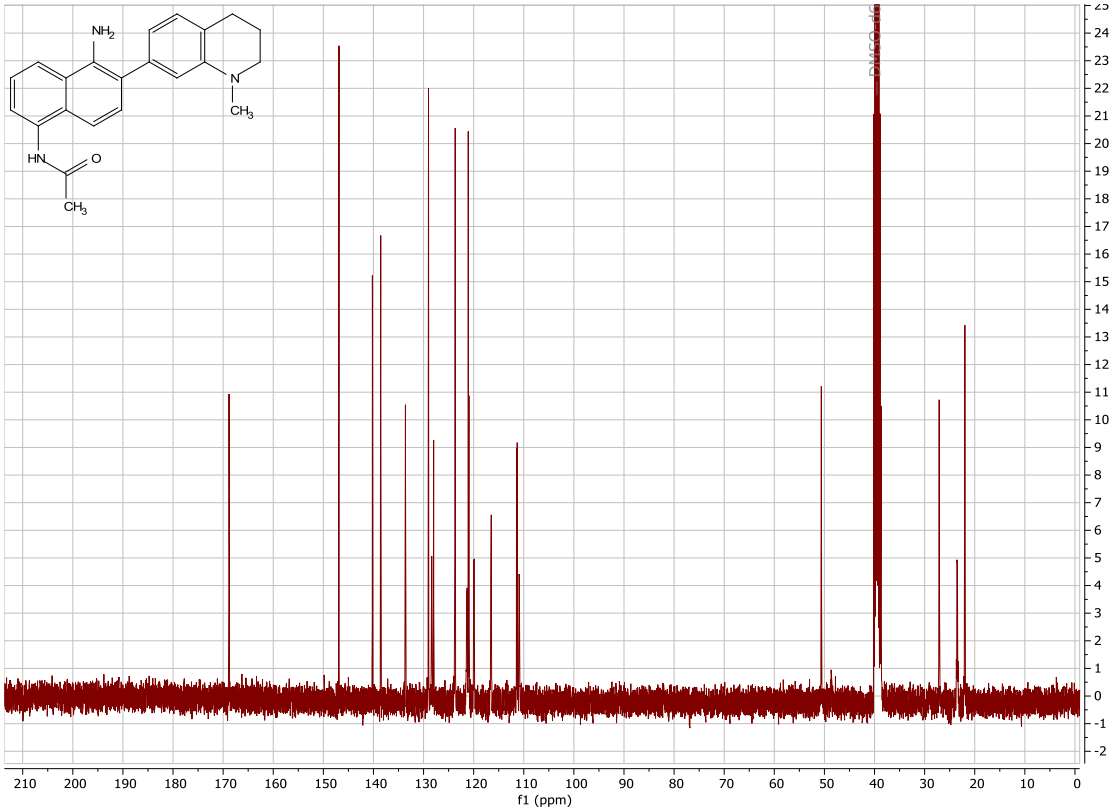

2-bromonaphthalen-1-amine

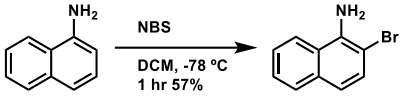

1.8 g (12.57 mmol) naphthylamine in 40 mL DCM was cooled to -78 °C in a dry ice/IPA bath for 10 min. 2.2 g (12.36 mmol, 1 eq) NBS were added in ten portions every five minutes. Thirty minutes after the final addition, the reaction was stripped of solvents under reduced pressure. SiO_2 column chromatography (2.5% EtOAc in hexanes) to remove starting material, dibromo and *para*-bromo impurities produced 2.0 g (57% yield). The *para* product is produced primarily by reacting in DMF at 0 °C. The dibromo product is produced in MeCN or MeCN/DCM, even at -78 °C, with very little monobromo product, and unreacted naphthylamine. The *para* product oxidizes readily on TLC under UV light, as does naphthylamine. The desired product oxidizes more

slowly, presumably due to the inductive effect of the bromide on the amine. The dibromo product shows very little oxidation. ^{1}H NMR (500 MHz, DMSO-d_6) δ 8.221 (dd, J = 7.3, 2.3 Hz, 1H), 7.770 (dd, J = 6.25, 2.5 Hz, 1H), 7.532 – 7.441 (m, 2H), 7.443 (d, J = 8.6 Hz, 1H), 7.070 (d, J = 8.7 Hz, 1H), 5.897 (s, 2H). ^{13}C NMR (126 MHz, DMSO) δ 141.22, 133.06, 129.78, 128.02, 126.08, 125.00, 123.10, 122.60, 116.98, 101.37. HRMS (ESI+): 221.9917 (M+H), Calculated $C_{10}H_9BrN$ 221.9918.

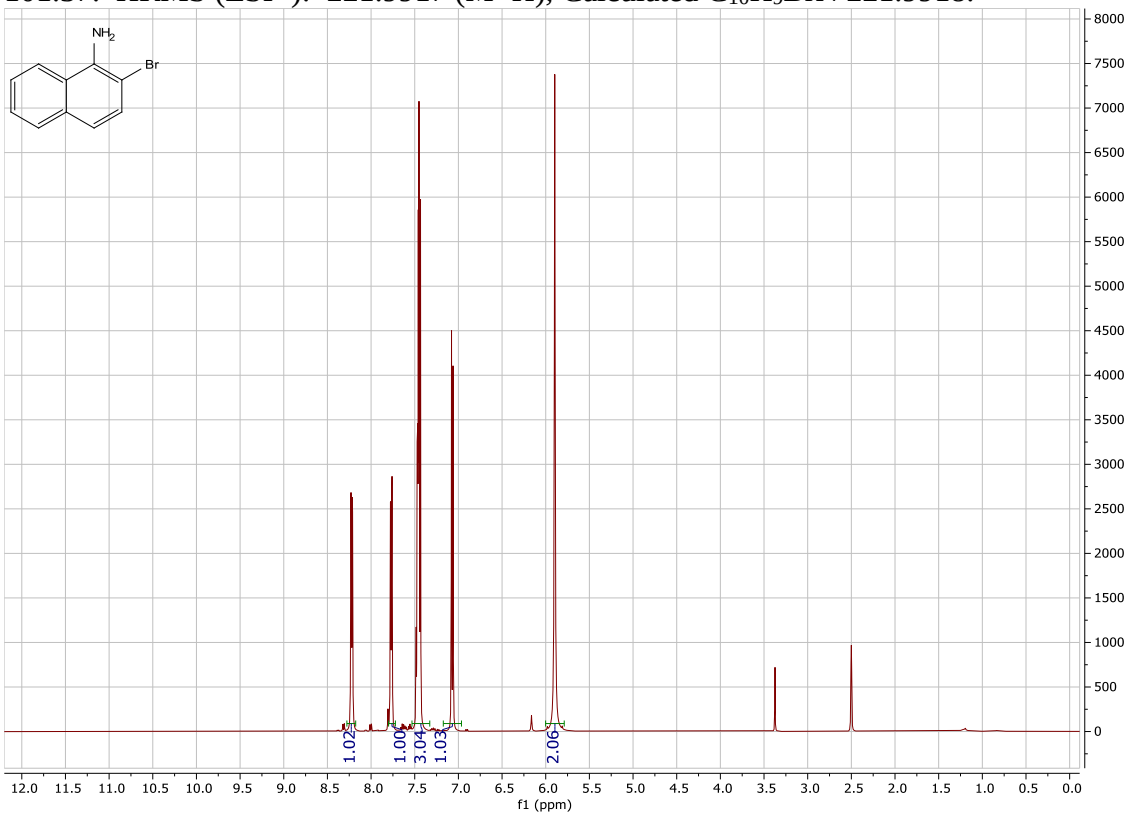

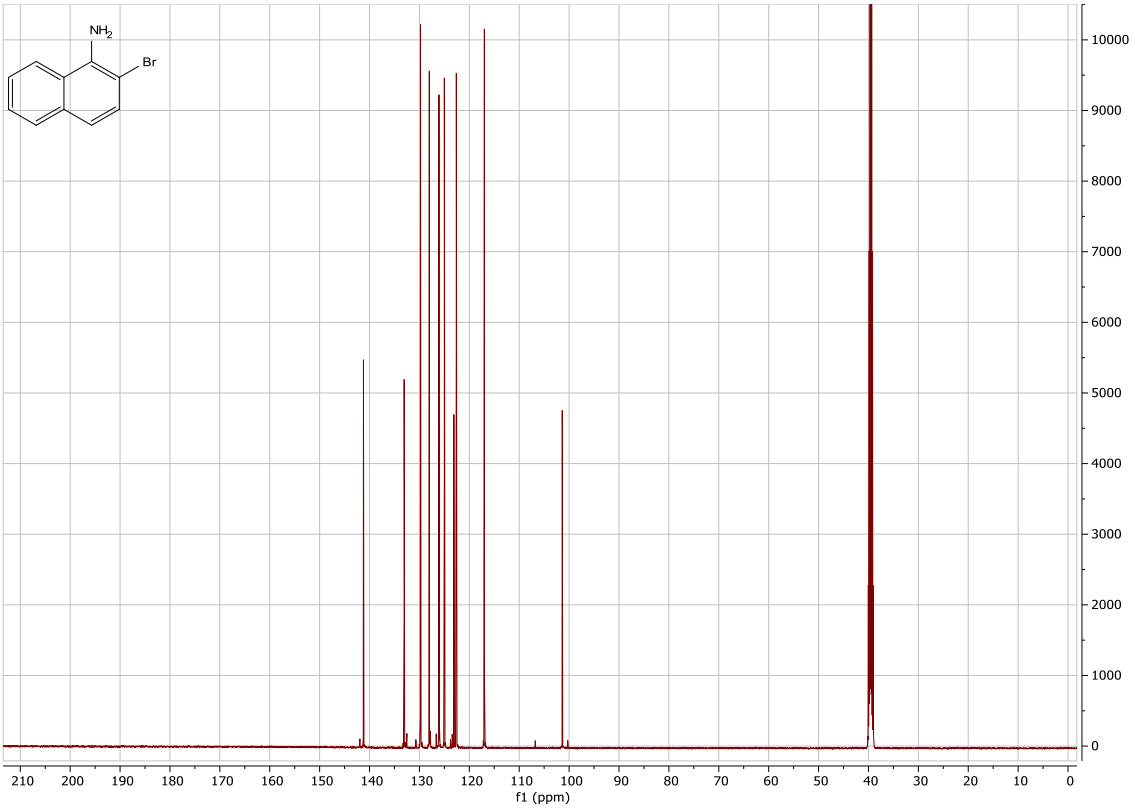

2-(2,3,6,7-tetrahydro-1H,5H-pyrido[3,2,1-ij]quinolin-8-yl)naphthalen-1-amine

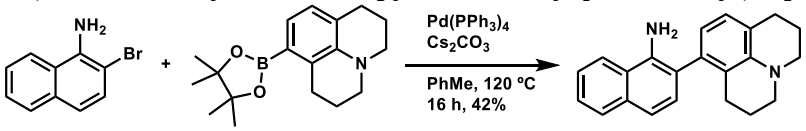

^{1}H NMR (400 MHz, Methanol-d_4) δ 7.990 (d, J = 8.3 Hz, 1H), 7.939 (d, J = 7.7 Hz, 1H), 7.702 (d, J = 8.4 Hz, 1H), 7.669 - 7.533 (m, 2H), 7.227 (d, J = 8.4 Hz, 1H), 7.044 (d, J = 7.6 Hz, 1H), 6.678 (d, J = 7.6 Hz, 1H), 3.454 – 3.327 (m, 2H), 3.326 – 3.198 (m, 2H), 2.919 (t, J = 6.8 Hz, 2H), 2.587 – 2.367 (m, 2H), 2.108 (p, J = 6.1 Hz, 2H), 1.960 (p, J = 6.5 Hz, 2H). HRMS (ESI+): 315.1858 (M+H), Calculated $C_{22}H_{23}N_2$ 315.1861.

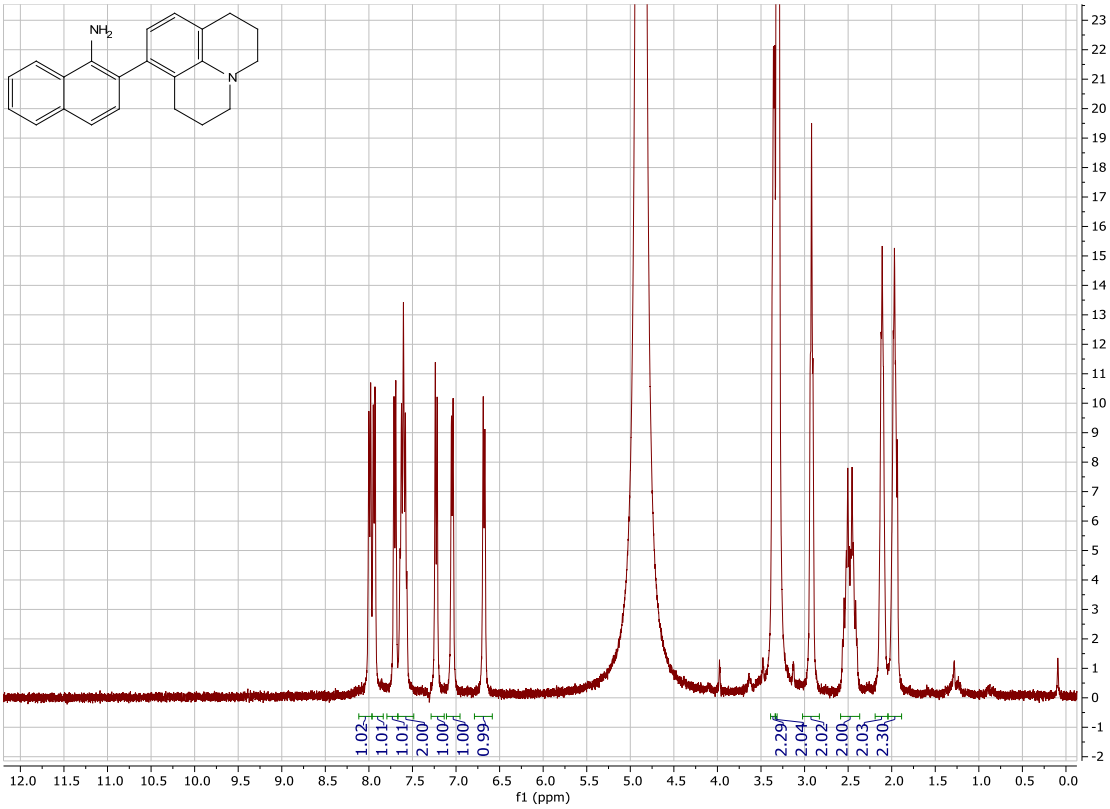

5-nitro-2-(2,3,6,7-tetrahydro-1H,5H-pyrido[3,2,1-ij]quinolin-8-yl)naphthalen-1-amine

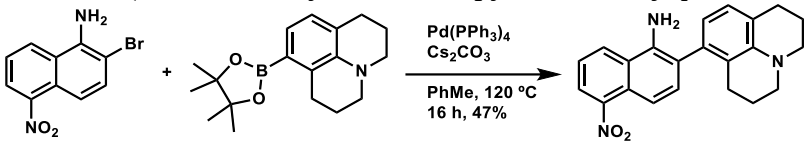

152.1 mg (0.570 mmol) of the bromide, 198.8 mg (0.664 mmol, 1.17 eq), and 557 mg (1.710 mmol, 3 eq) cesium carbonate in 10 mL toluene were sparged with N_2 for 20 min. to remove O_2. 66 mg (0.057 mmol, 0.1 eq) $Pd(PPh_3)_4$ were added quickly and the mixture was sparged with N_2 for another 10 min before refluxing at 120 °C under N_2 for 16 hrs. After cooling to RT, the reaction was diluted in EtOAc and washed with brine. The organics were dried over Na_2SO_4, filtered, and stripped of solvents under reduced pressure. SiO_2 column purification (10% EtOAc in DCM) provided 100 mg slightly impure product. Prep TLC (1000 mm SiO_2 F60) purification with 2:1 hexanes/EtOAc

provided 97 mg (47% yield). ^{1}H NMR (400 MHz, Chloroform-*d*) δ 8.165 (dt, *J* = 8.6, 1.1 Hz, 1H), 8.139 (dd, *J* = 7.6, 1.1 Hz, 1H), 7.917 (dd, *J* = 8.8, 1.0 Hz, 1H), 7.500 (dd, *J* = 8.5, 7.6 Hz, 1H), 7.380 (d, *J* = 8.8 Hz, 1H), 6.971 (d, *J* = 6.8 Hz, 1H), 6.602 (bs, 1H), 4.235 (bs, 2H), 3,394 – 3.086 (m, 4H), 2.884 (t, *J* = 6.7 Hz, 2H), 2.484 (t, *J* = 6.8 Hz, 2H), 2.271 – 2.023 (m, 2H), 2.023 – 1.828 (m, 2H).

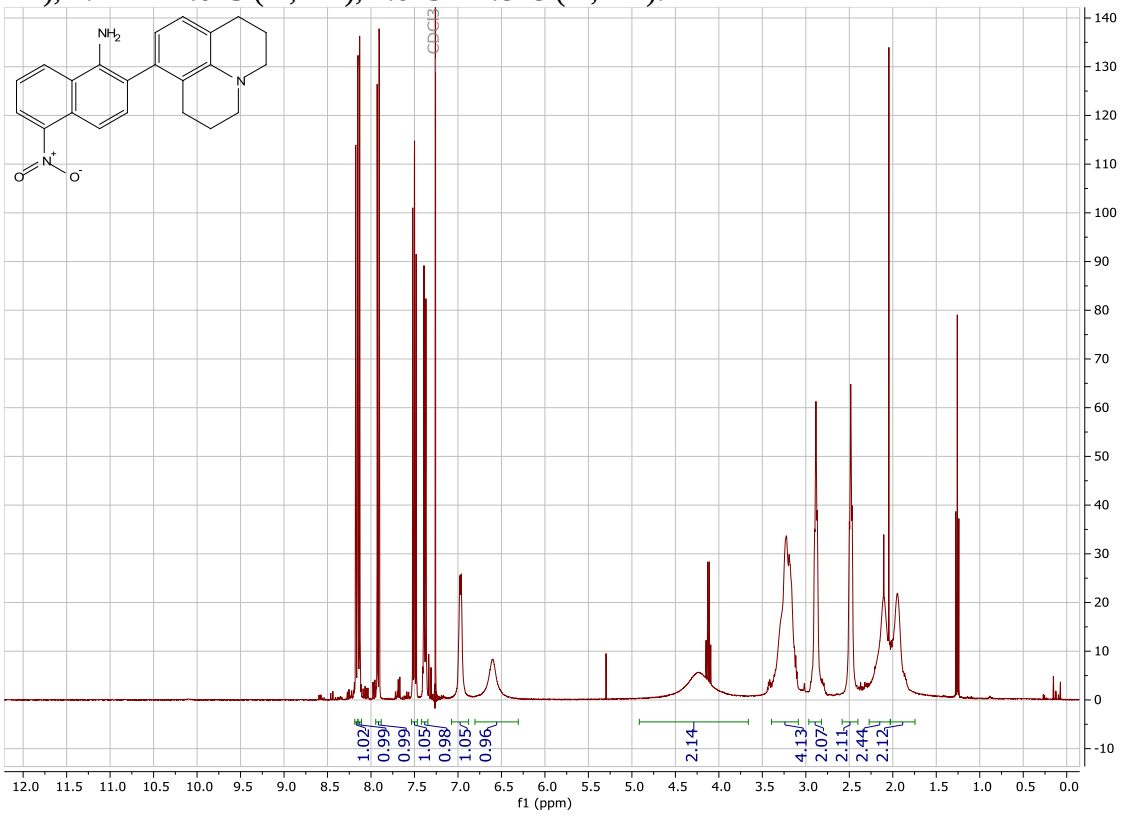

2-(2,3,6,7-tetrahydro-1H,5H-pyrido[3,2,1-ij]quinolin-8-yl)naphthalene-1,5-diamine

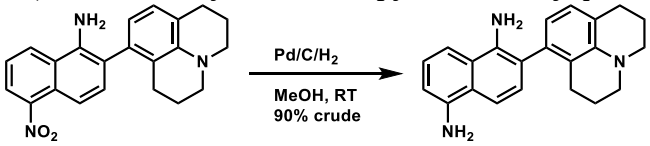

100 mg (0.278 mmol) were dispersed in 10 mL MeOH, and 20 mg 10% Pd/C were added. The suspension was sparged with H_2 for 15 min and then stirred at RT for 36 hrs.

The reaction was then filtered, and the filtrate was stripped of solvents at reduced pressure to give 83 mg (90% yield).

N-(5-amino-6-(2,3,6,7-tetrahydro-1H,5H-pyrido[3,2,1-ij]quinolin-8-yl)naphthalen-1-yl)acetamide

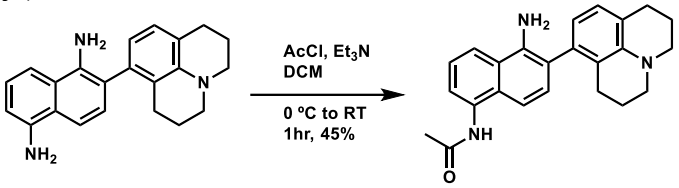

41 mg (0.124 mmol) diamine and 65 µL (0.467 mmol, 1.2 eq) triethylamine in 3 mL DCM were cooled in an ice bath for 10 min. 9 µL AcCl were added dropwise via syringe over 10 min. The ice bath was removed, and the reaction stirred while warming to RT. SiO_2 column chromatography (1-2% MeOH in Et_2O) gave 21 mg (45% yield) product after removing solvents at less than 30 °C under reduced pressure. ^{1}H NMR (400 MHz, DMSO-d_6) δ 9.759 (s, 1H), 7.953 (d, J = 8.6 Hz, 1H), 7.603 (d, J = 7.4 Hz, 1H), 7.362 (t, J = 8.6 Hz, 1H), 7.352 (d, J = 7.3 Hz), 7.044 (d, J = 8.6 Hz, 1H), 6.819 (d, J = 7.5 Hz, 1H), 6.319 (d, J = 7.5 Hz, 1H), 4.963 (s, 2H), 3.147 (dt, J = 5.6, 2.1 Hz, 2H), 3.093 (dt, J = 5.3, 3.3 Hz, 2H), 2.737 (t, J = 6.5 Hz, 2H), 2.441 – 2.241 (m, 2H), 2.164 (s, 3H), 1.995 – 1.846 (m, J = 6.7 Hz, 2H), 1.769 (p, J = 6.3 Hz, 2H). ^{13}C NMR (101 MHz, dmso) δ 169.21, 143.61, 140.67, 137.01, 134.02, 128.61, 128.51, 127.29, 123.96, 123.89, 121.73, 120.97, 120.65, 120.29, 117.54, 110.98, 50.07, 49.67, 27.84, 25.31, 23.90, 22.09, 21.98. HRMS (ESI+): 372.2059 (M+H), Calculated $C_{24}H_{26}N_3O$ 372.2076.

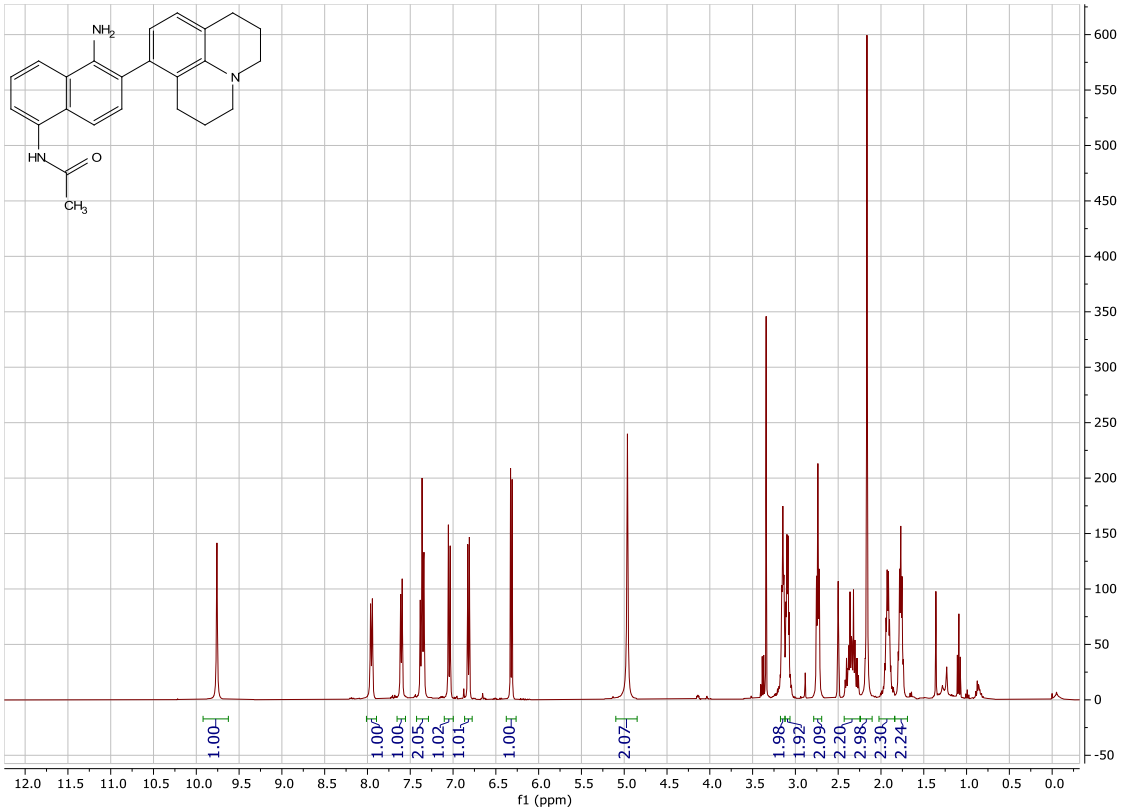
NH2
N
HN
O
CH3
1.00
1.00
1.00
2.05
1.02
1.01
1.00
2.07
1.98
1.92
2.09
2.20
2.98
2.30
2.24
f1 (ppm)

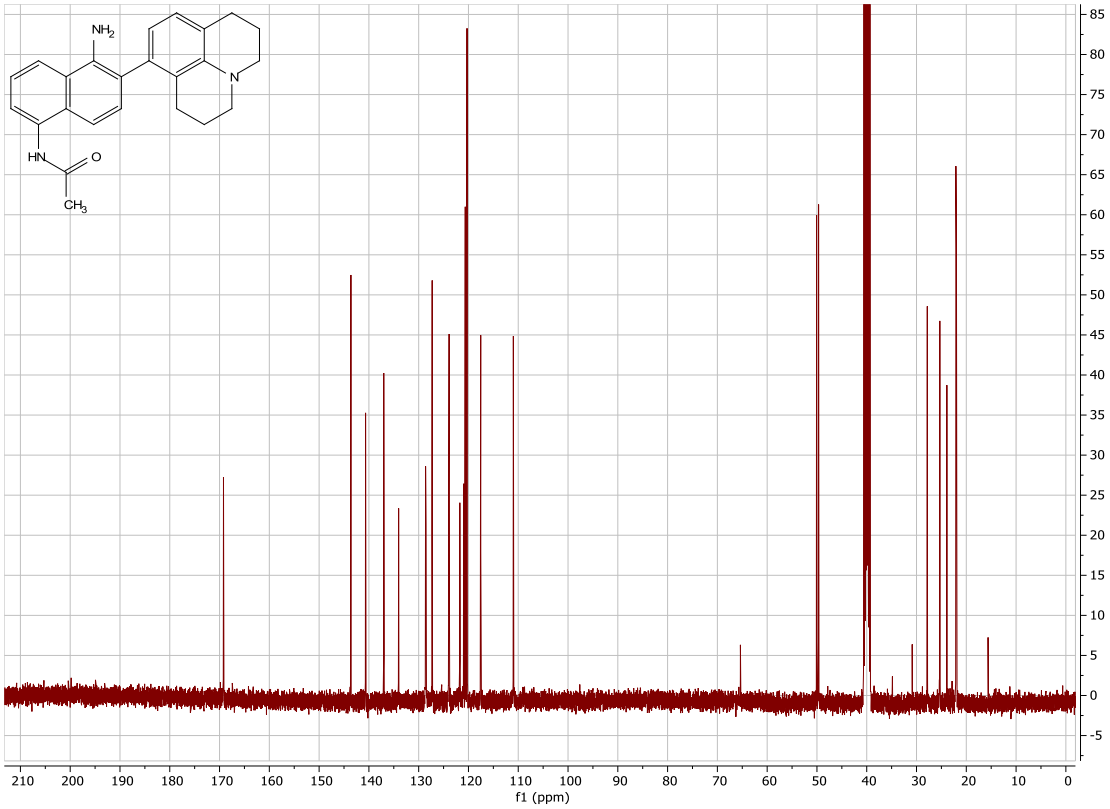

4-methyl-2-(1-methyl-1,2,3,4-tetrahydroquinolin-7-yl)aniline

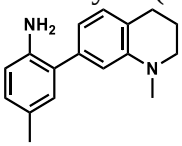

Probe **6**'s tendency to oxidize is much lower than that of **10**, **11**, and **13**. The sample from the Yang lab was fairly intact and could be purified by SiO_2 chromatography; no synthesis was required. Probe **6** is soluble in hexanes.

^{1}H NMR (500 MHz, Methanol-d_4) δ 6.955 (d, J = 7.5 Hz, 1H), 6.895 (dd, J = 8.0, 2.4 Hz, 1H), 6.870 (d, J = 2.4 Hz, 1H), 6.718 (d, J = 8.0 Hz, 1H), 6.587 (d, J = 1.8 Hz, 1H), 6.565 (dd, J = 7.5, 1.8 Hz, 1H), 3.222 (t, J = 5.7 Hz, 2H), 2.866 (s, 3H), 2.767 (t, J = 6.4 Hz, 2H), 2.226 (s, 3H), 1.992 (p, J = 6.5, 5.1 Hz, 2H), 1.284 (s, 1H). ^{13}C NMR (126 MHz, MeOD) δ 148.32, 142.16, 139.79, 131.49, 130.83, 130.01, 129.41, 128.95, 123.21, 118.10, 117.45, 112.90, 52.42, 39.53, 28.60, 23.66, 20.60.

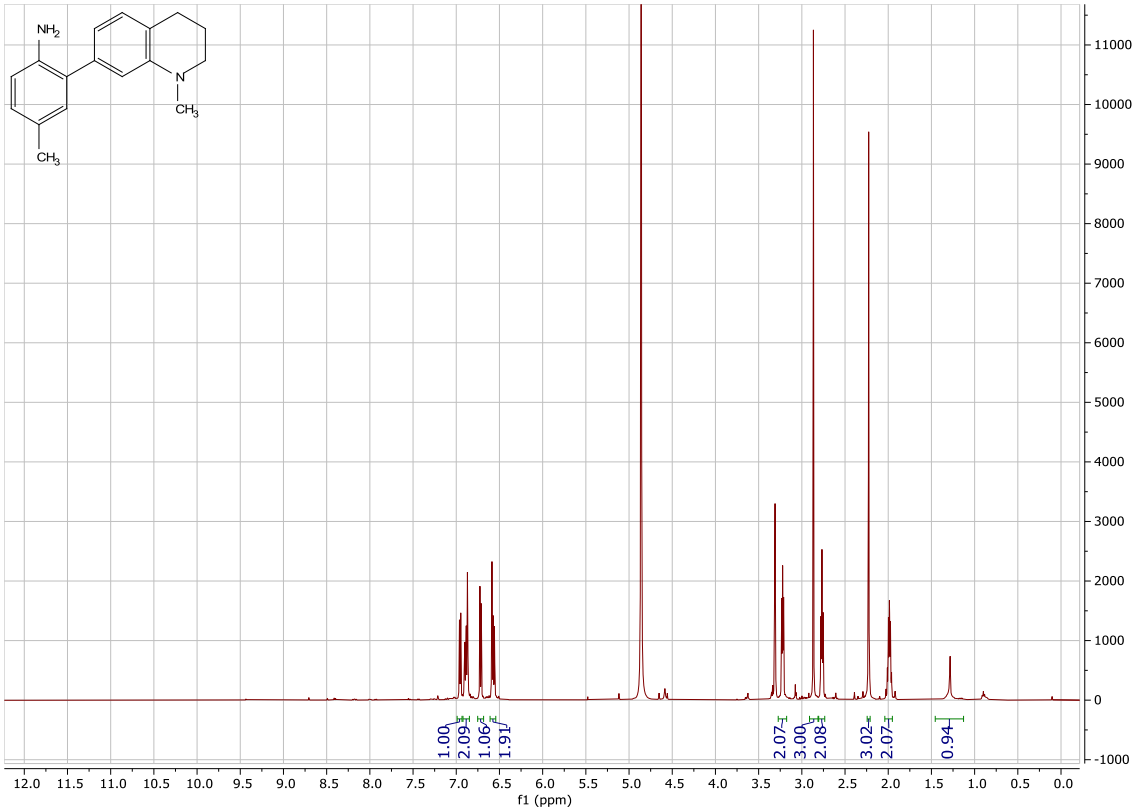
NH2
N
CH3
CH3
11000
10000
9000
8000
7000
6000
5000
4000
3000
2000
1000
0
-1000
1.00
2.09
1.06
1.91
2.07
3.00
2.08
3.02
2.07
0.94
12.0 11.5 11.0 10.5 10.0 9.5 9.0 8.5 8.0 7.5 7.0 6.5 6.0 5.5 5.0 4.5 4.0 3.5 3.0 2.5 2.0 1.5 1.0 0.5 0.0
f1 (ppm)

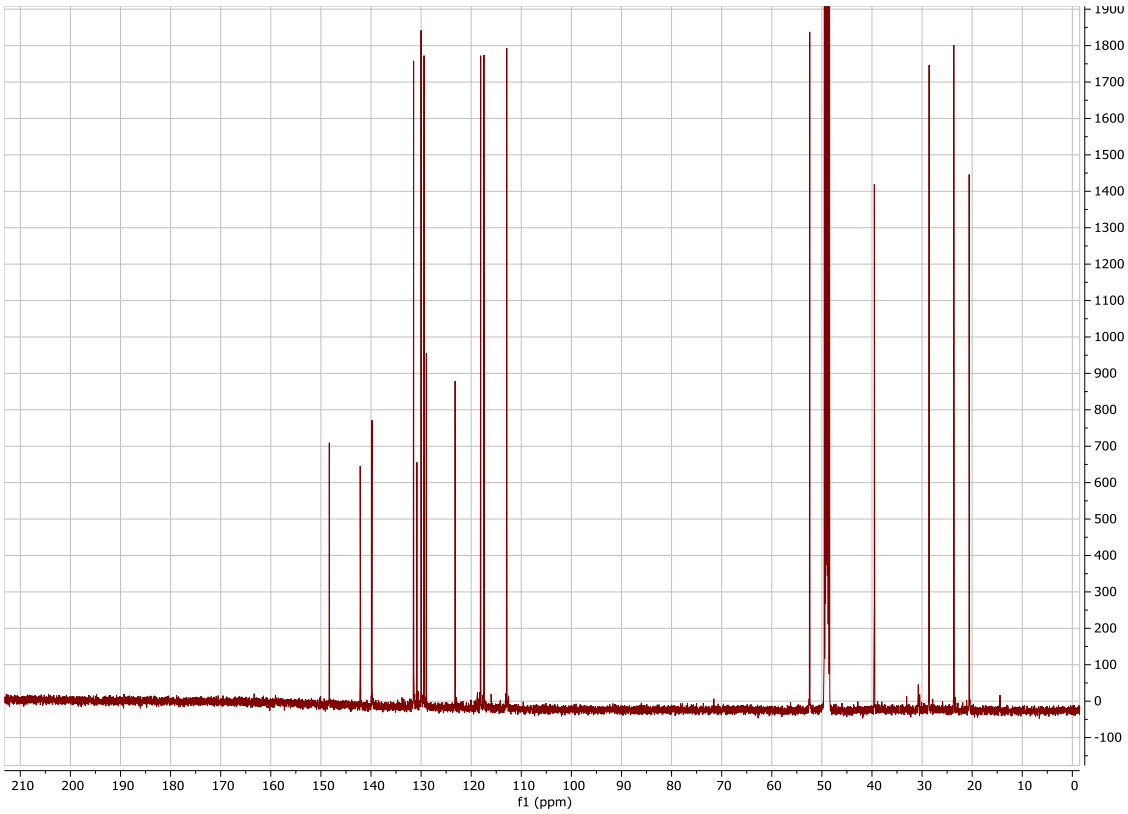

3,3'-oxybis(nitrobenzene)

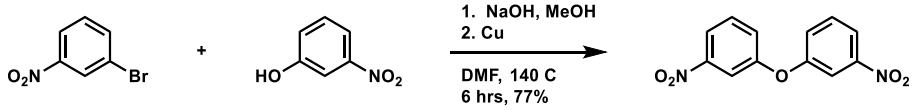

139 mg (1 mmol) *m*-nitrophenol and 40 mg NaOH were dissolved in MeOH to produce an orange solution. Solvents were removed at reduced pressure to give an orange solid, which was combined with 202 mg (1 mmol) 3-bromo-nitrobenzene and dissolved in 0.5 mL dry DMF. The mixture was sparged with N_2 for 5 min., and then 5 mg (0.08 mmol, 0.08 eq) copper powder were added. After sparging for another 10 min, the reaction was heated to 140 °C under N_2 balloon for six hours. The reaction was diluted with EtOAc and washed twice with 1 M aqueous citric acid and once with brine. The organics were

dried over Na_2SO_4, filtered free of solids, and stripped of solvents under reduced pressure. The resulting solid was triturated with MeOH to give 200 mg (77% yield). ^{1}H NMR (500 MHz, DMSO-d_6) δ 8.062 (m, *J* = 8.2, 2.6 Hz, 2H), 7.860 (t, *J* = 2.4 Hz, 2H), 7.725 (t, *J* = 8.2 Hz, 2H), 7.595 (dd, *J* = 8.2, 2.7 Hz, 2H). ^{13}C NMR (126 MHz, DMSO) δ 156.30, 148.94, 131.64, 125.67, 119.19, 113.75.

3,3'-oxydianiline

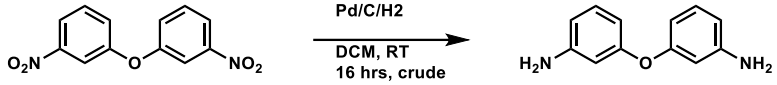

20 mg 10% Pd/C was added to a solution of 45 mg (0.25 mmol) dinitro compound in 5 mL DCM. The mixture was sparged with H_2 for 15 min and then stirred at RT overnight. It was next filtered through celite and stripped free of solvents under reduced pressure to give 34 mg (98% yield) crude. ^{1}H NMR (400 MHz, Methylene Chloride-d_2) δ 7.064 (t, *J* = 8.0 Hz, 1H), 6.399 (ddd, *J* = 8.0, 2.2, 1.0 Hz, 2H), 6.349 (ddd, *J* = 8.1, 2.2, 1.0 Hz, 2H), 6.301 (t, *J* = 2.2 Hz, 1H), 3.739 (s, 4H).

2,2',2",2"'-((oxybis(3,1-phenylene))bis(azanetriyl))tetrakis(ethan-1-ol)

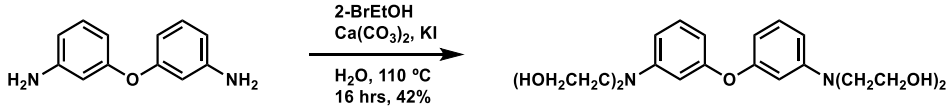

50 mg (0.25 mmol, crude) diamine, 141 µL (2 mmol, 8.0 eq) 2-bromoethanol, 100 mg (1.0 mmol, 4 eq) calcium carbonate, and 4 mg (0.025 mmol, 0.1 eq) KI in 1 mL water were refluxed under N_2 at 110 °C overnight. After cooling to RT, the reaction was diluted with brine and extracted with EtOAc. The organics were washed with brine, and the combined aqueous layers (pink) were extracted with 20% methanol in DCM. The

organics were comibined, dried over Na_2SO_4, and stripped of solvents under reduced pressure. SiO2 column chromatography (0-8% MeOH in EtOAc) gives 40 mg (42% yield). ^{1}H NMR (500 MHz, DMSO-d_6) δ 7.064 (t, J = 8.2 Hz, 2H), 6.413 (dd, J = 8.5, 2.5 Hz, 2H), 6.331 (d, J = 2.4 Hz, 2H), 6.096 (dd, J = 8.0, 2.1 Hz, 2H), 4.748 (t, J = 5.7 Hz, 4H), 3.511 (q, J = 6.0 Hz, 8H), 3.387 (d, J = 2.6 Hz, 8H). ^{13}C NMR (126 MHz, DMSO) δ 157.94, 149.55, 129.93, 106.47, 104.80, 101.86, 58.07, 53.31. HRMS (ESI+): 399.1890 (M+Na), Calculated $C_{20}H_{28}N_2O_5Na$ 399.1896.

tetraethyl 2,2',2",2'"-((oxybis(3,1-phenylene))bis(azanetriyl))tetraacetate

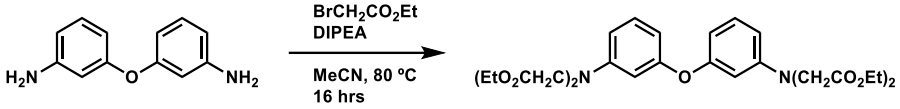

34 mg (0.170 mmol) diamine, 150 µL (1.36 mmol, 8 eq) ethyl bromoacetate , 178 µL (1.02 mmol, 6 eq) N,N-diisopropylethylamine in 2 mL MeCN were stirred at 80 °C overnight. The reaction was diluted in EtOAc, washed twice with brine, dried over Na_2SO_4, and stripped of solvents under reduced pressure. The crude product was loaded onto two 1mm prep TLC SiO_2 plates in DCM, eluted with hexanes/EtOAc, and extracted from the plates with EtOAc to give mg (% yield) after filtering and stripping solvents to dryness. ^{1}H NMR (400 MHz, Chloroform-d) δ 7.107 (t, J = 8.2 Hz, 2H), 6.358 (ddd, J = 8.1, 2.1, 0.80 Hz, 2H), 6.319 (ddd, J = 8.2, 2.6, 0.80 Hz, 2H), 6.285 (t, J = 2.4 Hz, 2H), 4.185 (q, J = 7.1, 8H), 4.092 (s, 8H), 1.377 – 1.121 (t, J = 7.2 Hz, 12H). HRMS (ESI+): 545.2508 (M+H), Calculated $C_{28}H_{37}N_2O_9$ 545.2499.

2-(4-(dimethylamino)-2-hydroxybenzoyl)benzoic acid

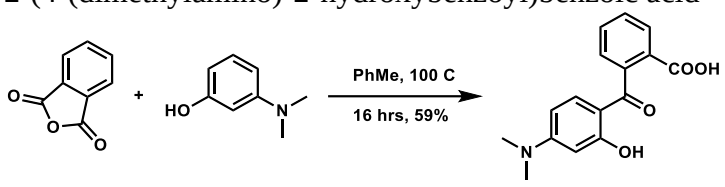

275 mg (2.0 mmol) N,N-dimethyl-3-aminophenol and 296 mg (2.0 mmol, 1 eq) phthalic anhydride were suspended in 10 mL toluene and refluxed at 100 °C overnight. After cooling, the crude mixture was purified free of tetramethyl rhodamine by SiO_2 chromatography (10% MeOH in $CHCl_3$) to give 337 mg (59% yield).

3'-amino-2'-bromo-6'-(dimethylamino)-3H-spiro[isobenzofuran-1,9'-xanthen]-3-one

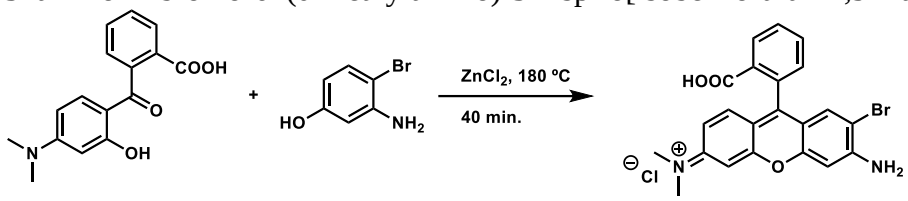

337 mg (1.18 mmol) ketone, 222 mg (1.18 mmol, 1 eq) 3-amino-4-bromophenol, and 100 mg (0.734 mmol) zinc chloride were melted at 180 °C and stirred until the mixture solidified (40 minutes). The solid was triturated with 0.5 M aq. HCl, filtered, and air-dried overnight. ^{1}H NMR (500 MHz, Methanol-d_4) δ 8.258 (d, J = 7.7 Hz, 1H), 7.778 (t, J = 7.4 Hz, 2H), 7.729 (t, J = 7.6 Hz, 2H), 7.329 (d, J = 7.4 Hz, 1H), 7.188 (s, 1H), 7.061 (d, J = 9.6 Hz, 1H), 7.006 (dd, J = 9.6, 2.4 Hz, 1H), 6.883 (s, 1H), 6.865 (d, J = 2.4 Hz, 1H), 3.219 (s, 6H). ^{13}C NMR (126 MHz, MeOD) δ 167.98, 161.67, 159.69, 159.36, 157.76, 156.74, 134.69, 134.40, 134.04, 132.65, 132.56, 132.19, 131.78, 131.43, 116.54, 115.68, 115.55, 110.20, 99.57, 97.53, 41.21, 39.47.

3'-amino-6'-(dimethylamino)-2'-(3-(dimethylamino)phenyl)-3H-spiro[isobenzofuran-1,9'-xanthen]-3-one

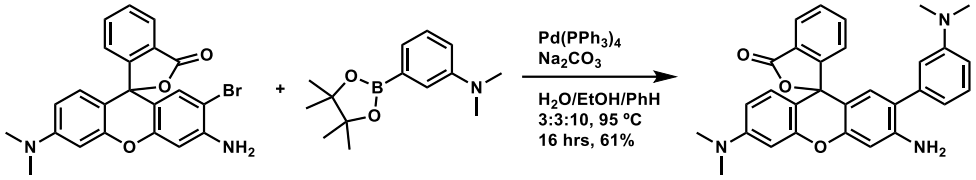

22 mg (0.050 mmol) bromide, 11 mg (0.067, 1.3 eq) boronate, and 54 mg (0.51 mmol, 10 eq) in 1 mL EtOH, 300 µL benzene, and 300 µL water were sparged with argon for 10 min. 4 mg (0.0035 mmol, 0.07 eq) $Pd(PPh_3)_4$ were quickly added, and the mixture was sparged with argon for another 5 min prior to stirring overnight at 95 °C under argon. The solvents evaporated off by the next morning. The solid was sonicated in EtOH, and the suspension was diluted with DCM and washed with pH 4 (adjusted with HCl) brine. The aqueous layer was extracted repeatedly with DCM until colorless. The combined organics were dried over Na2SO4, filtered, and stripped free of solvents at reduced pressure. The crude mixture was purified by prep HPLC (C_{18} column, MeOH/water binary gradient with 0.1% formic acid added) to remove major de-brominated rhodamine and other minor impurities. Combined pure fractions were stripped of solvents to 10 mL volume under reduced pressure, and the remaining solvents were removed by lyophilization to 16 mg (61 % yield). ^{1}H NMR (500 MHz, DMSO-d_6) δ 7.927 (d, *J* = 7.6 Hz, 1H), 7.769 (t, *J* = 7.5 Hz, 1H), 7.665 (t, *J* = 7.5 Hz, 1H), 7.288 (d, *J* = 7.6 Hz, 1H), 7.144 (t, *J* = 7.9 Hz, 1H), 6.640 (s, 1 H), 6.632 (dd, *J* = 8.875, 2.8 Hz, 1 H), 6.538 (d, *J* = 1.9 1.6 Hz, 1H), 6.515 – 6.441 (m, 3H), 6.397 (d, *J* = 7.4 Hz, 1H), 6.184 (s, 1H), 5.295 (s, 2H), 2.941 (s, 6H), 2.830 (s, 6H). ^{13}C NMR (126 MHz, DMSO) δ 168.82, 152.33, 152.22, 151.94, 151.50, 150.51, 147.70, 138.71, 135.36, 129.91, 129.47, 128.66, 128.32, 126.68, 124.41, 124.08, 123.86, 116.16, 112.07, 111.26, 108.95, 106.80,

106.05, 100.12, 98.20, 84.67, 48.61. HRMS (ESI+): 478.2130 (M+H), Calculated $C_{30}H_{28}N_3O_3$ 478.2131.

APPENDIX C: CELL EXPERIMENTS, MATERIALS, EQUIPMENT, AND IMAGING

Cell Cultures

NIH 3T3 and RAW 264.7 cells (ATCC) were cultured in high-glucose Dulbecco's Modified Eagle Medium (DMEM) or Leibovitz's L-15 Medium (L-15) with 10% BCS (NIH 3T3) or 10% FBS (RAW 264.7) added. For the bicarbonate-buffered DMEM medium, the cells were incubated in a humidified environment at 37 °C under 5% CO_2/air, whereas for the phosphate-buffered L-15 medium, no CO_2 was added. Cells were passaged at least three times prior to any imaging experiments. For fluorescence microscopy, cells were plated onto Lab-Tek II Chambered #1.5 German Coverglass sterile 8-well plates in DMEM or L-15 medium supplemented with 1% serum.

Passaging Cells

DMEM + 10% BCS medium was removed from 70-90% confluent NIH 3T3 cells in T25 culture flasks, and 0.05% trypsin-EDTA solution with phenol red was promptly added. The cells were incubated at 37 °C under 5% CO2 for one minute so they would detach, and then the cell suspension was transferred to a 15 mL centrifuge tube. The culture flask was rinsed with 3 mL DPBS,and the cells were centrifuged to a pellet. The supernatant was discarded, and the cells were suspended in 1 mL DMEM + 10% BCS. 80-100 μL of this suspension was added to a new culture flask containing 4 mL DMEM + 10% BCS, and the cells were incubated at 37 °C under 5% CO2 to complete the passage.

DMEM + 10% FBS was removed from 70-90% confluent RAW 264.7 cells, and 1 mL DPBS was added. The cells were detachedwith a cell scraper, and the cell

suspension was transferred to a 15 mL centrifuge tube. The culture flask was rinsed with 3 mL DPBS, and the cell suspension was centrifuged. The cell pellet was suspended in 1 mL DMEM + 10% FBS, and an 80-100 μL aliquot of this suspension was added to 4 mL DMEM + 10% FBS in a new culture flask. The cells were incubated at 37 °C under 5% CO2 to complete the passage.

Cell plating

Each well of a Nunc Lab-Tek II Chambered Coverglass 8-well plate was charged with 500 μL DMEM + 1% BCS (NIH 3T3) or FBS (RAW 264.7). The centrifuged cell pellet obtained as described in the section above was suspended in 1 mL DMEM + 1% serum. A 10-20 μL aliquot of this suspension was added to each well, and the cells were incubated at 37 °C under 5% CO2.

SNAP stimulus experiments

NIH 3T3 cells were plated into a Nunc 8-well plate in high-glucose DMEM + 1% BCS and incubated overnight at 37 °C under 5% CO_2/air. The DMEM was then replaced with Hepes Hanks Buffered Saline Solution (HHBSS) + 1% BCS, and the cells were incubated at 37°C for twenty minutes. 2 mM probe solutions of NO550 (**9**), NO530 (**10**), or NO562 (**13**) in DMSO were diluted in HHBSS + 1% BCS to give a 15 μM probe concentration, with 0.75% DMSO. The medium in a pair of wells was replaced with 15 μM probe loading solution – three probes, six wells total. To the no-probe pair of wells was added the same volume of DMSO without probe to give 0.75% DMSO. The cells were incubated in this loading solution for two hours at 37 °C. The loading solution was then replaced with HHBSS + 1% BCS. A 200 mM S-Nitroso N-acetyl D,L-penicillamine (SNAP) solution in DMSO was diluted into the medium of four wells (stimulated),

containing the three different probes and no probe, to give 1 mM SNAP, 1.23% DMSO. The same volume of DMSO was diluted into the medium of the remaining wells (non-stimulated) to give 1.23% DMSO. The cells were incubated for four hours at 37 °C. Brightfield and DAPI and FITC-filtered fluorescence images were acquired through 10x and 40x objectives.

RAW 264.7 cells were plated into a Nunc 8-well plate high-glucose DMEM + 1% FBS and incubated overnight at 37 °C under 5% CO_2/air. The DMEM was then replaced with Krebs-Ringer buffer (KRB) + 1% FBS. 2 mM probe solutions of **9**, **10**, or **13** in DMSO were diluted in KRB + 1% FBS to a final concentration of 10 μM, 0.5% DMSO, and the medium over cells was replaced with this 10 μM loading solution, two wells per probe, six wells total. A 25 mM SNAP solution in DMSO was diluted into the loading solution of three wells (stimulated), each containing a different probe, to give 200 μM SNAP, 1.3% DMSO. The three remaining wells (nonstimulated) were treated with the same volume of DMSO but without SNAP, to give 1.3% DMSO. The cells were incubated for four hours at 37 °C. The medium in all wells was replaced with KRB + 1% FBS. Brightfield and DAPI and FITC-filtered fluorescence images were acquired through 10x objective.

NO Solution Stimulus

To the wells containing NIH 3T3 cells - loaded with probes **9**, **10**, or **13** or with no probe at all - that had not been subjected to 1 mM SNAP (above) was added 1.9 mM aqueous NO solution to a final concentration of 250 μM. The cells were incubated at 37 °C for 10 minutes, and then brightfield and DAPI and FITC-filtered fluorescence images of the four wells were acquired through 10x and 40x objectives.

RAW 264.7 cells were plated into a Nunc 8-well plate high-glucose DMEM + 1% FBS and incubated overnight at 37 °C under 5% CO_2/air. The DMEM was then replaced with DPBS + 1% FBS. 2 mM probe solutions of **9**, **10**, or **13** in DMSO were diluted in DPBS + 1% FBS to a final concentration of 10 μM, 0.5% DMSO, and the medium over cells was replaced with this 10 μM loading solution, two wells per probe, six wells total. Two wells were left without probe, but DMSO was added to the medium to 0.5%. The cells were incubated at 37 °C for 9 hours, and then the 10 μM loading solutions were replaced with DPBS + 1% FBS. A 1.8 mM aqueous NO solution was diluted into the medium in three wells (stimulated), each containing a different probe, and one no-probe well (also stimulated), to a final concentration of 300 μM NO. Nothing was added to the remaining four wells (non-stimulated). The cells were incubated for ten minutes at 37 °C, and then brightfield and DAPI and FITC-filtered fluorescence images of all wells were acquired through 10x and 40x objectives.

L-Arginine Stimulus

NIH 3T3 cells were plated into a Nunc 8-well plate in high-glucose DMEM + 1% BCS and incubated overnight at 37 °C under 5% CO_2/air. A 2 mM probe **13** in DMSO was diluted in DMEM + 1% BCS to give 10 μM probe concentration, with 0.5% DMSO. The medium in two wells was replaced with 500 μL 10 μM probe loading solution. The cells were incubated in this loading solution for one hour at 37 °C. 4 μL of a 100 mM L-arginine solution were added to one of the wells (2 mM L-arginine diluted concentration); 4 μL water were added to the other well. The cells were incubated for twenty-four hours at 37 °C. The medium in both wells was replaced with Krebs-Ringers solution + 1% BCS for imaging. Brightfield and DAPI and FITC-filtered fluorescence images were acquired through a 10x objective.

LPS screen

Lipopolysaccharides from Escherichia coli: 026:B6 (L2654), 055:B5 (L6529), 0111:B4 (L4391) and purified by phenol extraction (L2630), and 0127:B8 (L4516) and from Salmonella enterica: serotype enteritidis (L7770), serotype Minnesota (L4641), and serotype typhimurium (L6143) were purchased from Sigma (catalog numbers in parentheses). 1 mg of each LPS variant was dissolved in 1 mL water sterilized by 0.2 μm filtration. To seven wells (stimulated) of an 8-well plate that had been plated with RAW 264.7 cells in DMEM + 1% FBS was added an appropriate aliquot of a different LPS variant so as to achieve a final concentration of 1 μg/mL LPS. No LPS was added to one well (non-stimulated). The cells were incubated for 90 minutes at 37 °C, 5% CO2. A 1 mM solution of DAF-FM diacetate in DMSO was diluted to 2 μM in DMEM + 1% FBS, and the medium in all wells was replaced with this 2 μM solution. After incubation at 37 °C, 5% CO2 for 30 minutes, the medium was replaced with KRB, and the cells were incubated for 5 minutes further at room temperature. They were then imaged through the FITC filter set. Cells stimulated with variant Escherichia coli 011:B4 (L4391) produced the greatest increase in DAF-FM brightness over the nonstimulated cells, although the same variant purified by phenol extraction (L2630) also produced a greater increase than the remaining variants.

Cell exposure to LPS

RAW 264.7 cells were plated into a Nunc 8-well plate in high-glucose DMEM + 1% FBS and incubated overnight at 37 °C under 5% CO_2/air. To four (stimulated) of the eight wells was added 1 mg/mL LPS in 0.2 μm filtered water to a final concentration of 1

μg/mL. Nothing was added to the remaining four wells (non-stimulated). The cells were incubated at 37 °C, 5% CO2 for 15 hours. The medium in all wells was replaced with L-15 + 1% FBS, and 1 mg/mL LPS solution was diluted to 1 μg/mL in the four stimulated wells. The cells were incubated at 37 °C for another six hours. A 2 mM solution of probes **9**, **10**, and **13** in DMSO was first diluted to 150 μM, 7% DMSO in L-15 + 1% FBS in order to avoid high localized concentrations of DMSO over the cells. Each 150 μM probe solution was further diluted to 15 μM, 0.7% DMSO into two wells, stimulated and non-stimulated, for a total of six wells, and the cells were incubated at 37 °C for 2.5 hours. A 1 mM DAF-FM diacetate solution in DMSO was diluted to 10 μM in L-15 + 1% FBS and then diluted further to 1 μM in the two remaining, one stimulated and one non-stimulated, wells. After 25 minutes at room temperature, the DAF-FM diacetate loading medium was replaced with L-15 + 1% FBS. The cells were left for another ten minutes at room temperature for non-specific esterases to finish hydrolyzing the two acetate functionalities. (This extra hydrolysis time must be counterbalanced with the propensity of the hydrolyzed form of DAF-FM to leak or get pumped out of cells.) Brightfield and DAPI and FITC-filtered fluorescence images were acquired for all wells (starting with the two containing the leakage-prone DAF-FM) through a 10x objective.

Calcein Blue/Propidium Iodide Cell Viability Assay

The membrane-permeable acetoxymethyl ester derivative of Calcein Blue is non-fluorescent until non-specific esterases in viable cells hydrolyze the esters to produce the membrane-impermeable blue fluorophore that remains in the cytosol of cells with intact membranes. Propidium iodide becomes red fluorescent when it intercalates into DNA. The membrane-impermeable propidium iodide cannot intercalate into the DNA of viable

cells with intact membranes. Therefore, blue fluorescent cells are deemed viable, whereas red fluorescent are not.

The DMEM + 1% FBS medium over RAW 264.7 cells was replaced with L-15 + 1% FBS; 4% DMSO in L-15 + 1% FBS; or 1.25, 2.5, 5, 10, 20, or 40 μM **10** (diluted from 2 mM probe **10** in DMSO) in L-15 + 1% FBS. Cells were incubated at 37 °C for two hours. A 2 mM Calcein Blue (AM) solution in DMSO was diluted to 50 μM in DPBS. A 1.5 mM propidium iodide solution in 0.2 μm-filtered water was diluted to 50 μM in the 50 μM Calcein Blue (AM) solution. The medium in all wells was replaced with DPBS, and then the 50 μM Calcein Blue (AM), 50 μM propidium iodide solution was diluted ten-fold into each well. Cells were incubated at 37 °C for 30 minutes prior to imaging. Brightfield and DAPI, FITC, and TRITC-filtered fluorescence images were acquired for all wells.

Image Processing

Images were saved as TIFFs. All images were processed with FIJI software, version 2.0.0-rc-65/1.52a.3 Brightfield images were processed with the Subtract Background command, typically with a rolling ball radius of 10 pixels and with smoothing disabled, followed by further processing with a variance filter set at a radius of 2-5 pixels. A threshold was applied to the background-subtracted and variance-filtered images to reduce them to 8-bit images from which a selection could be created. This selection was converted to a region of interest and served as a mask for areas occupied by cells. The rolling ball radius values in the Subtract Background command and the radius values in the variance filter were adjusted to achieve the best fit of the region of interest to the cells in the image. Each brightfield image-derived mask was applied to the corresponding FITC and DAPI channel images to obtain the mean pixel intensity within

the mask, which was treated as intracellular signal. An inverse of the selection produced a mask of the region not occupied by cells, and this mask was applied to the FITC and DAPI channel images to measure extracellular signal. An image 960 x 720 pixels in size contains 691,200 pixels. Processing Figure 12e and 12f gave a mean intensity value of 1316 for FITC and 705 for DAPI over 138,173 pixels for the intracellular signal. The inverse of the selection produced a mean of 636 for FITC and 604 for DAPI over 553,027 pixels for the extracellular signal. The intracellular and extracellular pixels totaled to 691,200 pixels.

These signals were corrected by subtracting the mean intracellular signal from cells not loaded with probe from those loaded with probe for experiments with SNAP, NO solution, and LPS stimuli in NIH 3T3 and RAW 264.7 cells. For LPS stimuli experiments in cells, images of cells not loaded with probes were not collected, so the lowest extracellular mean signal, no matter which probe was loaded into cells, in a certain experiment was subtracted from the mean intracellular signals for all loaded probes.

Furthermore, if at any point the intracellular signal from cells not loaded with probe was greater than that for cells loaded with probe, the lowest extracellular mean signal in the same experiment was subtracted from the mean intracellular signal for that probe.

Zeiss DAPI, FITC, and TRITC Filters

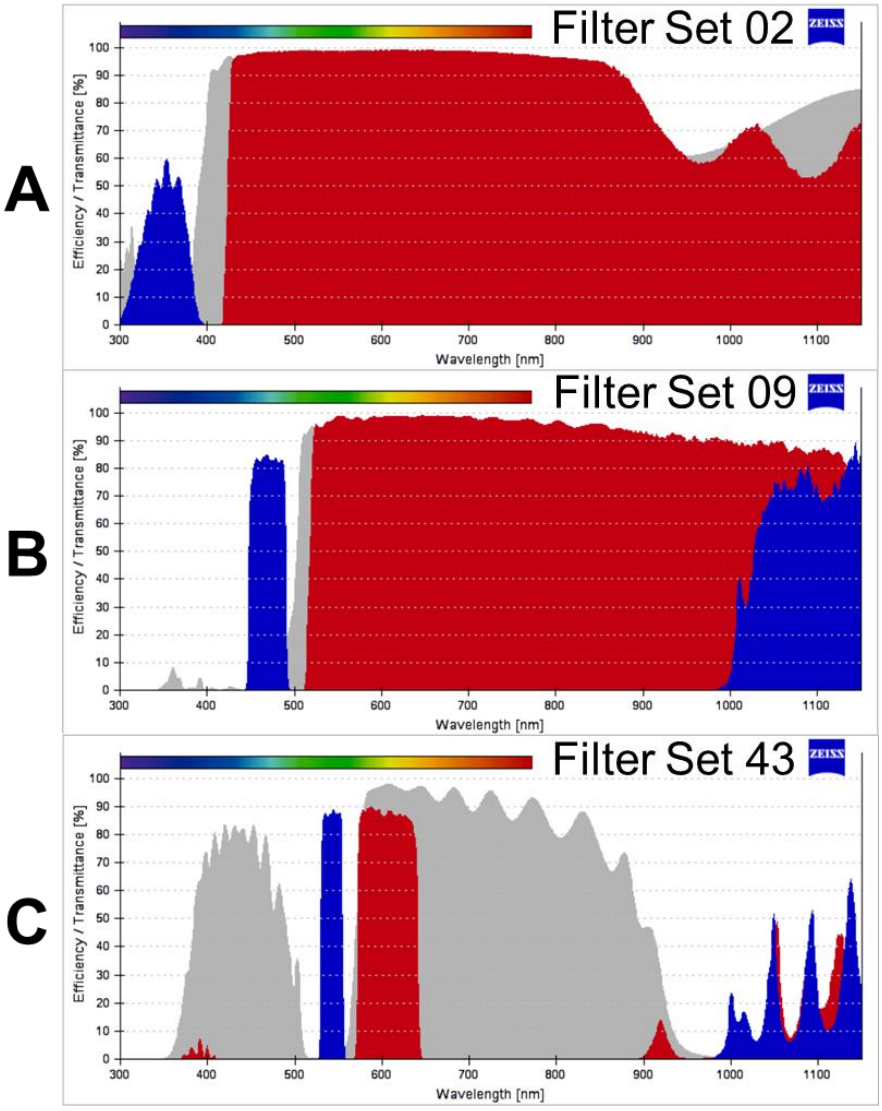

Percent transmittance versus wavelength graphs for DAPI (top), FITC (middle), and TRITC (bottom) filters.2 Excitation filter (blue), beam splitter (gray), and emission filter (red) parameters (listed in this order) for each set: DAPI (G 365, FT 395, LP 420), FITC (BP 450-490, FT 510, LP 515), and TRITC (545/25, FT 570, BP 605/70). From
(A) Carl Zeiss Microscopy, L. Filter Set 02.
https://www.microshop.zeiss.com/images/fat/chart.gif.php?l=en&a=v&ft=446431-0011-000&fa=000000-4242- 879&fe=447741-8001-000;
(B) Carl Zeiss Microscopy, L. Filter Set 09.
https://www.microshop.zeiss.com/images/fat/chart.gif.php?l=en&a=v&ft=446431-0011-000&fa=000000-4242- 879&fe=447741-8001-000;
(C) Carl Zeiss Microscopy, L. Filter Set 43.
https://www.microshop.zeiss.com/images/fat/chart.gif.php?l=en&a=v&ft=446431-0011-000&fa=000000-4242- 879&fe=447741-8001-000.

APPENDIX D: EXPERIMENTAL DETAILS AND SPECTRA FOR CHAPTER 2 COMPOUNDS

3,5-dimethoxyaniline handle

1-benzyl-3-(3,5-dimethoxyphenyl)-1-(2-hydroxyethyl)urea

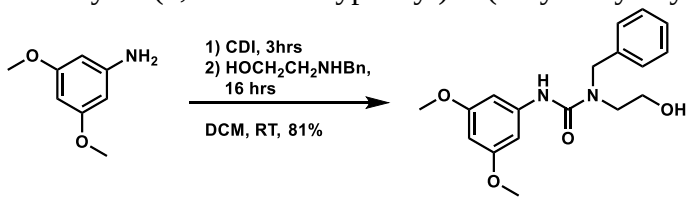

To a solution of 198 mg 84% CDI (16% imidazole, as determined by 1H NMR, 1 mmol, 1 eq) in 5 mL DCM was added via syringe a solution of 153 mg (1 mmol) 3,5-dimethoxyaniline in 1 mL DCM at a rate of 100 µL every two minutes. The reaction stirred at room temperature for four hours, and then 140 µL (1 mmol, 1 eq) N-benzyl-2-aminoethanol, and the reaction stirred at room temperature overnight. The reaction mixture was diluted with DCM, washed twice with 0.1 M HCl, and once with brine. The combined aqueous layers were back-extracted with DCM. The combined organics were dried over Na2SO4, filtered free of solids, and stripped free of solvents under reduced pressure. SiO2 column chromatography (1:1 hexanes/EtOAc) yielded 267 mg (81%). ^{1}H NMR (400 MHz, DMSO-d6) δ 8.647 (s, 1H), 7.371 – 7.283 (m, 2H), 7.283 – 7.193 (m, 3H), 6.705 (d, J = 2.3 Hz, 2H), 6.086 (t, J = 2.3 Hz, 1H), 5.263 (t, J = 4.8 Hz, 1H), 4.569 (s, 2H), 3.672 (s, 5H), 3.535 (q, J = 5.3 Hz, 2H), 3.379 – 3.299 (m, 1H). ^{13}C NMR (126 MHz, DMSO) δ 160.40, 155.65, 142.32, 138.86, 128.43, 127.31, 126.93, 97.36, 93.88, 59.92, 55.00, 50.00, 49.04. HRMS ESI+: 353.1483 (M+Na), Calculated $C_{18}H_{22}N_2O_4Na$ 353.1477.

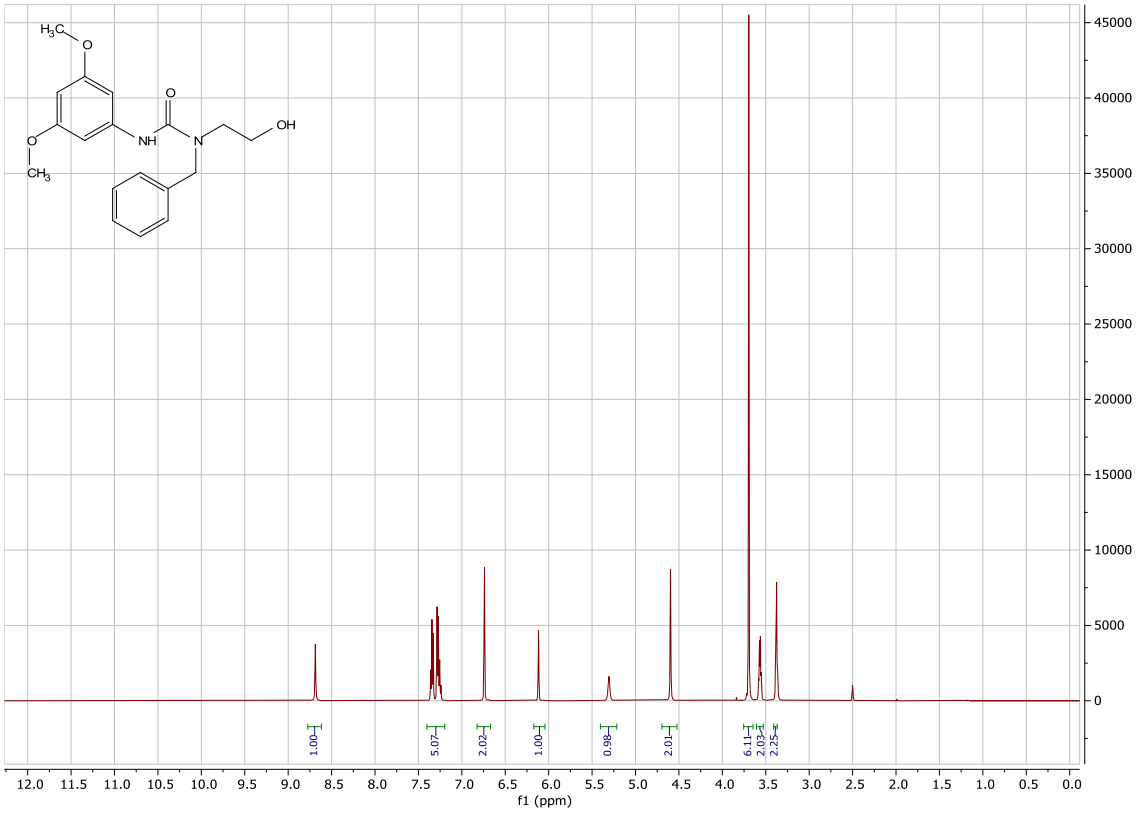
H3C
O
O
NH
N
OH
O
CH3
45000
40000
35000
30000
25000
20000
15000
10000
5000
0
1.00
5.07
2.02
1.00
0.98
2.01
6.11
2.03
2.25
12.0 11.5 11.0 10.5 10.0 9.5 9.0 8.5 8.0 7.5 7.0 6.5 6.0 5.5 5.0 4.5 4.0 3.5 3.0 2.5 2.0 1.5 1.0 0.5 0.0
f1 (ppm)

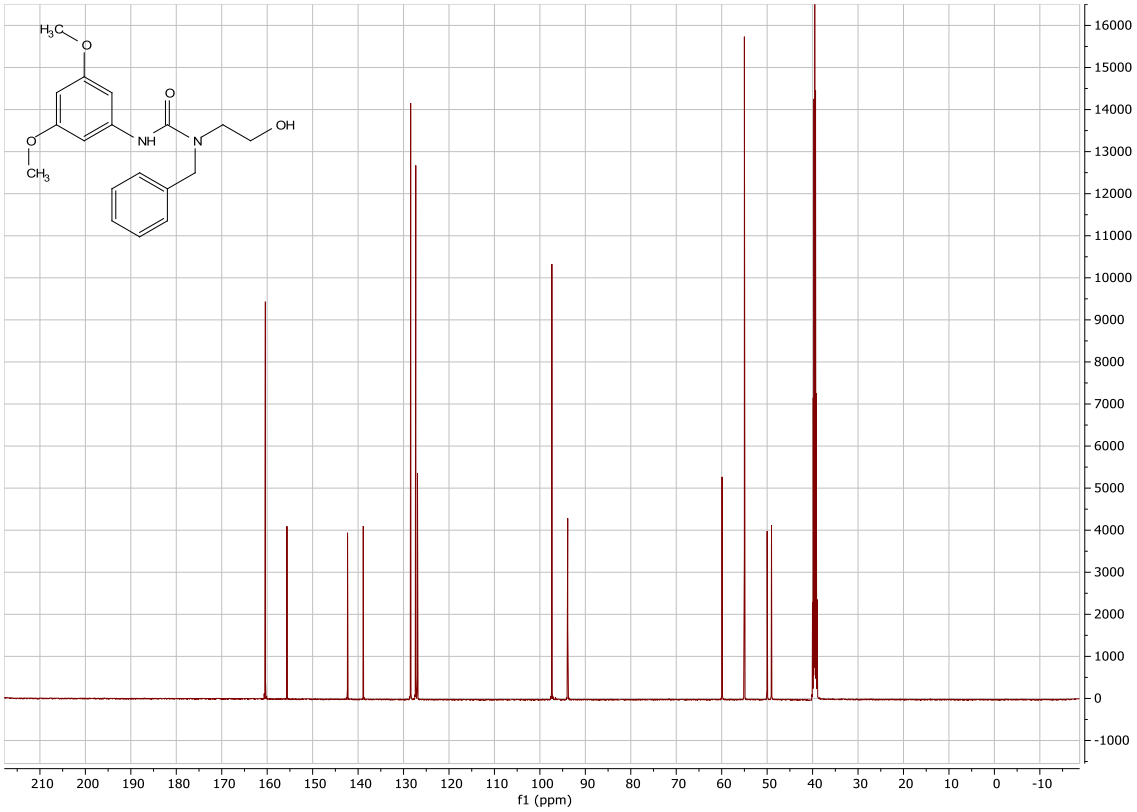

2-(1-benzyl-3-(3,5-dimethoxyphenyl)ureido)ethyl(2-hydroxyethyl)carbamate

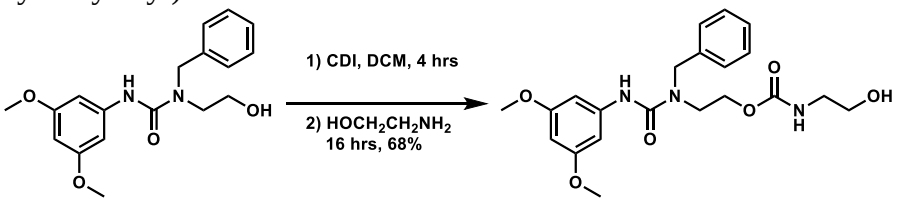

33 mg (0.1 mmol) of the mixed urea and 16 mg (0.1 mmol, 1.0 eq) CDI in 1 mL $CDCl_3$ were agitated on a mechanical shaker for one hour. 6 µL (0.1 mmol, 1 eq) 2-aminoethanol were added, and the reaction was shaken at room temperature for four days. The reaction mixture was diluted with DCM, washed twice with 0.1 M HCl, and once with brine. The combined aqueous layers were back-extracted with DCM. The combined organics were dried over Na_2SO_4, filtered free of solids, and stripped free of

solvents under reduced pressure. SiO_2 column chromatography (2:3 hexanes/EtOAc) yielded 39 mg (95%). 1H NMR (400 MHz, Chloroform-d) δ 7.898 (s, 1H), 7.571 (d, J = 1.0 Hz, 2H), 7.450 – 7.164 (m, 5H), 7.011 (d, J = 1.0 Hz, 4H), 6.831 – 6.660 (m, 2H), 6.585 (dd, J = 12.4, 2.2 Hz, 1H), 6.141 (q, J = 2.6 Hz, 1H), 5.894 (s, 1H), 4.563 (d, J = 7.0 Hz, 2H), 4.025 (t, J = 6.6 Hz, 2H), 3.695 (s, 4H), 3.670 (s, 1H), 3.664 – 3.585 (m, 2H), 3.514 (t, J = 6.5 Hz, 2H), 3.287 (q, J = 5.3 Hz, 2H). LCMS: 418 (M+H), 440 (M+Na), 452 (M+Cl), calculated $C_{21}H_{27}N_3O_6$ 417.1900

2-(1-benzyl-3-(3,5-dimethoxyphenyl)ureido)ethyl(2-(((2-hydroxyethyl)carbamoyl)oxy) ethyl)carbamate

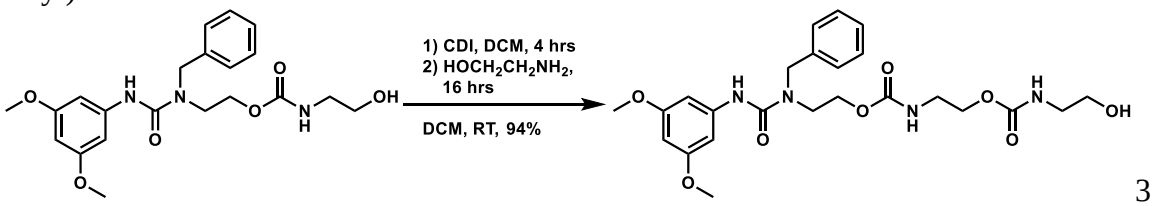

3

79 mg (0.91 mmol) dimer and 171 mg (1.05 mmol, 1.15 eq) in 10 mL DCM was stirred for four hours. Then 153 µL (2.53 mmol, 2.8 eq) 2-aminoethanol were added, and the reaction stirred overnight at room temperature. The reaction mixture was diluted with DCM, washed twice with 0.1 M HCl, and once with brine. The combined aqueous layers were back-extracted with DCM. The combined organics were dried over Na_2SO_4, filtered free of solids, and stripped free of solvents under reduced pressure. SiO_2 column chromatography (1:2 hexanes/EtOAc) yielded 430 mg (94%). LCMS 505 (M+H), 527 (M+Na), calculated $C_{24}H_{32}N_4O_8$ 504.2220

2-benzyl-1-((3,5-dimethoxyphenyl)amino)-1,6,11-trioxo-5,10-dioxa-2,7,12-triazatetra decan-14-yl 2-cyanoacetate

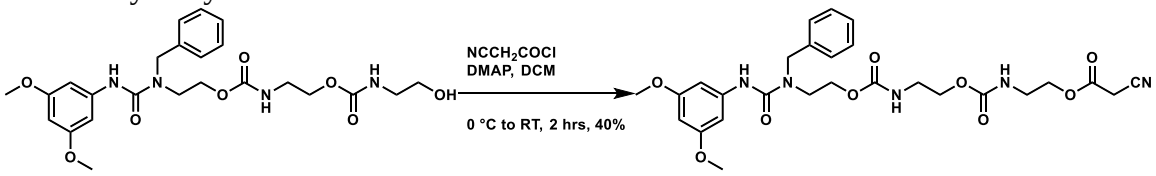

A solution of 25 mg (0.05 mmol) and 6 mg (0.05 mmol, 1.0 eq) DMAP in 0.5 mL DCM was cooled in an ice/brine bath for 10 minutes, and then 6 mg (0.05 mmol, 1.0 eq) cyanoacetyl chloride in 0.5 mL DCM were added. After 15 minutes stirring, the ice bath was removed, and the reaction stirred for two hours warming to room temperature. The reaction mixture was diluted with DCM, washed twice with 0.1 M HCl, and once with brine. The combined aqueous layers were back-extracted with DCM. The combined organics were dried over Na_2SO_4, filtered free of solids, and stripped free of solvents under reduced pressure. SiO_2 column chromatography (1:1 hexanes/EtOAc) yielded 11.4 mg (40%). LCMS APCI +/-: 572 (M+H), 594 (M+Na), 570 (M-1)

2-benzyl-1-((3,5-dimethoxyphenyl)amino)-1,6,11-trioxo-5,10-dioxa-2,7,12-triazatetradec an-14-yl 4-methylbenzenesulfonate

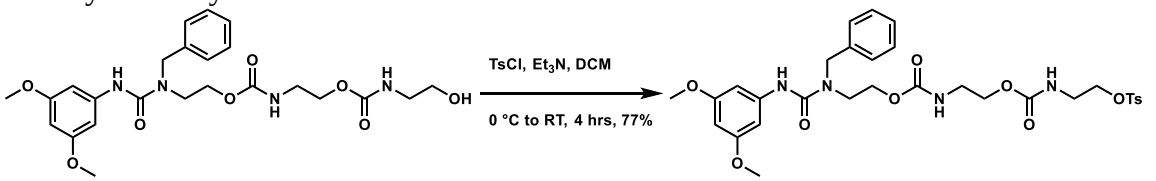

A solution of 50 mg (0.1 mmol) trimer-OH and 32 µL (0.23 mmol, 2.3 eq) in 1 mL DCM was cooled in an ice/brine bath for 10 minutes before 30 mg (0.16 mmol, 1.6 eq) tosyl chloride in 0.5 mL DCM were added. The ice-bath was removed after 15 minutes, and the reaction warmed to room temperature while stirring. After four hours, the reaction

mixture was diluted with DCM, washed twice with 0.1 M HCl, and once with brine. The combined aqueous layers were back-extracted with DCM. The combined organics were dried over Na_2SO_4, filtered free of solids, and stripped free of solvents under reduced pressure. SiO_2 column chromatography (1:2 hexanes/EtOAc) yielded 50 mg (77%). LCMS (APCI +/-): 659 (M+H), 681 (M+Na), 693 (M+Cl), Calculated $C_{31}H_{38}N_4O_{10}S$ 658.2309

2-(1-benzyl-3-(3,5-dimethoxyphenyl)ureido)ethyl(2-(((2-azidoethyl)carbamoyl)oxy) ethyl)carbamate

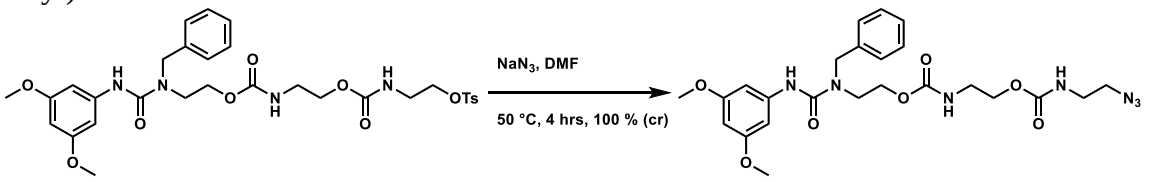

A solution of 50 mg (0.076 mmol) trimer-OTs and 10 mg (0.152 mmol, 2 eq) in 1 mL DMF was heated at 50 °C for four hours. After cooling to RT, it was poured into sodium bicarbonate, filtered, and rinsed with dI water. The solid was air-dried overnight to give 41 mg, 100% crude. LCMS (APCI +/-): 530 (M+H), 552 (M+Na), 564 (M+Cl) Calculated: $C_{24}H_{31}N_7O_7$ 529.2285.

2-(1-benzyl-3-(3,5-dimethoxyphenyl)ureido)ethyl(2-(((2-aminoethyl)carbamoyl)oxy) ethyl)carbamate

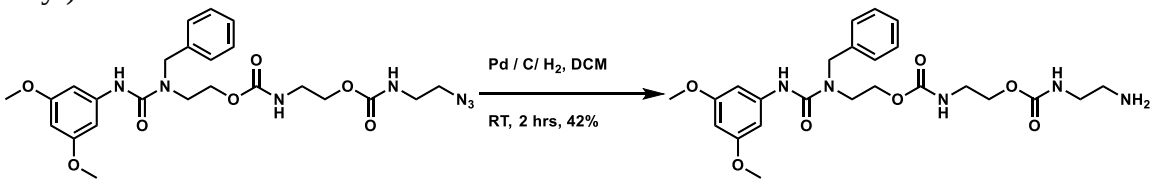

A dispersion of 40 mg (0.076 mmol) trimer-N_3 and 10 mg 5% Pd/C in 1 mL 1,2-dichloroethane was sparged with H_2 for 10 minutes and then stirred at RT for 2 hours.

The reaction mixture was filtered through hardened filter paper, and the filtrate was stripped of solvents under reduced temperature. SiO_2 column chromatography (2% MeOH in DCM + 5% Et_3N) yielded 32 mg still impure amine. This amine was sonicated in toluene and filtered to give 16 mg of ~89% pure product. LCMS (APCI +/-): 504 (M+H), 526 (M+Na), 538 (M+Cl) Calculated $C_{24}H_{33}N_5O_7$ 503.2380.

2-(1-benzyl-3-(3,5-dimethoxyphenyl)ureido)ethyl(2-(((2-(3-(3,5-dimethoxyphenyl) ureido)ethyl)carbamoyl)oxy)ethyl)carbamate

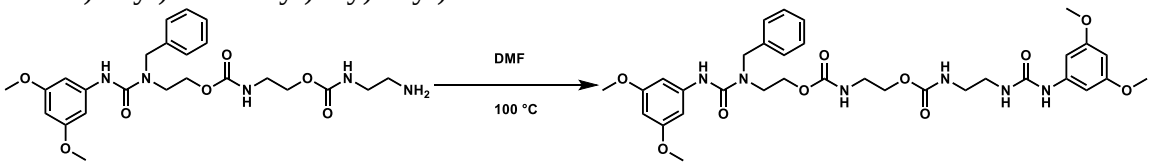

4 mg trimer-NH_2 (0.008 mmol) in 100 µL DMF were stirred at 90 °C overnight. LCMS (APCI +/-): 683 (M+H), 705 (M+Na), 717 (M+Cl) Calculated $C_{33}H_{42}N_6O_{10}$ 682.2962.

1-benzyl-3-(3,5-dimethoxyphenyl)-1-vinylurea

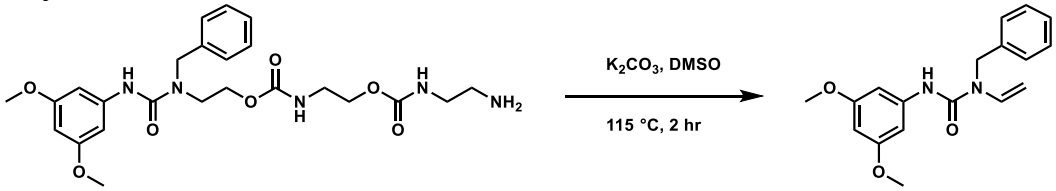

4 mg trimer-NH_2 (0.008 mmol) and 4 mg (0.029, 3.7 eq) K_2CO_3 in 100 µL DMSO were stirred at 115 °C for two hours. LCMS (APCI +/-): 313 (M+H), 335 (M+Na), Calculated $C_{18}H_{20}N_2O_3$ 312.1474.

2-(1-benzyl-3-(3,5-dimethoxyphenyl)ureido)ethyl(2-(((2-(3-phenylthioureido)ethyl)carbamoyl)oxy)ethyl)carbamate and 2-(1-benzyl-3-(3,5-dimethoxyphenyl)ureido)ethyl(4-oxo-9-thioxo-3-oxa-5,8,10-triaza tridecyl)carbamate

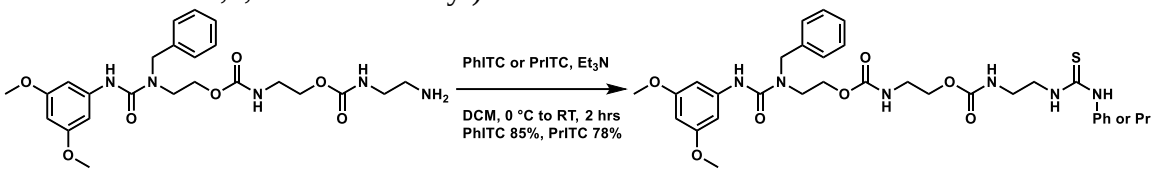

Two separate reactions: 4 mg trimer-NH2 (0.008 mmol), 0.95 µL (0.008 mmol, 1.0 eq) phenyl isothiocyanate or 0.82 µL (0.008 mmol, 1.0 eq) propyl isothiocyanate, 1.12 µL triethylamine (0.008 mmol, 1.0 eq), in 200 µL DCM were stirred at room temperature overnight. Two more equivalents of either PhITC or PrITC were added the next day to effect complete conversion of the amine to the thiourea after four hours stirring. The reaction mixture was diluted with DCM, washed once with 0.1 M HCl, and twice with brine. The combined aqueous layers were back-extracted with DCM. The combined organics were dried over Na_2SO_4, filtered free of solids, and stripped free of solvents under reduced pressure. SiO_2 prep TLC (1:2 hexanes/EtOAc) yielded 2 mg Ph and 2 mg Pr variants (40 % Ph, 42% Pr). LCMS (APCI +/-): 639 (M+H), 661 (M+Na). HRMS ESI+: 639.2597 (M+H) Calculated $C_{31}H_{39}N_6O_7S$ 639.2595 for Ph variant. 605 (M+H), 627 (M+Na), 603 (M-H), 639 (M+Cl), Calculated $C_{28}H_{40}N_6O_7S$ 604.2679 for Pr variant.

Edman degradation with phenyl or propyl thioureas.

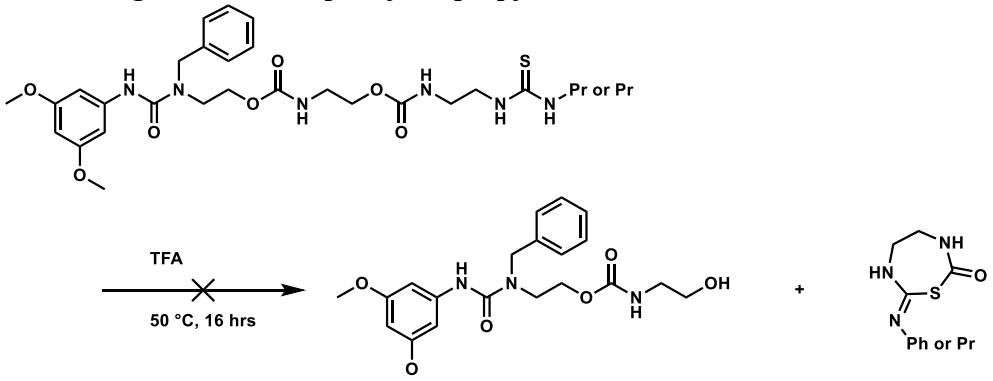

2 mg (0.003 mmol) of the thiourea was dissolved in 300 µL TFA and heated at 50 °C overnight. No peak with a mass equivalent to the sequenced product dimer-OH was observed. The main conversion was to a product 2 m/z less than the thiourea molecular mass, as if an oxidation (-2H) or a cyclization (also -2H) had occurred.

2,4-dimethoxybenzylamine handle

1-(2,4-dimethoxybenzyl)-3-(2-hydroxyethyl)urea

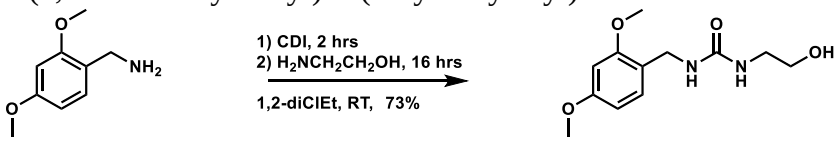

150 µL (1 mmol) 2,4-dimethoxybenzylamine and 186 mg (1.15 mmol, 1.15 eq) CDI in 1 mL 1,2-dichloroethane was stirred at room temperature for two hours. 78 µL (1.3 mmol, 1.3 eq) 2-aminoethanol were added, and the reaction stirred overnight. The mixture was poured into 1M HCl and thrice extracted with EtOAc. The combined organics were washed with 1M HCl, then brine, dried over Na_2SO_4, filtered, and stripped of solvents to dryness under reduced pressure. SiO_2 column chromatography (3:1 EtOAc / hexanes) gave 185 mg (73% yield). 1H NMR (500 MHz, DMSO-d6) δ 7.065 (d, J = 8.3 Hz, 1H), 6.526 (d, J = 2.4 Hz, 1H), 6.460 (dd, J = 8.3, 2.4 Hz, 1H), 6.155 (t, J = 5.9 Hz, 1H), 6.000

(t, J = 5.7 Hz, 1H), 4.670 (t, J = 5.1 Hz, 1H), 4.078 (d, J = 5.8 Hz, 2H), 3.776 (s, 3H), 3.733 (s, 3H), 3.370 (t, J = 5.5 Hz, 2H), 3.143 – 2.994 (m, 2H). 13C NMR (126 MHz, DMSO) δ 159.59, 158.26, 157.72, 128.78, 120.46, 104.18, 98.19, 60.91, 55.33, 55.18, 42.15, 37.89. LCMS (ESI/APCI +/-) 255 (M+H), 277 (M+Na), 531 (2M+Na) 253(M-1), 289 (M+Cl). HRMS ESI+: 255.1339, Calculated $C_{12}H_{19}N_2O_4$ 255.1339.

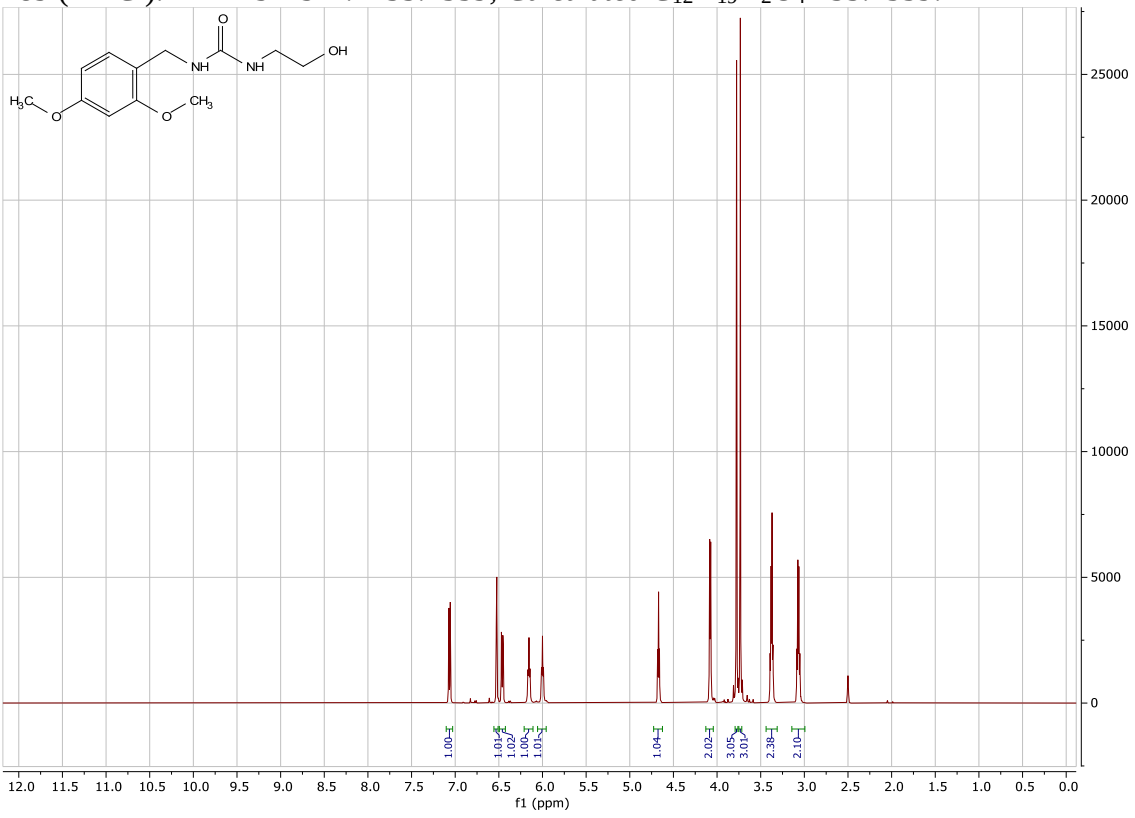

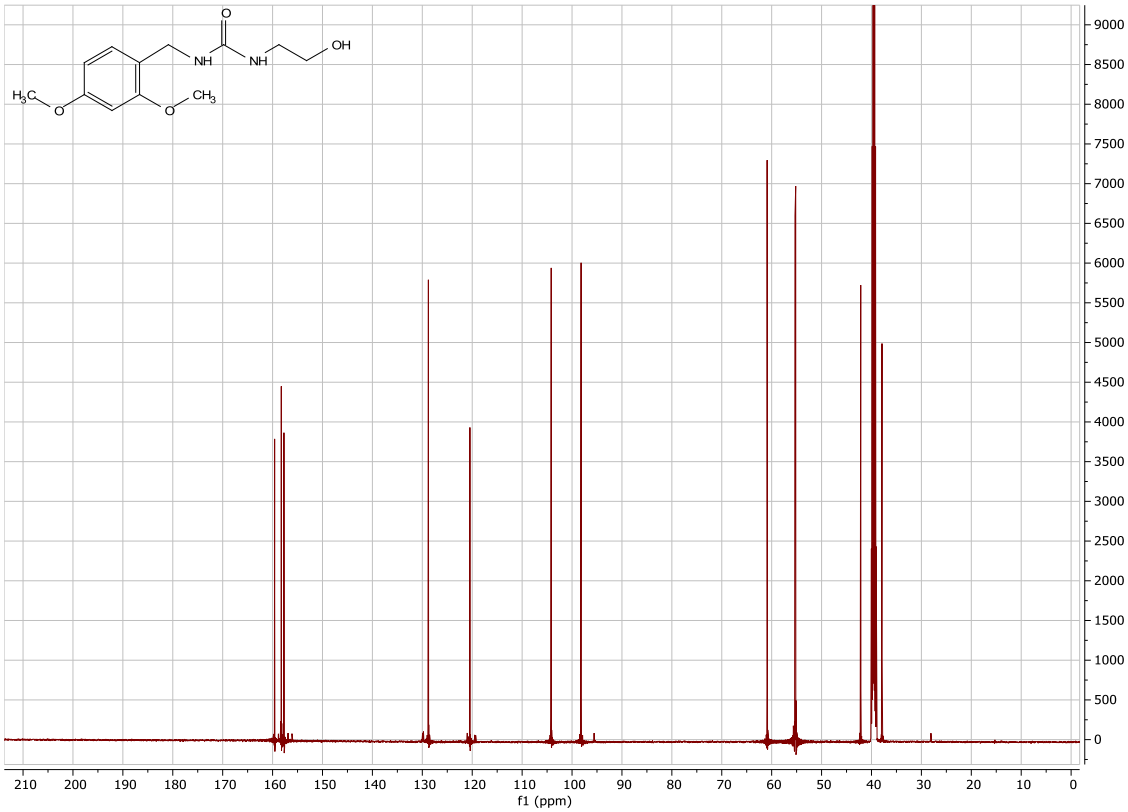

2-(3-(2,4-dimethoxybenzyl)ureido)ethyl (2-hydroxyethyl)carbamate

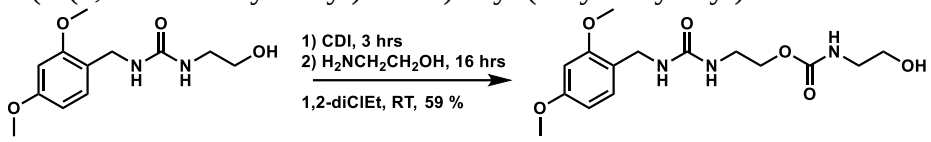

220 mg (0.865 mmol) and 162 mg (0.995 mmol, 1.15eq) CDI in 3 mL 1,2-dichlorethane were stirred at RT for 3 hours. 61 µL 2-aminoethanol were added, and the reaction stirred overnight. The mixture was poured into 1M HCl and thrice extracted with EtOAc. The combined organics were washed with 1M HCl, then brine, dried over Na_2SO_4, filtered, and stripped of solvents to dryness under reduced pressure. SiO_2 column chromatography (2% MeOH in EtOAc) gave 175 mg (59% yield). ^{1}H NMR (500 MHz, DMSO-d6) δ 7.059 (d, J = 8.3 Hz, 1H), 7.021 (t, J = 5.2 Hz, 1H), 6.525 (d, J = 1.9 Hz, 1H), 6.460 (dd, J = 8.2, 2.0 Hz, 1H), 6.146 (t, J = 5.6 Hz, 1H), 6.022 (t, J = 5.3 Hz, 1H),

4.618 (t, J = 5.5 Hz, 1H), 4.075 (d, J = 5.7 Hz, 2H), 3.903 (t, J = 5.6 Hz, 2H), 3.776 (s, 3H), 3.733 (s, 3H), 3.384 (d, J = 5.9 Hz, 2H), 3.192 (s, 2H), 3.036 (q, J = 6.1 Hz, 2H). ^{13}C NMR (126 MHz, DMSO) δ 159.61, 157.96, 157.72, 156.29, 128.83, 120.35, 104.20, 98.20, 63.42, 59.96, 55.35, 55.19, 43.04, 38.90, 37.90. HRMS ESI+: 342.1663 (M+H) Calculated $C_{15}H_{24}N_3O_6$ 342.1660

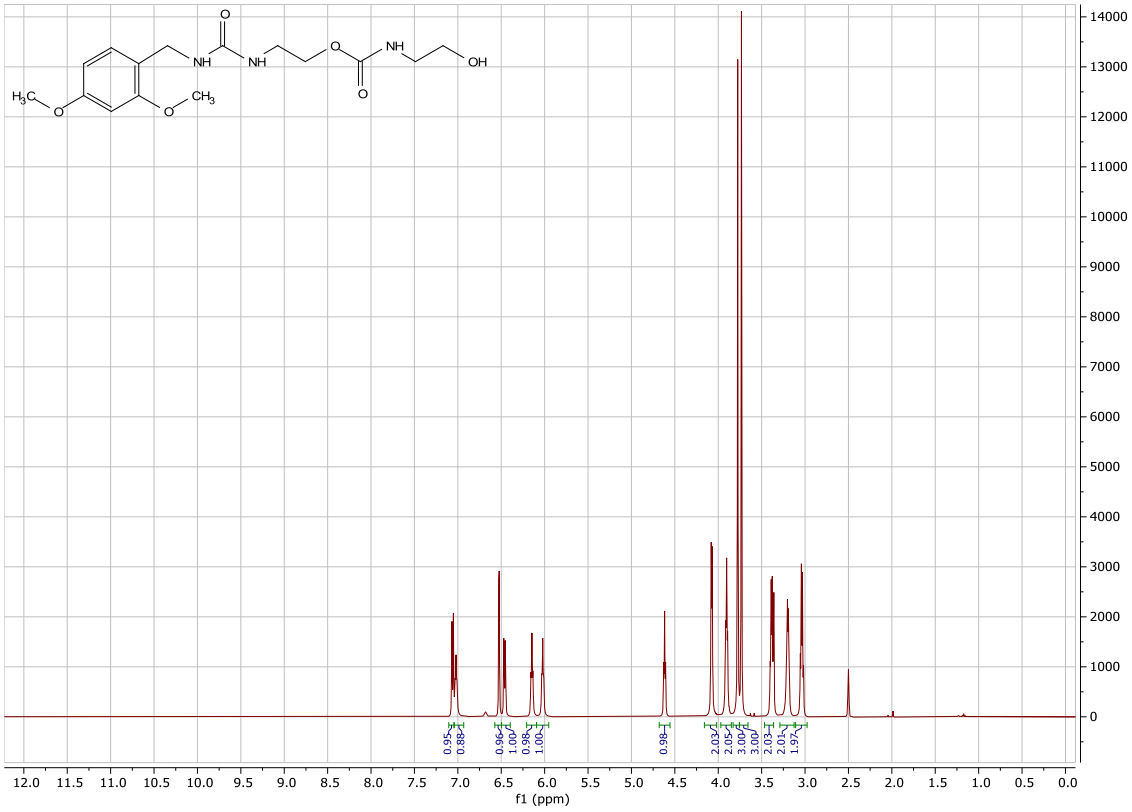

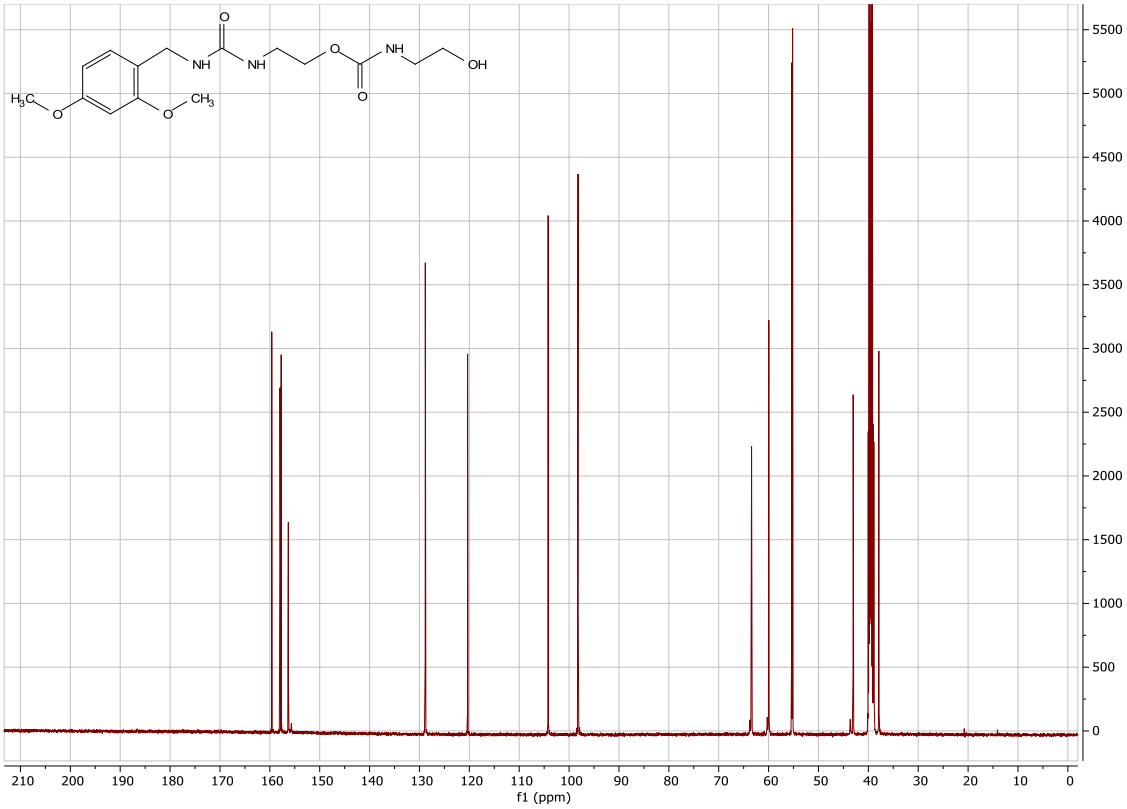

1-(2,4-dimethoxyphenyl)-3,8-dioxo-7-oxa-2,4,9-triazaundecan-11-yl4-methylbenzene sulfonate

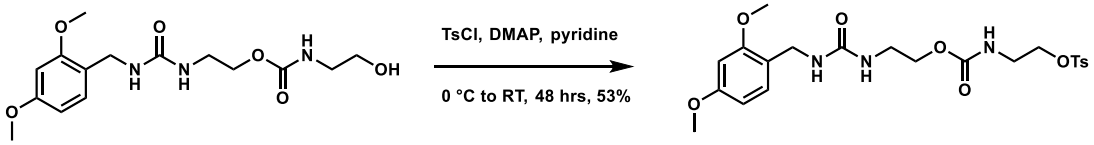

682 mg (2 mmol) dimer-OH and 12 mg (0.1 mmol, 0.05 eq) DMAP were dissolved in 4 mL pyridine and cooled in an ice/brine bath for 10 minutes. 572 mg (3 mmol, 1.5 eq) tosyl chloride were added in four portions every five minutes. The ice bath was removed 20 minutes after the last addition, and the reaction stirred overnight at RT. 230 mg (4.2 mmol, 2.1 eq total) tosyl chloride were added in two portions at RT, and the reaction stirred for another night. The reaction was diluted with DCM and washed twice with 1:1 citric acid/brine. The emulsion that formed on the second wash was filtered, and the

organic layer was dried over Na_2SO_4, filtered, and stripped of solvents under reduced pressure. SiO_2 column chromatography (1:3 hexanes/EtOAc) gave 525 mg (53% yield). LCMS (ESI/APCI +/-): 496 (M+H), 518 (M+2H), 530 (M+Cl). HRMS ESI+: 496.1749 (M+H), Calculated $C_{22}H_{30}N_3O_8S$ 496.1748.

2-(3-(2,4-dimethoxybenzyl)ureido)ethyl (2-azidoethyl)carbamate

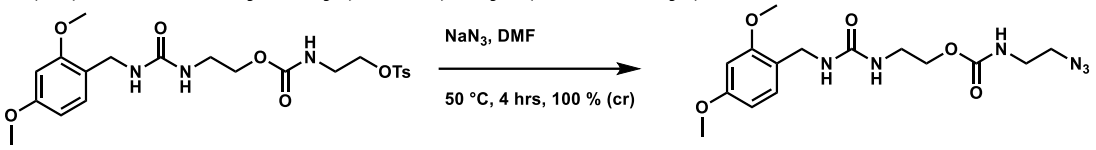

200 mg (0.59 mmol) dimer-OTs and 76 mg (1.172 mmol, 2 eq) sodium azide were reacted in 4 mL DMF at 50 °C for four hours. After cooling, the reaction was poured into sodium bicarbonate solution, filtered, and rinsed with dI water. The filtered solid was air-dried overnight to give 235 mg (110%, crude). LCMS (ESI/APCI +/-): 389 (M+Na), 755 (2M+Na), 401 (M+Cl), 411 (M+formate) Calculated: $C_{15}H_{22}N_6O_5$ 366.1652

2-(3-(2,4-dimethoxybenzyl)ureido)ethyl (2-aminoethyl)carbamate

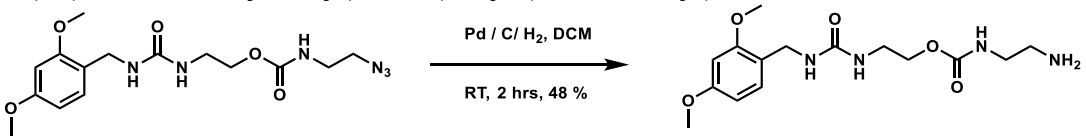

235 mg (0.59 mmol) dimer-N_3 and 30 mg 5% Pd/C in 10 mL DCM were sparged with H_2 for 10 min and then stirred for 2 hours. The reaction mixture was filtered through hardened filter paper, and the filtrate was stripped free of solvents under reduced pressure. Reverse-phase chromatography purification yielded 155 mg (48%) as the formate salt. ^{1}H NMR (500 MHz, DMSO-d6) δ 8.415 (s, 1H), 7.417 (s, 1H), 7.061 (d, J = 8.3 Hz, 1H), 6.517 (d, J = 2.4 Hz, 1H), 6.455 (dd, J = 8.3, 2.4 Hz, 1H), 6.403 (t, J = 5.8

Hz, 1H), 6.306 (t, J = 5.7 Hz, 1H), 5.764 (s, 3H), 4.069 (d, J = 5.6 Hz, 2H), 3.912 (t, J = 5.7 Hz, 2H), 3.769 (s, 3H), 3.729 (s, 3H), 3.192 (dd, J = 11.7, 5.9 Hz, 4H), 2.794 (s, 2H). ^{13}C NMR (126 MHz, DMSO) δ 159.54, 158.13, 157.65, 156.35, 128.71, 120.42, 104.19, 98.15, 63.72, 55.34, 55.19, 38.72, 37.79. LCMS (ESI/APCI +/-): 341 (M+H), 363 (M+Na), 681 (2M+H), 703 (2M+Na), 375 (M+Cl), 385 (M+formate). HRMS ESI+: 341.1826 (M+H), Calculated: $C_{15}H_{24}N_4O_5$ 341.1819.

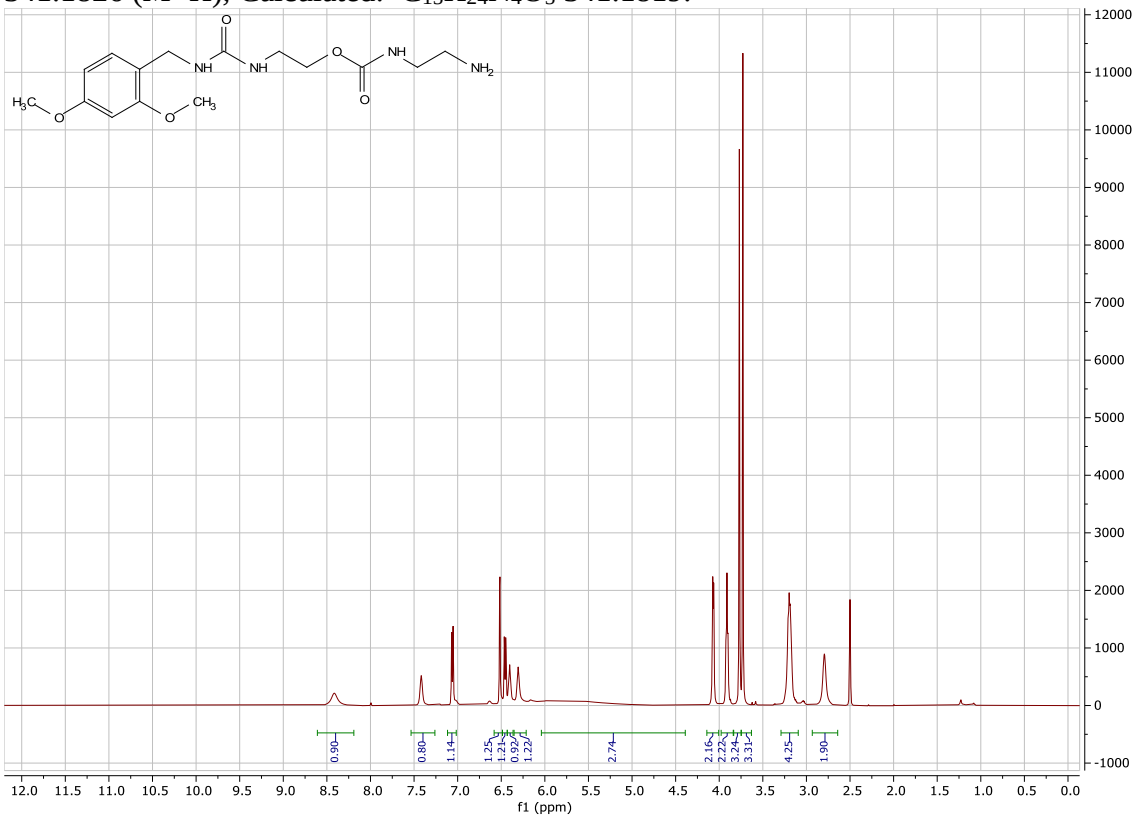

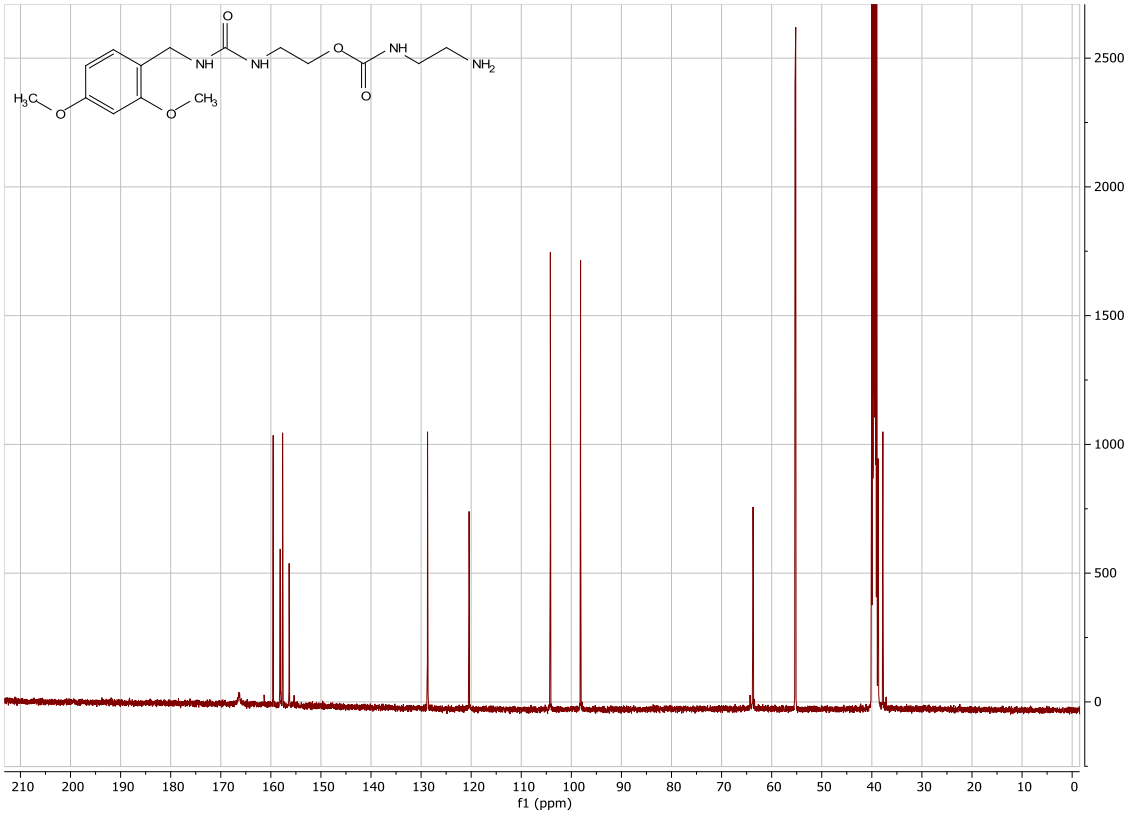

Dimer-NH_2 cyclization sequencing

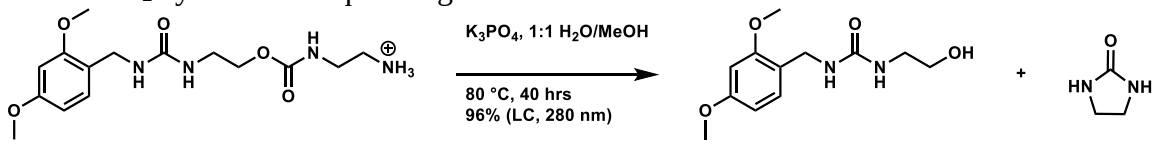

0.3 mg (0.09 mmol) of the formate salt of the dimer-NH_2 and 5 mg potassium phosphate in 200 µL H_2O and 200 µL MeOH in an LCMS vial was stirred at RT overnight. Since there was no reaction by LCMS, the reaction was stirred at 40 °C for 3 hours, then at 60 °C overnight. With about 15% conversion to the monomer, the reaction was then stirred at 80 °C overnight, with 78% conversion. Another 24 hours at 80 °C were necessary to drive the reaction to 96% completion.

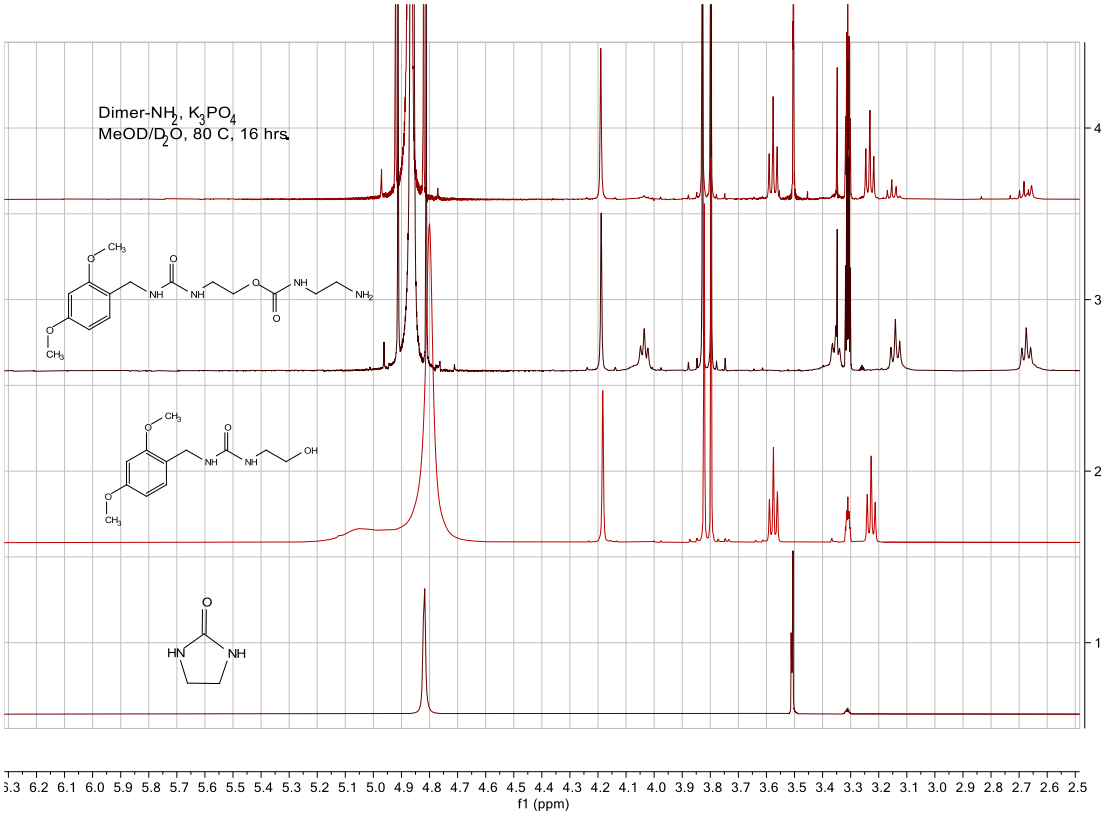

0.3 mg (0.09 mmol) of the formate salt of the dimer-NH_2 and 50 µL Hünig's base in 300 µL DMF were stirred at 50 °C for 1 hour. Since there was no reaction by LCMS, the reaction was stirred at 50 °C overnight. There was little conversion to the monomer-OH, only to a mixture of other unrecognizable products. The reaction was abandoned to the more favorable results with potassium phosphate/methanol/water.

F-OH: (S)-1-(2,4-dimethoxybenzyl)-3-(1-hydroxy-3-phenylpropan-2-yl)urea

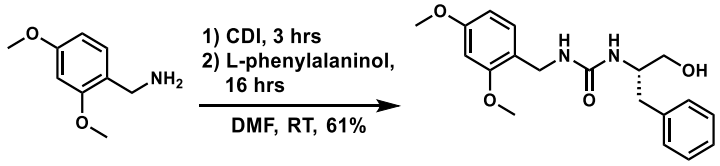

2.8 mL (18.65 mmol) 2,4-dimethoxybenzyl amime and 3.32 g (20.52 mmol, 1.1 eq) carbonyldiimidazole (CDI) in 50 mL anhydrous DMF were stirred at RT for three hours.

2.82 g (18.65, 1 eq) L-phenylalaninol were added, and the reaction stirred overnight at RT. The mixture was poured into 1M HCl and thrice extracted with EtOAc. The combined organics were washed with 1M HCl, then brine, dried over Na_2SO_4, filtered, and stripped of solvents to dryness under reduced pressure. SiO_2 column chromatography (3:1 EtOAc / DCM) gave 3.94 g (61% yield) F as a white solid. ^{1}H NMR (500 MHz, DMSO-d6) δ 7.32 – 7.23 (m, 2H), 7.23 – 7.14 (m, 3H), 6.98 (d, J = 8.3 Hz, 1H), 6.52 (d, J = 2.4 Hz, 1H), 6.44 (dd, J = 8.3, 2.4 Hz, 1H), 6.09 (t, J = 5.9 Hz, 1H), 5.89 (d, J = 8.3 Hz, 1H), 4.80 (dd, J = 5.5, 4.8 Hz, 1H), 4.04 (d, J = 5.9 Hz, 2H), 3.76 (s, 3H), 3.75 (m, 4H), 3.32 (dt, J = 10.6, 4.8 Hz, 1H), 3.24 (dt, J = 10.6, 5.5 Hz, 1H), 2.79 (dd, J = 13.5, 6.3 Hz, 1H), 2.60 (dd, J = 13.5, 7.5 Hz, 1H). ^{13}C NMR (126 MHz, DMSO-d6) δ 159.52, 157.68, 157.64, 139.39, 129.25, 128.63, 128.12, 125.87, 120.44, 104.15, 98.12, 62.72, 55.33, 55.20, 52.63, 37.74, 37.36. HRMS +ESI [M + K^+]: 383.1374, calculated $C_{19}H_{24}N_2O_4K$ 383.14.

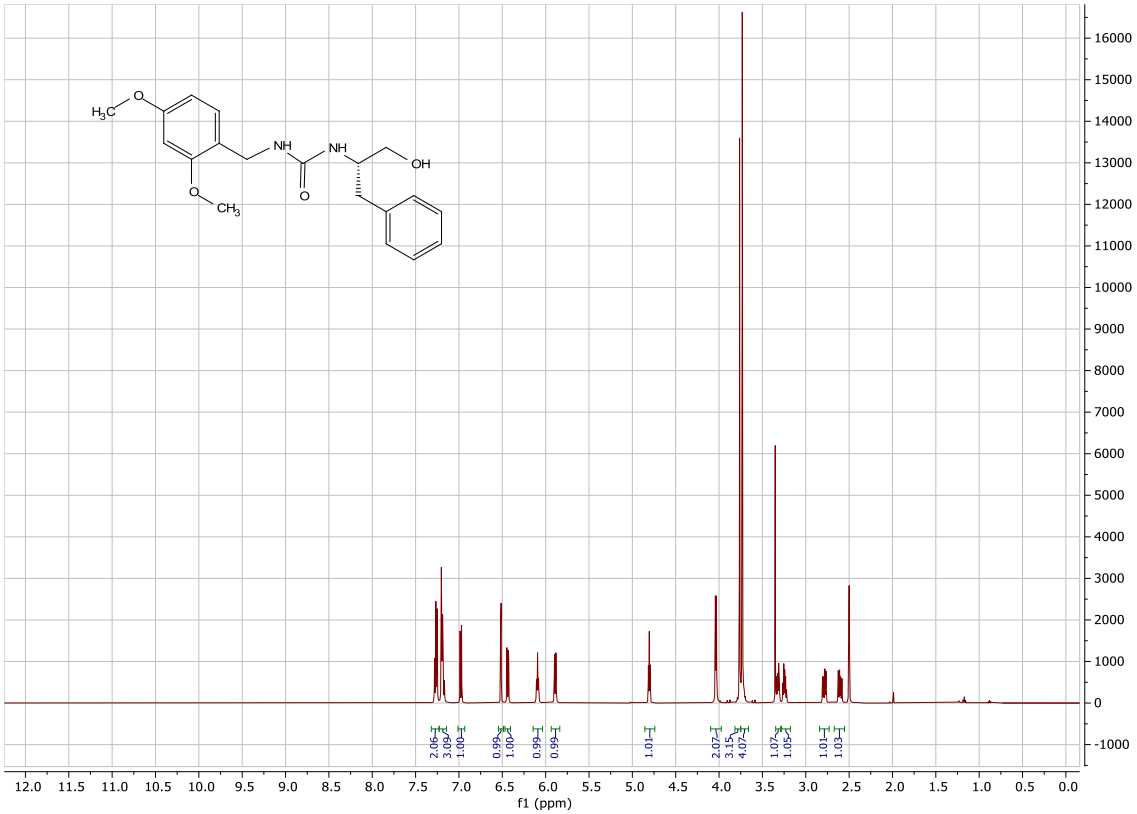
O
H3C
NH
NH
OH
O
O
CH3
16000
15000
14000
13000
12000
11000
10000
9000
8000
7000
6000
5000
4000
3000
2000
1000
0
-1000
2.06
3.09
1.00
0.99
1.00
0.99
0.99
1.01
2.07
3.15
4.07
1.07
1.05
1.01
1.03
12.0
11.5
11.0
10.5
10.0
9.5
9.0
8.5
8.0
7.5
7.0
6.5
6.0
5.5
5.0
4.5
4.0
3.5
3.0
2.5
2.0
1.5
1.0
0.5
0.0
f1 (ppm)

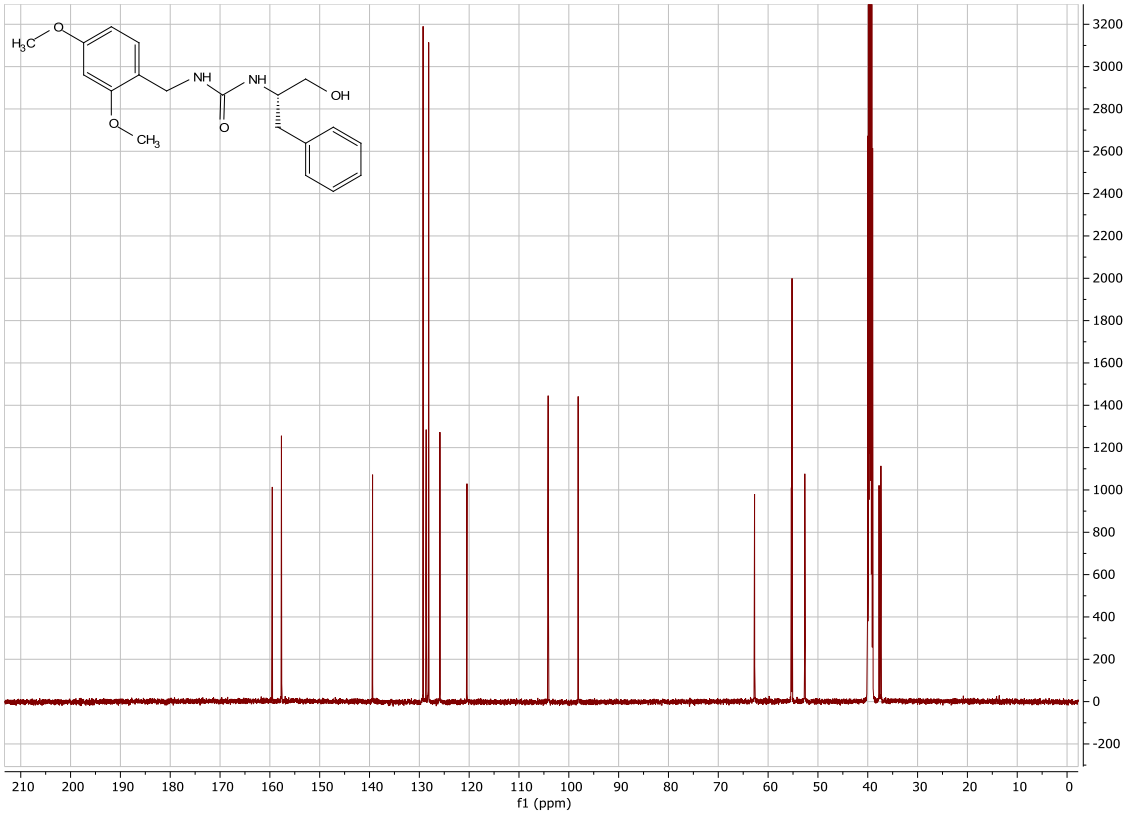

FA-OH: (S)-2-(3-(2,4-dimethoxybenzyl)ureido)-3-phenylpropyl((S)-1-hydroxypropan-2-yl)carbamate

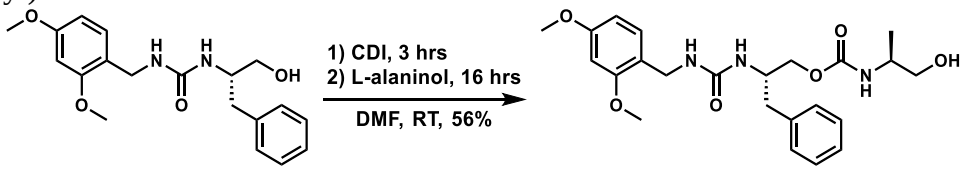

3.94 g (11.44 mmol) F and 1.95 g (12.01 mmol, 1.05 eq) CDI in 50 mL anhydrous DMF were stirred at RT for three hours. 0.945 g (12.584, 1.1 eq) L-alaninol were added, and the reaction stirred overnight at RT. The mixture was poured into 1M HCl and thrice extracted with EtOAc. The combined organics were washed with 1M HCl, then brine, dried over Na_2SO_4, filtered, and stripped of solvents to dryness under reduced pressure. SiO_2 column chromatography (2:1 EtOAc / hexanes, to 100% EtOAc) gave 2.86 g (56%

yield) FA as a white solid. ^{1}H NMR (500 MHz, DMSO-d_6) δ 7.29 (t, J = 7.4 Hz, 2H), 7.19 - 7.22 (m, 3H), 6.98 (d, J = 8.3 Hz, 1H), 6.94 (d, J = 8.1 Hz, 1H), 6.53 (d, J = 2.4 Hz, 1H), 6.45 (dd, J = 8.3, 2.4 Hz, 1H), 6.10 (t, J = 5.9 Hz, 1H), 5.97 (d, J = 8.1 Hz, 1H), 4.66 (t, J = 5.7 Hz, 1H), 4.05 (d, J = 5.9 Hz, 2H), 4.01 – 3.90 (m, 1H), 3.89 – 3.79 (m, 2H), 3.77 (s, 3H), 3.74 (s, 3H), 3.59 – 3.42 (m, J = 6.6 Hz, 1H), 3.34 (dt, J = 10.6, 5.5 Hz, 1H), 3.22 (dt, J = 10.6, 5.9 Hz, 1H), 2.77 (dd, J = 13.5, 6.0 Hz, 1H), 2.68 (dd, J = 13.5, 7.5 Hz, 1H), 1.02 (d, J = 6.6 Hz, 3H). ^{13}C NMR (126 MHz, DMSO-d_6) δ 159.99, 158.09, 157.87, 156.09, 138.92, 129.63, 129.12, 128.69, 126.57, 120.76, 104.59, 98.57, 65.56, 64.98, 55.77, 55.62, 50.46, 48.89, 38.20, 37.97, 17.78. HRMS +ESI [M^{+}H]: 446.2285, calculated $C_{23}H_{32}N_3O_6$ 446.23.

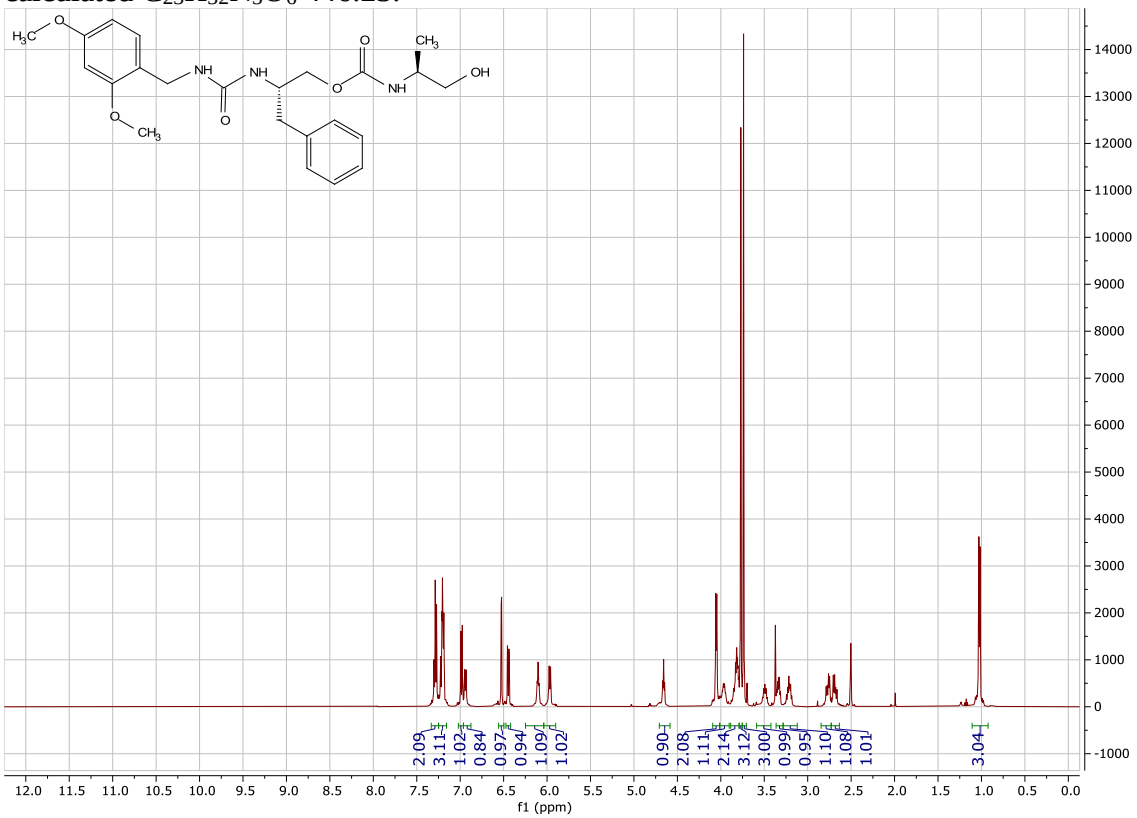

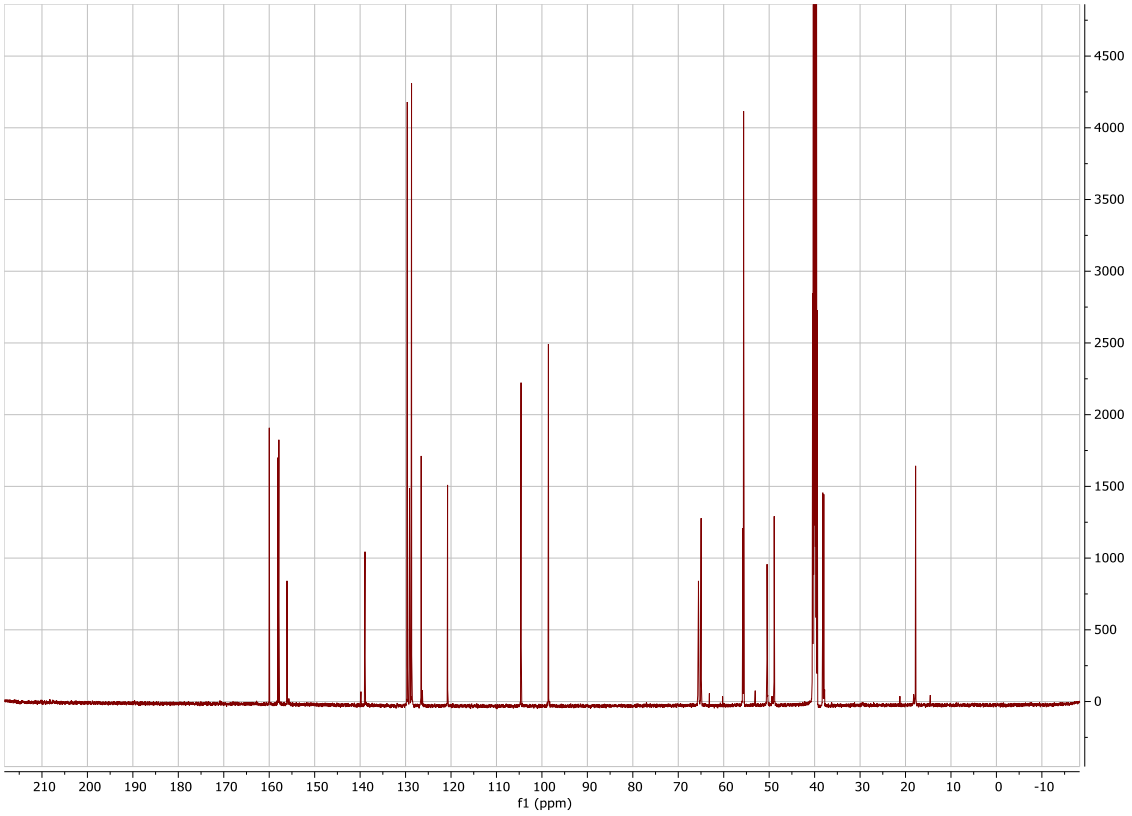

FAL-OH: (S)-2-(3-(2,4-dimethoxybenzyl)ureido)-3-phenylpropyl((S)-1-((((S)-1-hydroxy-4-methylpentan-2-yl)carbamoyl)oxy)propan-2-yl)carbamate

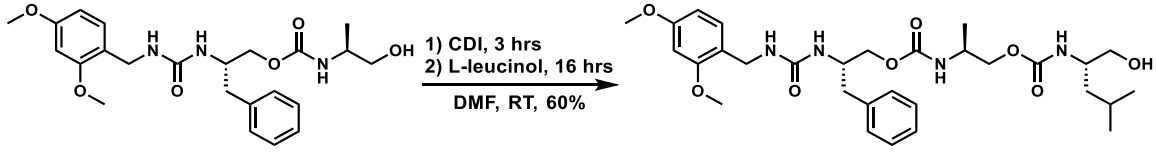

1.4 g (3.14 mmol) FA and 0.94 g (5.80 mmol, 1.85 eq) CDI in 20 mL anhydrous DMF were stirred at RT for three hours. 1.1 g (9.39 mmol, 3.0 eq) L-leucinol were added, and the reaction stirred overnight at RT. The mixture was poured into 1M HCl and thrice extracted with EtOAc. The combined organics were washed with 1M HCl, then brine, dried over Na_2SO_4, filtered, and stripped of solvents to dryness under reduced pressure. SiO_2 column chromatography (5:1 EtOAc / hexanes) gave 1.120 g (61% yield) FAL as a

white solid. ^{1}H NMR (500 MHz, DMSO-d_6) δ 7.28 (t, J = 7.4 Hz, 2H), 7.24 – 7.10 (m, 4H), 6.97 (d, J = 8.3 Hz, 1H), 6.82 (d, J = 8.9 Hz, 1H), 6.52 (d, J = 2.4 Hz, 1H), 6.44 (dd, J = 8.3, 2.4 Hz, 1H), 6.09 (t, J = 5.9 Hz, 1H), 5.96 (d, J = 8.1 Hz, 1H), 4.59 (t, J = 5.5 Hz, 1H), 4.05 (d, J = 5.9 Hz, 2H), 4.01 – 3.94 (m, 2H), 3.87 – 3.78 (m, 4H), 3.76 (s, 3H), 3.73 (s, 3H), 3.72 – 3.62 (m, 1H), 3.47 (dq, J = 10.6, 5.6 Hz, 1H), 3.30 (dt, J = 10.6, 5.5 Hz, 1H), 3.20 (dt, J = 10.6, 6.2 Hz, 1H), 2.76 (dd, J = 13.6, 6.1 Hz, 1H), 2.68 (dd, J = 13.6, 7.5 Hz, 1H), 1.73 – 1.44 (m, 1H), 1.33 – 1.13 (m, 2H), 1.03 (d, J = 6.5 Hz, 3H), 0.83 (dd, J = 9.4, 6.6 Hz, 6H). ^{13}C NMR (126 MHz, DMSO-d_6) δ 159.56, 157.66, 157.43, 155.96, 155.64, 138.44, 129.21, 128.71, 128.26, 126.15, 120.32, 104.16, 98.14, 66.13, 65.29, 64.09, 55.35, 55.20, 50.87, 50.02, 45.93, 37.77, 37.62, 24.22, 23.44, 21.80, 17.40. HRMS +ESI [M^{+}H]: 589.3232, calculated ($C_{30}H_{45}N_4O_8$): 589.32

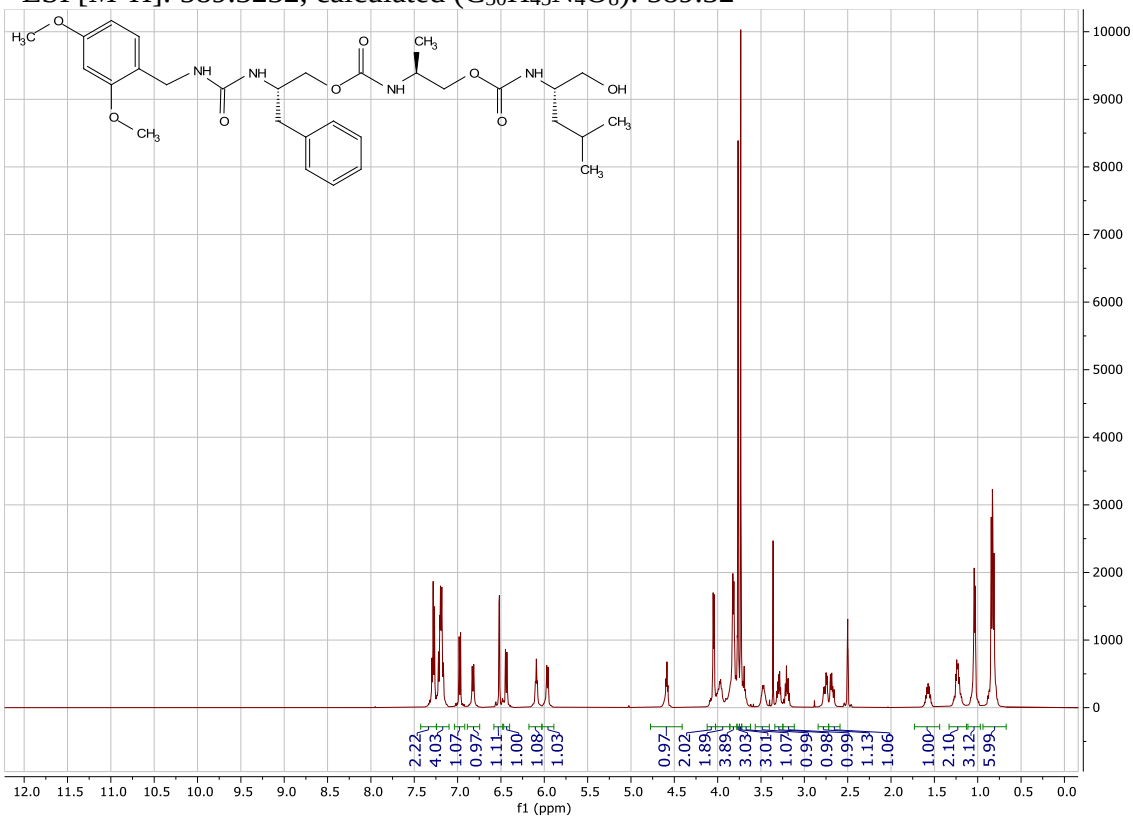

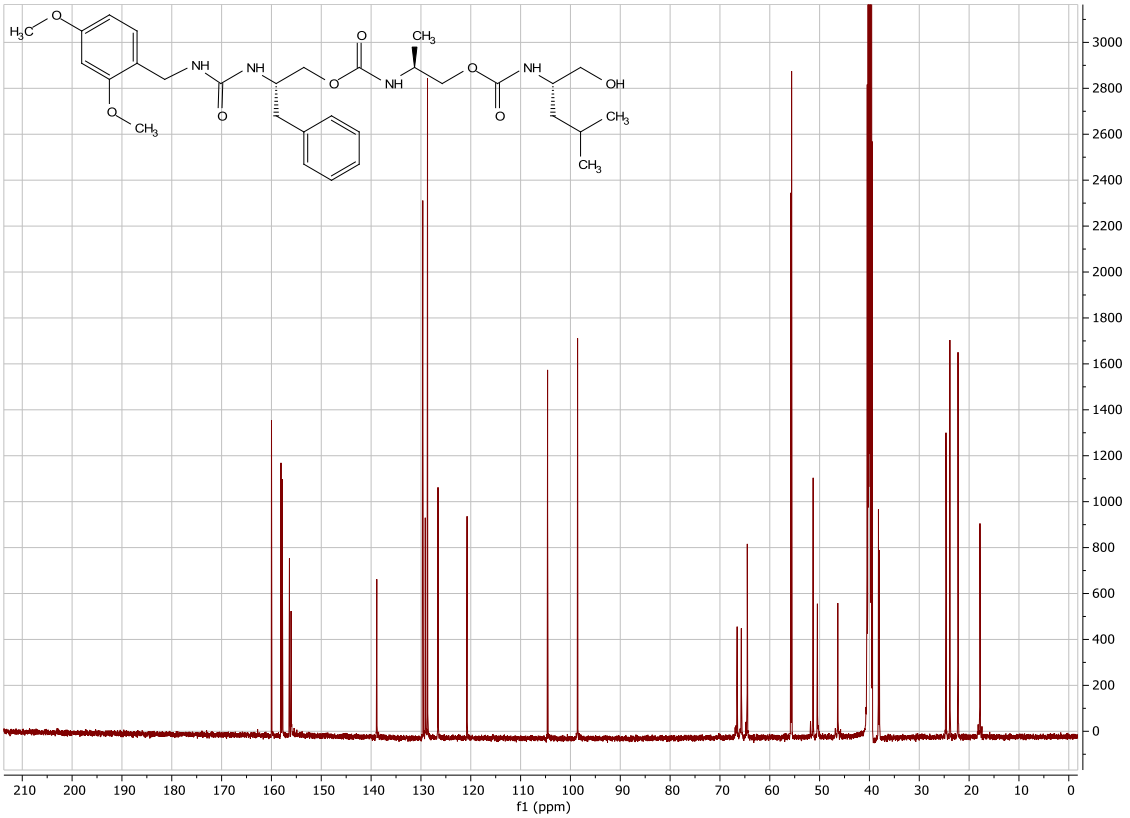

FAL-phthalimide: (S)-2-(3-(2,4-dimethoxybenzyl)ureido)-3-phenylpropyl ((S)-1-((((S)-1-(1,3-dioxoisoindolin-2-yl)-4-methylpentan-2-yl)carbamoyl)oxy)propan-2-yl)carbamate

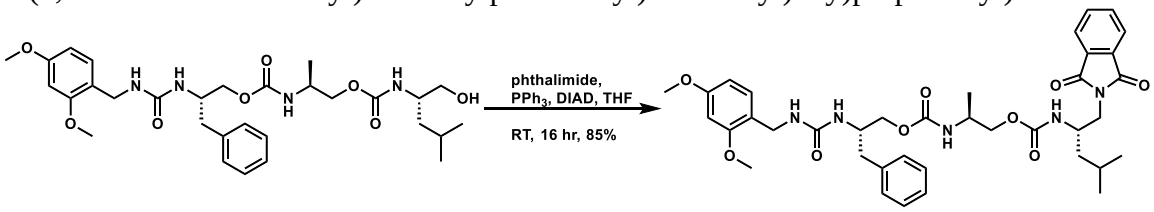

100 mg (0.169 mmol) FAL-OH, 58 mg (0.22 mmol, 1.3 eq) PPh_3, 43 µL (0.22 mol, 1.3 eq) DIAD, and 32 mg (0.22 mol, 1.3 eq) phthalimide were stirred in 4 mL THF at room temperature overnight. LCMS showed FAL-OH was still present. PPh_3, DIAD, and phthalimide quantities were doubled, and the reaction stirred overnight. Only 62% had converted to FAL-phthalimide, and so another 1.3 eq phthalimide were added. After stirring one more night, the reaction reached 89% product with 11% FAL-OH. The

reaction was filtered free of solids, poured into water, and extracted twice with DCM. The organics were washed twice with brine, dried over Na_2SO_4, filtered of solids, and stripped of solvents under reduced pressure. SiO_2 chromatography (slow gradient 3:1 Hexanes/EtOAc to 100% EtOAc to 2% MeOH in EtOAc) to remove excess reagents and triphenylphosphonium oxide gave 103 mg (85% yield) product. LCMS (ESI / APCI +/-): 718 (M+H), 740 (M+Na), 762 (M+formate), Calculated $C_{38}H_{47}N_5O_9$, 717.3374.

FAL-NH_2: (S)-2-(3-(2,4-dimethoxybenzyl)ureido)-3-phenylpropyl ((S)-1-((((S)-1-amino-4-methylpentan-2-yl)carbamoyl)oxy)propan-2-yl)carbamate

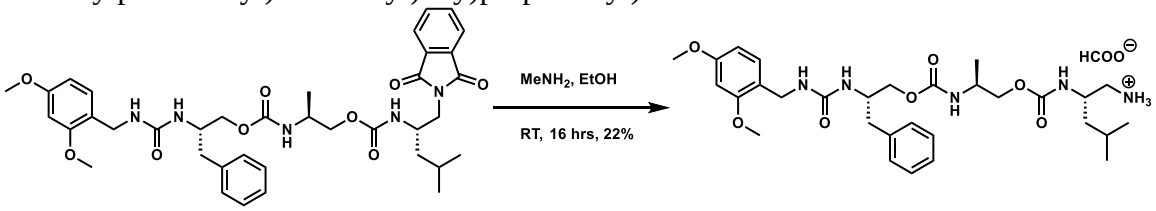

To 50 mg (0.0697 mmol) in 0.5 mL ethanol were added 10 µL (0.0837 mmol, 1.15 eq) 8M methylamine in ethanol, and the reaction was stirred at room temperature overnight. 18% of the phthalimide remained. Two µL more methylamine solution were added, and the reaction stirred another night. Formic acid was added to pH 3, and the reaction was stripped of ethanol and methyl amine solvents at reduced pressure. Reverse-phase purification produced 9 mg (22% yield) of the amine as the ammonium formate salt. Pure fractions were lyophilized free of water overnight. LCMS (ESI/APCI +/-): 588 (M+H), Calculated: $C_{30}H_{45}N_5O_7$, 587.3319

FALM-OH:(5S,10S)-5-benzyl-1-(2,4-dimethoxyphenyl)-10-methyl-3,8-dioxo-7-oxa-2,4,9-triazaundecan-11-yl((S)-1-((((S)-1-hydroxy-4-(methylthio)butan-2-yl)carbamoyl)oxy)-4-methylpentan-2-yl)carbamate

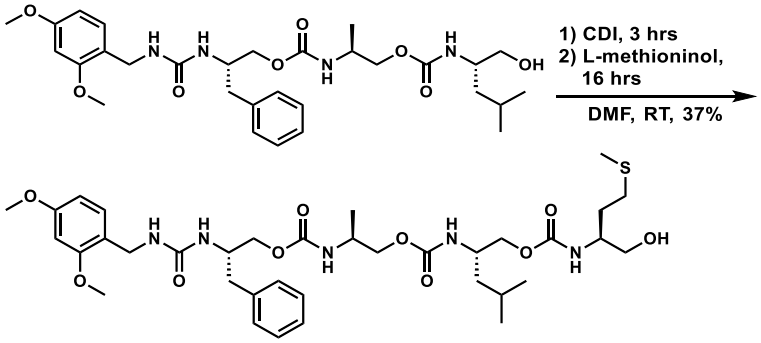

265 mg (0.450 mmol) FAL and 265 mg (1.638 mmol, 3.64 eq) CDI in 4 mL anhydrous DMF were stirred at RT for three hours. 444 mg (3.28 mmol, 7.3 eq) L-methioninol were added, and the reaction stirred overnight at RT. The mixture was poured into 1M HCl and thrice extracted with EtOAc. The combined organics were washed with 1M HCl, then brine, dried over Na_2SO_4, filtered, and stripped of solvents to dryness under reduced pressure. SiO_2 column chromatography to remove sulfoxide (oxidized FALM) (4:1 EtOAc / hexanes to 100% EtOAc) gave 125 mg (37% yield) FALM. ^{1}H NMR (500 MHz, DMSO-d_6) δ 7.29 (t, *J* = 7.4 Hz, 2H), 7.24-7.12 (m, 4H), 7.01 (d, *J* = 8.8 Hz, 1H), 6.98 (d, *J* = 8.2, 1H), 6.86 (d, *J* = 8.6 Hz, 1H), 6.53 (d, *J* = 2.4 Hz, 1H), 6.44 (dd, *J* = 8.2, 2.4 Hz, 1H), 6.08 (t, *J* = 5.9 Hz, 1H), 5.95 (d, *J* = 8.1 Hz, 1H), 4.64 (t, *J* = 5.7 Hz, 1H), 4.05 (d, *J* = 5.9 Hz, 2H), 4.0 – 3.93 (m, 1H), 3.90 – 3.78 (m, 5H), 3.77 (s, 4H), 3.74 (s, 3H), 3.72 – 3.63 (m, 2H), 3.50 (tq, *J* = 9.5, 5.2 Hz, 1H), 3.40 – 3.35 (m, 1H), 3.25 (dt, *J* = 11.4, 6.4 Hz, 1H), 2.77 (dd, *J* = 13.8, 6.2 Hz, 1H), 2.69 (dd, *J* = 13.7, 7.5 Hz, 1H), 2.46 (dd, *J* = 9.4, 5.0 Hz, 1H), 2.40 (dq, *J* = 13.1, 7.1 Hz, 1H), 2.02 (s, 3H), 1.78 (td, *J* = 9.2, 4.6 Hz, 1H), 1.57 (dqt, *J* = 14.5, 9.6, 5.6, 4.7 Hz, 2H), 1.28 (ddt, *J* = 17.2, 12.2, 6.0 Hz, 1H), 1.19 (q, *J* = 7.3, 6.3 Hz, 2H), 1.05 (d, *J* = 6.9 Hz, 3H), 0.84 (dd, *J* = 11.3, 6.6 Hz,

6H). ^{13}C NMR (126 MHz, DMSO-d_6) δ 159.55, 157.40, 155.93, 155.88, 155.61, 138.40, 129.16, 128.70, 128.22, 126.11, 120.31, 104.18, 98.14, 66.23, 63.26, 59.77, 55.32, 55.17, 51.99, 50.01, 48.16, 45.90, 37.75, 37.60, 30.60, 29.99, 24.06, 23.20, 21.68, 20.76, 17.39, 14.65, 14.09. HRMS +ESI [M$^+$H]: 750.3727, calculated ($C_{36}H_{56}N_5O_{10}S$): 750.37

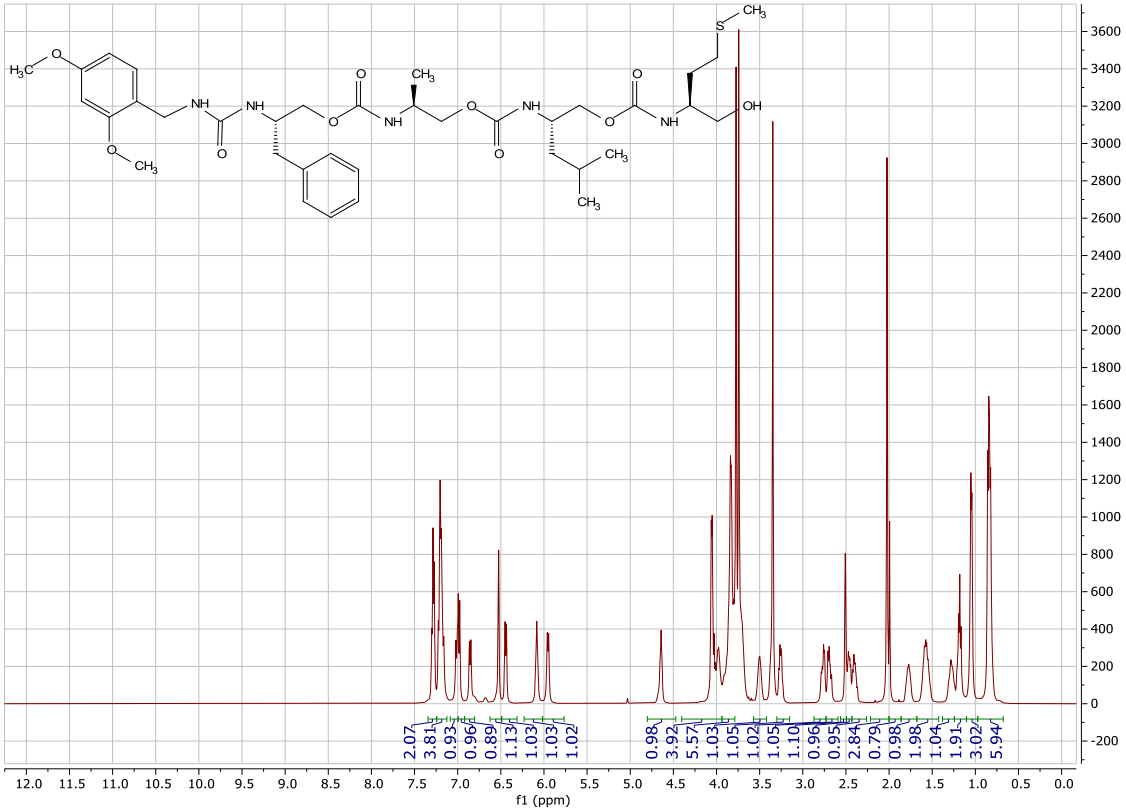

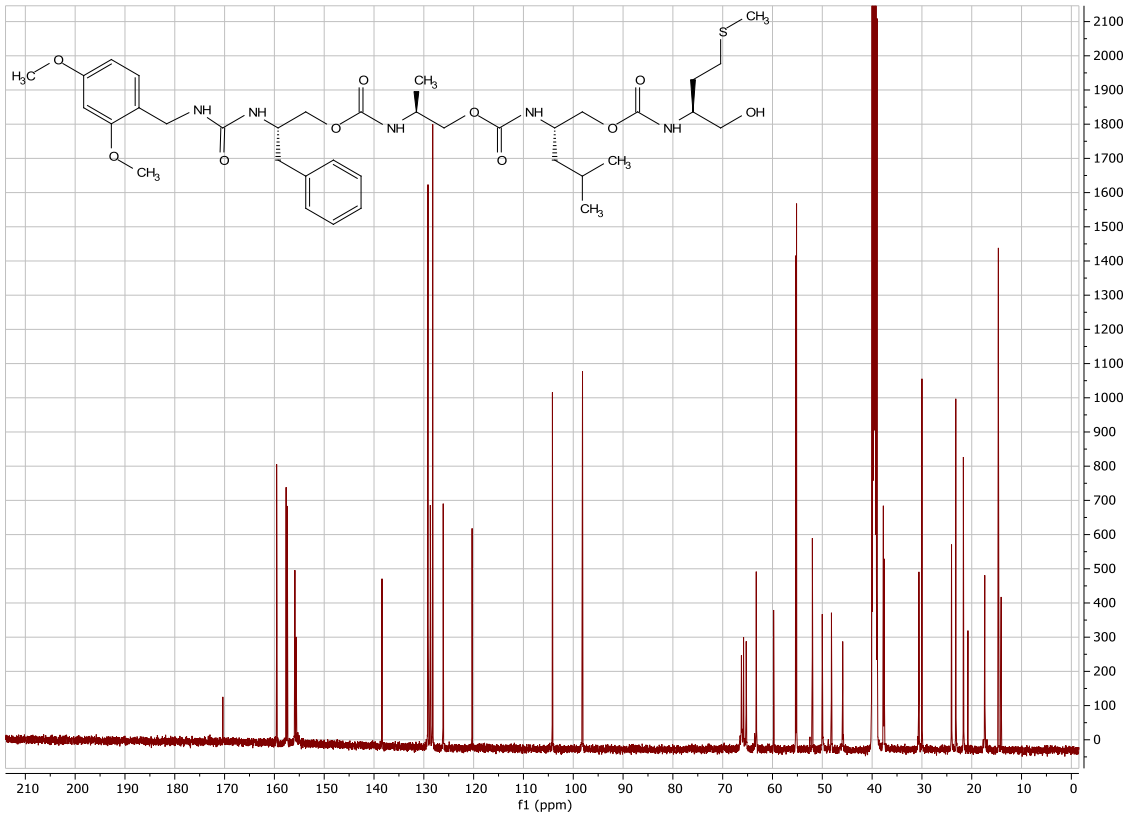

FALMW-OH: (5S,10S)-5-benzyl-1-(2,4-dimethoxyphenyl)-10-methyl-3,8-dioxo-7-oxa-2,4,9-triazaundecan-11-yl ((2S,7S,12S)-2-((1H-indol-3-yl)methyl)-1-hydroxy-14-methyl-7-(2-(methylthio)ethyl)-4,9-dioxo-5,10-dioxa-3,8-diazapentadecan-12-yl)carbamate

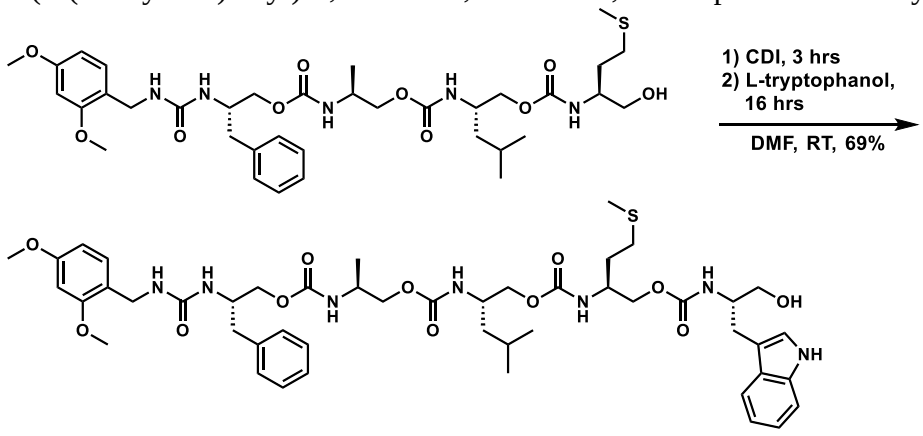

95 mg (0.127 mmol) FALM and 31 mg (0.190 mmol, 1.5 eq) CDI in 4 mL anhydrous DMF under argon balloon (to prevent sulfide oxidation to sulfoxide) were stirred at RT for three hours. 53 mg (0.280 mmol, 2.2 eq) L-tryptophanol were added, and the reaction stirred overnight at RT. The mixture was poured into 1M HCl and thrice extracted with EtOAc. The combined organics were washed with 1M HCl, then brine, dried over Na_2SO_4, filtered, and stripped of solvents to dryness under reduced pressure. SiO_2 column chromatography (4:1 EtOAc / hexanes to 100% EtOAc) gave 85 mg (69% yield) FALMW. ^{1}H NMR (500 MHz, DMSO-d_6) δ 10.76 (d, *J* = 2.5 Hz, 1H), 7.58 (d, *J* = 7.9 Hz, 1H), 7.32 (d, *J* = 8.1 Hz, 1H), 7.28 (t, *J* = 7.5 Hz, 2H), 7.24 – 7.13 (m, 4H), 7.09 (d, *J* = 2.3 Hz, 1H), 7.05 (t, *J* = 7.5 Hz, 2H), 7.02 (s, 1H), 6.99 – 6.94 (m, 2H), 6.92 (d, *J* = 8.4 Hz, 1H), 6.52 (d, *J* = 2.4 Hz, 1H), 6.44 (dd, *J* = 8.3, 2.4 Hz, 1H), 6.08 (t, *J* = 5.9 Hz, 1H), 5.95 (d, *J* = 8.2 Hz, 1H), 4.65 (t, *J* = 5.7 Hz, 1H), 4.05 (d, *J* = 5.8 Hz, 2H), 4.00 – 3.94 (m, 1H), 3.94 – 3.86 (m, 2H), 3.86 – 3.78 (m, 6H), 3.76 (s, 3H), 3.73 (s, 3H), 3.73 – 3.61 (m, 4H), 3.28 – 3.20 (m, 1H), 2.89 (dd, *J* = 14.6, 6.6 Hz, 1H), 2.82 -2.71 (m, 2H), 2.68 (dd, *J* = 13.7, 7.5 Hz, 1H), 2.45 (dd, *J* = 8.9, 5.1 Hz, 1H), 2.42 – 2.29 (m, 1H), 2.01 (s, 3H), 1.76 – 1.64 (m, 1H), 1.64 – 1.48 (m, 2H), 1.27 (dq, *J* = 16.9, 9.2, 7.1 Hz, 1H), 1.22 – 1.11 (m, 1H), 1.11 – 0.96 (m, 4H), 0.87 – 0.76 (m, 6H). ^{13}C NMR (126 MHz, DMSO-d_6) δ 159.56, 157.66, 157.43, 155.90, 155.80, 155.62, 138.40, 136.18, 129.17, 128.71, 128.23, 127.51, 126.12, 123.16, 120.81, 120.31, 118.42, 118.18, 111.42, 111.31, 104.20, 98.15, 66.25, 65.97, 65.29, 65.03, 62.72, 55.34, 55.18, 53.79, 50.03, 49.33, 48.16, 45.92, 45.71, 37.76, 37.60, 30.71, 29.64, 26.73, 24.05, 23.21, 21.68, 17.40, 14.64. HRMS +ESI [M^+H]: 966.4663, calculated ($C_{48}H_{68}N_7O_{12}S$): 966.46

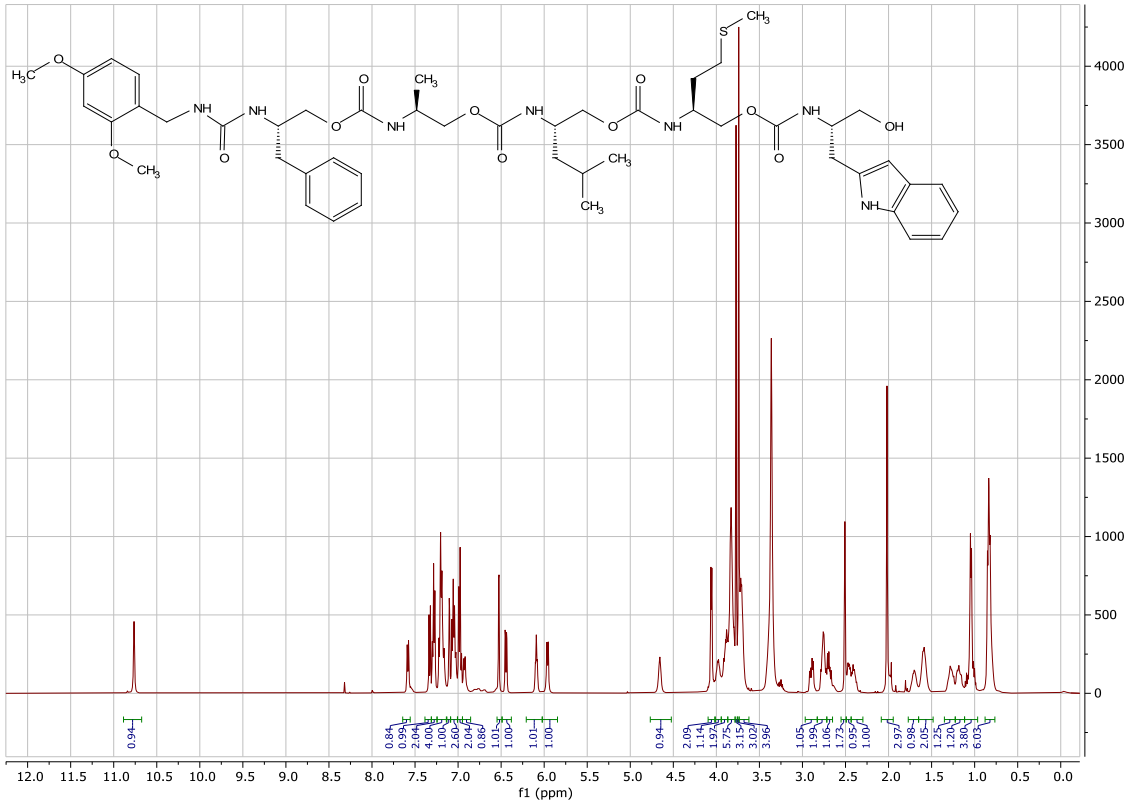
f1 (ppm)

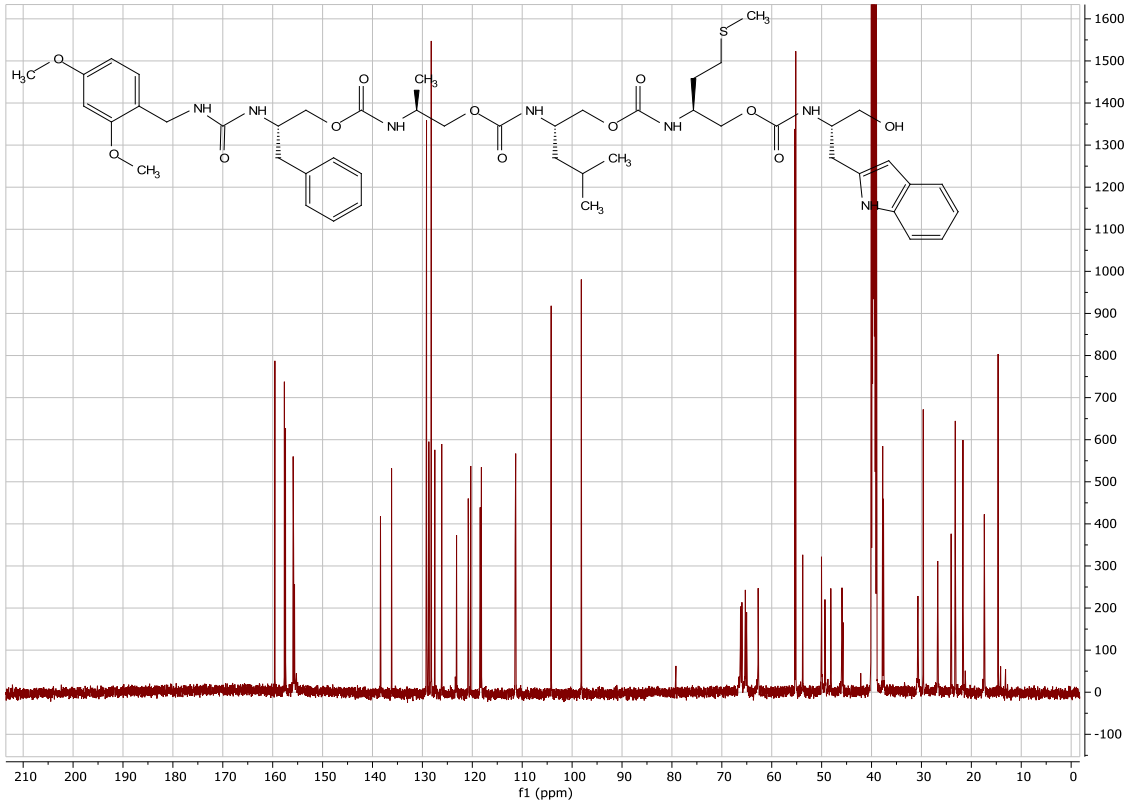
f1 (ppm)

References

REFERENCES FOR CHAPTER 1

1. Neumann, R. M., High-Precision Radiofrequency Spectrum of ^{14}N ^{16}O. *The Astrophysical Journal* **1970,** *161*, 779.
2. Armor, J. N., Influence of pH and ionic strength upon solubility of nitric oxide in aqueous solution. *Journal of Chemical & Engineering Data* **1974,** *19* (1), 82-84.
3. Oxides of Nitrogen. In *Solubility Data Series*, Young, C. L., Ed. Pergamon: Amsterdam, 1981; Vol. 8, pp 1-367.
4. Kelm, M., Nitric oxide metabolism and breakdown. *Biochimica et Biophysica Acta (BBA) - Bioenergetics* **1999,** *1411* (2), 273-289.
5. Lancaster, J. R., A Tutorial on the Diffusibility and Reactivity of Free Nitric Oxide. *Nitric Oxide* **1997,** *1* (1), 18-30.
6. Bartberger, M. D.; Liu, W.; Ford, E.; Miranda, K. M.; Switzer, C.; Fukuto, J. M.; Farmer, P. J.; Wink, D. A.; Houk, K. N., The reduction potential of nitric oxide (NO) and its importance to NO biochemistry. *Proc Natl Acad Sci USA* **2002,** *99* (17), 10958.
7. Shafirovich, V.; Lymar, S. V., Nitroxyl and its anion in aqueous solutions: Spin states, protic equilibria, and reactivities toward oxygen and nitric oxide. *Proc Natl Acad Sci USA* **2002,** *99* (11), 7340.
8. Lee, K. Y.; Kuchynka, D. J.; Kochi, J. K., Redox equilibria of the nitrosonium cation and of its nonbonded complexes. *Inorg. Chem.* **1990,** *29* (21), 4196-4204.
9. Stanbury, D. M., Recent advances in electron-transfer reactions. *Adv. Inorg. Chem* **2003,** *54*, 351-393.
10. Pollock, J. S.; Förstermann, U.; Mitchell, J. A.; Warner, T. D.; Schmidt, H. H.; Nakane, M.; Murad, F., Purification and characterization of particulate endothelium-derived relaxing factor synthase from cultured and native bovine aortic endothelial cells. *Proc Natl Acad Sci U S A* **1991,** *88* (23), 10480-10484.
11. Schmidt, H. H.; Pollock, J. S.; Nakane, M.; Gorsky, L. D.; Förstermann, U.; Murad, F., Purification of a soluble isoform of guanylyl cyclase-activating-factor synthase. *Proc Natl Acad Sci USA* **1991,** *88* (2), 365.
12. Kone, B. C.; Kuncewicz, T.; Zhang, W.; Yu, Z.-Y., Protein interactions with nitric oxide synthases: controlling the right time, the right place, and the right amount of nitric oxide. *American Journal of Physiology-Renal Physiology* **2003,** *285* (2), F178-F190.
13. Hevel, J. M.; White, K. A.; Marletta, M. A., Purification of the inducible murine macrophage nitric oxide synthase. Identification as a flavoprotein. *Journal of Biological Chemistry* **1991,** *266* (34), 22789-22791.
14. Stuehr, D. J.; Cho, H. J.; Kwon, N. S.; Weise, M. F.; Nathan, C. F., Purification and characterization of the cytokine-induced macrophage nitric oxide synthase: an FAD- and FMN-containing flavoprotein. *Proc Natl Acad Sci USA* **1991,** *88* (17), 7773.

15. MacMicking, J.; Xie, Q.-w.; Nathan, C., NITRIC OXIDE AND MACROPHAGE FUNCTION. *Annual Review of Immunology* **1997,** *15* (1), 323-350.
16. Lorsbach, R. B.; Murphy, W. J.; Lowenstein, C. J.; Snyder, S. H.; Russell, S. W., Expression of the nitric oxide synthase gene in mouse macrophages activated for tumor cell killing. Molecular basis for the synergy between interferon-gamma and lipopolysaccharide. *Journal of Biological Chemistry* **1993,** *268* (3), 1908-1913.
17. Stuehr, D. J.; Marletta, M. A., Mammalian nitrate biosynthesis: mouse macrophages produce nitrite and nitrate in response to Escherichia coli lipopolysaccharide. *Proc Natl Acad Sci U S A* **1985,** *82* (22), 7738-7742.
18. Cortese-Krott, M. M.; Rodriguez-Mateos, A.; Sansone, R.; Kuhnle, G. G. C.; Thasian-Sivarajah, S.; Krenz, T.; Horn, P.; Krisp, C.; Wolters, D.; Heiß, C.; Kröncke, K.-D.; Hogg, N.; Feelisch, M.; Kelm, M., Human red blood cells at work: identification and visualization of erythrocytic eNOS activity in health and disease. *Blood* **2012,** *120* (20), 4229-4237.
19. Kleinbongard, P.; Schulz, R.; Rassaf, T.; Lauer, T.; Dejam, A.; Jax, T.; Kumara, I.; Gharini, P.; Kabanova, S.; Özüyaman, B.; Schnürch, H.-G.; Gödecke, A.; Weber, A.-A.; Robenek, M.; Robenek, H.; Bloch, W.; Rösen, P.; Kelm, M., Red blood cells express a functional endothelial nitric oxide synthase. *Blood* **2006,** *107* (7), 2943-2951.
20. Picón-Pagès, P.; Garcia-Buendia, J.; Muñoz, F. J., Functions and dysfunctions of nitric oxide in brain. *Biochimica et Biophysica Acta (BBA) - Molecular Basis of Disease* **2019,** *1865* (8), 1949-1967.
21. Cinelli, M. A.; Do, H. T.; Miley, G. P.; Silverman, R. B., Inducible nitric oxide synthase: Regulation, structure, and inhibition. *Medicinal Research Reviews* **2020,** *40* (1), 158-189.
22. Marsden, P. A.; Heng, H. H.; Scherer, S. W.; Stewart, R. J.; Hall, A. V.; Shi, X. M.; Tsui, L. C.; Schappert, K. T., Structure and chromosomal localization of the human constitutive endothelial nitric oxide synthase gene. *Journal of Biological Chemistry* **1993,** *268* (23), 17478-17488.
23. Xu, W.; Gorman, P.; Sheer, D.; Bates, G.; Kishimoto, J.; Lizhi, L.; Emson, P., Regional localization of the gene coding for human brain nitric oxide synthase (NOS1) to 12q24.2→24.31 by fluorescent in situ hybridization. *Cytogenetic and Genome Research* **1993,** *64* (1), 62-63.
24. Aoyagi, M.; Arvai, A. S.; Tainer, J. A.; Getzoff, E. D., Structural basis for endothelial nitric oxide synthase binding to calmodulin. *The EMBO Journal* **2003,** *22* (4), 766-775.
25. Bredt, D. S.; Snyder, S. H., Isolation of nitric oxide synthetase, a calmodulin-requiring enzyme. *Proc Natl Acad Sci USA* **1990,** *87* (2), 682.
26. Salerno, J. C.; Harris, D. E.; Irizarry, K.; Patel, B.; Morales, A. J.; Smith, S. M. E.; Martasek, P.; Roman, L. J.; Masters, B. S. S.; Jones, C. L.; Weissman, B. A.; Lane, P.; Liu, Q.; Gross, S. S., An Autoinhibitory Control Element Defines Calcium-regulated Isoforms of Nitric Oxide Synthase. *Journal of Biological Chemistry* **1997,** *272* (47), 29769-29777.

27. Daff, S.; Sagami, I.; Shimizu, T., The 42-amino acid insert in the FMN domain of neuronal nitric-oxide synthase exerts control over Ca(2+)/calmodulin-dependent electron transfer. *The Journal of biological chemistry* **1999,** *274* (43), 30589-95.
28. Lane, P.; Gross, S. S., The autoinhibitory control element and calmodulin conspire to provide physiological modulation of endothelial and neuronal nitric oxide synthase activity. *Acta physiologica Scandinavica* **2000,** *168* (1), 53-63.
29. Roman, L. J.; Miller, R. T.; de la Garza, M. A.; Kim, J.-J. P.; Siler Masters, B. S., The C Terminus of Mouse Macrophage Inducible Nitric-oxide Synthase Attenuates Electron Flow through the Flavin Domain. *Journal of Biological Chemistry* **2000,** *275* (29), 21914-21919.
30. Roman, L. J.; Martásek, P.; Miller, R. T.; Harris, D. E.; de la Garza, M. A.; Shea, T. M.; Kim, J.-J. P.; Masters, B. S. S., The C Termini of Constitutive Nitric-oxide Synthases Control Electron Flow through the Flavin and Heme Domains and Affect Modulation by Calmodulin. *Journal of Biological Chemistry* **2000,** *275* (38), 29225-29232.
31. Tiso, M.; Tejero, J.; Panda, K.; Aulak, K. S.; Stuehr, D. J., Versatile Regulation of Neuronal Nitric Oxide Synthase by Specific Regions of Its C-Terminal Tail. *Biochemistry* **2007,** *46* (50), 14418-14428.
32. Brenman, J. E.; Chao, D. S.; Gee, S. H.; McGee, A. W.; Craven, S. E.; Santillano, D. R.; Wu, Z.; Huang, F.; Xia, H.; Peters, M. F.; Froehner, S. C.; Bredt, D. S., Interaction of Nitric Oxide Synthase with the Postsynaptic Density Protein PSD-95 and α1-Syntrophin Mediated by PDZ Domains. *Cell* **1996,** *84* (5), 757-767.
33. Roman, L. J.; Martásek, P.; Masters, B. S. S., Intrinsic and Extrinsic Modulation of Nitric Oxide Synthase Activity. *Chem. Rev.* **2002,** *102* (4), 1179-1190.
34. Ghosh, D. K.; Wu, C.; Pitters, E.; Moloney, M.; Werner, E. R.; Mayer, B.; Stuehr, D. J., Characterization of the Inducible Nitric Oxide Synthase Oxygenase Domain Identifies a 49 Amino Acid Segment Required for Subunit Dimerization and Tetrahydrobiopterin Interaction. *Biochemistry* **1997,** *36* (35), 10609-10619.
35. Garcin, E. D.; Bruns, C. M.; Lloyd, S. J.; Hosfield, D. J.; Tiso, M.; Gachhui, R.; Stuehr, D. J.; Tainer, J. A.; Getzoff, E. D., Structural basis for isozyme-specific regulation of electron transfer in nitric-oxide synthase. *The Journal of biological chemistry* **2004,** *279* (36), 37918-27.
36. Iyanagi, T.; Xia, C.; Kim, J.-J. P., NADPH–cytochrome P450 oxidoreductase: Prototypic member of the diflavin reductase family. *Archives of Biochemistry and Biophysics* **2012,** *528* (1), 72-89.
37. Oprian, D. D.; Coon, M. J., Oxidation-reduction states of FMN and FAD in NADPH-cytochrome P-450 reductase during reduction by NADPH. *The Journal of biological chemistry* **1982,** *257* (15), 8935-44.
38. Panda, K.; Ghosh, S.; Stuehr, D. J., Calmodulin Activates Intersubunit Electron Transfer in the Neuronal Nitric-oxide Synthase Dimer. *Journal of Biological Chemistry* **2001,** *276* (26), 23349-23356.

39. Sagami, I.; Daff, S.; Shimizu, T., Intra-subunit and inter-subunit electron transfer in neuronal nitric-oxide synthase: effect of calmodulin on heterodimer catalysis. *The Journal of biological chemistry* **2001,** *276* (32), 30036-42.
40. Siddhanta, U.; Presta, A.; Fan, B.; Wolan, D.; Rousseau, D. L.; Stuehr, D. J., Domain swapping in inducible nitric-oxide synthase. Electron transfer occurs between flavin and heme groups located on adjacent subunits in the dimer. *The Journal of biological chemistry* **1998,** *273* (30), 18950-8.
41. Daff, S., NO synthase: Structures and mechanisms. *Nitric Oxide* **2010,** *23* (1), 1-11.
42. Raman, C. S.; Li, H.; Martásek, P.; Král, V.; Masters, B. S. S.; Poulos, T. L., Crystal Structure of Constitutive Endothelial Nitric Oxide Synthase: A Paradigm for Pterin Function Involving a Novel Metal Center. *Cell* **1998,** *95* (7), 939-950.
43. Chreifi, G.; Li, H.; McInnes, C. R.; Gibson, C. L.; Suckling, C. J.; Poulos, T. L., Communication between the Zinc and Tetrahydrobiopterin Binding Sites in Nitric Oxide Synthase. *Biochemistry* **2014,** *53* (25), 4216-4223.
44. Förstermann, U.; Münzel, T., Endothelial Nitric Oxide Synthase in Vascular Disease. *Circulation* **2006,** *113* (13), 1708-1714.
45. Hemmens, B.; Mayer, B., Enzymology of Nitric Oxide Synthases. In *Nitric Oxide Protocols*, Titheradge, M. A., Ed. Humana Press: Totowa, NJ, 1998; pp 1-32.
46. Kretsinger, R. H.; Nockolds, C. E., Carp muscle calcium-binding protein. II. Structure determination and general description. *The Journal of biological chemistry* **1973,** *248* (9), 3313-26.
47. Venema, R. C.; Sayegh, H. S.; Kent, J. D.; Harrison, D. G., Identification, Characterization, and Comparison of the Calmodulin-binding Domains of the Endothelial and Inducible Nitric Oxide Synthases. *Journal of Biological Chemistry* **1996,** *271* (11), 6435-6440.
48. Abu-Soud, H. M.; Stuehr, D. J., Nitric oxide synthases reveal a role for calmodulin in controlling electron transfer. *Proc Natl Acad Sci U S A* **1993,** *90* (22), 10769-10772.
49. Abu-Soud, H. M.; Yoho, L. L.; Stuehr, D. J., Calmodulin controls neuronal nitric-oxide synthase by a dual mechanism. Activation of intra- and interdomain electron transfer. *Journal of Biological Chemistry* **1994,** *269* (51), 32047-50.
50. Garcin, E. D.; Bruns, C. M.; Lloyd, S. J.; Hosfield, D. J.; Tiso, M.; Gachhui, R.; Stuehr, D. J.; Tainer, J. A.; Getzoff, E. D., Structural Basis for Isozyme-specific Regulation of Electron Transfer in Nitric-oxide Synthase. *Journal of Biological Chemistry* **2004,** *279* (36), 37918-37927.
51. Gorren, A. C. F.; Mayer, B., Nitric-oxide synthase: A cytochrome P450 family foster child. *Biochimica et Biophysica Acta (BBA) - General Subjects* **2007,** *1770* (3), 432-445.
52. Spiro, T. G.; Jarzecki, A. A., Heme-based sensors: theoretical modeling of heme-ligand–protein interactions. *Current Opinion in Chemical Biology* **2001,** *5* (6), 715-723.
53. Giroud, C.; Moreau, M.; Mattioli, T. A.; Balland, V.; Boucher, J.-L.; Xu-Li, Y.; Stuehr, D. J.; Santolini, J., Role of Arginine Guanidinium Moiety in Nitric-oxide

Synthase Mechanism of Oxygen Activation. *Journal of Biological Chemistry* **2010,** *285* (10), 7233-7245.
54. Li, H.; Poulos, T. L., Structure–function studies on nitric oxide synthases. *Journal of Inorganic Biochemistry* **2005,** *99* (1), 293-305.
55. Stuehr, D. J.; Santolini, J.; Wang, Z.-Q.; Wei, C.-C.; Adak, S., Update on Mechanism and Catalytic Regulation in the NO Synthases. *Journal of Biological Chemistry* **2004,** *279* (35), 36167-36170.
56. Borek, E.; Clarke, H. T., COMPOUNDS RELATED TO CANALINE AND CANAVANINE. *Journal of Biological Chemistry* **1938,** *125* (2), 479-494.
57. Davydov, R.; Sudhamsu, J.; Lees, N. S.; Crane, B. R.; Hoffman, B. M., EPR and ENDOR Characterization of the Reactive Intermediates in the Generation of NO by Cryoreduced Oxy-Nitric Oxide Synthase from Geobacillus stearothermophilus. *J. Am. Chem. Soc.* **2009,** *131* (40), 14493-14507.
58. Hord, N. G.; Tang, Y.; Bryan, N. S., Food sources of nitrates and nitrites: the physiologic context for potential health benefits. *The American Journal of Clinical Nutrition* **2009,** *90* (1), 1-10.
59. Sparacino-Watkins, C. E.; Tejero, J.; Sun, B.; Gauthier, M. C.; Thomas, J.; Ragireddy, V.; Merchant, B. A.; Wang, J.; Azarov, I.; Basu, P.; Gladwin, M. T., Nitrite reductase and nitric-oxide synthase activity of the mitochondrial molybdopterin enzymes mARC1 and mARC2. *The Journal of biological chemistry* **2014,** *289* (15), 10345-10358.
60. Weitzberg, E.; Lundberg, J., Nonenzymatic nitric oxide production in humans. *Nitric Oxide* **1998,** *2* (1), 1-7.
61. Spiegelhalder, B.; Eisenbrand, G.; Preussmann, R., Influence of dietary nitrate on nitrite content of human saliva: possible relevance to in vivo formation of N-nitroso compounds. *Food and cosmetics toxicology* **1976,** *14* (6), 545-548.
62. MILLAR, T. M.; STEVENS, C. R.; BLAKE, D. R., Xanthine oxidase can generate nitric oxide from nitrate in ischaemia. *Biochemical Society Transactions* **1997,** *25* (3), 528S-528S.
63. Jansson, E. Å.; Huang, L.; Malkey, R.; Govoni, M.; Nihlén, C.; Olsson, A.; Stensdotter, M.; Petersson, J.; Holm, L.; Weitzberg, E.; Lundberg, J. O., A mammalian functional nitrate reductase that regulates nitrite and nitric oxide homeostasis. *Nature Chemical Biology* **2008,** *4* (7), 411-417.
64. Benjamin, N.; O'Driscoll, F.; Dougall, H.; Duncan, C.; Smith, L.; Golden, M.; McKenzie, H., Stomach NO synthesis. *Nature* **1994,** *368* (6471), 502.
65. Licht, W. R.; Schultz, D. S.; Fox, J. G.; Tannenbaum, S. R.; Deen, W. M., Mechanisms for nitrite loss from the stomach. *Carcinogenesis* **1986,** *7* (10), 1681-1687.
66. Kapil, V.; Khambata, R. S.; Jones, D. A.; Rathod, K.; Primus, C.; Massimo, G.; Fukuto, J. M.; Ahluwalia, A., The Noncanonical Pathway for In Vivo Nitric Oxide Generation: The Nitrate-Nitrite-Nitric Oxide Pathway. *Pharmacol Rev* **2020,** *72* (3), 692-766.
67. Li, H.; Cui, H.; Kundu, T. K.; Alzawahra, W.; Zweier, J. L., Nitric oxide production from nitrite occurs primarily in tissues not in the blood critical role of

xanthine oxidase and aldehyde oxidase. *Journal of Biological Chemistry* **2008,** *283* (26), 17855-17863.
68. Thomas, D. D.; Liu, X.; Kantrow, S. P.; Lancaster, J. R., The biological lifetime of nitric oxide: Implications for the perivascular dynamics of NO and O₂. *Proc Natl Acad Sci USA* **2001,** *98* (1), 355-360.
69. Eich, R. F.; Li, T.; Lemon, D. D.; Doherty, D. H.; Curry, S. R.; Aitken, J. F.; Mathews, A. J.; Johnson, K. A.; Smith, R. D.; Phillips, G. N.; Olson, J. S., Mechanism of NO-Induced Oxidation of Myoglobin and Hemoglobin. *Biochemistry* **1996,** *35* (22), 6976-6983.
70. Jia, L.; Bonaventura, C.; Bonaventura, J.; Stamler, J. S., S-nitrosohaemoglobin: a dynamic activity of blood involved in vascular control. *Nature* **1996,** *380* (6571), 221-6.
71. Ferranti, P.; Malorni, A.; Mamone, G.; Sannolo, N.; Marino, G., Characterisation of S-nitrosohaemoglobin by mass spectrometry. *FEBS Letters* **1997,** *400* (1), 19-24.
72. Chan, N. L.; Rogers, P. H.; Arnone, A., Crystal structure of the S-nitroso form of liganded human hemoglobin. *Biochemistry* **1998,** *37* (47), 16459-64.
73. Stamler, J. S.; Jaraki, O.; Osborne, J.; Simon, D. I.; Keaney, J.; Vita, J.; Singel, D.; Valeri, C. R.; Loscalzo, J., Nitric oxide circulates in mammalian plasma primarily as an S-nitroso adduct of serum albumin. *Proc Natl Acad Sci U S A* **1992,** *89* (16), 7674-7.
74. Stone, J. R.; Marletta, M. A., Soluble guanylate cyclase from bovine lung: activation with nitric oxide and carbon monoxide and spectral characterization of the ferrous and ferric states. *Biochemistry* **1994,** *33* (18), 5636-5640.
75. Denninger, J. W.; Marletta, M. A., Guanylate cyclase and the ·NO/cGMP signaling pathway. *Biochimica et Biophysica Acta (BBA) - Bioenergetics* **1999,** *1411* (2), 334-350.
76. Stone, J. R.; Sands, R. H.; Dunham, W. R.; Marletta, M. A., Electron paramagnetic resonance spectral evidence for the formation of a pentacoordinate nitrosyl-heme complex on soluble guanylate cyclase. *Biochemical and biophysical research communications* **1995,** *207* (2), 572-577.
77. Hunt, A. P.; Lehnert, N., Heme-Nitrosyls: Electronic Structure Implications for Function in Biology. *Acc. Chem. Res.* **2015,** *48* (7), 2117-2125.
78. Brown, G. C., Nitric oxide regulates mitochondrial respiration and cell functions by inhibiting cytochrome oxidase. *FEBS letters* **1995,** *369* (2-3), 136-139.
79. Wink, D. A.; Osawa, Y.; Darbyshire, J. F.; Jones, C. R.; Eshenaur, S. C.; Nims, R. W., Inhibition of cytochromes P450 by nitric oxide and a nitric oxide-releasing agent. *Arch Biochem Biophys* **1993,** *300* (1), 115-23.
80. Brouwer, M.; Chamulitrat, W.; Ferruzzi, G.; Sauls, D.; Weinberg, J., Nitric oxide interactions with cobalamins: biochemical and functional consequences. *Blood* **1996,** *88* (5), 1857-1864.
81. Sekkaï, D.; Aillet, F.; Israël, N.; Lepoivre, M., Inhibition of NF-κB and HIV-1 long terminal repeat transcriptional activation by inducible nitric oxide synthase 2 activity. *Journal of Biological Chemistry* **1998,** *273* (7), 3895-3900.
82. Lander, H. M.; Sehajpal, P. K.; Novogrodsky, A., Nitric oxide signaling: a possible role for G proteins. *The Journal of Immunology* **1993,** *151* (12), 7182-7187.

83. Li, J.; Billiar, T. R.; Talanian, R. V.; Kim, Y. M., Nitric oxide reversibly inhibits seven members of the caspase family via S-nitrosylation. *Biochemical and biophysical research communications* **1997,** *240* (2), 419-424.
84. Kim, Y.-M.; Bombeck, C. A.; Billiar, T. R., Nitric oxide as a bifunctional regulator of apoptosis. *Circulation research* **1999,** *84* (3), 253-256.
85. Durzan, D. J.; Pedroso, M. C., Nitric oxide and reactive nitrogen oxide species in plants. *Biotechnology and Genetic Engineering Reviews* **2002,** *19* (1), 293-338.
86. Gow, A. J.; Stamler, J. S., Reactions between nitric oxide and haemoglobin under physiological conditions. *Nature* **1998,** *391* (6663), 169-173.
87. Toledo, J. C.; Bosworth, C. A.; Hennon, S. W.; Mahtani, H. A.; Bergonia, H. A.; Lancaster, J. R., Nitric oxide-induced conversion of cellular chelatable iron into macromolecule-bound paramagnetic dinitrosyliron complexes. *Journal of Biological Chemistry* **2008,** *283* (43), 28926-28933.
88. Xu, L.; Eu, J. P.; Meissner, G.; Stamler, J. S., Activation of the cardiac calcium release channel (ryanodine receptor) by poly-S-nitrosylation. *Science* **1998,** *279* (5348), 234-237.
89. Lipton, S.; Stamler, J., Actions of redox-related congeners of nitric oxide at the NMDA receptor. *Neuropharmacology* **1994,** *33* (11), 1229-1233.
90. Bolotina, V. M.; Najibi, S.; Palacino, J. J.; Pagano, P. J.; Cohen, R. A., Nitric oxide directly activates calcium-dependent potassium channels in vascular smooth muscle. *Nature* **1994,** *368* (6474), 850-853.
91. Uppu, R. M.; Squadrito, G. L.; Pryor, W. A., Acceleration of peroxynitrite oxidations by carbon dioxide. *Arch Biochem Biophys* **1996,** *327* (2), 335-43.
92. Beckman, J. S.; Koppenol, W. H., Nitric oxide, superoxide, and peroxynitrite: the good, the bad, and ugly. *American Journal of Physiology-Cell Physiology* **1996,** *271* (5), C1424-C1437.
93. Liu, X.; Miller, M. J. S.; Joshi, M. S.; Thomas, D. D.; Lancaster, J. R., Accelerated reaction of nitric oxide with O₂ within the hydrophobic interior of biological membranes. *Proc Natl Acad Sci USA* **1998,** *95* (5), 2175-2179.
94. Furchgott, R. F.; Vanhoutte, P. M., Endothelium-derived relaxing and contracting factors. *The FASEB Journal* **1989,** *3* (9), 2007-2018.
95. Wareham, L. K.; Buys, E. S.; Sappington, R. M., The nitric oxide-guanylate cyclase pathway and glaucoma. *Nitric oxide : biology and chemistry* **2018,** *77*, 75-87.
96. Jeremy, J. Y.; Rowe, D.; Emsley, A. M.; Newby, A. C., Nitric oxide and the proliferation of vascular smooth muscle cells. *Cardiovascular Research* **1999,** *43* (3), 580-594.
97. Irwin, C.; Roberts, W.; Naseem, K. M., Nitric oxide inhibits platelet adhesion to collagen through cGMP-dependent and independent mechanisms: the potential role for S-nitrosylation. *Platelets* **2009,** *20* (7), 478-86.
98. Laroux, F. S.; Lefer, D. J.; Kawachi, S.; Scalia, R.; Cockrell, A. S.; Gray, L.; Van der Heyde, H.; Hoffman, J. M.; Grisham, M. B., Role of nitric oxide in the regulation of acute and chronic inflammation. *Antioxid Redox Signal* **2000,** *2* (3), 391-6.

99. Boueiz, A.; Hassoun, P. M., Regulation of endothelial barrier function by reactive oxygen and nitrogen species. *Microvascular research* **2009,** *77* (1), 26-34.
100. McQuaid, K. E.; Keenan, A. K., Endothelial barrier dysfunction and oxidative stress: roles for nitric oxide? *Experimental physiology* **1997,** *82* (2), 369-76.
101. Sessa, W. C., Molecular control of blood flow and angiogenesis: role of nitric oxide. *Journal of thrombosis and haemostasis : JTH* **2009,** *7 Suppl 1*, 35-7.
102. Cooke, J. P., NO and angiogenesis. *Atherosclerosis. Supplements* **2003,** *4* (4), 53-60.
103. Pearson, J. D., Endothelial cell function and thrombosis. *Best Practice & Research Clinical Haematology* **1999,** *12* (3), 329-341.
104. Ricciardolo, F. L. M., Multiple roles of nitric oxide in the airways. *Thorax* **2003,** *58* (2), 175-182.
105. Khan, S. A.; Skaf, M. W.; Harrison, R. W.; Lee, K.; Minhas, K. M.; Kumar, A.; Fradley, M.; Shoukas, A. A.; Berkowitz, D. E.; Hare, J. M., Nitric oxide regulation of myocardial contractility and calcium cycling: independent impact of neuronal and endothelial nitric oxide synthases. *Circulation research* **2003,** *92* (12), 1322-1329.
106. Davis, B. J.; Flanagan, B. F.; Gilfillan, A. M.; Metcalfe, D. D.; Coleman, J. W., Nitric Oxide Inhibits IgE-Dependent Cytokine Production and Fos and Jun Activation in Mast Cells. *The Journal of Immunology* **2004,** *173* (11), 6914-6920.
107. Frank, S.; Kämpfer, H.; Wetzler, C.; Pfeilschifter, J., Nitric oxide drives skin repair: novel functions of an established mediator. *Kidney international* **2002,** *61* (3), 882-8.
108. Filippin, L. I.; Moreira, A. J.; Marroni, N. P.; Xavier, R. M., Nitric oxide and repair of skeletal muscle injury. *Nitric Oxide* **2009,** *21* (3-4), 157-63.
109. Burnett, A. L.; Lowenstein, C. J.; Bredt, D. S.; Chang, T. S.; Snyder, S. H., Nitric oxide: a physiologic mediator of penile erection. *Science* **1992,** *257* (5068), 401-3.
110. Thaler, C. D.; Epel, D., Nitric oxide in oocyte maturation, ovulation, fertilization, cleavage and implantation: a little dab'll do ya. *Current pharmaceutical design* **2003,** *9* (5), 399-409.
111. Rolle, U.; Nemeth, L.; Puri, P., Nitrergic innervation of the normal gut and in motility disorders of childhood. *Journal of Pediatric Surgery* **2002,** *37* (4), 551-567.
112. Blantz, R. C.; Deng, A.; Lortie, M.; Munger, K.; Vallon, V.; Gabbai, F. B.; Thomson, S. C., The complex role of nitric oxide in the regulation of glomerular ultrafiltration. *Kidney international* **2002,** *61* (3), 782-5.
113. Kurtz, A.; Wagner, C., Role of nitric oxide in the control of renin secretion. *American Journal of Physiology-Renal Physiology* **1998,** *275* (6), F849-F862.
114. Toda, N.; Ayajiki, K.; Okamura, T., Cerebral blood flow regulation by nitric oxide: recent advances. *Pharmacol Rev* **2009,** *61* (1), 62-97.
115. Gerstberger, R., Nitric Oxide and Body Temperature Control. *Physiology* **1999,** *14* (1), 30-36.
116. Vincent, S. R., Nitric oxide neurons and neurotransmission. *Progress in neurobiology* **2010,** *90* (2), 246-55.

117. Toda, N.; Okamura, T., The pharmacology of nitric oxide in the peripheral nervous system of blood vessels. *Pharmacol Rev* **2003,** *55* (2), 271-324.
118. PÖÜN, Ş.; KUHAR, M. J., Regulation of Neurotransmitter Reuptake by Nitric Oxide. *Annals of the New York Academy of Sciences* **1994,** *738* (1), 305-315.
119. Kilduff, T. S.; Cauli, B.; Gerashchenko, D., Activation of cortical interneurons during sleep: an anatomical link to homeostatic sleep regulation? *Trends in neurosciences* **2011,** *34* (1), 10-19.
120. Freire, M. A. M.; Guimarães, J. S.; Leal, W. G.; Pereira, A., Pain modulation by nitric oxide in the spinal cord. *Front Neurosci* **2009,** *3* (2), 175-181.
121. Cury, Y.; Picolo, G.; Gutierrez, V. P.; Ferreira, S. H., Pain and analgesia: The dual effect of nitric oxide in the nociceptive system. *Nitric Oxide* **2011,** *25* (3), 243-254.
122. Alicja Kasperska-Zając, B. R., Role of nitric oxide (NO) in hormone secretion – part II. *CaseRepClinPractRev* **2003,** *4* (2), 146-148.
123. Alicja Kasperska-Zając, B. R., Role of nitric oxide (NO) in hormone secretion – part I. *CaseRepClinPractRev* **2003,** *4* (2), 141-145.
124. Kourosh-Arami, M.; Hosseini, N.; Mohsenzadegan, M.; Komaki, A.; Joghataei, M. T., Neurophysiologic implications of neuronal nitric oxide synthase. *Reviews in the Neurosciences* **2020,** *31* (6), 617.
125. Ivanova, V. O.; Balaban, P. M.; Bal, N. V., Modulation of AMPA Receptors by Nitric Oxide in Nerve Cells. *International Journal of Molecular Sciences* **2020,** *21* (3), 981.
126. Shefa, U.; Kim, D.; Kim, M.-S.; Jeong, N. Y.; Jung, J., Roles of Gasotransmitters in Synaptic Plasticity and Neuropsychiatric Conditions. *Neural Plasticity* **2018,** *2018*, 1824713.
127. Ogasawara, H.; Doi, T.; Doya, K.; Kawato, M., Nitric oxide regulates input specificity of long-term depression and context dependence of cerebellar learning. *PLoS Comput Biol* **2007,** *3* (1), e179.
128. Carreira, B. P.; Morte, M. I.; Inácio, Â.; Costa, G.; Rosmaninho-Salgado, J.; Agasse, F.; Carmo, A.; Couceiro, P.; Brundin, P.; Ambrósio, A. F., Nitric oxide stimulates the proliferation of neural stem cells bypassing the epidermal growth factor receptor. *Stem cells* **2010,** *28* (7), 1219-1230.
129. Bonafè, F.; Guarnieri, C.; Muscari, C., Nitric oxide regulates multiple functions and fate of adult progenitor and stem cells. *Journal of Physiology and Biochemistry* **2015,** *71* (1), 141-153.
130. Bogdan, C., Nitric oxide synthase in innate and adaptive immunity: an update. *Trends in Immunology* **2015,** *36* (3), 161-178.
131. Vannini, F.; Kashfi, K.; Nath, N., The dual role of iNOS in cancer. *Redox Biology* **2015,** *6*, 334-343.
132. Ignarro, L. J.; Kadowitz, P. J., The pharmacological and physiological role of cyclic GMP in vascular smooth muscle relaxation. *Annu Rev Pharmacol Toxicol* **1985,** *25*, 171-91.

133. Ignarro, L. J.; Buga, G. M.; Wood, K. S.; Byrns, R. E.; Chaudhuri, G., Endothelium-derived relaxing factor produced and released from artery and vein is nitric oxide. *Proc Natl Acad Sci USA* **1987,** *84* (24), 9265.
134. Nisoli, E.; Clementi, E.; Paolucci, C.; Cozzi, V.; Tonello, C.; Sciorati, C.; Bracale, R.; Valerio, A.; Francolini, M.; Moncada, S.; Carruba, M. O., Mitochondrial biogenesis in mammals: the role of endogenous nitric oxide. *Science* **2003,** *299* (5608), 896-9.
135. Lipton, S. A.; Choi, Y.-B.; Pan, Z.-H.; Lei, S. Z.; Chen, H.-S. V.; Sucher, N. J.; Loscalzo, J.; Singel, D. J.; Stamler, J. S., A redox-based mechanism for the neuroprotective and neurodestructive effects of nitric oxide and related nitroso-compounds. *Nature* **1993,** *364* (6438), 626-632.
136. Hess, D. T.; Matsumoto, A.; Kim, S.-O.; Marshall, H. E.; Stamler, J. S., Protein S-nitrosylation: purview and parameters. *Nature reviews Molecular cell biology* **2005,** *6* (2), 150-166.
137. Gu, Z.; Kaul, M.; Yan, B.; Kridel, S. J.; Cui, J.; Strongin, A.; Smith, J. W.; Liddington, R. C.; Lipton, S. A., S-nitrosylation of matrix metalloproteinases: signaling pathway to neuronal cell death. *Science* **2002,** *297* (5584), 1186-90.
138. Luchsinger, B. P.; Rich, E. N.; Gow, A. J.; Williams, E. M.; Stamler, J. S.; Singel, D. J., Routes to S-nitroso-hemoglobin formation with heme redox and preferential reactivity in the β subunits. *Proc Natl Acad Sci USA* **2003,** *100* (2), 461-466.
139. Marozkina, N.; Gaston, B., An Update on Thiol Signaling: S-Nitrosothiols, Hydrogen Sulfide and a Putative Role for Thionitrous Acid. *Antioxidants* **2020,** *9* (3), 225.
140. Patel, R. P.; Yuan, S.; Kevil, C. G., Chapter 4 - S-Nitrosothiols and Nitric Oxide Biology. In *Nitric Oxide (Third Edition)*, Ignarro, L. J.; Freeman, B. A., Eds. Academic Press: 2017; pp 45-56.
141. Xu, W.; Charles, I. G.; Moncada, S., Nitric oxide: orchestrating hypoxia regulation through mitochondrial respiration and the endoplasmic reticulum stress response. *Cell Research* **2005,** *15* (1), 63-65.
142. Rubbo, H.; Parthasarathy, S.; Barnes, S.; Kirk, M.; Kalyanaraman, B.; Freeman, B. A., Nitric oxide inhibition of lipoxygenase-dependent liposome and low-density lipoprotein oxidation: termination of radical chain propagation reactions and formation of nitrogen-containing oxidized lipid derivatives. *Arch Biochem Biophys* **1995,** *324* (1), 15-25.
143. Chong, Z.; Li, F.; Maiese, a., K, Activating Akt and the brain's resources to drive cellular survival and prevent inflammatory injury. *Histology and histopathology* **2005,** *20* (1), 299.
144. Ridnour, L. A.; Thomas, D. D.; Mancardi, D.; Espey, M. G.; Miranda, K. M.; Paolocci, N.; Feelisch, M.; Fukuto, J.; Wink, D. A., The chemistry of nitrosative stress induced by nitric oxide and reactive nitrogen oxide species. Putting perspective on stressful biological situations. *Biological chemistry* **2004,** *385* (1), 1-10.
145. Thomas, D. D., Breathing new life into nitric oxide signaling: A brief overview of the interplay between oxygen and nitric oxide. *Redox Biology* **2015,** *5*, 225-233.

146. Napoli, C.; Ignarro, L. J., Nitric oxide and pathogenic mechanisms involved in the development of vascular diseases. *Archives of pharmacal research* **2009,** *32* (8), 1103-8.
147. Reddy, Y. S.; Kiranmayi, V. S.; Bitla, A. R.; Krishna, G. S.; Rao, P. V. L. N. S.; Sivakumar, V., Nitric oxide status in patients with chronic kidney disease. *Indian J Nephrol* **2015,** *25* (5), 287-291.
148. Edwards, T. M.; Rickard, N. S., New perspectives on the mechanisms through which nitric oxide may affect learning and memory processes. *Neuroscience & Biobehavioral Reviews* **2007,** *31* (3), 413-425.
149. Steinert, J. R.; Chernova, T.; Forsythe, I. D., Nitric oxide signaling in brain function, dysfunction, and dementia. *The Neuroscientist* **2010,** *16* (4), 435-452.
150. Austin, S. A.; Santhanam, A. V.; Hinton, D. J.; Choi, D. S.; Katusic, Z. S., Endothelial nitric oxide deficiency promotes Alzheimer's disease pathology. *Journal of neurochemistry* **2013,** *127* (5), 691-700.
151. Gebhart, V.; Reiß, K.; Kollau, A.; Mayer, B.; Gorren, A. C. F., Site and mechanism of uncoupling of nitric-oxide synthase: Uncoupling by monomerization and other misconceptions. *Nitric Oxide* **2019,** *89*, 14-21.
152. Pfeiffer, S.; Gorren, A. C. F.; Schmidt, K.; Werner, E. R.; Hansert, B.; Bohle, D. S.; Mayer, B., Metabolic Fate of Peroxynitrite in Aqueous Solution: REACTION WITH NITRIC OXIDE AND pH-DEPENDENT DECOMPOSITION TO NITRITE AND OXYGEN IN A 2:1 STOICHIOMETRY. *Journal of Biological Chemistry* **1997,** *272* (6), 3465-3470.
153. Lymar, S. V.; Hurst, J. K., CO2-catalyzed one-electron oxidations by peroxynitrite: properties of the reactive intermediate. *Inorg. Chem.* **1998,** *37* (2), 294-301.
154. Kaur, H.; Halliwell, B., Evidence for nitric oxide-mediated oxidative damage in chronic inflammation Nitrotyrosine in serum and synovial fluid from rheumatoid patients. *FEBS Letters* **1994,** *350* (1), 9-12.
155. Fukuyama, N.; Takebayashi, Y.; Hida, M.; Ishida, H.; Ichimori, K.; Nakazawa, H., Clinical evidence of peroxynitrite formation in chronic renal failure patients with septic shock. *Free Radic Biol Med* **1997,** *22* (5), 771-4.
156. ter Steege, J. C.; Koster-Kamphuis, L.; van Straaten, E. A.; Forget, P. P.; Buurman, W. A., Nitrotyrosine in plasma of celiac disease patients as detected by a new sandwich ELISA. *Free Radic Biol Med* **1998,** *25* (8), 953-63.
157. Cuzzocrea, S.; Mazzon, E.; Costantino, G.; Serraino, I.; Dugo, L.; Calabrò, G.; Cucinotta, G.; De Sarro, A.; Caputi, A. P., Beneficial effects of n-acetylcysteine on ischaemic brain injury. *British journal of pharmacology* **2000,** *130* (6), 1219-26.
158. Bandookwala, M.; Sengupta, P., 3-Nitrotyrosine: a versatile oxidative stress biomarker for major neurodegenerative diseases. *The International journal of neuroscience* **2020,** *130* (10), 1047-1062.
159. Pryor, W. A.; Lightsey, J. W., Mechanisms of nitrogen dioxide reactions: initiation of lipid peroxidation and the production of nitrous acid. *Science* **1981,** *214* (4519), 435-437.

160. Kennedy, L. J.; Moore, K.; Caulfield, J. L.; Tannenbaum, S. R.; Dedon, P. C., Quantitation of 8-oxoguanine and strand breaks produced by four oxidizing agents. *Chem. Res. Toxicol.* **1997,** *10* (4), 386-392.
161. Burney, S.; Caulfield, J. L.; Niles, J. C.; Wishnok, J. S.; Tannenbaum, S. R., The chemistry of DNA damage from nitric oxide and peroxynitrite. *Mutation research* **1999,** *424* (1-2), 37-49.
162. Jaiswal, M.; LaRusso, N. F.; Gores, G. J., Nitric oxide in gastrointestinal epithelial cell carcinogenesis: linking inflammation to oncogenesis. *American Journal of Physiology-Gastrointestinal and Liver Physiology* **2001,** *281* (3), G626-G634.
163. Jourd'heuil, D.; Kang, D.; Grisham, M. B., Interactions between superoxide and nitric oxide: implications in DNA damage and mutagenesis. *Frontiers in bioscience : a journal and virtual library* **1997,** *2*, d189-96.
164. Marnett, L. J.; Riggins, J. N.; West, J. D., Endogenous generation of reactive oxidants and electrophiles and their reactions with DNA and protein. *The Journal of clinical investigation* **2003,** *111* (5), 583-93.
165. Brown, G. C.; Borutaite, V., Nitric oxide, mitochondria, and cell death. *IUBMB life* **2001,** *52* (3-5), 189-95.
166. Bal-Price, A.; Brown, G. C., Inflammatory neurodegeneration mediated by nitric oxide from activated glia-inhibiting neuronal respiration, causing glutamate release and excitotoxicity. *The Journal of neuroscience : the official journal of the Society for Neuroscience* **2001,** *21* (17), 6480-91.
167. Touil, T.; Deloire-Grassin, M. S.; Vital, C.; Petry, K. G.; Brochet, B., In vivo damage of CNS myelin and axons induced by peroxynitrite. *Neuroreport* **2001,** *12* (16), 3637-44.
168. Scott, G. S.; Spitsin, S. V.; Kean, R. B.; Mikheeva, T.; Koprowski, H.; Hooper, D. C., Therapeutic intervention in experimental allergic encephalomyelitis by administration of uric acid precursors. *Proc Natl Acad Sci USA* **2002,** *99* (25), 16303-16308.
169. Burai, R.; Ait-Bouziad, N.; Chiki, A.; Lashuel, H. A., Elucidating the Role of Site-Specific Nitration of α-Synuclein in the Pathogenesis of Parkinson's Disease via Protein Semisynthesis and Mutagenesis. *J Am Chem Soc* **2015,** *137* (15), 5041-52.
170. Bates, J. N., Nitric oxide measurement by chemiluminescence detection. *Neuroprotocols* **1992,** *1* (2), 141-149.
171. Adler-Golden, S. M., The nitric oxide + oxygen atom and nitric oxide + ozone reactions. 2. Analysis of nitrogen dioxide continuum chemiluminescence. *The Journal of Physical Chemistry* **1989,** *93* (2), 691-697.
172. Gudem, M.; Hazra, A., Mechanism of the Chemiluminescent Reaction between Nitric Oxide and Ozone. *The Journal of Physical Chemistry A* **2019,** *123* (4), 715-722.
173. Clyne, M. A. A.; Thrush, B. A.; Wayne, R. P., Kinetics of the chemiluminescent reaction between nitric oxide and ozone. *Transactions of the Faraday Society* **1964,** *60* (0), 359-370.
174. Samouilov, A.; Zweier, J. L., Development of Chemiluminescence-Based Methods for Specific Quantitation of Nitrosylated Thiols. *Analytical Biochemistry* **1998,** *258* (2), 322-330.

175. Zhang, X.; Cardosa, L.; Broderick, M.; Fein, H.; Lin, J., An Integrated Nitric Oxide Sensor Based on Carbon Fiber Coated with Selective Membranes. *Electroanalysis* **2000,** *12* (14), 1113-1117.
176. Bedioui, F.; Villeneuve, N., Electrochemical Nitric Oxide Sensors for Biological Samples – Principle, Selected Examples and Applications. *Electroanalysis* **2003,** *15* (1), 5-18.
177. Brown, M. D.; Schoenfisch, M. H., Electrochemical Nitric Oxide Sensors: Principles of Design and Characterization. *Chem. Rev.* **2019,** *119* (22), 11551-11575.
178. Xu, T.; Scafa, N.; Xu, L.-P.; Su, L.; Li, C.; Zhou, S.; Liu, Y.; Zhang, X., Electrochemical Sensors for Nitric Oxide Detection in Biological Applications. *Electroanalysis* **2014,** *26* (3), 449-468.
179. Elbert, D. L.; Hubbell, J. A., Surface treatments of polymers for biocompatibility. *Annual Review of Materials Science* **1996,** *26* (1), 365-394.
180. Bedioui, F.; Villeneuve, N., Electrochemical nitric oxide sensors for biological samples–principle, selected examples and applications. *Electroanalysis: An International Journal Devoted to Fundamental and Practical Aspects of Electroanalysis* **2003,** *15* (1), 5-18.
181. Liu, Y.-L.; Wang, X.-Y.; Xu, J.-Q.; Xiao, C.; Liu, Y.-H.; Zhang, X.-W.; Liu, J.-T.; Huang, W.-H., Functionalized graphene-based biomimetic microsensor interfacing with living cells to sensitively monitor nitric oxide release. *Chemical science* **2015,** *6* (3), 1853-1858.
182. Shin, J. H.; Privett, B. J.; Kita, J. M.; Wightman, R. M.; Schoenfisch, M. H., Fluorinated Xerogel-Derived Microelectrodes for Amperometric Nitric Oxide Sensing. *Anal. Chem.* **2008,** *80* (18), 6850-6859.
183. Pailleret, A.; Oni, J.; Reiter, S.; Isik, S.; Etienne, M.; Bedioui, F.; Schuhmann, W., In situ formation and scanning electrochemical microscopy assisted positioning of NO-sensors above human umbilical vein endothelial cells for the detection of nitric oxide release. *Electrochemistry Communications* **2003,** *5* (10), 847-852.
184. Elliott, J.; Duay, J.; Simoska, O.; Shear, J. B.; Stevenson, K. J., Gold Nanoparticle Modified Transparent Carbon Ultramicroelectrode Arrays for the Selective and Sensitive Electroanalytical Detection of Nitric Oxide. *Anal. Chem.* **2017,** *89* (2), 1267-1274.
185. Guo, C. X.; Ng, S. R.; Khoo, S. Y.; Zheng, X.; Chen, P.; Li, C. M., RGD-Peptide Functionalized Graphene Biomimetic Live-Cell Sensor for Real-Time Detection of Nitric Oxide Molecules. *ACS Nano* **2012,** *6* (8), 6944-6951.
186. Oni, J.; Pailleret, A.; Isik, S.; Diab, N.; Radtke, I.; Blöchl, A.; Jackson, M.; Bedioui, F.; Schuhmann, W., Functionalised electrode array for the detection of nitric oxide released by endothelial cells using different NO-sensing chemistries. *Analytical and Bioanalytical Chemistry* **2004,** *378* (6), 1594-1600.
187. Yaoita, M.; Ikariyama, Y.; Aizawa, M., Electrical effects on the proliferation of living HeLa cells cultured on optically transparent electrode surface. *Journal of biotechnology* **1990,** *14* (3-4), 321-332.
188. Hall, C. N.; Garthwaite, J., What is the real physiological NO concentration in vivo? *Nitric Oxide* **2009,** *21* (2), 92-103.

189. Chen, K.; Pittman, R. N.; Popel, A. S., Nitric oxide in the vasculature: where does it come from and where does it go? A quantitative perspective. *Antioxid Redox Signal* **2008,** *10* (7), 1185-98.
190. Bohlen, H. G., Is the real in vivo nitric oxide concentration pico or nano molar? Influence of electrode size on unstirred layers and NO consumption. *Microcirculation (New York, N.Y. : 1994)* **2013,** *20* (1), 30-41.
191. Hogg, N., Detection of nitric oxide by electron paramagnetic resonance spectroscopy. *Free Radical Biology and Medicine* **2010,** *49* (2), 122-129.
192. Hogg, N., Detection of Nitric Oxide by Electron Paramagnetic Resonance Spectroscopy. *Free radical biology & medicine* **2010,** *49* (2), 122-129.
193. Haseloff, R. F.; Zöllner, S.; Kirilylik, I. a.; Grigorev, I. a.; Reszka, R.; Bernhardt, R.; Mertsch, K.; Roloff, B.; Blasig, I. e., Superoxide-Mediated Reduction of the Nitroxide Group Can Prevent Detection of Nitric Oxide by Nitronyl Nitroxides. *Free Radical Research* **1997,** *26* (1), 7-17.
194. Nagano, T.; Yoshimura, T., Bioimaging of Nitric Oxide. *Chem. Rev.* **2002,** *102* (4), 1235-1270.
195. Yoshimura, T.; Yokoyama, H.; Fujii, S.; Takayama, F.; Oikawa, K.; Kamada, H., In vivo EPR detection and imaging of endogenous nitric oxide in lipopolysaccharide-treated mice. *Nature Biotechnology* **1996,** *14* (8), 992-994.
196. Quaresima, V.; Takehara, H.; Tsushima, K.; Ferrari, M.; Utsumi, H., In vivodetection of mouse liver nitric oxide generation by spin trapping electron paramagnetic resonance spectroscopy. *Biochemical and biophysical research communications* **1996,** *221* (3), 729-734.
197. Maia, L. B.; Moura, J. J. G., Detection of Nitric Oxide by Electron Paramagnetic Resonance Spectroscopy: Spin-Trapping with Iron-Dithiocarbamates. In *Plant Nitric Oxide: Methods and Protocols*, Gupta, K. J., Ed. Springer New York: New York, NY, 2016; pp 81-102.
198. Kleschyov, A. L.; Muller, B.; Keravis, T.; Stoeckel, M.-E.; Stoclet, J.-C., Adventitia-derived nitric oxide in rat aortas exposed to endotoxin: cell origin and functional consequences. *American Journal of Physiology-Heart and Circulatory Physiology* **2000,** *279* (6), H2743-H2751.
199. Misra, H. P., Reaction of copper-zinc superoxide dismutase with diethyldithiocarbamate. *The Journal of biological chemistry* **1979,** *254* (22), 11623-8.
200. Mülsch, A.; Schray-Utz, B.; Mordvintcev, P. I.; Hauschildt, S.; Busse, R., Diethyldithiocarbamate inhibits induction of macrophage NO synthase. *FEBS Lett* **1993,** *321* (2-3), 215-8.
201. Yoneyama, H.; Kosaka, H.; Ohnishi, T.; Kawazoe, T.; Mizoguchi, K.; Ichikawa, Y., Reaction of neuronal nitric oxide synthase with the nitric oxide spin-trapping agent, iron complexed with N-dithiocarboxysarcosine. *European journal of biochemistry* **1999,** *266* (3), 771-7.
202. Reiter, C. D.; Wang, X.; Tanus-Santos, J. E.; Hogg, N.; Cannon, R. O.; Schechter, A. N.; Gladwin, M. T., Cell-free hemoglobin limits nitric oxide bioavailability in sickle-cell disease. *Nature medicine* **2002,** *8* (12), 1383-1389.

203. Gladwin, M. T.; Shelhamer, J. H.; Schechter, A. N.; Pease-Fye, M. E.; Waclawiw, M. A.; Panza, J. A.; Ognibene, F. P.; Cannon, R. O., Role of circulating nitrite and S-nitrosohemoglobin in the regulation of regional blood flow in humans. *Proc Natl Acad Sci USA* **2000,** *97* (21), 11482-11487.
204. de Silva, A. P.; Gunaratne, H. Q. N.; Gunnlaugsson, T.; Huxley, A. J. M.; McCoy, C. P.; Rademacher, J. T.; Rice, T. E., Signaling Recognition Events with Fluorescent Sensors and Switches. *Chem. Rev.* **1997,** *97* (5), 1515-1566.
205. Dahlhauser, S. D.; Escamilla, P. R.; VandeWalle, A. N.; York, J. T.; Rapagnani, R. M.; Shei, J. S.; Glass, S. A.; Coronado, J. N.; Moor, S. R.; Saunders, D. P.; Anslyn, E. V., Sequencing of Sequence-Defined Oligourethanes via Controlled Self-Immolation. *J. Am. Chem. Soc.* **2020,** *142* (6), 2744-2749.
206. Chudakov, D. M.; Matz, M. V.; Lukyanov, S.; Lukyanov, K. A., Fluorescent Proteins and Their Applications in Imaging Living Cells and Tissues. *Physiological Reviews* **2010,** *90* (3), 1103-1163.
207. Lambert, G. G.; Depernet, H.; Gotthard, G.; Schultz, D. T.; Navizet, I.; Lambert, T.; Adams, S. R.; Torreblanca-Zanca, A.; Chu, M.; Bindels, D. S.; Levesque, V.; Nero Moffatt, J.; Salih, A.; Royant, A.; Shaner, N. C., Aequorea's secrets revealed: New fluorescent proteins with unique properties for bioimaging and biosensing. *PLOS Biology* **2020,** *18* (11), e3000936.
208. Thorn, K., Genetically encoded fluorescent tags. *Molecular Biology of the Cell* **2017,** *28* (7), 848-857.
209. Chudakov, D. M.; Lukyanov, S.; Lukyanov, K. A., Fluorescent proteins as a toolkit for in vivo imaging. *Trends in biotechnology* **2005,** *23* (12), 605-13.
210. Park, S.-H.; Kwon, N.; Lee, J.-H.; Yoon, J.; Shin, I., Synthetic ratiometric fluorescent probes for detection of ions. *Chemical Society Reviews* **2020,** *49* (1), 143-179.
211. Chan, J.; Dodani, S. C.; Chang, C. J., Reaction-based small-molecule fluorescent probes for chemoselective bioimaging. *Nature Chemistry* **2012,** *4* (12), 973-984.
212. Fu, Y.; Finney, N. S., Small-molecule fluorescent probes and their design. *RSC Advances* **2018,** *8* (51), 29051-29061.
213. Domaille, D. W.; Que, E. L.; Chang, C. J., Synthetic fluorescent sensors for studying the cell biology of metals. *Nature Chemical Biology* **2008,** *4* (3), 168-175.
214. Yin, J.; Hu, Y.; Yoon, J., Fluorescent probes and bioimaging: alkali metals, alkaline earth metals and pH. *Chemical Society Reviews* **2015,** *44* (14), 4619-4644.
215. Nagano, T., Development of fluorescent probes for bioimaging applications. *Proc Jpn Acad Ser B Phys Biol Sci* **2010,** *86* (8), 837-847.
216. de Silva, A. P.; Moody, T. S.; Wright, G. D., Fluorescent PET (Photoinduced Electron Transfer) sensors as potent analytical tools. *Analyst* **2009,** *134* (12), 2385-2393.
217. Zhang, W.; Ma, Z.; Du, L.; Li, M., Design strategy for photoinduced electron transfer-based small-molecule fluorescent probes of biomacromolecules. *Analyst* **2014,** *139* (11), 2641-9.
218. Sun, W.; Li, M.; Fan, J.; Peng, X., Activity-Based Sensing and Theranostic Probes Based on Photoinduced Electron Transfer. *Acc. Chem. Res.* **2019,** *52* (10), 2818-2831.

219. Lee, M. H.; Kim, J. S.; Sessler, J. L., Small molecule-based ratiometric fluorescence probes for cations, anions, and biomolecules. *Chem Soc Rev* **2015,** *44* (13), 4185-91.
220. Hochreiter, B.; Garcia, A.; Schmid, J., Fluorescent Proteins as Genetically Encoded FRET Biosensors in Life Sciences. *Sensors* **2015,** *15*, 26281-26314.
221. Wu, L.; Huang, C.; Emery, B. P.; Sedgwick, A. C.; Bull, S. D.; He, X.-P.; Tian, H.; Yoon, J.; Sessler, J. L.; James, T. D., Förster resonance energy transfer (FRET)-based small-molecule sensors and imaging agents. *Chemical Society Reviews* **2020,** *49* (15), 5110-5139.
222. Doose, S.; Neuweiler, H.; Sauer, M., Fluorescence Quenching by Photoinduced Electron Transfer: A Reporter for Conformational Dynamics of Macromolecules. *ChemPhysChem* **2009,** *10* (9-10), 1389-1398.
223. Church, J. E.; Fulton, D., Differences in eNOS Activity Because of Subcellular Localization Are Dictated by Phosphorylation State Rather than the Local Calcium Environment. *Journal of Biological Chemistry* **2006,** *281* (3), 1477-1488.
224. Sowa, G.; Liu, J.; Papapetropoulos, A.; Rex-Haffner, M.; Hughes, T. E.; Sessa, W. C., Trafficking of Endothelial Nitric-oxide Synthase in Living Cells: QUANTITATIVE EVIDENCE SUPPORTING THE ROLE OF PALMITOYLATION AS A KINETIC TRAPPING MECHANISM LIMITING MEMBRANE DIFFUSION*. *Journal of Biological Chemistry* **1999,** *274* (32), 22524-22531.
225. Eroglu, E.; Gottschalk, B.; Charoensin, S.; Blass, S.; Bischof, H.; Rost, R.; Madreiter-Sokolowski, C. T.; Pelzmann, B.; Bernhart, E.; Sattler, W.; Hallström, S.; Malinski, T.; Waldeck-Weiermair, M.; Graier, W. F.; Malli, R., Development of novel FP-based probes for live-cell imaging of nitric oxide dynamics. *Nature Communications* **2016,** *7*, 10623.
226. Charoensin, S.; Eroglu, E.; Opelt, M.; Bischof, H.; Madreiter-Sokolowski, C. T.; Kirsch, A.; Depaoli, M. R.; Frank, S.; Schrammel, A.; Mayer, B.; Waldeck-Weiermair, M.; Graier, W. F.; Malli, R., Intact mitochondrial Ca2+ uniport is essential for agonist-induced activation of endothelial nitric oxide synthase (eNOS). *Free Radical Biology and Medicine* **2017,** *102*, 248-259.
227. Pearce, L. L.; Gandley, R. E.; Han, W.; Wasserloos, K.; Stitt, M.; Kanai, A. J.; McLaughlin, M. K.; Pitt, B. R.; Levitan, E. S., Role of metallothionein in nitric oxide signaling as revealed by a green fluorescent fusion protein. *Proc Natl Acad Sci U S A* **2000,** *97* (1), 477-82.
228. Eroglu, E.; Charoensin, S.; Bischof, H.; Ramadani, J.; Gottschalk, B.; Depaoli, M. R.; Waldeck-Weiermair, M.; Graier, W. F.; Malli, R., Genetic biosensors for imaging nitric oxide in single cells. *Free Radical Biology and Medicine* **2018**.
229. Croix, C. M. S.; Wasserloos, K. J.; Dineley, K. E.; Reynolds, I. J.; Levitan, E. S.; Pitt, B. R., Nitric oxide-induced changes in intracellular zinc homeostasis are mediated by metallothionein/thionein. *American Journal of Physiology-Lung Cellular and Molecular Physiology* **2002,** *282* (2), L185-L192.

230. Sato, M.; Hida, N.; Ozawa, T.; Umezawa, Y., Fluorescent indicators for cyclic GMP based on cyclic GMP-dependent protein kinase Ialpha and green fluorescent proteins. *Anal Chem* **2000,** *72* (24), 5918-24.
231. Sato, M.; Hida, N.; Umezawa, Y., Imaging the nanomolar range of nitric oxide with an amplifier-coupled fluorescent indicator in living cells. *Proc Natl Acad Sci U S A* **2005,** *102* (41), 14515-14520.
232. Sato, M.; Nakajima, T.; Goto, M.; Umezawa, Y., Cell-Based Indicator to Visualize Picomolar Dynamics of Nitric Oxide Release from Living Cells. *Anal. Chem.* **2006,** *78* (24), 8175-8182.
233. Nausch, L. W. M.; Ledoux, J.; Bonev, A. D.; Nelson, M. T.; Dostmann, W. R., Differential patterning of cGMP in vascular smooth muscle cells revealed by single GFP-linked biosensors. *Proc Natl Acad Sci USA* **2008,** *105* (1), 365-370.
234. Hidaka, M.; Gotoh, A.; Shimizu, T.; Minamisawa, K.; Imamura, H.; Uchida, T., Visualization of $NO3^{-}$/$NO2^{-}$ Dynamics in Living Cells by Fluorescence Resonance Energy Transfer (FRET) Imaging Employing a Rhizobial Two-component Regulatory System. *The Journal of biological chemistry* **2016,** *291* (5), 2260-2269.
235. Stephens, D. J.; Pepperkok, R., The many ways to cross the plasma membrane. *Proc Natl Acad Sci U S A* **2001,** *98* (8), 4295-8.
236. Gao, P.; Pan, W.; Li, N.; Tang, B., Fluorescent probes for organelle-targeted bioactive species imaging. *Chemical Science* **2019,** *10* (24), 6035-6071.
237. Perry, S. W.; Norman, J. P.; Barbieri, J.; Brown, E. B.; Gelbard, H. A., Mitochondrial membrane potential probes and the proton gradient: a practical usage guide. *BioTechniques* **2011,** *50* (2), 98-115.
238. Keppler, A.; Gendreizig, S.; Gronemeyer, T.; Pick, H.; Vogel, H.; Johnsson, K., A general method for the covalent labeling of fusion proteins with small molecules in vivo. *Nature Biotechnology* **2003,** *21* (1), 86-89.
239. Los, G. V.; Encell, L. P.; McDougall, M. G.; Hartzell, D. D.; Karassina, N.; Zimprich, C.; Wood, M. G.; Learish, R.; Ohana, R. F.; Urh, M.; Simpson, D.; Mendez, J.; Zimmerman, K.; Otto, P.; Vidugiris, G.; Zhu, J.; Darzins, A.; Klaubert, D. H.; Bulleit, R. F.; Wood, K. V., HaloTag: a novel protein labeling technology for cell imaging and protein analysis. *ACS chemical biology* **2008,** *3* (6), 373-82.
240. Bätz, M.; Korth, H.-G.; Sustmann, R., A Novel Method for Detecting Nitric Oxide (NO) by Formation of Fluorescent Products Based on Cheletropic Spin Traps. *Angewandte Chemie International Edition in English* **1997,** *36* (13-14), 1501-1503.
241. Meineke, P.; Rauen, U.; de Groot, H.; Korth, H.-G.; Sustmann, R., Cheletropic Traps for the Fluorescence Spectroscopic Detection of Nitric Oxide (Nitrogen Monoxide) in Biological Systems. *Chemistry – A European Journal* **1999,** *5* (6), 1738-1747.
242. Yoshiki, K.; Nobuaki, S.; Mizuo, M., Strategies and Development of Molecular Probes for Nitrogen Monoxide Monitoring. *Bulletin of the Chemical Society of Japan* **2002,** *75* (8), 1681-1691.
243. Katayama, Y.; Takahashi, S.; Maeda, M., Design, synthesis and characterization of a novel fluorescent probe for nitric oxide (nitrogen monoxide). *Analytica Chimica Acta* **1998,** *365* (1), 159-167.

244. Lim, M. H.; Xu, D.; Lippard, S. J., Visualization of nitric oxide in living cells by a copper-based fluorescent probe. *Nature Chemical Biology* **2006,** *2*, 375.
245. Lim, M. H.; Wong, B. A.; Pitcock, W. H.; Mokshagundam, D.; Baik, M.-H.; Lippard, S. J., Direct Nitric Oxide Detection in Aqueous Solution by Copper(II) Fluorescein Complexes. *J. Am. Chem. Soc.* **2006,** *128* (44), 14364-14373.
246. McQuade, L. E.; Lippard, S. J., Fluorescence-Based Nitric Oxide Sensing by Cu(II) Complexes That Can Be Trapped in Living Cells. *Inorg. Chem.* **2010,** *49* (16), 7464-7471.
247. McQuade, L. E.; Ma, J.; Lowe, G.; Ghatpande, A.; Gelperin, A.; Lippard, S. J., Visualization of nitric oxide production in the mouse main olfactory bulb by a cell-trappable copper(II) fluorescent probe. *Proc Natl Acad Sci USA* **2010,** *107* (19), 8525-8530.
248. Hu, X.; Wang, J.; Zhu, X.; Dong, D.; Zhang, X.; Wu, S.; Duan, C., A copper(ii) rhodamine complex with a tripodal ligand as a highly selective fluorescence imaging agent for nitric oxide. *Chem. Commun.* **2011,** *47* (41), 11507-11509.
249. Srivastava, P.; Verma, M.; Sivakumar, S.; Patra, A. K., A smart FRET probe exhibiting a molecular keypad lock device based on rapid detection of nitric oxide mediated by Cu2+ ion. *Sensors and Actuators B: Chemical* **2019,** *291*, 478-484.
250. Zhu, X.-Q.; Zhao, B.-J.; Cheng, J.-P., Mechanisms of the Oxidations of NAD(P)H Model Hantzsch 1,4-Dihydropyridines by Nitric Oxide and Its Donor N-Methyl-N-nitrosotoluene-p-sulfonamide. *The Journal of Organic Chemistry* **2000,** *65* (24), 8158-8163.
251. Itoh, T.; Nagata, K.; Matsuya, Y.; Miyazaki, M.; Ohsawa, A., Reaction of Nitric Oxide with Amines. *The Journal of Organic Chemistry* **1997,** *62* (11), 3582-3585.
252. Ma, S.; Sun, X.; Yu, Q.; Liu, R.; Lu, Z.; He, L., Dihydropyridine-coumarin-based fluorescent probe for imaging nitric oxide in living cells. *Photochemical & Photobiological Sciences* **2020,** *19* (9), 1230-1235.
253. Gao, C.; Lin, L.; Sun, W.; Tan, Z.-L.; Huang, J.-R.; He, L.; Lu, Z.-L., Dihydropyridine-derived BODIPY probe for detecting exogenous and endogenous nitric oxide in mitochondria. *Talanta* **2018,** *176*, 382-388.
254. Li, H.; Zhang, D.; Gao, M.; Huang, L.; Tang, L.; Li, Z.; Chen, X.; Zhang, X., Highly specific C–C bond cleavage induced FRET fluorescence for in vivo biological nitric oxide imaging. *Chemical Science* **2017,** *8* (3), 2199-2203.
255. Miles, A. M.; Wink, D. A.; Cook, J. C.; Grisham, M. B., Determination of nitric oxide using fluorescence spectroscopy. *Methods in enzymology* **1996,** *268*, 105-20.
256. Biswas, S.; Rajesh, Y.; Barman, S.; Bera, M.; Paul, A.; Mandal, M.; Pradeep Singh, N. D., A dual-analyte probe: hypoxia activated nitric oxide detection with phototriggered drug release ability. *Chem. Commun.* **2018,** *54* (57), 7940-7943.
257. Yu, H.; Xiao, Y.; Jin, L., A Lysosome-Targetable and Two-Photon Fluorescent Probe for Monitoring Endogenous and Exogenous Nitric Oxide in Living Cells. *J. Am. Chem. Soc.* **2012,** *134* (42), 17486-17489.

258. Zhang, X.; Wang, B.; Xiao, Y.; Wang, C.; He, L., Targetable, two-photon fluorescent probes for local nitric oxide capture in the plasma membranes of live cells and brain tissues. *Analyst* **2018,** *143* (17), 4180-4188.
259. Gabe, Y.; Urano, Y.; Kikuchi, K.; Kojima, H.; Nagano, T., Highly Sensitive Fluorescence Probes for Nitric Oxide Based on Boron Dipyrromethene ChromophoreRational Design of Potentially Useful Bioimaging Fluorescence Probe. *J. Am. Chem. Soc.* **2004,** *126* (10), 3357-3367.
260. Gabe, Y.; Ueno, T.; Urano, Y.; Kojima, H.; Nagano, T., Tunable design strategy for fluorescence probes based on 4-substituted BODIPY chromophore: improvement of highly sensitive fluorescence probe for nitric oxide. *Analytical and Bioanalytical Chemistry* **2006,** *386* (3), 621-626.
261. Yao, H.-W.; Zhu, X.-Y.; Guo, X.-F.; Wang, H., An Amphiphilic Fluorescent Probe Designed for Extracellular Visualization of Nitric Oxide Released from Living Cells. *Anal. Chem.* **2016,** *88* (18), 9014-9021.
262. Kojima, H.; Nakatsubo, N.; Kikuchi, K.; Kawahara, S.; Kirino, Y.; Nagoshi, H.; Hirata, Y.; Nagano, T., Detection and Imaging of Nitric Oxide with Novel Fluorescent Indicators: Diaminofluoresceins. *Anal. Chem.* **1998,** *70* (13), 2446-2453.
263. Kojima, H.; Urano, Y.; Kikuchi, K.; Higuchi, T.; Hirata, Y.; Nagano, T., Fluorescent Indicators for Imaging Nitric Oxide Production. *Angewandte Chemie International Edition* **1999,** *38* (21), 3209-3212.
264. Nagano, T., Bioimaging Probes for Reactive Oxygen Species and Reactive Nitrogen Species. *Journal of Clinical Biochemistry and Nutrition* **2009,** *45* (2), 111-124.
265. Kojima, H.; Hirotani, M.; Nakatsubo, N.; Kikuchi, K.; Urano, Y.; Higuchi, T.; Hirata, Y.; Nagano, T., Bioimaging of Nitric Oxide with Fluorescent Indicators Based on the Rhodamine Chromophore. *Anal. Chem.* **2001,** *73* (9), 1967-1973.
266. Sasaki, E.; Kojima, H.; Nishimatsu, H.; Urano, Y.; Kikuchi, K.; Hirata, Y.; Nagano, T., Highly Sensitive Near-Infrared Fluorescent Probes for Nitric Oxide and Their Application to Isolated Organs. *J. Am. Chem. Soc.* **2005,** *127* (11), 3684-3685.
267. Tang, C.; Wang, M.; Shang, X.; Chen, X.; Huang, D.; Zheng, Q., Real-time monitoring of intracellular nitric oxide using a long-wavelength-emitting probe via one-photon or two-photon excitation. *Journal of Materials Chemistry C* **2019,** *7* (11), 3246-3252.
268. Mao, Z.; Feng, W.; Li, Z.; Zeng, L.; Lv, W.; Liu, Z., NIR in, far-red out: developing a two-photon fluorescent probe for tracking nitric oxide in deep tissue. *Chemical Science* **2016,** *7* (8), 5230-5235.
269. Rodriguez, J.; Specian, V.; Maloney, R.; Jourd'heuil, D.; Feelisch, M., Performance of diamino fluorophores for the localization of sources and targets of nitric oxide. *Free Radical Biology and Medicine* **2005,** *38* (3), 356-368.
270. Meadows, M. K.; Sun, X.; Kolesnichenko, I. V.; Hinson, C. M.; Johnson, K. A.; Anslyn, E. V., Mechanistic studies of a “Declick” reaction. *Chemical Science* **2019,** *10* (38), 8817-8824.

271. Wang, Q.; Jiao, X.; Liu, C.; He, S.; Zhao, L.; Zeng, X., A rhodamine-based fast and selective fluorescent probe for monitoring exogenous and endogenous nitric oxide in live cells. *Journal of Materials Chemistry B* **2018,** *6* (24), 4096-4103.
272. Zheng, H.; Shang, G.-Q.; Yang, S.-Y.; Gao, X.; Xu, J.-G., Fluorogenic and Chromogenic Rhodamine Spirolactam Based Probe for Nitric Oxide by Spiro Ring Opening Reaction. *Org. Lett.* **2008,** *10* (12), 2357-2360.
273. Huo, Y.; Miao, J.; Han, L.; Li, Y.; Li, Z.; Shi, Y.; Guo, W., Selective and sensitive visualization of endogenous nitric oxide in living cells and animals by a Si-rhodamine deoxylactam-based near-infrared fluorescent probe. *Chem Sci* **2017,** *8* (10), 6857-6864.
274. Wang, T.; Douglass, E. F.; Fitzgerald, K. J.; Spiegel, D. A., A "Turn-On" Fluorescent Sensor for Methylglyoxal. *J. Am. Chem. Soc.* **2013,** *135* (33), 12429-12433.
275. Jourd'heuil, D., Increased nitric oxide-dependent nitrosylation of 4,5-diaminofluorescein by oxidants: implications for the measurement of intracellular nitric oxide. *Free Radical Biology and Medicine* **2002,** *33* (5), 676-684.
276. Espey, M. G.; Thomas, D. D.; Miranda, K. M.; Wink, D. A., Focusing of nitric oxide mediated nitrosation and oxidative nitrosylation as a consequence of reaction with superoxide. *Proc Natl Acad Sci USA* **2002,** *99* (17), 11127-11132.
277. Figueroa, J. D.; Fuentes-Lemus, E.; Dorta, E.; Melin, V.; Cortés-Ríos, J.; Faúndez, M.; Contreras, D.; Denicola, A.; Álvarez, B.; Davies, M. J.; López-Alarcón, C., Quantification of carbonate radical formation by the bicarbonate-dependent peroxidase activity of superoxide dismutase 1 using pyrogallol red bleaching. *Redox biology* **2019,** *24*, 101207-101207.
278. Puppo, A.; Halliwell, B., Formation of Hydroxyl Radicals in Biological Systems. Does Myoglobin Stimulate Hydroxyl Radical Formation from Hydrogen Peroxide? *Free Radical Research Communications* **1988,** *4* (6), 415-422.
279. Miao, J.; Huo, Y.; Lv, X.; Li, Z.; Cao, H.; Shi, H.; Shi, Y.; Guo, W., Fast-response and highly selective fluorescent probes for biological signaling molecule NO based on N-nitrosation of electron-rich aromatic secondary amines. *Biomaterials* **2016,** *78*, 11-19.
280. Huo, Y.; Miao, J.; Fang, J.; Shi, H.; Wang, J.; Guo, W., Aromatic secondary amine-functionalized fluorescent NO probes: improved detection sensitivity for NO and potential applications in cancer immunotherapy studies. *Chemical Science* **2019,** *10* (1), 145-152.
281. Liu, Y.; Fan, H.; Wen, Y.; Jia, T.; Su, Q.; Li, F., ICT-based near infrared fluorescent switch-on probe for nitric oxide bioimaging in vivo. *Dyes and Pigments* **2019,** *166*, 211-216.
282. Yang, Y.; Seidlits, S. K.; Adams, M. M.; Lynch, V. M.; Schmidt, C. E.; Anslyn, E. V.; Shear, J. B., A Highly Selective Low-Background Fluorescent Imaging Agent for Nitric Oxide. *J. Am. Chem. Soc.* **2010,** *132* (38), 13114-13116.
283. Ghebremariam, Y. T.; Huang, N. F.; Kambhampati, S.; Volz, K. S.; Joshi, G. G.; Anslyn, E. V.; Cooke, J. P., Characterization of a Fluorescent Probe for Imaging Nitric Oxide. *Journal of Vascular Research* **2014,** *51* (1), 68-79.

284. Fakhari M, A.; Rokita, S. E., A new solvatochromic fluorophore for exploring nonpolar environments created by biopolymers. *Chem. Commun.* **2011,** *47* (14), 4222-4224.
285. Lv, X.; Wang, Y.; Zhang, S.; Liu, Y.; Zhang, J.; Guo, W., A specific fluorescent probe for NO based on a new NO-binding group. *Chem. Commun.* **2014,** *50* (56), 7499-7502.
286. Dai, C.-G.; Wang, J.-L.; Fu, Y.-L.; Zhou, H.-P.; Song, Q.-H., Selective and Real-Time Detection of Nitric Oxide by a Two-Photon Fluorescent Probe in Live Cells and Tissue Slices. *Anal. Chem.* **2017,** *89* (19), 10511-10519.
287. Zhu, X.; Chen, J.-Q.; Ma, C.; Liu, X.; Cao, X.-P.; Zhang, H., A ratiometric mitochondria-targeting two-photon fluorescent probe for imaging of nitric oxide in vivo. *Analyst* **2017,** *142* (24), 4623-4628.
288. Escamilla, P. R.; Shen, Y.; Zhang, Q.; Hernandez, D. S.; Howard, C. J.; Qian, X.; Filonov, D. Y.; Kinev, A. V.; Shear, J. B.; Anslyn, E. V.; Yang, Y., 2-Amino-3′-dialkylaminobiphenyl-based fluorescent intracellular probes for nitric oxide surrogate N2O3. *Chemical Science* **2020,** *11* (5), 1394-1403.
289. Vogel, M.; Rettig, W.; Sens, R.; Drexhage, K. H., Structural relaxation of rhodamine dyes with different N-substitution patterns: A study of fluorescence decay times and quantum yields. *Chemical Physics Letters* **1988,** *147* (5), 452-460.
290. Grabowski, Z. R.; Rotkiewicz, K.; Rettig, W., Structural Changes Accompanying Intramolecular Electron Transfer: Focus on Twisted Intramolecular Charge-Transfer States and Structures. *Chem. Rev.* **2003,** *103* (10), 3899-4032.
291. Segado, M.; Gomez, I.; Reguero, M., Intramolecular charge transfer in aminobenzonitriles and tetrafluoro counterparts: fluorescence explained by competition between low-lying excited states and radiationless deactivation. Part I: A mechanistic overview of the parent system ABN. *Physical Chemistry Chemical Physics* **2016,** *18* (9), 6861-6874.
292. Lee, J.-K.; Fujiwara, T.; Kofron, W. G.; Zgierski, M. Z.; Lim, E. C., The low-lying πσ* state and its role in the intramolecular charge transfer of aminobenzonitriles and aminobenzethyne. *The Journal of Chemical Physics* **2008,** *128* (16), 164512.
293. Yang, Y.; Lowry, M.; Xu, X.; Escobedo, J. O.; Sibrian-Vazquez, M.; Wong, L.; Schowalter, C. M.; Jensen, T. J.; Fronczek, F. R.; Warner, I. M.; Strongin, R. M., Seminaphthofluorones are a family of water-soluble, low molecular weight, NIR-emitting fluorophores. *Proc Natl Acad Sci USA* **2008,** *105* (26), 8829.
294. Lee Linda, G.; Berry Gillian, M.; Chen, C. H., Vita blue: A new 633-nm excitable fluorescent dye for cell analysis. *Cytometry* **1989,** *10* (2), 151-164.
295. Whitaker, J. E.; Haugland, R. P.; Prendergast, F. G., Spectral and photophysical studies of benzo[c]xanthene dyes: Dual emission pH sensors. *Analytical Biochemistry* **1991,** *194* (2), 330-344.
296. The sigma plus substituent constant for a substituent X was determined by taking the negative logarithm of the ratio of the rate constant for the solvolysis of 2-chloro-2-para-X-phenylpropane versus that for 2-chloro-2-phenylpropane (X = H for the latter). A negative sigma plus value means that the substituent enhanced the rate of solvolysis by

electron-donating resonance stabilization. The more negative the value, the more electron donating is a substituent.
297. Lewis, M.; Bagwill, C.; Hardebeck, L. K. E.; Wireduaah, S., THE USE OF HAMMETT CONSTANTS TO UNDERSTAND THE NON-COVALENT BINDING OF AROMATICS. *Computational and Structural Biotechnology Journal* **2012,** *1* (1), e201204004.
298. C. Challis, B.; Kyrtopoulos, S., *The chemistry of nitroso compounds. Part 12. The mechanism of nitrosation and nitration of aqueous piperidine by gaseous dinitrogen tetraoxide and dinitrogen trioxide in aqueous alkaline solutions. Evidence for the existence of molecular isomers of dinitrogen tetraoxide and dinitrogen trioxide*. 1978.
299. O'Connor, N.; Silver, R. B., Chapter 16 - Ratio Imaging: Practical Considerations for Measuring Intracellular Ca2+ and pH in Living Cells. In *Methods in Cell Biology*, Sluder, G.; Wolf, D. E., Eds. Academic Press: 2013; Vol. 114, pp 387-406.
300. Hernandez, D. S. Multiphoton techniques for dynamic manipulation of cellular microenvironments. Dissertation, University of Texas at Austin, UT Electronic Theses and Dissertations, 2014.
301. Schindelin, J.; Arganda-Carreras, I.; Frise, E.; Kaynig, V.; Longair, M.; Pietzsch, T.; Preibisch, S.; Rueden, C.; Saalfeld, S.; Schmid, B.; Tinevez, J.-Y.; White, D. J.; Hartenstein, V.; Eliceiri, K.; Tomancak, P.; Cardona, A., Fiji: an open-source platform for biological-image analysis. *Nature Methods* **2012,** *9*, 676.
302. Kitamura, Y.; Uzawa, T.; Oka, K.; Komai, Y.; Ogawa, H.; Takizawa, N.; Kobayashi, H.; Tanishita, K., Microcoaxial Electrode for in Vivo Nitric Oxide Measurement. *Anal. Chem.* **2000,** *72* (13), 2957-2962.
303. Ferrero, R.; Rodríguez-Pascual, F.; Miras-Portugal, M. T.; Torres, M., Comparative effects of several nitric oxide donors on intracellular cyclic GMP levels in bovine chromaffin cells: correlation with nitric oxide production. *Br J Pharmacol* **1999,** *127* (3), 779-787.
304. Fujiwara, T.; Kanazawa, S.; Ichibori, R.; Tanigawa, T.; Magome, T.; Shingaki, K.; Miyata, S.; Tohyama, M.; Hosokawa, K., L-arginine stimulates fibroblast proliferation through the GPRC6A-ERK1/2 and PI3K/Akt pathway. *PLoS One* **2014,** *9* (3), e92168-e92168.
305. Pilar, F. L., Rates and equilibria of organic reactions (Leffler, John E.; Grunwald, Ernest). *Journal of Chemical Education* **1964,** *41* (7), 407.
306. Hartrampf, N.; Saebi, A.; Poskus, M.; Gates, Z. P.; Callahan, A. J.; Cowfer, A. E.; Hanna, S.; Antilla, S.; Schissel, C. K.; Quartararo, A. J.; Ye, X.; Mijalis, A. J.; Simon, M. D.; Loas, A.; Liu, S.; Jessen, C.; Nielsen, T. E.; Pentelute, B. L., Synthesis of proteins by automated flow chemistry. *Science* **2020,** *368* (6494), 980-987.
307. Piovesan, A.; Pelleri, M. C.; Antonaros, F.; Strippoli, P.; Caracausi, M.; Vitale, L., On the length, weight and GC content of the human genome. *BMC Research Notes* **2019,** *12* (1), 106.
308. Silverman, S. K., DNA as a versatile chemical component for catalysis, encoding, and stereocontrol. *Angewandte Chemie (International ed. in English)* **2010,** *49* (40), 7180-7201.

309. Silverman, S. K., Catalytic DNA: Scope, Applications, and Biochemistry of Deoxyribozymes. *Trends in Biochemical Sciences* **2016,** *41* (7), 595-609.
310. Ma, L.; Liu, J., Catalytic nucleic acids: biochemistry, chemical biology, biosensors, and nanotechnology. *Iscience* **2020,** *23* (1), 100815.
311. Wang, F.; Lu, C.-H.; Willner, I., From cascaded catalytic nucleic acids to enzyme–DNA nanostructures: controlling reactivity, sensing, logic operations, and assembly of complex structures. *Chem. Rev.* **2014,** *114* (5), 2881-2941.
312. Rivilla, I.; de Cózar, A.; Schäfer, T.; Hernandez, F. J.; Bittner, A. M.; Eleta-Lopez, A.; Aboudzadeh, A.; Santos, J. I.; Miranda, J. I.; Cossío, F. P., Catalysis of a 1,3-dipolar reaction by distorted DNA incorporating a heterobimetallic platinum(ii) and copper(ii) complex. *Chemical Science* **2017,** *8* (10), 7038-7046.
313. Park, S. V.; Yang, J.-S.; Jo, H.; Kang, B.; Oh, S. S.; Jung, G. Y., Catalytic RNA, ribozyme, and its applications in synthetic biology. *Biotechnology Advances* **2019,** *37* (8), 107452.
314. Müller, S.; Appel, B.; Balke, D.; Hieronymus, R.; Nübel, C., Thirty-five years of research into ribozymes and nucleic acid catalysis: where do we stand today? *F1000Res* **2016,** *5*, F1000 Faculty Rev-1511.
315. Dunn, M. R.; Jimenez, R. M.; Chaput, J. C., Analysis of aptamer discovery and technology. *Nature Reviews Chemistry* **2017,** *1* (10), 0076.
316. Adachi, T.; Nakamura, Y., Aptamers: A Review of Their Chemical Properties and Modifications for Therapeutic Application. *Molecules (Basel, Switzerland)* **2019,** *24* (23), 4229.
317. Zou, X.; Wu, J.; Gu, J.; Shen, L.; Mao, L., Application of Aptamers in Virus Detection and Antiviral Therapy. *Frontiers in Microbiology* **2019,** *10* (1462).
318. Begum, A.; Dodoala, S.; Prasad, K.; Koganti, B., A Review on Azapeptides: The Promising Peptidomimetics. *Asian Journal of Chemistry* **2017,** *29*, 1879-1887.
319. Li, X.; Yang, D., Peptides of aminoxy acids as foldamers. *Chem. Commun.* **2006,** (32), 3367-3379.
320. Salaün, A.; Potel, M.; Roisnel, T.; Gall, P.; Le Grel, P., Crystal Structures of Aza-β3-peptides, A New Class of Foldamers Relying on a Framework of Hydrazinoturns. *The Journal of Organic Chemistry* **2005,** *70* (16), 6499-6502.
321. Del Borgo, M. P.; Kulkarni, K.; Aguilar, M. I., Using β-Amino Acids and β-Peptide Templates to Create Bioactive Ligands and Biomaterials. *Current pharmaceutical design* **2017,** *23* (26), 3772-3785.
322. Pilsl, L. K. A.; Reiser, O., α/β-Peptide foldamers: state of the art. *Amino Acids* **2011,** *41* (3), 709-718.
323. Cheng, R. P.; Gellman, S. H.; DeGrado, W. F., β-Peptides: From Structure to Function. *Chem. Rev.* **2001,** *101* (10), 3219-3232.
324. Teng, P.; Shi, Y.; Sang, P.; Cai, J., γ-AApeptides as a New Class of Peptidomimetics. *Chemistry (Weinheim an der Bergstrasse, Germany)* **2016,** *22* (16), 5458-66.

325. Vasudev, P. G.; Chatterjee, S.; Shamala, N.; Balaram, P., Structural Chemistry of Peptides Containing Backbone Expanded Amino Acid Residues: Conformational Features of β, γ, and Hybrid Peptides. *Chem. Rev.* **2011,** *111* (2), 657-687.
326. Seebach, D.; Beck, A. K.; Bierbaum, D. J., The world of beta- and gamma-peptides comprised of homologated proteinogenic amino acids and other components. *Chemistry & biodiversity* **2004,** *1* (8), 1111-239.
327. Gangloff, N.; Ulbricht, J.; Lorson, T.; Schlaad, H.; Luxenhofer, R., Peptoids and Polypeptoids at the Frontier of Supra- and Macromolecular Engineering. *Chem. Rev.* **2016,** *116* (4), 1753-1802.
328. Ganesh, S. D.; Saha, N.; Zandraa, O.; Zuckermann, R. N.; Sáha, P., Peptoids and polypeptoids: biomimetic and bioinspired materials for biomedical applications. *Polymer Bulletin* **2017,** *74* (8), 3455-3466.
329. Reese, H. R.; Shanahan, C. C.; Proulx, C.; Menegatti, S., Peptide science: A "rule model" for new generations of peptidomimetics. *Acta Biomaterialia* **2020,** *102*, 35-74.
330. Cho, C. Y.; Moran, E. J.; Cherry, S. R.; Stephans, J. C.; Fodor, S. P.; Adams, C. L.; Sundaram, A.; Jacobs, J. W.; Schultz, P. G., An unnatural biopolymer. *Science* **1993,** *261* (5126), 1303-5.
331. Cussol, L.; Mauran-Ambrosino, L.; Buratto, J.; Belorusova, A. Y.; Neuville, M.; Osz, J.; Fribourg, S.; Fremaux, J.; Dolain, C.; Goudreau, S. R.; Rochel, N.; Guichard, G., Structural Basis for α-Helix Mimicry and Inhibition of Protein–Protein Interactions with Oligourea Foldamers. *Angewandte Chemie International Edition* **2021,** *60* (5), 2296-2303.
332. Semetey, V.; Rognan, D.; Hemmerlin, C.; Graff, R.; Briand, J.-P.; Marraud, M.; Guichard, G., Stable Helical Secondary Structure in Short-Chain N,N′-Linked Oligoureas Bearing Proteinogenic Side Chains. *Angewandte Chemie International Edition* **2002,** *41* (11), 1893-1895.
333. Diemer, V.; Fischer, L.; Kauffmann, B.; Guichard, G., Anion Recognition by Aliphatic Helical Oligoureas. *Chemistry (Weinheim an der Bergstrasse, Germany)* **2016,** *22* (44), 15684-15692.
334. Appella, D. H., Non-natural nucleic acids for synthetic biology. *Curr Opin Chem Biol* **2009,** *13* (5-6), 687-96.
335. Delaney, J. C.; Gao, J.; Liu, H.; Shrivastav, N.; Essigmann, J. M.; Kool, E. T., Efficient replication bypass of size-expanded DNA base pairs in bacterial cells. *Angewandte Chemie (International ed. in English)* **2009,** *48* (25), 4524-7.
336. Chen, Z.; Lichtor, P. A.; Berliner, A. P.; Chen, J. C.; Liu, D. R., Evolution of sequence-defined highly functionalized nucleic acid polymers. *Nature Chemistry* **2018,** *10* (4), 420-427.
337. Kimoto, M.; Kawai, R.; Mitsui, T.; Yokoyama, S.; Hirao, I., An unnatural base pair system for efficient PCR amplification and functionalization of DNA molecules. *Nucleic acids research* **2009,** *37* (2), e14.
338. Kong, D.; Lei, Y.; Yeung, W.; Hili, R., Enzymatic Synthesis of Sequence-Defined Synthetic Nucleic Acid Polymers with Diverse Functional Groups. *Angewandte Chemie (International ed. in English)* **2016,** *55* (42), 13164-13168.

339. Duffy, K.; Arangundy-Franklin, S.; Holliger, P., Modified nucleic acids: replication, evolution, and next-generation therapeutics. *BMC Biology* **2020,** *18* (1), 112.
340. Shivalingam, A.; Brown, T., Synthesis of chemically modified DNA. *Biochemical Society transactions* **2016,** *44* (3), 709-15.
341. Eremeeva, E.; Abramov, M.; Margamuljana, L.; Herdewijn, P., Base-Modified Nucleic Acids as a Powerful Tool for Synthetic Biology and Biotechnology. *Chemistry (Weinheim an der Bergstrasse, Germany)* **2017,** *23* (40), 9560-9576.
342. Ziach, K.; Chollet, C.; Parissi, V.; Prabhakaran, P.; Marchivie, M.; Corvaglia, V.; Bose, P. P.; Laxmi-Reddy, K.; Godde, F.; Schmitter, J.-M.; Chaignepain, S.; Pourquier, P.; Huc, I., Single helically folded aromatic oligoamides that mimic the charge surface of double-stranded B-DNA. *Nature Chemistry* **2018,** *10* (5), 511-518.
343. Quan, G.; Ying, W.; Hua, J., Aromatic Oligoamide Foldamers: A Paradigm for Structure – Property Relationship. *Current Organic Chemistry* **2011,** *15* (9), 1293-1301.
344. Hu, H.-Y.; Chen, C.-F., Artificial Supersecondary Structures Based on Aromatic Oligoamides. In *Protein Supersecondary Structures*, Kister, A. E., Ed. Humana Press: Totowa, NJ, 2013; pp 219-234.
345. Ferrand, Y.; Kendhale, A. M.; Garric, J.; Kauffmann, B.; Huc, I., Parallel and Antiparallel Triple Helices of Naphthyridine Oligoamides. *Angewandte Chemie International Edition* **2010,** *49* (10), 1778-1781.
346. Gan, Q.; Bao, C.; Kauffmann, B.; Grélard, A.; Xiang, J.; Liu, S.; Huc, I.; Jiang, H., Quadruple and Double Helices of 8-Fluoroquinoline Oligoamides. *Angewandte Chemie International Edition* **2008,** *47* (9), 1715-1718.
347. Kline, M. A.; Wei, X.; Horner, I. J.; Liu, R.; Chen, S.; Chen, S.; Yung, K. Y.; Yamato, K.; Cai, Z.; Bright, F. V.; Zeng, X. C.; Gong, B., Extremely strong tubular stacking of aromatic oligoamide macrocycles. *Chemical Science* **2015,** *6* (1), 152-157.
348. Ahn, S.-H.; Grate, J. W., Foldamer Architectures of Triazine-Based Sequence-Defined Polymers Investigated with Molecular Dynamics Simulations and Enhanced Sampling Methods. *The Journal of Physical Chemistry B* **2019,** *123* (44), 9364-9377.
349. Gunasekaran, P.; Kim, E. Y.; Lee, J.; Ryu, E. K.; Shin, S. Y.; Bang, J. K., Synthesis of Fmoc-Triazine Amino Acids and Its Application in the Synthesis of Short Antibacterial Peptidomimetics. *International Journal of Molecular Sciences* **2020,** *21* (10), 3602.
350. Nanjan, P.; Porel, M., Sequence-defined non-natural polymers: synthesis and applications. *Polymer Chemistry* **2019,** *10* (40), 5406-5424.
351. Guichard, G.; Huc, I., Synthetic foldamers. *Chemical communications (Cambridge, England)* **2011,** *47* (21), 5933-41.
352. Meier, M. A. R.; Barner-Kowollik, C., A New Class of Materials: Sequence-Defined Macromolecules and Their Emerging Applications. *Advanced Materials* **2019,** *31* (26), 1806027.
353. Goodman, C. M.; Choi, S.; Shandler, S.; DeGrado, W. F., Foldamers as versatile frameworks for the design and evolution of function. *Nature Chemical Biology* **2007,** *3* (5), 252-262.

354. Lutz, J.-F., Coding Macromolecules: Inputting Information in Polymers Using Monomer-Based Alphabets. *Macromolecules* **2015,** *48* (14), 4759-4767.
355. Gunay, Ufuk S.; Petit, Benoît E.; Karamessini, D.; Al Ouahabi, A.; Amalian, J.-A.; Chendo, C.; Bouquey, M.; Gigmes, D.; Charles, L.; Lutz, J.-F., Chemoselective Synthesis of Uniform Sequence-Coded Polyurethanes and Their Use as Molecular Tags. *Chem* **2016,** *1* (1), 114-126.
356. Amalian, J.-A.; Poyer, S.; Petit, B. E.; Telitel, S.; Monnier, V.; Karamessini, D.; Gigmes, D.; Lutz, J.-F.; Charles, L., Negative mode MS/MS to read digital information encoded in sequence-defined oligo(urethane)s: A mechanistic study. *International Journal of Mass Spectrometry* **2017,** *421*, 271-278.
357. Martens, S.; Landuyt, A.; Espeel, P.; Devreese, B.; Dawyndt, P.; Du Prez, F., Multifunctional sequence-defined macromolecules for chemical data storage. *Nature Communications* **2018,** *9* (1), 4451.
358. Tossi, A.; Sandri, L.; Giangaspero, A., Amphipathic, alpha-helical antimicrobial peptides. *Biopolymers* **2000,** *55* (1), 4-30.
359. Venkatesh, M.; Barathi, V. A.; Goh, E. T. L.; Anggara, R.; Fazil, M. H. U. T.; Ng, A. J. Y.; Harini, S.; Aung, T. T.; Fox, S. J.; Liu, S.; Yang, L.; Barkham, T. M. S.; Loh, X. J.; Verma, N. K.; Beuerman, R. W.; Lakshminarayanan, R., Antimicrobial Activity and Cell Selectivity of Synthetic and Biosynthetic Cationic Polymers. *Antimicrobial Agents and Chemotherapy* **2017,** *61* (10), e00469-17.
360. McHenry, A. J.; Sciacca, M. F. M.; Brender, J. R.; Ramamoorthy, A., Does cholesterol suppress the antimicrobial peptide induced disruption of lipid raft containing membranes? *Biochimica et Biophysica Acta (BBA) - Biomembranes* **2012,** *1818* (12), 3019-3024.
361. Gunasekaran, P.; Fan, m.; Kim, E. Y.; Shin, J. H.; Lee, J. E.; Son, E. J.; Kim, J.; Hwang, E.; Yim, M. S.; Kim, E.-H.; Choi, Y.-J.; Lee, Y.-H.; Chung, Y.-H.; Kim, H. N.; Ryu, E. K.; Shin, S. Y.; Kim, E.-K.; Bang, J. K., Amphiphilic Triazine Polymer Derivatives as Antibacterial And Anti-atopic Agents in Mice Model. *Scientific Reports* **2019,** *9* (1), 15161.
362. Porel, M.; Thornlow, D. N.; Artim, C. M.; Alabi, C. A., Sequence-Defined Backbone Modifications Regulate Antibacterial Activity of OligoTEAs. *ACS Chemical Biology* **2017,** *12* (3), 715-723.
363. Bécart, D.; Diemer, V.; Salaün, A.; Oiarbide, M.; Nelli, Y. R.; Kauffmann, B.; Fischer, L.; Palomo, C.; Guichard, G., Helical Oligourea Foldamers as Powerful Hydrogen Bonding Catalysts for Enantioselective C–C Bond-Forming Reactions. *J. Am. Chem. Soc.* **2017,** *139* (36), 12524-12532.
364. Lin, Y., What's happened over the last five years with high-throughput protein crystallization screening? *Expert Opinion on Drug Discovery* **2018,** *13* (8), 691-695.
365. Edman, P., Method for Determination of the Amino Acid Sequence in Peptides. *Acta Scandinavica* **1950,** *4*, 283-293.
366. Edman, P.; Begg, G., A Protein Sequenator. *European Journal of Biochemistry* **1967,** *1* (1), 80-91.

367. Schlesinger, D. H., PROTEINS | Traditional Methods of Sequence Determination. In *Encyclopedia of Analytical Science (Second Edition)*, Worsfold, P.; Townshend, A.; Poole, C., Eds. Elsevier: Oxford, 2005; pp 352-357.
368. Berg, J. M. T., J.L.; Stryer, L., Amino Acid Sequences Can Be Determined by Automated Edman Degradation. In *Biochemistry*, 5 ed.; W H Freeman: New York, 2002.
369. Cottrell, J. S., Protein identification using MS/MS data. *Journal of Proteomics* **2011,** *74* (10), 1842-1851.
370. Lu, B.; Chen, T., Algorithms for de novo peptide sequencing using tandem mass spectrometry. *Drug Discovery Today: BIOSILICO* **2004,** *2* (2), 85-90.
371. Wang, R.; Chait, B. T.; Kent, S. B. H., Protein Ladder Sequencing: A Conceptually Novel Approach To Protein Sequencing Using Cycling Chemical Degradation and One-Step Readout by Matrix-Assisted Laser Desorption Mass Spectrometry. In *Techniques in Protein Chemistry IV*, Angeletti, R. H., Ed. Academic Press: 1993; pp 471-478.
372. Hernandez, E. T.; Swaminathan, J.; Marcotte, E. M.; Anslyn, E. V., Solution-phase and solid-phase sequential, selective modification of side chains in KDYWEC and KDYWE as models for usage in single-molecule protein sequencing. *New journal of chemistry = Nouveau journal de chimie* **2017,** *41* (2), 462-469.
373. Swaminathan, J.; Boulgakov, A. A.; Hernandez, E. T.; Bardo, A. M.; Bachman, J. L.; Marotta, J.; Johnson, A. M.; Anslyn, E. V.; Marcotte, E. M., Highly parallel single-molecule identification of proteins in zeptomole-scale mixtures. *Nature Biotechnology* **2018**, 10.1038/nbt.4278.
374. Kanelis, V.; Forman-Kay, J. D.; Kay, L. E., Multidimensional NMR methods for protein structure determination. *IUBMB life* **2001,** *52* (6), 291-302.
375. Wüthrich, K., NMR with proteins and nucleic acids. *Europhysics News* **1986,** *17* (1), 11-13.
376. Riek, R.; Hornemann, S.; Wider, G.; Billeter, M.; Glockshuber, R.; Wüthrich, K., NMR structure of the mouse prion protein domain PrP (121–231). *Nature* **1996,** *382* (6587), 180-182.
377. Jiang, Y.; Kalodimos, C. G., NMR studies of large proteins. *Journal of molecular biology* **2017,** *429* (17), 2667-2676.
378. Cavanagh, J.; Fairbrother, W. J.; Palmer III, A. G.; Skelton, N. J., *Protein NMR spectroscopy: principles and practice*. Elsevier: 1995.
379. Cavalli, A.; Salvatella, X.; Dobson, C. M.; Vendruscolo, M., Protein structure determination from NMR chemical shifts. *Proc Natl Acad Sci USA* **2007,** *104* (23), 9615-9620.
380. Zhang, P.; Seth, A.; Fernandes, H., Other Post-PCR Detection Technologies. In *Pathobiology of Human Disease*, McManus, L. M.; Mitchell, R. N., Eds. Academic Press: San Diego, 2014; pp 4074-4088.
381. Davis, L. G.; Dibner, M. D.; Battey, J. F., SECTION 5-4 - Restriction Endonucleases (REs) and Their Use. In *Basic Methods in Molecular Biology*, Davis, L. G.; Dibner, M. D.; Battey, J. F., Eds. Elsevier: 1986; pp 51-57.

382. Pareek, C. S.; Smoczynski, R.; Tretyn, A., Sequencing technologies and genome sequencing. *J Appl Genet* **2011,** *52* (4), 413-435.
383. Timp, W.; Timp, G., Beyond mass spectrometry, the next step in proteomics. *Science Advances* **2020,** *6* (2), eaax8978.
384. Heerma, W.; Versluis, C.; De Koster, C.; Kruijtzer, J.; Zigrovic, I.; Liskamp, R., Comparing mass spectrometric characteristics of peptides and peptoids. *Rapid communications in mass spectrometry* **1996,** *10* (4), 459-464.
385. Roy, R. K.; Meszynska, A.; Laure, C.; Charles, L.; Verchin, C.; Lutz, J.-F., Design and synthesis of digitally encoded polymers that can be decoded and erased. *Nature Communications* **2015,** *6* (1), 1-8.
386. Al Ouahabi, A.; Amalian, J.-A.; Charles, L.; Lutz, J.-F., Mass spectrometry sequencing of long digital polymers facilitated by programmed inter-byte fragmentation. *Nature Communications* **2017,** *8* (1), 967.
387. David, D.; Emma, C.; Graham, K.; Emma, C.; Cole, M.; Leroy, C., *A Universal Sequencing System for Unknown Oligomers*. 2020.
388. Proulx, C.; Noë, F.; Yoo, S.; Connolly, M. D.; Zuckermann, R. N., On-resin N-terminal peptoid degradation: Toward mild sequencing conditions. *Biopolymers* **2016,** *106* (5), 726-36.
389. Weinstain, R.; Sagi, A.; Karton, N.; Shabat, D., Self-Immolative Comb-Polymers: Multiple-Release of Side-Reporters by a Single Stimulus Event. *Chemistry – A European Journal* **2008,** *14* (23), 6857-6861.
390. Erez, R.; Shabat, D., The azaquinone-methide elimination: comparison study of 1,6- and 1,4-eliminations under physiological conditions. *Organic & Biomolecular Chemistry* **2008,** *6* (15), 2669-2672.
391. Sirianni, Q. E. A.; Gillies, E. R., The architectural evolution of self-immolative polymers. *Polymer* **2020,** *202*, 122638.
392. Dewit, M. A.; Beaton, A.; Gillies, E. R., A reduction sensitive cascade biodegradable linear polymer. *Journal of Polymer Science Part A: Polymer Chemistry* **2010,** *48* (18), 3977-3985.
393. Montaudo, G.; Puglisi, C.; Scamporrino, E.; Vitalini, D., Mechanism of thermal degradation of polyurethanes. Effect of ammonium polyphosphate. *Macromolecules* **1984,** *17* (8), 1605-1614.
394. Mondal, T.; Charles, L.; Lutz, J.-F., Damage and Repair in Informational Poly(N-substituted urethane)s. *Angewandte Chemie International Edition* **2020,** *59* (46), 20390-20393.

REFERENCES FOR CHAPTER 2

1. Hartrampf, N.; Saebi, A.; Poskus, M.; Gates, Z. P.; Callahan, A. J.; Cowfer, A. E.; Hanna, S.; Antilla, S.; Schissel, C. K.; Quartararo, A. J.; Ye, X.; Mijalis, A. J.; Simon, M. D.; Loas, A.; Liu, S.; Jessen, C.; Nielsen, T. E.; Pentelute, B. L., Synthesis of proteins by automated flow chemistry. *Science* **2020,** *368* (6494), 980-987.

2. Piovesan, A.; Pelleri, M. C.; Antonaros, F.; Strippoli, P.; Caracausi, M.; Vitale, L., On the length, weight and GC content of the human genome. *BMC Research Notes* **2019,** *12* (1), 106.
3. Silverman, S. K., DNA as a versatile chemical component for catalysis, encoding, and stereocontrol. *Angewandte Chemie (International ed. in English)* **2010,** *49* (40), 7180-7201.
4. Silverman, S. K., Catalytic DNA: Scope, Applications, and Biochemistry of Deoxyribozymes. *Trends in Biochemical Sciences* **2016,** *41* (7), 595-609.
5. Ma, L.; Liu, J., Catalytic nucleic acids: biochemistry, chemical biology, biosensors, and nanotechnology. *Iscience* **2020,** *23* (1), 100815.
6. Wang, F.; Lu, C.-H.; Willner, I., From cascaded catalytic nucleic acids to enzyme–DNA nanostructures: controlling reactivity, sensing, logic operations, and assembly of complex structures. *Chem. Rev.* **2014,** *114* (5), 2881-2941.
7. Rivilla, I.; de Cózar, A.; Schäfer, T.; Hernandez, F. J.; Bittner, A. M.; Eleta-Lopez, A.; Aboudzadeh, A.; Santos, J. I.; Miranda, J. I.; Cossío, F. P., Catalysis of a 1,3-dipolar reaction by distorted DNA incorporating a heterobimetallic platinum(ii) and copper(ii) complex. *Chemical Science* **2017,** *8* (10), 7038-7046.
8. Park, S. V.; Yang, J.-S.; Jo, H.; Kang, B.; Oh, S. S.; Jung, G. Y., Catalytic RNA, ribozyme, and its applications in synthetic biology. *Biotechnology Advances* **2019,** *37* (8), 107452.
9. Müller, S.; Appel, B.; Balke, D.; Hieronymus, R.; Nübel, C., Thirty-five years of research into ribozymes and nucleic acid catalysis: where do we stand today? *F1000Res* **2016,** *5*, F1000 Faculty Rev-1511.
10. Dunn, M. R.; Jimenez, R. M.; Chaput, J. C., Analysis of aptamer discovery and technology. *Nature Reviews Chemistry* **2017,** *1* (10), 0076.
11. Adachi, T.; Nakamura, Y., Aptamers: A Review of Their Chemical Properties and Modifications for Therapeutic Application. *Molecules (Basel, Switzerland)* **2019,** *24* (23), 4229.
12. Zou, X.; Wu, J.; Gu, J.; Shen, L.; Mao, L., Application of Aptamers in Virus Detection and Antiviral Therapy. *Frontiers in Microbiology* **2019,** *10* (1462).
13. Begum, A.; Dodoala, S.; Prasad, K.; Koganti, B., A Review on Azapeptides: The Promising Peptidomimetics. *Asian Journal of Chemistry* **2017,** *29*, 1879-1887.
14. Li, X.; Yang, D., Peptides of aminoxy acids as foldamers. *Chem. Commun.* **2006,** (32), 3367-3379.
15. Salaün, A.; Potel, M.; Roisnel, T.; Gall, P.; Le Grel, P., Crystal Structures of Aza-β3-peptides, A New Class of Foldamers Relying on a Framework of Hydrazinoturns. *The Journal of Organic Chemistry* **2005,** *70* (16), 6499-6502.
16. Del Borgo, M. P.; Kulkarni, K.; Aguilar, M. I., Using β-Amino Acids and β-Peptide Templates to Create Bioactive Ligands and Biomaterials. *Current pharmaceutical design* **2017,** *23* (26), 3772-3785.
17. Pilsl, L. K. A.; Reiser, O., α/β-Peptide foldamers: state of the art. *Amino Acids* **2011,** *41* (3), 709-718.

18. Cheng, R. P.; Gellman, S. H.; DeGrado, W. F., β-Peptides: From Structure to Function. *Chem. Rev.* **2001,** *101* (10), 3219-3232.
19. Teng, P.; Shi, Y.; Sang, P.; Cai, J., γ-AApeptides as a New Class of Peptidomimetics. *Chemistry (Weinheim an der Bergstrasse, Germany)* **2016,** *22* (16), 5458-66.
20. Vasudev, P. G.; Chatterjee, S.; Shamala, N.; Balaram, P., Structural Chemistry of Peptides Containing Backbone Expanded Amino Acid Residues: Conformational Features of β, γ, and Hybrid Peptides. *Chem. Rev.* **2011,** *111* (2), 657-687.
21. Seebach, D.; Beck, A. K.; Bierbaum, D. J., The world of beta- and gamma-peptides comprised of homologated proteinogenic amino acids and other components. *Chemistry & biodiversity* **2004,** *1* (8), 1111-239.
22. Gangloff, N.; Ulbricht, J.; Lorson, T.; Schlaad, H.; Luxenhofer, R., Peptoids and Polypeptoids at the Frontier of Supra- and Macromolecular Engineering. *Chem. Rev.* **2016,** *116* (4), 1753-1802.
23. Ganesh, S. D.; Saha, N.; Zandraa, O.; Zuckermann, R. N.; Sáha, P., Peptoids and polypeptoids: biomimetic and bioinspired materials for biomedical applications. *Polymer Bulletin* **2017,** *74* (8), 3455-3466.
24. Reese, H. R.; Shanahan, C. C.; Proulx, C.; Menegatti, S., Peptide science: A "rule model" for new generations of peptidomimetics. *Acta Biomaterialia* **2020,** *102*, 35-74.
25. Cho, C. Y.; Moran, E. J.; Cherry, S. R.; Stephans, J. C.; Fodor, S. P.; Adams, C. L.; Sundaram, A.; Jacobs, J. W.; Schultz, P. G., An unnatural biopolymer. *Science* **1993,** *261* (5126), 1303-5.
26. Cussol, L.; Mauran-Ambrosino, L.; Buratto, J.; Belorusova, A. Y.; Neuville, M.; Osz, J.; Fribourg, S.; Fremaux, J.; Dolain, C.; Goudreau, S. R.; Rochel, N.; Guichard, G., Structural Basis for α-Helix Mimicry and Inhibition of Protein–Protein Interactions with Oligourea Foldamers. *Angewandte Chemie International Edition* **2021,** *60* (5), 2296-2303.
27. Semetey, V.; Rognan, D.; Hemmerlin, C.; Graff, R.; Briand, J.-P.; Marraud, M.; Guichard, G., Stable Helical Secondary Structure in Short-Chain N,N′-Linked Oligoureas Bearing Proteinogenic Side Chains. *Angewandte Chemie International Edition* **2002,** *41* (11), 1893-1895.
28. Diemer, V.; Fischer, L.; Kauffmann, B.; Guichard, G., Anion Recognition by Aliphatic Helical Oligoureas. *Chemistry (Weinheim an der Bergstrasse, Germany)* **2016,** *22* (44), 15684-15692.
29. Appella, D. H., Non-natural nucleic acids for synthetic biology. *Curr Opin Chem Biol* **2009,** *13* (5-6), 687-96.
30. Delaney, J. C.; Gao, J.; Liu, H.; Shrivastav, N.; Essigmann, J. M.; Kool, E. T., Efficient replication bypass of size-expanded DNA base pairs in bacterial cells. *Angewandte Chemie (International ed. in English)* **2009,** *48* (25), 4524-7.
31. Chen, Z.; Lichtor, P. A.; Berliner, A. P.; Chen, J. C.; Liu, D. R., Evolution of sequence-defined highly functionalized nucleic acid polymers. *Nature Chemistry* **2018,** *10* (4), 420-427.

32. Kimoto, M.; Kawai, R.; Mitsui, T.; Yokoyama, S.; Hirao, I., An unnatural base pair system for efficient PCR amplification and functionalization of DNA molecules. *Nucleic acids research* **2009,** *37* (2), e14.
33. Kong, D.; Lei, Y.; Yeung, W.; Hili, R., Enzymatic Synthesis of Sequence-Defined Synthetic Nucleic Acid Polymers with Diverse Functional Groups. *Angewandte Chemie (International ed. in English)* **2016,** *55* (42), 13164-13168.
34. Duffy, K.; Arangundy-Franklin, S.; Holliger, P., Modified nucleic acids: replication, evolution, and next-generation therapeutics. *BMC Biology* **2020,** *18* (1), 112.
35. Shivalingam, A.; Brown, T., Synthesis of chemically modified DNA. *Biochemical Society transactions* **2016,** *44* (3), 709-15.
36. Eremeeva, E.; Abramov, M.; Margamuljana, L.; Herdewijn, P., Base-Modified Nucleic Acids as a Powerful Tool for Synthetic Biology and Biotechnology. *Chemistry (Weinheim an der Bergstrasse, Germany)* **2017,** *23* (40), 9560-9576.
37. Ziach, K.; Chollet, C.; Parissi, V.; Prabhakaran, P.; Marchivie, M.; Corvaglia, V.; Bose, P. P.; Laxmi-Reddy, K.; Godde, F.; Schmitter, J.-M.; Chaignepain, S.; Pourquier, P.; Huc, I., Single helically folded aromatic oligoamides that mimic the charge surface of double-stranded B-DNA. *Nature Chemistry* **2018,** *10* (5), 511-518.
38. Quan, G.; Ying, W.; Hua, J., Aromatic Oligoamide Foldamers: A Paradigm for Structure – Property Relationship. *Current Organic Chemistry* **2011,** *15* (9), 1293-1301.
39. Hu, H.-Y.; Chen, C.-F., Artificial Supersecondary Structures Based on Aromatic Oligoamides. In *Protein Supersecondary Structures*, Kister, A. E., Ed. Humana Press: Totowa, NJ, 2013; pp 219-234.
40. Ferrand, Y.; Kendhale, A. M.; Garric, J.; Kauffmann, B.; Huc, I., Parallel and Antiparallel Triple Helices of Naphthyridine Oligoamides. *Angewandte Chemie International Edition* **2010,** *49* (10), 1778-1781.
41. Gan, Q.; Bao, C.; Kauffmann, B.; Grélard, A.; Xiang, J.; Liu, S.; Huc, I.; Jiang, H., Quadruple and Double Helices of 8-Fluoroquinoline Oligoamides. *Angewandte Chemie International Edition* **2008,** *47* (9), 1715-1718.
42. Kline, M. A.; Wei, X.; Horner, I. J.; Liu, R.; Chen, S.; Chen, S.; Yung, K. Y.; Yamato, K.; Cai, Z.; Bright, F. V.; Zeng, X. C.; Gong, B., Extremely strong tubular stacking of aromatic oligoamide macrocycles. *Chemical Science* **2015,** *6* (1), 152-157.
43. Ahn, S.-H.; Grate, J. W., Foldamer Architectures of Triazine-Based Sequence-Defined Polymers Investigated with Molecular Dynamics Simulations and Enhanced Sampling Methods. *The Journal of Physical Chemistry B* **2019,** *123* (44), 9364-9377.
44. Gunasekaran, P.; Kim, E. Y.; Lee, J.; Ryu, E. K.; Shin, S. Y.; Bang, J. K., Synthesis of Fmoc-Triazine Amino Acids and Its Application in the Synthesis of Short Antibacterial Peptidomimetics. *International Journal of Molecular Sciences* **2020,** *21* (10), 3602.
45. Nanjan, P.; Porel, M., Sequence-defined non-natural polymers: synthesis and applications. *Polymer Chemistry* **2019,** *10* (40), 5406-5424.
46. Guichard, G.; Huc, I., Synthetic foldamers. *Chemical communications (Cambridge, England)* **2011,** *47* (21), 5933-41.

47. Meier, M. A. R.; Barner-Kowollik, C., A New Class of Materials: Sequence-Defined Macromolecules and Their Emerging Applications. *Advanced Materials* **2019,** *31* (26), 1806027.
48. Goodman, C. M.; Choi, S.; Shandler, S.; DeGrado, W. F., Foldamers as versatile frameworks for the design and evolution of function. *Nature Chemical Biology* **2007,** *3* (5), 252-262.
49. Lutz, J.-F., Coding Macromolecules: Inputting Information in Polymers Using Monomer-Based Alphabets. *Macromolecules* **2015,** *48* (14), 4759-4767.
50. Gunay, Ufuk S.; Petit, Benoît E.; Karamessini, D.; Al Ouahabi, A.; Amalian, J.-A.; Chendo, C.; Bouquey, M.; Gigmes, D.; Charles, L.; Lutz, J.-F., Chemoselective Synthesis of Uniform Sequence-Coded Polyurethanes and Their Use as Molecular Tags. *Chem* **2016,** *1* (1), 114-126.
51. Amalian, J.-A.; Poyer, S.; Petit, B. E.; Telitel, S.; Monnier, V.; Karamessini, D.; Gigmes, D.; Lutz, J.-F.; Charles, L., Negative mode MS/MS to read digital information encoded in sequence-defined oligo(urethane)s: A mechanistic study. *International Journal of Mass Spectrometry* **2017,** *421*, 271-278.
52. Martens, S.; Landuyt, A.; Espeel, P.; Devreese, B.; Dawyndt, P.; Du Prez, F., Multifunctional sequence-defined macromolecules for chemical data storage. *Nature Communications* **2018,** *9* (1), 4451.
53. Tossi, A.; Sandri, L.; Giangaspero, A., Amphipathic, alpha-helical antimicrobial peptides. *Biopolymers* **2000,** *55* (1), 4-30.
54. Venkatesh, M.; Barathi, V. A.; Goh, E. T. L.; Anggara, R.; Fazil, M. H. U. T.; Ng, A. J. Y.; Harini, S.; Aung, T. T.; Fox, S. J.; Liu, S.; Yang, L.; Barkham, T. M. S.; Loh, X. J.; Verma, N. K.; Beuerman, R. W.; Lakshminarayanan, R., Antimicrobial Activity and Cell Selectivity of Synthetic and Biosynthetic Cationic Polymers. *Antimicrobial Agents and Chemotherapy* **2017,** *61* (10), e00469-17.
55. McHenry, A. J.; Sciacca, M. F. M.; Brender, J. R.; Ramamoorthy, A., Does cholesterol suppress the antimicrobial peptide induced disruption of lipid raft containing membranes? *Biochimica et Biophysica Acta (BBA) - Biomembranes* **2012,** *1818* (12), 3019-3024.
56. Gunasekaran, P.; Fan, m.; Kim, E. Y.; Shin, J. H.; Lee, J. E.; Son, E. J.; Kim, J.; Hwang, E.; Yim, M. S.; Kim, E.-H.; Choi, Y.-J.; Lee, Y.-H.; Chung, Y.-H.; Kim, H. N.; Ryu, E. K.; Shin, S. Y.; Kim, E.-K.; Bang, J. K., Amphiphilic Triazine Polymer Derivatives as Antibacterial And Anti-atopic Agents in Mice Model. *Scientific Reports* **2019,** *9* (1), 15161.
57. Porel, M.; Thornlow, D. N.; Artim, C. M.; Alabi, C. A., Sequence-Defined Backbone Modifications Regulate Antibacterial Activity of OligoTEAs. *ACS Chemical Biology* **2017,** *12* (3), 715-723.
58. Bécart, D.; Diemer, V.; Salaün, A.; Oiarbide, M.; Nelli, Y. R.; Kauffmann, B.; Fischer, L.; Palomo, C.; Guichard, G., Helical Oligourea Foldamers as Powerful Hydrogen Bonding Catalysts for Enantioselective C–C Bond-Forming Reactions. *J. Am. Chem. Soc.* **2017,** *139* (36), 12524-12532.

59. Lin, Y., What's happened over the last five years with high-throughput protein crystallization screening? *Expert Opinion on Drug Discovery* **2018,** *13* (8), 691-695.
60. Edman, P., Method for Determination of the Amino Acid Sequence in Peptides. *Acta Scandinavica* **1950,** *4*, 283-293.
61. Edman, P.; Begg, G., A Protein Sequenator. *European Journal of Biochemistry* **1967,** *1* (1), 80-91.
62. Schlesinger, D. H., PROTEINS | Traditional Methods of Sequence Determination. In *Encyclopedia of Analytical Science (Second Edition)*, Worsfold, P.; Townshend, A.; Poole, C., Eds. Elsevier: Oxford, 2005; pp 352-357.
63. Berg, J. M. T., J.L.; Stryer, L., Amino Acid Sequences Can Be Determined by Automated Edman Degradation. In *Biochemistry*, 5 ed.; W H Freeman: New York, 2002.
64. Cottrell, J. S., Protein identification using MS/MS data. *Journal of Proteomics* **2011,** *74* (10), 1842-1851.
65. Lu, B.; Chen, T., Algorithms for de novo peptide sequencing using tandem mass spectrometry. *Drug Discovery Today: BIOSILICO* **2004,** *2* (2), 85-90.
66. Wang, R.; Chait, B. T.; Kent, S. B. H., Protein Ladder Sequencing: A Conceptually Novel Approach To Protein Sequencing Using Cycling Chemical Degradation and One-Step Readout by Matrix-Assisted Laser Desorption Mass Spectrometry. In *Techniques in Protein Chemistry IV*, Angeletti, R. H., Ed. Academic Press: 1993; pp 471-478.
67. Hernandez, E. T.; Swaminathan, J.; Marcotte, E. M.; Anslyn, E. V., Solution-phase and solid-phase sequential, selective modification of side chains in KDYWEC and KDYWE as models for usage in single-molecule protein sequencing. *New journal of chemistry = Nouveau journal de chimie* **2017,** *41* (2), 462-469.
68. Swaminathan, J.; Boulgakov, A. A.; Hernandez, E. T.; Bardo, A. M.; Bachman, J. L.; Marotta, J.; Johnson, A. M.; Anslyn, E. V.; Marcotte, E. M., Highly parallel single-molecule identification of proteins in zeptomole-scale mixtures. *Nature Biotechnology* **2018**, 10.1038/nbt.4278.
69. Kanelis, V.; Forman-Kay, J. D.; Kay, L. E., Multidimensional NMR methods for protein structure determination. *IUBMB life* **2001,** *52* (6), 291-302.
70. Wüthrich, K., NMR with proteins and nucleic acids. *Europhysics News* **1986,** *17* (1), 11-13.
71. Riek, R.; Hornemann, S.; Wider, G.; Billeter, M.; Glockshuber, R.; Wüthrich, K., NMR structure of the mouse prion protein domain PrP (121–231). *Nature* **1996,** *382* (6587), 180-182.
72. Jiang, Y.; Kalodimos, C. G., NMR studies of large proteins. *Journal of molecular biology* **2017,** *429* (17), 2667-2676.
73. Cavanagh, J.; Fairbrother, W. J.; Palmer III, A. G.; Skelton, N. J., *Protein NMR spectroscopy: principles and practice*. Elsevier: 1995.
74. Cavalli, A.; Salvatella, X.; Dobson, C. M.; Vendruscolo, M., Protein structure determination from NMR chemical shifts. *Proc Natl Acad Sci USA* **2007,** *104* (23), 9615-9620.

75. Zhang, P.; Seth, A.; Fernandes, H., Other Post-PCR Detection Technologies. In *Pathobiology of Human Disease*, McManus, L. M.; Mitchell, R. N., Eds. Academic Press: San Diego, 2014; pp 4074-4088.
76. Davis, L. G.; Dibner, M. D.; Battey, J. F., SECTION 5-4 - Restriction Endonucleases (REs) and Their Use. In *Basic Methods in Molecular Biology*, Davis, L. G.; Dibner, M. D.; Battey, J. F., Eds. Elsevier: 1986; pp 51-57.
77. Pareek, C. S.; Smoczynski, R.; Tretyn, A., Sequencing technologies and genome sequencing. *J Appl Genet* **2011,** *52* (4), 413-435.
78. Timp, W.; Timp, G., Beyond mass spectrometry, the next step in proteomics. *Science Advances* **2020,** *6* (2), eaax8978.
79. Heerma, W.; Versluis, C.; De Koster, C.; Kruijtzer, J.; Zigrovic, I.; Liskamp, R., Comparing mass spectrometric characteristics of peptides and peptoids. *Rapid communications in mass spectrometry* **1996,** *10* (4), 459-464.
80. Roy, R. K.; Meszynska, A.; Laure, C.; Charles, L.; Verchin, C.; Lutz, J.-F., Design and synthesis of digitally encoded polymers that can be decoded and erased. *Nature Communications* **2015,** *6* (1), 1-8.
81. Al Ouahabi, A.; Amalian, J.-A.; Charles, L.; Lutz, J.-F., Mass spectrometry sequencing of long digital polymers facilitated by programmed inter-byte fragmentation. *Nature Communications* **2017,** *8* (1), 967.
82. David, D.; Emma, C.; Graham, K.; Emma, C.; Cole, M.; Leroy, C., *A Universal Sequencing System for Unknown Oligomers*. 2020.
83. Proulx, C.; Noë, F.; Yoo, S.; Connolly, M. D.; Zuckermann, R. N., On-resin N-terminal peptoid degradation: Toward mild sequencing conditions. *Biopolymers* **2016,** *106* (5), 726-36.
84. Weinstain, R.; Sagi, A.; Karton, N.; Shabat, D., Self-Immolative Comb-Polymers: Multiple-Release of Side-Reporters by a Single Stimulus Event. *Chemistry – A European Journal* **2008,** *14* (23), 6857-6861.
85. Erez, R.; Shabat, D., The azaquinone-methide elimination: comparison study of 1,6- and 1,4-eliminations under physiological conditions. *Organic & Biomolecular Chemistry* **2008,** *6* (15), 2669-2672.
86. Sirianni, Q. E. A.; Gillies, E. R., The architectural evolution of self-immolative polymers. *Polymer* **2020,** *202*, 122638.
87. Dewit, M. A.; Beaton, A.; Gillies, E. R., A reduction sensitive cascade biodegradable linear polymer. *Journal of Polymer Science Part A: Polymer Chemistry* **2010,** *48* (18), 3977-3985.
88. Montaudo, G.; Puglisi, C.; Scamporrino, E.; Vitalini, D., Mechanism of thermal degradation of polyurethanes. Effect of ammonium polyphosphate. *Macromolecules* **1984,** *17* (8), 1605-1614.
89. Dahlhauser, S. D.; Escamilla, P. R.; VandeWalle, A. N.; York, J. T.; Rapagnani, R. M.; Shei, J. S.; Glass, S. A.; Coronado, J. N.; Moor, S. R.; Saunders, D. P.; Anslyn, E. V., Sequencing of Sequence-Defined Oligourethanes via Controlled Self-Immolation. *J. Am. Chem. Soc.* **2020,** *142* (6), 2744-2749.

90. Mondal, T.; Charles, L.; Lutz, J.-F., Damage and Repair in Informational Poly(N-substituted urethane)s. *Angewandte Chemie International Edition* **2020,** *59* (46), 20390-20393.